AREVA

DOCKET 71–9341

BEA Research Reactor Package

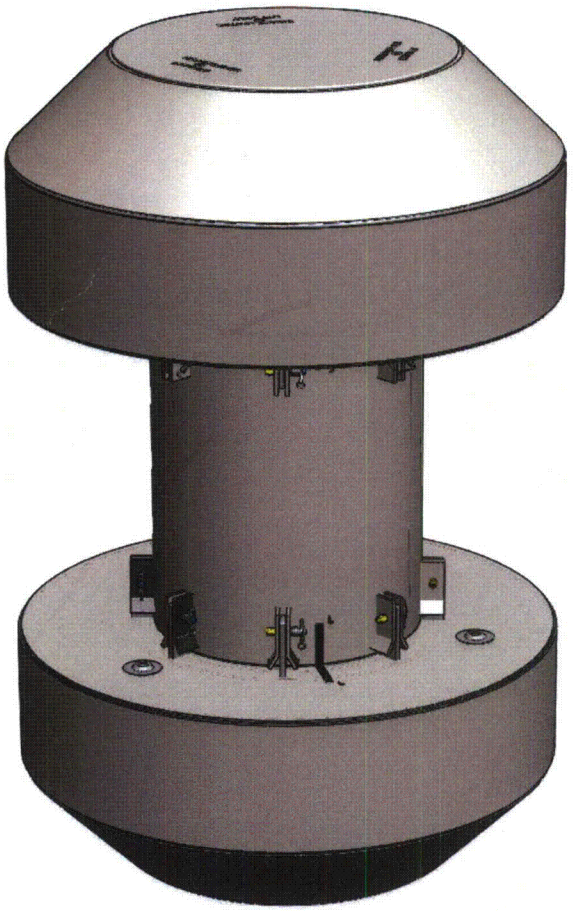

Safety Analysis Report

Revision 4

AREVA Federal Services LLC

December 2010

TABLE OF CONTENTS

1.0 GENERAL INFORMATION

This section presents a general introduction and description of the BEA Research Reactor (BRR) package. The BRR package is used to transport fuel elements that have been irradiated in various test and research reactors, including the University of Missouri Research Reactor (MURR), the Massachusetts Institute of Technology Nuclear Research Reactor (MITR–II), Advanced Test Reactor (ATR), and Training, Research, Isotopes, General Atomics (TRIGA) reactors. This application seeks authorization of the BRR package as a Type B(U)F–96 shipping container in accordance with the provisions of Title 10, Part 71 of the Code of Federal Regulations [1].

The major components comprising the package are discussed in Section 1.2.1, *Packaging*, and illustrated in Figure 1.2-1 through Figure 1.2-7. A glossary of terms is presented in Appendix 1.3.2, *Glossary of Terms and Acronyms*. Detailed drawings of the package design are presented in Appendix 1.3.3, *Packaging General Arrangement Drawings*.

1.1 Introduction

The BRR package has been developed to transport irradiated research reactor fuel. The fuel is primarily of two basic types: highly enriched aluminum–uranium plate fuel, and TRIGA fuel of varying enrichments. Within the package, the fuel is contained in basket structures specifically designed for each fuel type, and that provide for optimum heat rejection and criticality control.

The packaging consists of a payload basket, a lead–shielded cask body, an upper shield plug, a closure lid, and upper and lower impact limiters. The package is of conventional design and utilizes ASTM Type 304 stainless steel as its primary structural material. The package is designed to provide leaktight containment of the radioactive contents under all NCT and HAC.[1]

The BRR package may be used in a pool or hot cell environment. The cask body is provided with a drain port, and is intended for use with a drying system to ensure that water is not present during transport. The package is designed to be transported singly, with its longitudinal axis vertical, by highway truck or by rail in exclusive use. When loaded and prepared for transport, the BRR package is 119.5 inches long, 78 inches in diameter (over the impact limiters), and weighs 32,000 lb.

Based on the criticality assessment provided in Chapter 6, *Criticality Evaluation*, the criticality safety index for the BRR package is zero.

[1] Leaktight is defined as a maximum of 1×10^{-7} reference–cm^3/sec, air leakage per ANSI N14.5–1997 [2].

1.2 Package Description

This section presents a basic description of the BRR package components and construction. General arrangement drawings are provided in Appendix 1.3.3, *Packaging General Arrangement Drawings*.

1.2.1 Packaging

The BRR package consists of a payload basket (of a design that is specific for the fuel being transported), a lead–shielded cask body, a separate, removable upper shield plug, a closure lid, twelve closure bolts, and upper and lower impact limiters containing polyurethane foam. Except for the closure bolts and impact limiter attachments, the package is of primarily welded construction, using Type 304 austenitic stainless steel. These components will now be discussed in detail.

1.2.1.1 Cask Body

The BRR cask body is a right circular cylinder 77.1 inches long and 38 inches in diameter (not including the impact limiter attachments and the thermal shield). It is composed of upper and lower massive end structures connected by inner and outer shells. Thick lead shielding is located between the two circular shells, in the lower end structure, and in the shield plug. The payload cavity has a diameter of 16 inches and a length of 54 inches.

The massive end structures may be cast from ASTM A351, Grade CF8A, or forged from ASTM A182, Type F304. The lower end structure contains a drain to allow removal of water from the payload cavity. The inner shell may be cast from ASTM A451, Grade CPF8A, or forged from ASTM A182, Type F304. The outer shell may be made from ASTM A240, Type 304 plate, or optionally cast from ASTM A451, Grade CPF8A or forged from ASTM A182, Type F304. The outer shell may have up to two, full penetration longitudinal seam welds. The inner shell is one inch thick, and is welded to each end structure using a full penetration weld. The outer shell is two inches thick, and is connected to each end structure using a full penetration weld. The weld of the outer shell to the upper end structure is made after lead pour.

The cask is lifted using four, 1–8 UNC threaded holes in the upper end structure, that may be optionally fitted with heavy duty thread inserts. See Zone D2 of sheet 3 of drawing 1910–01–01–SAR.

On the outside of the outer shell, in the region not covered by the impact limiters, is a thermal shield composed of an outer sheet of 12 gauge (0.105–inch thick) Type 304 stainless steel, separated from the outer shell by small strips of the same 12 gauge material.

A set of eight receptacles are attached to the outer shell at each end of the exposed region of the cask (total of 16 receptacles), that serve as impact limiter attachments (see Zone A4 of sheet 2 of drawing 1910–01–01–SAR). The receptacles consist of two closely spaced plates, 1/2–inches thick, that pass through the thermal shield and attach directly to the outer shell using a full penetration groove weld with a 1/2–inch fillet reinforcement on one side. Each impact limiter features eight, 3/4–inch thick blades that pass between the receptacle plates on the cask body. The attachment is completed by passing a one inch diameter, stainless steel ball lock pin through the three plates. The ball lock pins therefore act in double shear. Each impact limiter is retained by eight such attachments.

All lead shielding is made from ASTM B29, chemical lead, or optionally, from lead per Federal Specification QQ–L–171E, Grade A or C. The lead shield on the side of the cask body is cast–

in–place through the upper end structure, and is nominally 8 inches thick. The shield at the bottom is made from lead sheet material that is packed firmly into place, and is 7.7 inches thick. The bottom lead cavity is closed using a one inch thick plate secured with a full penetration groove weld, see Zone A6/7 of sheet 3 of drawing 1910–01–01–SAR.

The removable shield plug is located at the top of the payload cavity. The outer shell is made from Type 304 plate material of 1/2–inch, 3/8–inch, 1–inch, and 1½–inch thickness. See Zone D2 of sheet 4 of drawing 1910–01–01–SAR. The cavity is filled with lead sheet material that is packed firmly into place. The total thickness of the plug is 11.2 inches, and the lead thickness is 9.7 inches. The plug rests on a shoulder located approximately half way along the length of the plug. A corresponding shoulder is located in the upper end structure of the cask body to support the shield plug. A 3/4–inch diameter pipe passes through the plug to ensure proper draining and drying of the cask. The pipe is oriented approximately diagonally to prevent a deleterious shine path. The shield plug is lifted using a central, 1/2–13 UNC threaded hole.

The closure lid is made from 2–inch thick, ASTM A240, Type 304 stainless steel plate. It is attached to the cask using 12, 1–8 UNC bolts made of ASTM A320, Grade L43 material, with hardened steel washers. The bolts are plated with electroless nickel per MIL–DTL–26074 Rev. F Class 1 Grade B, and tightened to a torque of 220 ± 20 ft-lb. The mating holes in the cask body may be optionally fitted with heavy duty thread inserts. The mating surface of the lid features a step relief located at the bolt circle. This relief prevents any contact from occurring between the lid and the body outside of the bolt circle, thus preventing prying loads from being applied to the closure bolts. The closure lid includes two O–ring seals made from butyl rubber of 3/8–inch cross sectional diameter. The inner O–ring is the containment seal, and the outer is the test seal. The seals are retained in dovetail grooves in the lid. The O–ring material (including the sealing washers, see below) is made from Rainier Rubber R-0405–70, and subject to the tests given in Section 8.1.5.2.

The BRR package provides a single level of leaktight containment. The containment boundary of the BRR package consists of the following elements. Unless noted, all elements are made of ASTM Type 304 stainless steel in various product forms.

- The lower massive end structure (including the passage to the drain port)
- The inner cylindrical shell
- The upper massive end structure
- The containment elastomer O–ring seal (the inner seal in the closure lid)
- The closure lid
- The vent port in the closure lid including elastomer sealing washer
- The drain port in the lower end structure including elastomer sealing washer

The containment boundary is shown in Figure 1.2-12.

As noted above, the BRR package features two ports that are part of the containment boundary: a vent port in the closure lid, and a drain port in the lower end structure. Both ports are closed with threaded plugs made of ASTM B16 brass and sealed with butyl rubber sealing washers. A

threaded brass cover is used to protect the port plugs. A seal test port is located between the containment O–ring seal and test O–ring seals, and is not part of containment.

1.2.1.2 Impact Limiters

Impact limiters are attached to each end of the BRR package, having essentially identical design, and are shown in drawing 1910–01–02–SAR. Each limiter is 78 inches in diameter and 34.6 inches long overall, with a conical section 15 inches long towards the outer end. The impact limiter design consists of Type 304 stainless steel shells and approximately 9 lb/ft^3 polyurethane foam. The external shells (except for the end plate) are 1/4 inches thick, and the internal shells (that interface with the cask body) are 1/2 inches thick. The outer end plate is 1/2 inches thick. The closure end impact limiter features three reinforced, 1/2–13UNC holes for lifting of the impact limiter only. An optional drain tube, aligned along the long axis of the cask, may be included in the lower impact limiter. The polyurethane foam is rigid, closed–cell, and is poured in place. On the side that mates with the cask, the annular sheet features three plastic melt–out plugs designed to relieve pressure in the HAC fire event. The attachment of the impact limiters to the cask body is described in Section 1.2.1.1, *Cask Body.*

1.2.1.3 Baskets

There are four baskets used with the BRR package, one for each type of fuel transported, and are shown in drawing 1910–01–03–SAR. The baskets are made from welded construction using Type 304 stainless steel in plate, bar, pipe, and tubular forms. Each basket has a diameter of 15.63 inches and a length of 53.45 inches, and features a number of cavities that fit the size and shape of the fuel. The cavities are sized to minimize free play between the fuel and the basket, while ensuring free insertion and removal of the elements. The baskets are open on the top, and the fuel is located at the top end, nearest the shield plug. The baskets are designed to freely drain water when the cask is lifted out of the spent fuel pool.

1.2.1.3.1 MURR

The MURR basket consists of an outer rolled shell, an inner pipe, and thick radial plates that form eight pie–shaped cavities for the fuel in a circular array. The bottom of the fuel cavities is formed by a 3/8–inch thick plate that is welded to the inside of the shell. The lifting bar divides the interior of the inner tube in half and prevents loading any fuel within the inner tube. The MURR basket is shown in Figure 1.2-4.

1.2.1.3.2 MITR–II

The MITR-II basket consists of a cylindrical weldment supported by a 14 inch diameter pedestal. Twenty-nine (29) flat plates of variable thicknesses are machined and stacked to create eight (8) diamond shaped fuel cavities. Fuel cavities are arranged symmetrically about the center axis of the basket. The top plate of the weldment is machined to prevent the loading of fuel into the central cavity of the basket. The bottom plate of the weldment provides support for the fuel and allows for drainage of water from the fuel cavities. The MITR–II basket is shown in Figure 1.2-5.

1.2.1.3.3 ATR

The ATR basket consists of a rolled outer shell, an inner pipe, and radial plates that form eight pie–shaped cavities for the fuel in a circular array. Since the outer shell is somewhat smaller than the cask cavity, the ATR basket features four circular ribs having an outer diameter of 15.63 inches. The bottom support plate is 1/2–inches thick. The lifting bar divides the interior of the inner tube in half and prevents loading any fuel within the inner tube. The ATR basket is shown in Figure 1.2-6.

1.2.1.3.4 TRIGA

The TRIGA basket consists of an array of 19 tubes having a 2–inch outer diameter and an 11–gauge wall thickness. The tubes are held in place by a top plate, a bottom support plate, and a central support plate. A 13–inch diameter, 1/4–inch thick circular shell forms the lower portion of the basket. The short spacer pedestal and the adjustable spacer pedestal are used to customize the fuel cavity for various TRIGA fuel lengths. The TRIGA basket is shown in Figure 1.2-7.

1.2.1.4 Gross Weight

The gross weight of the BRR package, including the cask, impact limiters, and maximum payload, is 32,000 lb. A summary of overall component weights is shown in Table 2.1-2 and discussed in Section 2.1.3, *Weights and Centers of Gravity.*

1.2.1.5 Neutron Moderation and Absorption

The BRR package maintains criticality control by means of limitation of the quantity of fissile material present and by maintaining a safe configuration of the material under all NCT and HAC. The design of the BRR package does not include any components whose principal purpose is the absorption of neutrons. A more detailed description of the package criticality control functions is given in Chapter 6, *Criticality Evaluation.*

1.2.1.6 Receptacles, Valves, Testing and Sampling Ports

The BRR package closure lid contains a vent port and a containment seal test port. A body drain port is located on the side of the lower end of the cask. There are no valves or receptacles used in the BRR package.

1.2.1.7 Heat Dissipation

The dissipation of heat from the BRR package is entirely passive. The impact limiters are painted white to reduce the absorption of solar heat. A thermal shield is used on the cask body to limit the temperature of the lead gamma shield in the HAC fire event. A more detailed description of the package thermal design is given in Chapter 3, *Thermal Evaluation.*

1.2.1.8 Lifting and Tie–down Devices

Other than the threaded holes in the top of the cask body, there are no lifting or tie–down devices that are a structural part of the BRR package. The package is secured to the transport vehicle

using structures that interface with the surfaces of the upper and lower impact limiters. The package rests on a lower frame that is attached to the vehicle. An upper frame contacts the upper impact limiter and is attached to the vehicle using cables or the equivalent. There are no provisions to lift the package with the impact limiters installed.

1.2.1.9 Pressure Relief System

There is no pressure relief system in the BRR package.

1.2.1.10 Shielding

Biological shielding of gamma radiation is provided by a combination of lead and the thick steel shells of the BRR package. Hydrogenous neutron shielding is not necessary and none is included in the package design. Details of the gamma shielding are provided in Section 1.2.1.1, *Cask Body*. A full assessment of the shielding design is provided in Chapter 5, *Shielding Evaluation.*

1.2.2 Contents

The BRR package may contain up to 8 irradiated MURR fuel elements, up to 8 irradiated MITR–II fuel elements, up to 8 irradiated ATR fuel elements, and up to 19 irradiated TRIGA fuel elements. Only one fuel element is allowed per basket location. Details for each fuel type are provided in the following paragraphs.

1.2.2.1 MURR

The MURR fuel element may be irradiated to a maximum burnup of 180 MWD (218,196 MWD/MTU, or a U-235 depletion of 30.9%). The minimum cooling time is 180 days after reactor shutdown.

Each fresh MURR element contains 775.0 ± 7.8 g U–235, with an enrichment of 93 ± 1 wt.%. The weight percents of the remaining uranium isotopes are 1.2 wt.% U–234, 0.7 wt.% U–236, and 5.0 – 7.0 wt.% U–238. The MURR fuel element fissile material is uranium aluminide (UAl_x).

Each MURR fuel element contains 24 curved fuel plates. Fuel plate 1 has the smallest radius, while fuel plate 24 has the largest radius, as shown in Figure 1.2-8. The fuel "meat" is a mixture of uranium metal and aluminum, while the cladding and structural materials are an aluminum alloy. The fuel plates are rolled to shape and swaged into the two fuel element side plates. The fissile material (uranium aluminide) is nominally 0.02–in thick for all 24 plates. Fuel element side plates are fabricated of ASTM B 209, aluminum alloy 6061–T6 or 6061–T651 and are approximately 0.15–in thick. The averaged measured channel spacing between fuel plates, over the entire fuel element, is less than or equal to 0.088–in at the time of fabrication.

The MURR element overall length, including irradiation growth, is 32.75 inches. The bounding weight of one assembly is 15 lb. The maximum decay heat per fuel element is 158 W.

1.2.2.2 MITR–II

The MITR–II fuel element may be irradiated to a maximum burnup of 165 MWD (306,900 MWD/MTU, or a U–235 depletion of 43.9%). The minimum cooling time is 120 days after reactor shutdown.

Each fresh MITR–II element contains 510.0 +3.0/-10.0 g U–235, with an enrichment of 93 ± 1 wt.%. The weight percents of the remaining uranium isotopes are 1.2 wt.% U–234, 0.7 wt.% U–236, and 5.0 – 7.0 wt.% U–238. Like the MURR fuel element, the MITR–II fuel element fissile material is uranium aluminide (UAl_x).

Each MITR–II fuel element contains 15 flat fuel plates, as shown in Figure 1.2-9. The fuel plates are fabricated and swaged into the two fuel element side plates. The fuel "meat" is a mixture of uranium metal and aluminum, while the cladding and structural materials are an aluminum alloy. The fissile material (uranium aluminide) is nominally 0.03–in thick and the cladding is nominally 0.025–in thick. Fuel element side plates are fabricated of ASTM B 209, aluminum alloy 6061–T6 and are approximately 0.19–in thick. The averaged measured channel spacing between fuel plates, over the entire fuel element, is less than or equal to 0.082–in at the time of fabrication.

The MITR–II element overall length, including irradiation growth, is 26.52 inches. The bounding weight of one assembly is 10 lb. The maximum decay heat per assembly is 150 W.

1.2.2.3 ATR

The ATR fuel element may be irradiated to a maximum burnup of 480 MWD[1] (491,155 MWD/MTU, or a U–235 depletion of 58.6%). The minimum cooling time is 1,670 days (4.6 years) after reactor shutdown.

There are two general classes of ATR fuel element, XA and YA. The XA fuel element has a fresh fuel loading of 1,075 ± 10 g U–235, with an enrichment of 93 ± 1 wt.%. The weight percents of the remaining uranium isotopes are 1.2 wt.% U–234 (max), 0.7 wt.% U–236 (max), and 5.0 – 7.0 wt.% U–238. Like the MURR and MITR–II fuel elements, the fuel element fissile material is uranium aluminide (UAl_x).

The XA fuel element is further subdivided into fuel element types 7F, 7NB, 7NBH. In the 7F fuel element, all 19 fuel plates are loaded with enriched uranium in an aluminum matrix with the eight outer plates (1 through 4 and 16 through 19) containing boron as a burnable poison. The fuel element with the greatest reactivity is the 7NB that contains no burnable poison. The 7NBH fuel element is similar to the 7NB fuel element except that it contains one or two borated plates. The YA fuel element is identical to the 7F fuel element except that plate 19 of the YA fuel element is an aluminum alloy plate containing neither uranium fuel nor boron burnable poison. The YA fuel element has a fresh fuel loading of 1,022.4 ± 10 g U–235. A second YA fuel element design (YA–M) has the side plate width reduced by 15 mils.

[1] The element burnup of 480 MWD should not be a limit for licensing purposes because the element burnup is typically not known in units of MWD. The final U-235 mass within an element is computed and recorded by ATR staff.

The ATR fuel elements contain 19 curved fuel plates. A section view of an ATR fuel element is given in Figure 1.2-10. Note that an intact ATR fuel element has end boxes (as shown on Figure 1.2-10), although these end boxes are removed prior to insertion in the BRR package. The fuel plates are rolled to shape and swaged into the two fuel element side plates. Fuel plate 1 has the smallest radius, while fuel plate 19 has the largest radius. The fissile material (uranium aluminide) is nominally 0.02–in thick for all 19 plates. Fuel element side plates are fabricated of ASTM B 209, aluminum alloy 6061–T6 or 6061–T651 and are approximately 0.19–in thick. The averaged measured channel spacing between fuel plates, over the entire fuel element, is less than or equal to 0.085–in at the time of fabrication.

The ATR element overall length, after removal of the end box structures, 51.0 inches max. The bounding weight of one assembly is 25 lb. The maximum decay heat per assembly is 30 W.

1.2.2.4 TRIGA

Many different types of TRIGA fuel elements have been fabricated over the past several decades. TRIGA fuel elements utilize a zirconium hydride fuel matrix. The BRR package is limited to five specific TRIGA fuel types:

1. 8 wt.% uranium aluminum clad element (General Atomics catalog number 101)
2. 8.5 wt.% uranium stainless steel clad element (General Atomics catalog number 103)
3. 8.5 wt.% uranium stainless steel clad element, high enriched uranium (General Atomics catalog number 109). This fuel element is sometimes referred to in the literature as a Fuel Life Improvement Program (FLIP) element.
4. 20 wt.% uranium stainless steel clad element (General Atomics catalog number 117). This fuel element is sometimes referred to in the literature as a FLIP–LEU–I element.
5. 8.5 wt.% uranium stainless steel clad element, instrumented (General Atomics catalog number 203).

Basic fresh fuel data used to describe the various TRIGA fuel elements are summarized in Table 1.2-1. The maximum length of an element, including irradiation growth, is 45.50 inches. Non–instrumented fuel elements are somewhat shorter. For all fuel elements, spacers are utilized within the TRIGA baskets.

The maximum burnup and minimum cooling time varies for the five fuel element types and is summarized in Table 1.2-2. The two FLIP elements have significantly higher U–235 loadings and hence much larger burnups and longer cooling times. The bounding weight of any TRIGA fuel element is 10 lb. The maximum decay heat per element is 20 W.

1.2.3 Special Requirements for Plutonium

The BRR package may contain plutonium in excess of 20 Ci as a consequence of irradiation of the reactor fuel. As such, the plutonium is in solid form within the fuel matrix. Table 1.2-3 summarizes the plutonium activity for each of the four fuel types, both on a per-element and per-cask basis. The maximum quantity of plutonium for the BRR package is 873 Ci.

1.2.4 Operational Features

The BRR package is of conventional design and is not complex to operate. Operational features are depicted on the drawings provided in Appendix 1.3.3, *Packaging General Arrangement Drawings*. Operating procedures and instructions for loading, unloading, and preparing an empty package for transport are provided in Chapter 7, *Package Operations*.

Table 1.2-1 – TRIGA Fresh Fuel Characteristics

Parameter	GA Cat. # 101	GA Cat. # 103	GA Cat. # 109	GA Cat. # 117	GA Cat. # 203
General Description	8 wt.% aluminum clad	8.5 wt.% stainless steel clad	8.5 wt.% stainless steel clad, HEU	20 wt.% stainless steel clad	8.5 wt.% instrumented stainless steel clad
Active Fuel Length (in)	14	15	15	15	15
Fuel Pellet OD (in)	1.41	1.44	1.44	1.44	1.44
U (wt.% in fuel)	8.0	8.5	8.5	20	8.5
U (g)	180	195	196	504	195
U–235 (wt.% in U)	20	20	70	20	20
U–235 (g)	36	39	137	101	39
H/Zr	1.0	1.7	1.6	1.6	1.7
Erbium (wt.%)	0	0	1.3	0.5	0
Zirconium Center Rod Length (in)	n/a	15.0	15.0	15.0	15.0
Overall Element Length (in)**	28.37	28.90	28.90	29.68	45.25
Cladding OD (in)	1.48	1.48	1.48	1.48	1.48
Cladding Thickness (in)	0.03	0.02	0.02	0.02	0.02
Graphite Reflector Length Top/Bottom (in)	4.0 / 4.0*	2.6 / 3.7	2.6 / 3.7	2.6 / 3.7	3.1 / 3.4
Graphite Reflector OD (in)	1.4	1.4	1.4	1.4	1.4
Molybdenum Disc (Y/N)	No	Yes	Yes	Yes	Yes
Samarium Trioxide Disc (Y/N)	Yes (prior to 1964)	Yes (prior to 1964)	No	No	No
Zr Fuel Matrix Mass (g)	2,070	2,088	2,060	2,060	2,088

* Graphite reflector dimensions provided for an active fuel length of 14–in. If the active fuel length is reduced, the top and bottom reflectors increase equally in length, and the overall column stackup of fuel and reflector remains fixed at 22–in.

** Length does not include irradiation growth.

Table 1.2-2 – TRIGA Fuel Parameters

Fuel Type	Maximum U–235 depletion (%)	Maximum Burnup (MWD/MTU)	Minimum Decay Time
GA Cat. # 101 (Aluminum–clad standard)	22.42	36,953	28 days
GA Cat. # 103/203 (Stainless steel–clad standard)	20.72	34,111	28 days
GA Cat. # 109 (FLIP)	59.74	339,368	1 year
GA Cat. # 117 (FLIP–LEU–I)	43.81	75,415	1 year

Table 1.2-3 – Plutonium Activity

Plutonium Activity per Fuel Element (Ci)				
Isotope	**MURR**	**MITR–II**	**ATR**	**TRIGA**
Pu–238	1.63E+00	5.16E+00	8.38E+00	7.19E-01
Pu–239	1.03E-01	9.80E-02	1.90E-01	2.33E-01
Pu–240	4.91E-02	5.81E-02	1.38E-01	1.70E-01
Pu–241	1.19E+01	2.61E+01	4.60E+01	4.48E+01
Pu–242	3.66E-05	1.35E-04	4.93E-04	2.44E-04
Total	1.37E+01	3.14E+01	5.48E+01	4.59E+01
Plutonium Activity per BRR Package (Ci)				
Isotope	**MURR**	**MITR–II**	**ATR**	**TRIGA**
Pu–238	1.30E+01	4.13E+01	6.70E+01	1.37E+01
Pu–239	8.26E-01	7.84E-01	1.52E+00	4.42E+00
Pu–240	3.93E-01	4.65E-01	1.10E+00	3.23E+00
Pu–241	9.56E+01	2.09E+02	3.68E+02	8.51E+02
Pu–242	2.93E-04	1.08E-03	3.95E-03	4.64E-03
Total	1.10E+02	2.51E+02	4.38E+02	8.73E+02

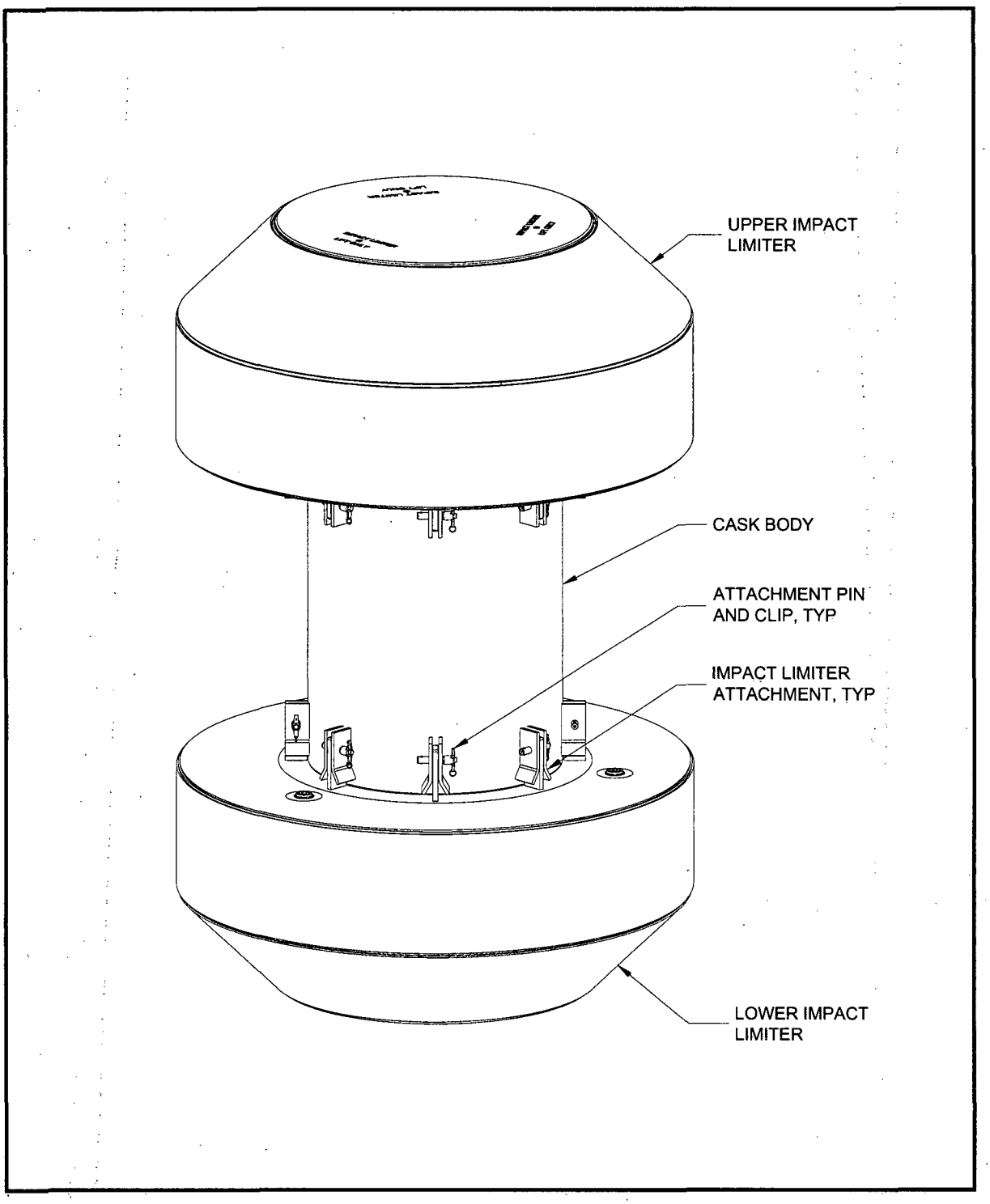

Figure 1.2-1 – BRR Packaging Components

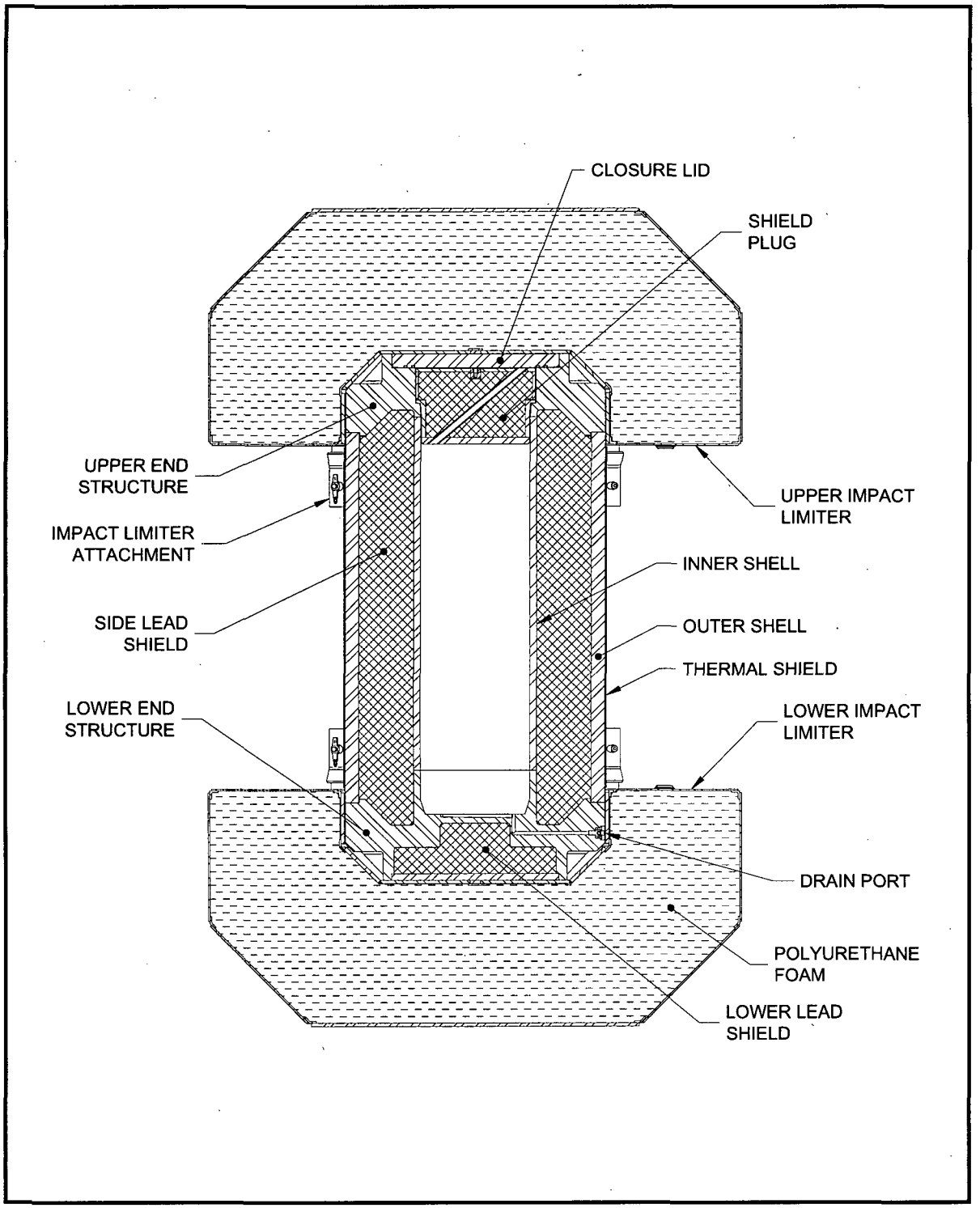

Figure 1.2-2 – BRR Package Cross Section

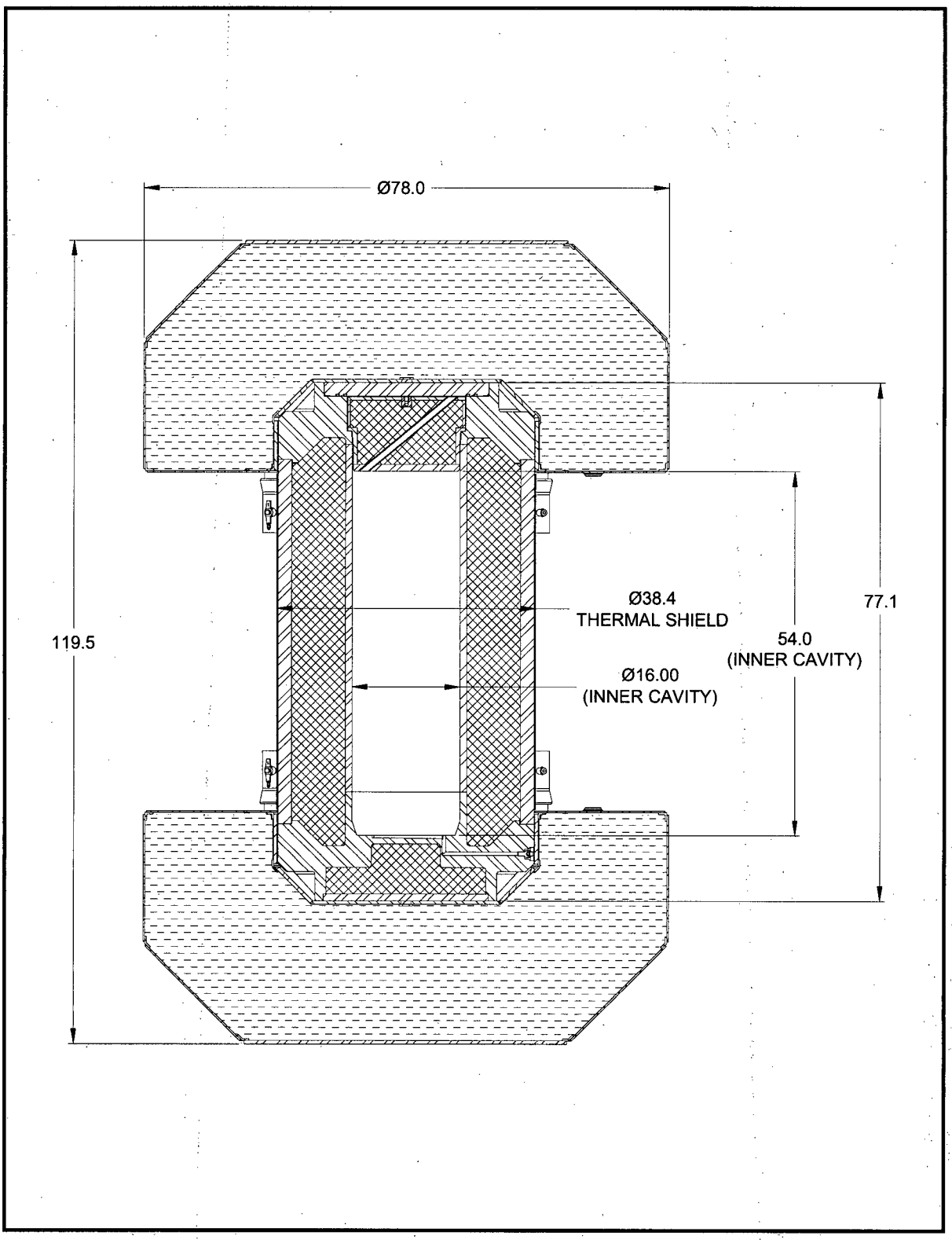

Figure 1.2-3 – BRR Package Dimensions

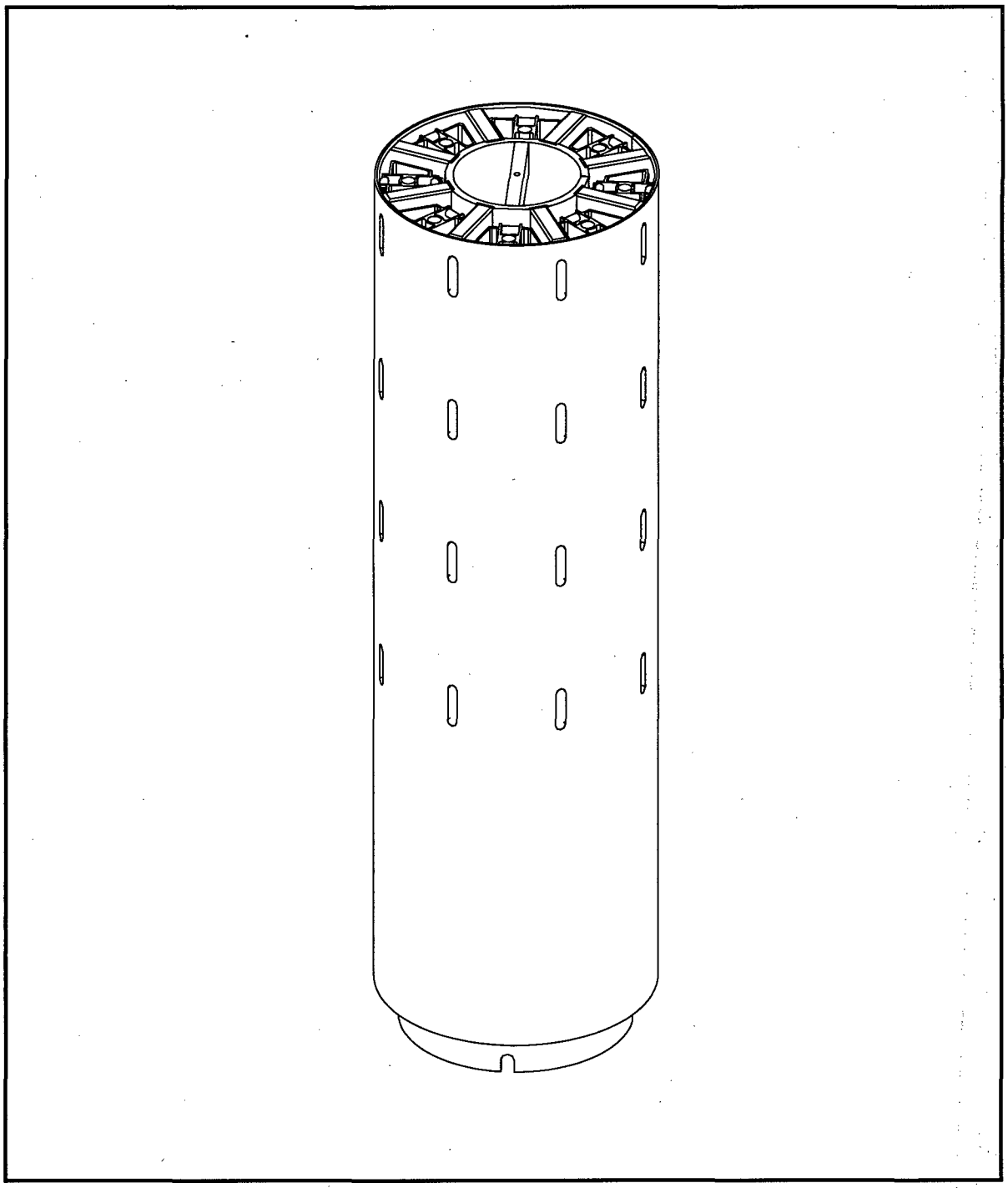

Figure 1.2-4 – MURR Fuel Basket

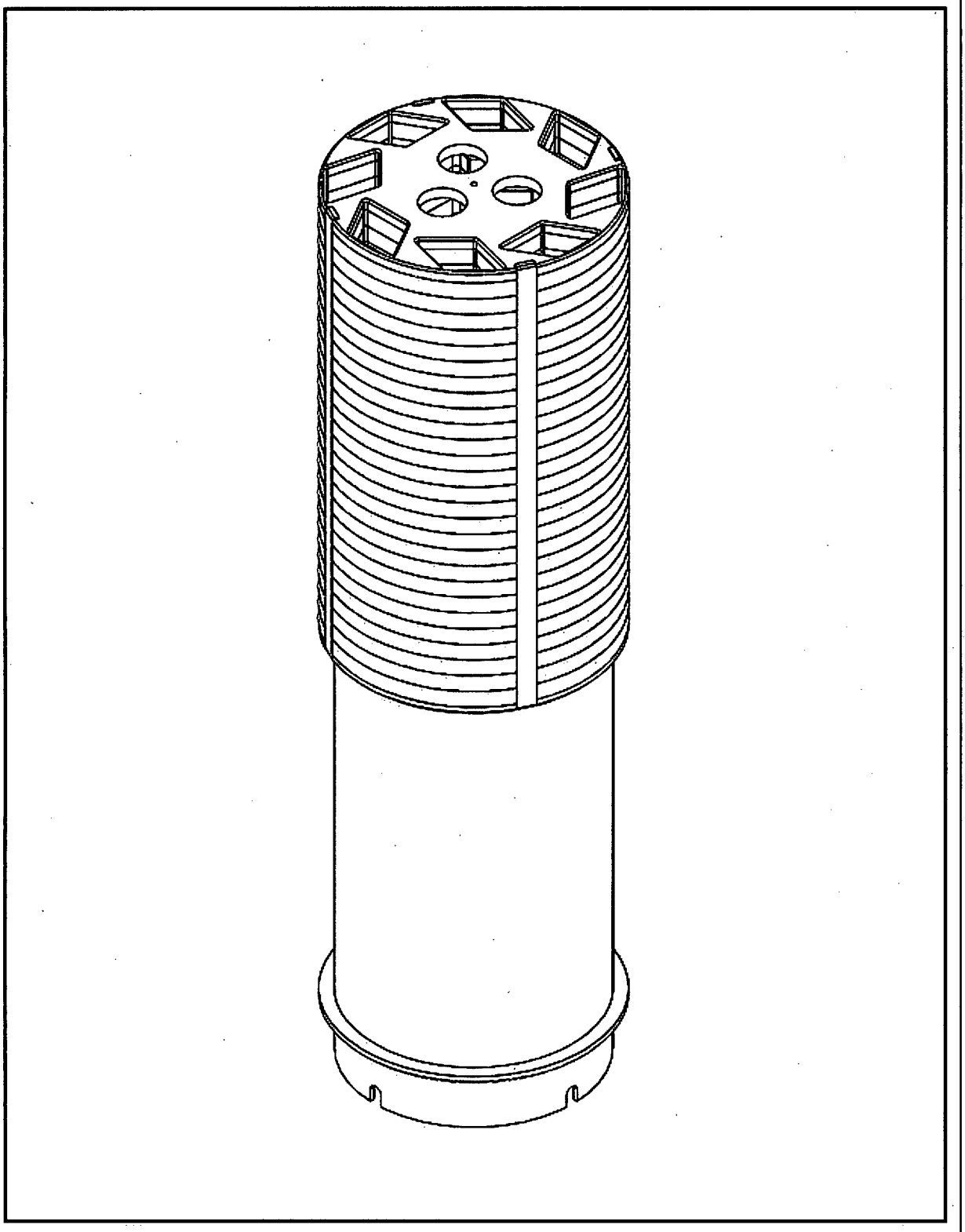

Figure 1.2-5 – MITR–II Fuel Basket

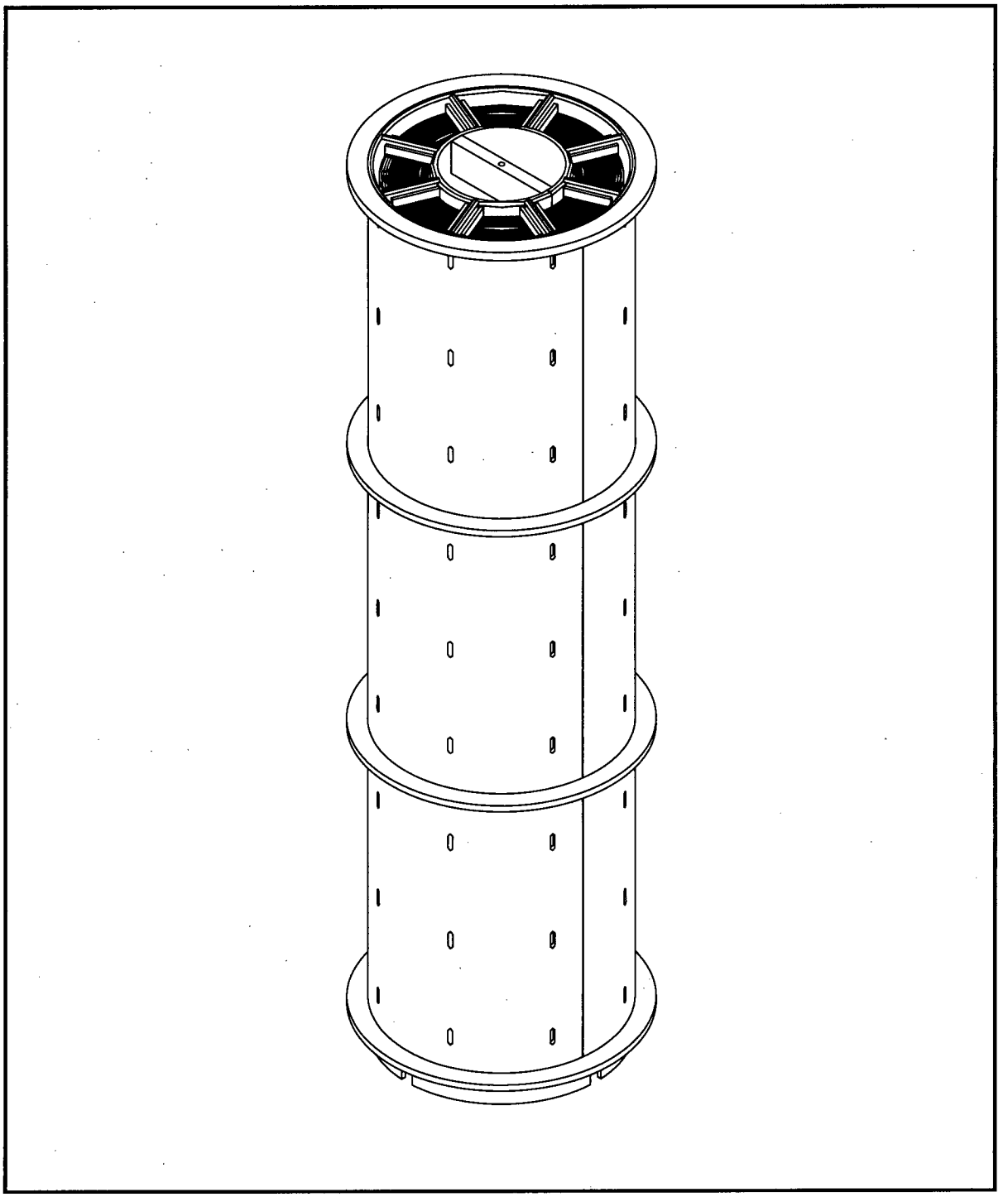

Figure 1.2-6 –ATR Fuel Basket

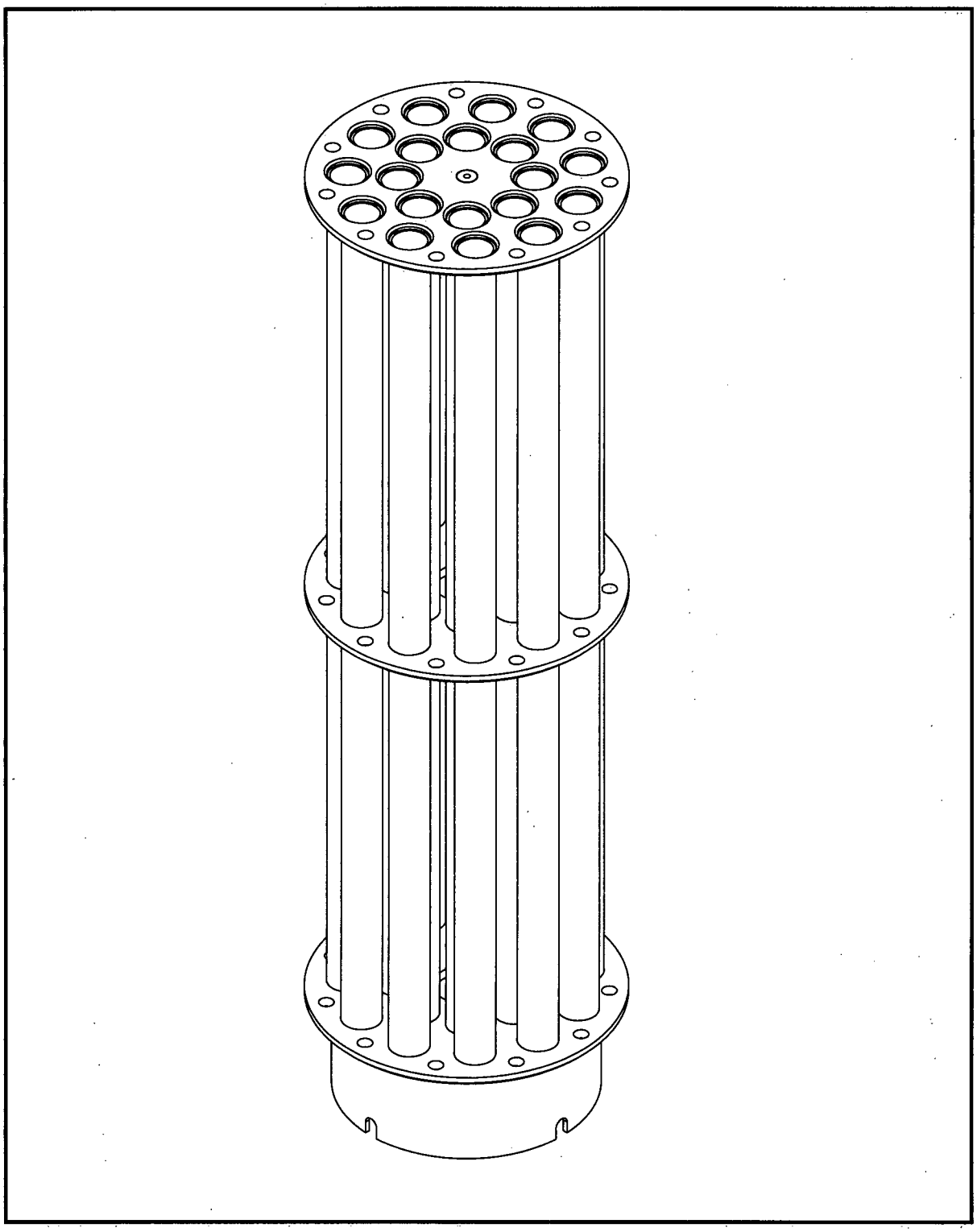

Figure 1.2-7 – TRIGA Fuel Basket

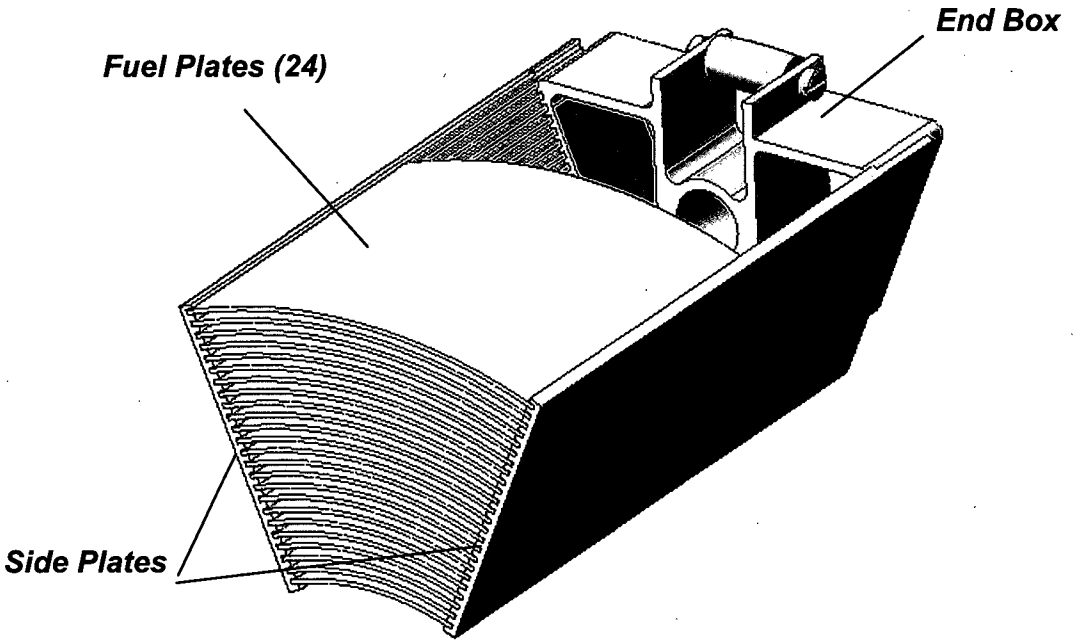

Figure 1.2-8 – MURR Fuel Element – Section View

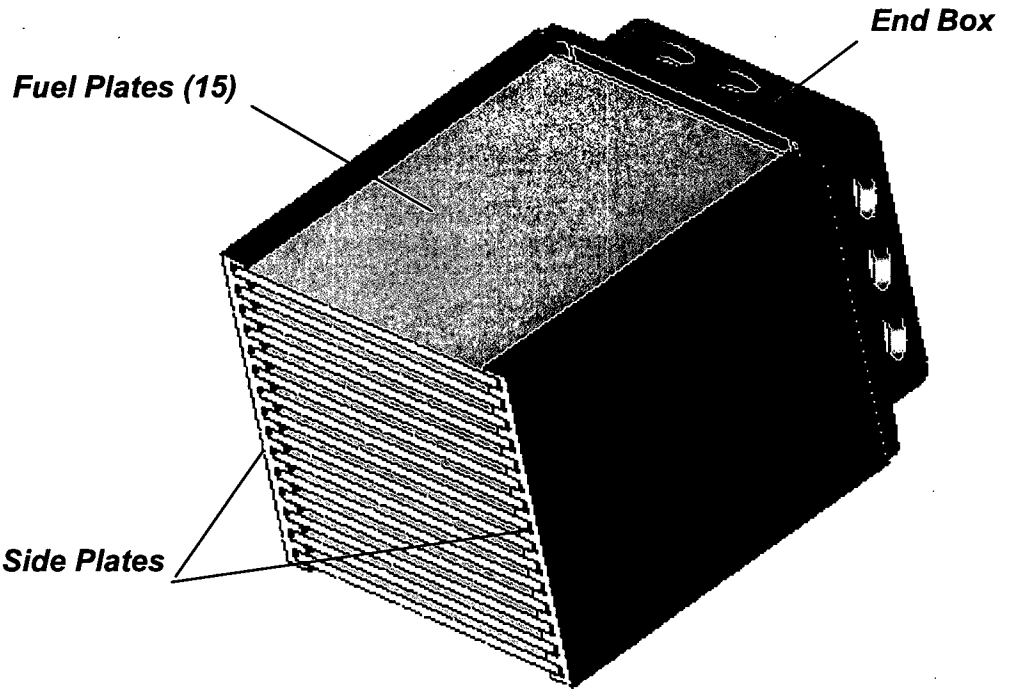

Figure 1.2-9 – MITR–II Fuel Element – Section View

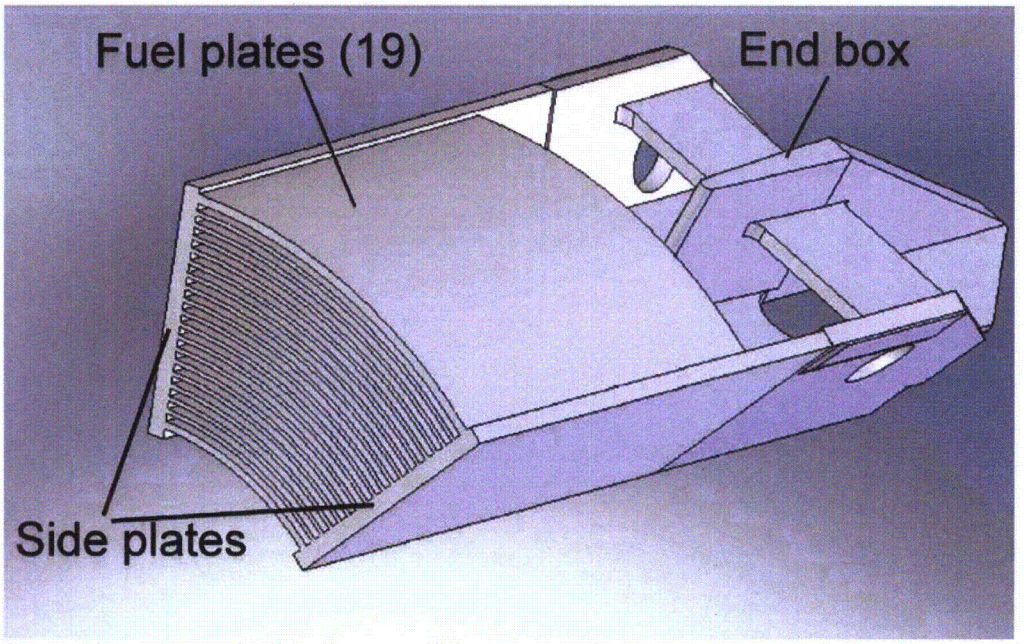

Note: The end box shown in this figure will be removed prior to insertion in the BRR package.

Figure 1.2-10 – ATR Fuel Element – Section View

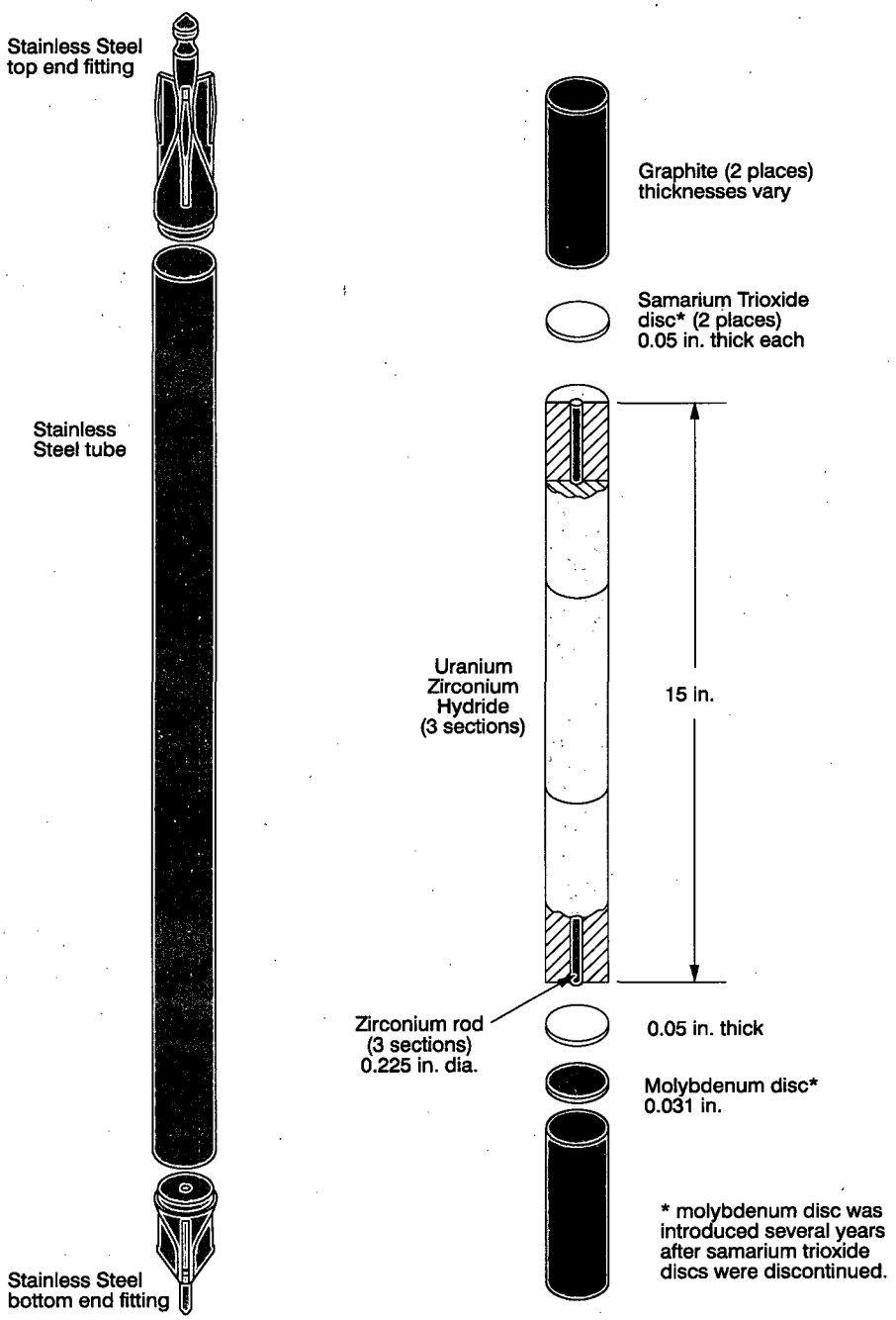

Figure 1.2-11 – TRIGA Fuel Element (Stainless Steel Clad)

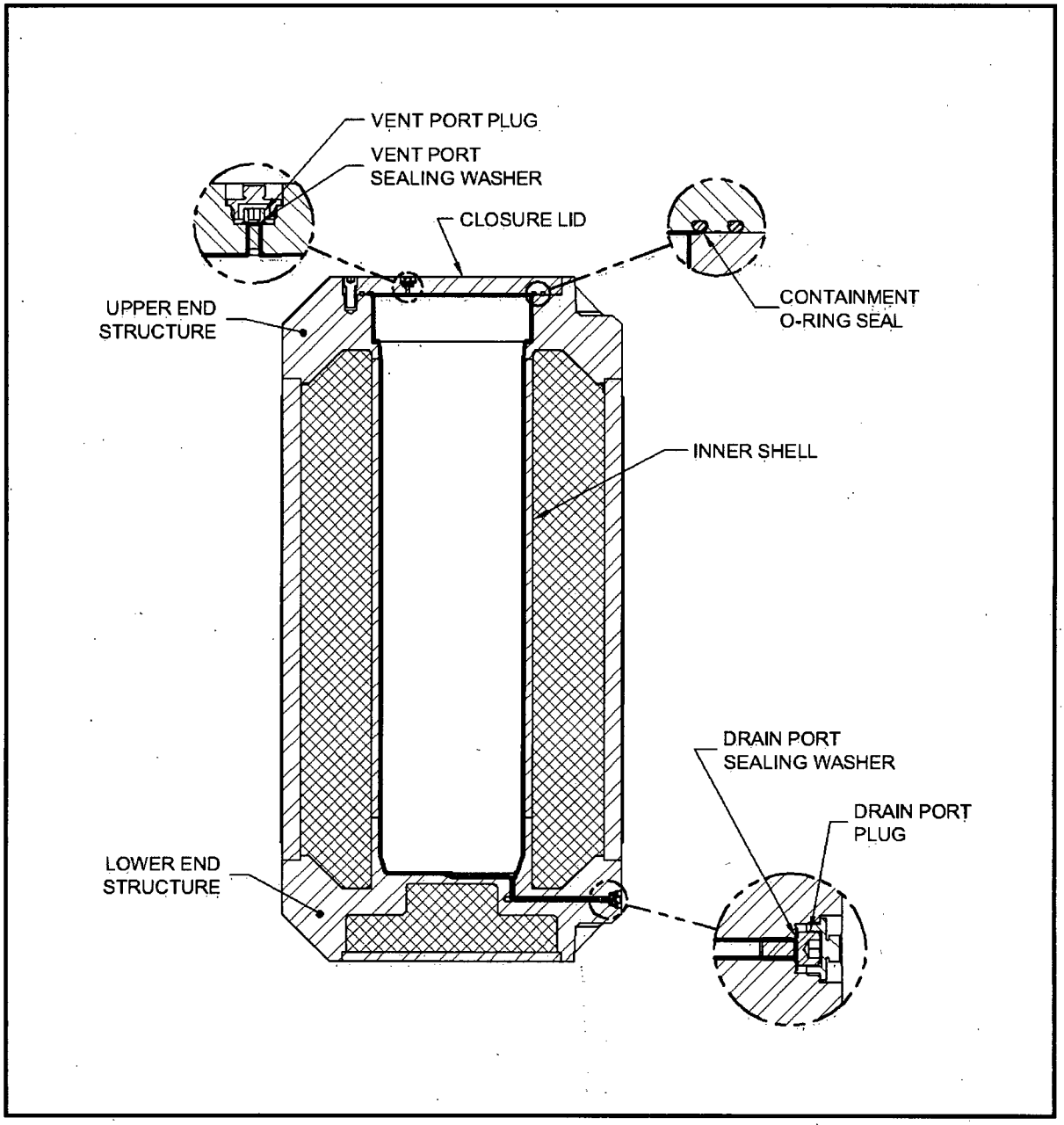

Figure 1.2-12 – BRR Package Containment Boundary

1.3 Appendices

1.3.1 References

1. Title 10, Code of Federal Regulations, Part 71 (10 CFR 71), Packaging and Transportation of Radioactive Material, 1–1–08 Edition.
2. ANSI N14.5–1997, *American National Standard for Radioactive Materials – Leakage Tests on Packages for Shipment*, American National Standards Institute (ANSI), Inc.

1.3.2 Glossary of Terms and Acronyms

ANSI –	American National Standards Institute.
ASME B&PV Code –	American Society of Mechanical Engineers Boiler and Pressure Vessel Code.
ASTM –	American Society for Testing and Materials.
ATR –	Advanced Test Reactor.
AWS –	American Welding Society.
Basket –	Structure that supports the fuel within the payload cavity.
Blade –	Part of impact limiter attachment, integral with the impact limiter. See *Receptacle*, below.
Cask Body –	BRR package component consisting of the inner shell, outer shell, upper and lower end structures, side and lower lead shielding.
Closure Lid –	Plate that completes the containment boundary. It contains the vent port, the test port, the containment O–ring seal, and the test O–ring seal.
Closure Bolts –	Fasteners that secure the closure lid to the body.
Containment O–ring Seal –	Inner elastomeric seal, retained in the closure lid, that forms part of the containment boundary.
Drain port –	Containment penetration at the lower end of the cask body through which water is drained from the cask during operations. Closed with the drain port plug, that is protected by a dust cover.
FLIP –	Fuel Life Improvement Program
GA –	General Atomics.
HAC –	Hypothetical Accident Conditions.
HEU –	High Enriched Uranium.
LEU –	Low Enriched Uranium.
Lower End Structure –	Part of the cask body. Massive structural element made of casting or forging that connects to both inner and outer cask body shells, and that contains the lower lead shielding and drain port. Interfaces with the lower impact limiter.
MITR–II –	Massachusetts Institute of Technology Nuclear Research Reactor.
MNOP –	Maximum Normal Operating Pressure.
MURR –	University of Missouri Research Reactor.

NCT –	Normal Conditions of Transport.
OD –	Outer Diameter.
Sealing Washers –	Integrated metal and elastomer seals that are used with the vent, test, and drain ports.
Shield Plug –	A removable plug that serves as the upper shielding.
Receptacle –	The pair of plates, attached to the cask, that accepts the impact limiter blade and create the impact limiter attachment.
Test O–ring Seal –	Outer elastomeric seal, retained in the closure lid, used to allow leakage rate testing of the containment seal.
Test port –	Opening located between the containment O–ring seal and the test O–ring seal in the closure lid, used to test the leakage rate of the containment O–ring seal. Closed with the test port plug, which is protected by a dust cover.
Thermal Shield –	Thin sheet attached to the outside of the outer shell, forming a thin air gap that inhibits heat transfer into the package during the HAC fire event.
TRIGA –	Training, Research, Isotopes, General Atomics.
Upper End Structure –	Part of the cask body. Massive structural element made of casting or forging that connects to both inner and outer cask body shells, and interfaces with the closure lid, shield plug, and upper impact limiter.
Vent port –	Containment penetration located in the closure lid which is used to vent the cavity and to introduce helium for leakage rate testing during operations. Closed with the vent port plug, that is protected by a dust cover.

1.3.3 Packaging General Arrangement Drawings

The packaging general arrangement drawings consist of:

- 1910–01–01–SAR, BRR Package Assembly SAR Drawing, 4 sheets
- 1910–01–02–SAR, BRR Package Impact Limiter SAR Drawing, 2 sheets
- 1910–01–03–SAR, BRR Package Fuel Baskets SAR Drawing, 3 sheets

Figure Withheld Under 10 CFR 2.390

AREVA	AREVA Federal Services LLC Packaging Projects Tacoma, WA 98402
DWG TITLE	BRR PACKAGE ASSEMBLY SAR DRAWING
	SCALE: SHOWN WT. ~ LBS
	REV. 4 SHEET 1 OF 4
	DWG SIZE D DWG NO. 1910-01-01-SAR
	CAD FILE: 1910C1901SAR4.ELDGRW

Figure Withheld Under 10 CFR 2.390

Figure Withheld Under 10 CFR 2.390

Figure Withheld Under 10 CFR 2.390

Figure Withheld Under 10 CFR 2.390

AREVA

AREVA Federal Services LLC
Packaging Projects
Tacoma, WA 98402

DWG TITLE
BRR PACKAGE IMPACT LIMITER
SAR DRAWING

SCALE: NOTED	WT. ~ 2252 LBS
REV: 1	SHEET 1 OF 2
DWG SIZE: D	DWG NO. 1910-01-02-SAR
CADFILE: 1910102SAR1.SLDDRW	

Figure Withheld Under 10 CFR 2.390

Figure Withheld Under 10 CFR 2.390

AREVA

AREVA Federal Services LLC
Packaging Projects
Tacoma, WA 98402

DWG TITLE
BRR PACKAGE FUEL BASKETS
SAR DRAWING

SCALE: SHOWN | WT. ~ LBS
REV: 4 | SHEET 1 OF 3
DWG SIZE D | DWG NO. 1910-01-03-SAR
CADFILE: 1910010303ARK.SLDDRW

Figure Withheld Under 10 CFR 2.390

Figure Withheld Under 10 CFR 2.390

2.0 STRUCTURAL EVALUATION

This section presents evaluations demonstrating that the BRR package meets all applicable structural criteria. The BRR package, consisting of a fuel basket, cask assembly, and impact limiters, is evaluated and shown to provide adequate protection for the payload. Normal conditions of transport (NCT) and hypothetical accident condition (HAC) evaluations are performed to address 10 CFR 71 [1] performance requirements. The primary method of performance demonstration is by analysis. Analytic demonstration techniques comply with the methodology presented in NRC Regulatory Guides 7.6 [2] and 7.8 [3]. Impact limiter performance in the free drop and puncture drop events is demonstrated by certification testing utilizing a half-scale certification test unit (CTU). A discussion of the tests performed is given in Appendix 2.12.2, *Certification Test Plan*, and results of the certification tests are provided in Appendix 2.12.3, *Certification Test Results*.

2.1 Structural Design

2.1.1 Discussion

The BRR package is designed to transport irradiated research reactor fuel. An isometric view of the cask is shown in Figure 1.2-1, a cross section view is shown Figure 1.2-2, and basic dimensions in Figure 1.2-3. The four types of fuel basket are shown in Figure 1.2-4 through Figure 1.2-7. The BRR package consists of a fuel basket, a cask body (which includes the gamma shielding), a shield plug, a closure lid, and two impact limiters. The payload cavity is 16 inches in diameter and 54 inches long. A lead shield plug of 11.2 inches in thickness is located at the top of the cavity. The inner (containment) shell is 1 inch thick, and the outer structural shell is 2 inches thick. The shells are welded to massive cast or forged end structures. The radial lead thickness is 8 inches, and the bottom lead thickness is 7.7 inches. A 12-gauge thermal shield is attached to the outside of the structural shell.

The closure lid is 2 inches thick and is attached with 12, 1-8 UNC socket head cap screws. Containment is afforded by a 3/8-inch cross-sectional diameter butyl O-ring seal. A test O-ring seal is used to provide a cavity for helium leak testing of the containment seal. The closure lid features vent and test ports and the bottom of the cask features a drain port. Impact limiters are located at each end of the cask to mitigate free drop and puncture drop impact. Each impact limiter has a ¼-inch thick outer stainless steel shell which envelops a nominally 9 lb/ft^3 polyurethane foam impact absorbing material. Each impact limiter is attached using eight, 1-inch diameter ball-lock pins.

There are four different kinds of payload basket, one each for MURR, MITR-II, ATR, and TRIGA fuel elements. Each fuel element cavity conforms to the overall geometric shape of the fuel, to ensure a nominally uniform support for the fuel elements under impact conditions.

All important structures are made from ASTM Type 304 stainless steel. The closure bolts are made from ASTM A320, Grade L43 alloy steel. Gamma shielding is made from ASTM B29, Chemical Lead, or equivalent lead. A comprehensive discussion of the BRR package design and configuration is provided in Section 1.2, *Package Description*.

2.1.2 Design Criteria

Proof of performance for the BRR package is achieved primarily by analysis. Impact limiter performance is demonstrated by half-scale certification testing. The acceptance criteria for analytic assessments are in accordance with Regulatory Guide 7.6. These design criteria meet the following safety requirements of 10 CFR §71.51:

1. For normal conditions of transport, there shall be no loss or dispersal of radioactive contents, as demonstrated to a sensitivity of 10^{-6} A_2 per hour, no significant increase in external radiation levels, and no substantial reduction in the effectiveness of the packaging.
2. For hypothetical accident conditions, there shall be no escape of radioactive material exceeding a total amount A_2 in one week, and no external radiation dose rate exceeding one rem per hour at one meter from the external surface of the package.

The BRR package is conservatively designated a Category I container, which is the highest and most stringent category [4]. Per NUREG/CR-3019 [5] and NUREG/CR-3854 [6], the cask components are classified as follows:

- Containment components are classified as ASME Code, Section III, Subsection NB [7].
- Fuel basket components are classified as ASME Code, Section III, Subsection NG [8].
- The outer shell, thermal shield, and impact limiter attachments are classified as ASME Code, Section III, Subsection NF [9]. However, the outer shell is conservatively analyzed to the requirements of Subsection NB.

The remainder of this section presents the detailed acceptance criteria used for analytic structural assessments of the BRR package.

2.1.2.1 Containment and Criticality Control Structures

A summary of allowable stresses used for containment and criticality control structures is presented in Table 2.1-1. Containment structures include the inner shell, massive end structures, and the closure lid. Criticality control structures include the fuel baskets. The allowable stresses shown in Table 2.1-1 are consistent with Regulatory Guide 7.6, and the ASME Code, Section III, Subsections NB and NG, and Appendix F. Peak stresses are further discussed in Section 2.1.2.3.2, *Fatigue Assessment*, and buckling in Section 2.1.2.3.3, *Buckling Assessment*. Closure bolts are evaluated utilizing NUREG/CR-6007 [10]. Furthermore, stress intensity in the cask closure region which could affect compression of the containment O-ring seal is limited to the lesser of the value shown in Table 2.1-1, or the yield strength.

2.1.2.2 Other Structures

Impact limiter structures, including the steel shells, energy-absorbing foam, and attachment structures, are expected to permanently deform under NCT and HAC. The impact limiter performance criteria are:

- Limit impact magnitude such that cask component stress and deflection criteria are met.
- Prevent "hard" contact of a rigid part of the cask with the ground due to excessive deformation of the foam.

- Maintain attachment to the cask and sufficient structural integrity subsequent to the HAC free drop and puncture drop events that the containment O-ring seal is protected from excessive temperature in the subsequent HAC fire event.

The performance of the impact limiters is discussed in Sections 2.7.1, *Free Drop*, and 2.7.3, *Puncture*. The thermal performance of the undamaged and damaged limiters is evaluated in Chapter 3, *Thermal Evaluation*.

The allowable stress for lifting components of the BRR package is limited to a maximum of one-third of the minimum yield strength of the material in the lifting load path, per the requirements of 10 CFR §71.45(a).

Since the BRR package is not attached to the conveyance using any structural part of the package, tiedown structural criteria are not required.

2.1.2.3 Miscellaneous Structural Failure Modes

2.1.2.3.1 Brittle Fracture

With the exception of the closure lid bolts, all structural components of the BRR package are fabricated of austenitic stainless steel. Austenitic stainless steels do not undergo a ductile-to-brittle transition in the temperature range of interest (i.e., down to -40 °F), and thus do not need to be evaluated for brittle fracture. The closure lid bolts are fabricated from ASTM A320, Grade L43 alloy steel bolting material. This material is specifically intended for low temperature service. In addition, per Section 5 of NUREG/CR-1815 [11], bolts are not considered as fracture-critical components because multiple load paths exist and bolting systems are generally redundant, as is the case with the BRR package. Therefore, brittle fracture is not a failure mode of concern.

2.1.2.3.2 Fatigue Assessment

2.1.2.3.2.1 Normal Operating Cycles

Normal operating cycles do not present a fatigue concern for the BRR package components over its service life. The basis for this conclusion is reached using the six criteria of Article NB-3222.4(d) of the ASME Boiler and Pressure Vessel Code. A summary of the six criteria and their application are discussed below. The service life of the package is 25 years with up to 20 shipments per year for a maximum of 500 shipments in the service life.

(1) Atmospheric to Service Pressure Cycle: The total number of atmospheric-to-operating pressure cycles during normal operations does not exceed the number of cycles on the fatigue curve corresponding to a value of $S_a = 3S_m$ for Type 304 stainless steel. From Section 2.2.1, *Material Properties and Specifications* at a bounding temperature of 250 °F per Section 2.6.1.1, *Summary of Pressures and Temperatures*, the S_m value for Type 304 stainless steel is 20 ksi, which corresponds to an alternating stress value of $S_a = 3S_m = 60$ ksi. The corresponding number of cycles for a value of $S_a = 60$ ksi is greater than 10,000 from Figure I-9.2.1 and Table I-9.1 of the ASME Code [12]. The package undergoes one atmospheric-to-operating pressure cycle per shipment, therefore the package will experience 500 atmospheric-to-operating pressure cycles in its life. Since the

allowable number of cycles is greater than the maximum expected number of cycles, the first criterion is satisfied.

(2) Normal Service Pressure Fluctuation: The specified full range of pressure fluctuations during normal service does not exceed the quantity 1/3 × Design Pressure × (S_a/S_m), where the Design Pressure is 25 psi, S_a is the value obtained from the Type 304 stainless steel design fatigue curve for the total specified number of significant pressure fluctuations (SPF), and S_m is the allowable stress intensity for the material at the service temperature. The total number of service cycles is based on the fill gas extreme temperature range as stated below. Conservatively, two complete temperature cycles are assumed to occur for each of the 500 lifetime shipments for a total quantity of 1,000 pressure fluctuation cycles. From Table I-9.1, S_a = 119,000 psi for 1,000 cycles. The value of S_m was defined above as 20 ksi at service temperature. The limiting full range of pressure fluctuations (FRF) becomes:

$$FRF_{LIMIT} = 1/3 \times \text{Design Pressure} \times (S_a/S_m) = 49.6 \text{ psi}$$

Next, the maximum pressure fluctuations in the package will be determined. Of note, the maximum pressure fluctuations will be conservatively assumed to be above the significance level, and therefore the value SPF does not need to be computed. The bulk average fill gas temperature varies between the extremes of T_1 = -40 °F and a conservative bounding temperature of T_2 = 400 °F. The maximum pressure (conservatively assuming that atmospheric pressure corresponds to -40 °F) is:

$$\frac{P_2}{P_1} = \frac{T_2}{T_1} \Rightarrow P_2 = P_1\left(\frac{T_2}{T_1}\right) = 14.7\left(\frac{400+460}{-40+460}\right) = 30.1 \text{ psia}$$

The resulting pressure fluctuation is FRF = 30.1 – 14.7 = 15.4 psi, which is less than FRF_{LIMIT} = 49.6 psi presented above and therefore, the second criterion is satisfied.

(3) Temperature Difference — Startup and Shutdown: The temperature between adjacent points of a package component during normal service does not exceed 1/2(S_a/Eα), where S_a is the design fatigue curve value taken from Table I-9.1 for Figure I-9.2.1 of the ASME Code for Type 304 stainless steel for the total specified number of temperature difference fluctuations, E is the modulus of elasticity, and α is the mean coefficient of thermal expansion, all evaluated at temperature. The total number of temperature fluctuations will not exceed the number of uses of the package, which is 500 as calculated above. It will be conservative to use the value of S_a from Table I-9.1 of the ASME Code for 1,000 cycles, which is 119,000 psi. From Section 2.2.1, *Material Properties and Specifications* at a bounding temperature of 250 °F, the value of the mean thermal expansion coefficient is $\alpha = 9.1(10^{-6})$/ °F and the modulus of elasticity, $E = 27.3(10^6)$ psi. Therefore, the value of 1/2(S_a/Eα) = 1/2(119,000/[$27.3(10^6)9.1(10^{-6})$] = 240 °F. Since the package design temperature is 250 °F under ambient conditions of 100 °F, the temperature difference between any two adjacent points cannot approach the 240 °F value. Thus, the third criterion is satisfied.

(4) Temperature Difference — Normal Service: The temperature difference between any two adjacent points does not change during normal service by more than the quantity 1/2(S_a/Eα), where S_a, E, and α are as defined above. However, normal operating temperatures of the containment boundary are largely determined by the steady heat load, and any changes in

temperature due to changes in ambient conditions, warm-up, or cool-down will be relatively slow and even due to the large thermal mass of the package. Therefore, the fourth criterion is satisfied.

(5) Temperature Difference — Dissimilar Materials: The fifth criterion is concerned with dissimilar materials. Since the containment boundary is constructed entirely of Type 304 stainless steel, dissimilar materials are not of concern. Therefore the fifth criterion is satisfied.

(6) Mechanical Loads: The specified full range of mechanical loads does not result in load stresses whose range exceeds the S_a design fatigue curve for the total specified number of load fluctuations. The only repeating mechanical loads will be those associated with lifting the package and tightening of the closure bolts.

Lifting. As the containment boundary is handled twice for each transport cycle (load and unload), the maximum number of cycles is $2 \times 500 = 1{,}000$. From Table I-9.1, $S_a = 119{,}000$ psi for 1,000 cycles. Of note, each load stress excursion will be conservatively assumed to be above the significance level, and therefore the actual significance level does not need to be computed. Lifting stress is limited by 10 CFR §71.45(a) to a value of one-third of the material's minimum yield strength. For a design temperature of 250 °F, the minimum yield strength of Type 304 stainless steel is 23,700 psi. Thus, one-third of the minimum yield strength is 23,700/3 = 7,900 psi. As 119,000 psi >> 7,900 psi, the sixth criterion is satisfied for lifting.

Closure bolts. The maximum stress intensity developed in the closure bolts during normal operations, given in Section 2.6.1.5, *Closure Bolts*, is bounded by a value of $S_{max} = 55{,}000$ psi. This stress includes preload stress, thermal stress, and a conservative inclusion of 50% of the applied preload torque as a residual torsion stress. From Table 2.2-3, the ASME allowable stress for the bolting material, S_m, at 250 °F is 32,450 psi. As defined by Table I-9.1 of the ASME B&PV Code, the Maximum Nominal Stress (MNS) of 55,000 psi is less than $2.7S_m$ (i.e., 2.7(32,450) = 87,615 psi). Per NB-3232.3(c), a stress concentration factor of four shall be applied to one-half the value of S_{max}, i.e., $4(0.5S_{max}) = 4 \times 0.5 \times 55{,}000 = 110{,}000$ psi. Per NB-3232.3(d), the alternating stress must be adjusted for the elastic modulus used in the fatigue curves. The modulus at a temperature of 250 °F is $26.9(10^6)$ psi and the modulus used for the fatigue curve, per Table I-9.1 is $30(10^6)$ psi. The adjusted alternating stress is:

$$S_{ALT} = \frac{30}{26.9} 110 = 123 \text{ ksi}$$

From Table I-9.1 for figure I-9.4, the service cycles allowed for a stress of 123 ksi is 670. Since closure bolts are tightened twice per package service cycle, the allowable number of package service cycles is half of this value. Therefore the closure bolts should be replaced every 670/2 = 335 service cycles for the package, and the sixth criterion is satisfied for closure bolts.

Summary: The previous discussion verifies that fatigue failure of the packaging containment boundary due to normal operating cycles is not a concern, per Section III, Subsection NB, Article NB-3222.4(d) of the ASME Code. Therefore the resistance of the BRR package to fatigue is adequate to ensure a minimum 25 year service life of up to 20 shipments per year.

2.1.2.3.2.2 Normal Vibration Over the Road

Fatigue associated with normal vibration over the road is addressed in Section 2.6.5, *Vibration.*

2.1.2.3.3 Buckling Assessment

Buckling, per Regulatory Guide 7.6, is an unacceptable failure mode for the containment vessel. The intent of this provision is to preclude large deformations that would compromise the validity of linear analysis assumptions and quasi-linear stress allowable limits, as given in Paragraph C.6 of Regulatory Guide 7.6.

Buckling investigations contained herein consider the outer shell of the BRR package. The outer and inner shells of the cask are closely connected through the massive end structures, thus, the two shells act to strengthen each other. One shell cannot buckle independently of the other. However, the strength of the inner shell for buckling considerations is conservatively ignored.

The shell buckling analysis is performed using the methodology of ASME B&PV Code Case N-284-2 [13]. Consistent with Regulatory Guide 7.6 philosophy, factors of safety corresponding to ASME Boiler and Pressure Vessel Code, Level A and Level D service conditions are employed. For NCT (Service Level A), the factor of safety is 2.0, and for HAC (Service Level D), the factor of safety is 1.34. Buckling analysis details are provided in Section 2.6.4, *Increased External Pressure*, Section 2.7.1, *Free Drop*, and Section 2.7.6, *Immersion – All Packages*.

2.1.3 Weights and Centers of Gravity

The maximum gross weight of the BRR package is 32,000 lb. The packaging component weights are summarized in Table 2.1-2, and the fuel basket and fuel weights in Table 2.1-3. The center of gravity (CG) of the package is located 38.7 inches from the bottom outside surface of the cask body. Note that this is directly on the geometric center of the package. The mass moment of inertia of the cask about a transverse axis through the center of gravity (including impact limiters, as prepared for transport) is 63,246 in-lb-s^2.

2.1.4 Identification of Codes and Standards for Package Design

The BRR package, without regard to content, is conservatively designated a Category I package. Per the guidance of NUREG/CR-3854, the appropriate design criteria for the containment is Section III, Subsection NB of the ASME B&PV Code. Consequently, the design of the containment boundary is based on the methodology of Regulatory Guide 7.6, and load cases are applied and combined according to Regulatory Guide 7.8. The outer shell is conservatively included under the NB criteria. The closure bolts are designed using the guidance of NUREG/CR-6007.

For the design of the baskets as criticality control components, the criteria is taken from Section III, Subsection NG of the ASME B&PV Code. For other structures such as the thermal shield, impact limiter shells, and impact limiter attachments, the criteria is taken from Section III, Subsection NF of the ASME B&PV Code.

Table 2.1-1 – Containment and Criticality Control Structure Allowable Stress Limits

Stress Category	NCT	HAC
General Primary Membrane Stress Intensity	S_m	Lesser of: $2.4S_m$, $0.7S_u$
Local Primary Membrane Stress Intensity①	$1.5S_m$	Lesser of: $3.6S_m$, S_u
Primary Membrane + Bending Stress Intensity	$1.5S_m$	Lesser of: $3.6S_m$, S_u
Range of Primary + Secondary Stress Intensity	$3.0S_m$	Not Applicable
Pure Shear Stress	$0.6S_m$	$0.42S_u$②
Peak	Per Section 2.1.2.2.2, *Fatigue Assessment*	
Buckling	Per Section 2.1.2.2.3, *Buckling Assessment*	
*Containment Fasteners:*③		
Average Tensile Stress Intensity	S_m④	Lesser of: S_y, $0.7S_u$
Average Tensile + Average Shear + Bending + Residual Torsion Stress Intensity	$1.35S_m$ for $S_u > 100$ ksi	Not Applicable

Notes:

1. This stress category does not apply to criticality control structures (Subsection NG).
2. For criticality control structures, the limit is the lesser of twice the NCT limit ($2 \times 0.6S_m = 1.2S_m$) or $0.42S_u$, per NG-3225.
3. Containment fastener stress limits are in accordance with NUREG/CR-6007.
4. S_m is defined as $(2/3)S_y$ as recommended by NUREG/CR-6007.

Table 2.1-2 – BRR Package Component Weights

Item	Weight, lb	CG, inches
Cask body①	25,400	---
Removable shield plug	950	---
Closure lid	280	---
Upper impact limiter	2,300	---
Lower impact limiter	2,300	---
Total empty package	31,230	38.6④
MURR Fuel basket② (loaded)	770	32.7③
MITR-II Fuel basket② (loaded)	640	35.5③
ATR Fuel basket② (loaded)	650	27.1③
TRIGA Fuel basket② (loaded)	480	28.1③
Total package, including MURR fuel (maximum)	**32,000**	**38.7④**
Total package, including MITR-II fuel	31,870	38.7④
Total package, including ATR fuel	31,880	38.6④
Total package, including TRIGA fuel	31,710	38.6④

Notes:

1. Includes all shells, end structures, and lead.
2. Individual basket and fuel weights are given in Table 2.1-3. Although ATR fuel is the heaviest at 200 lb, the MURR basket plus fuel weight is greatest overall.
3. Measured from the bottom surface of the basket.
4. Measured from the bottom outside surface of the cask body.

Table 2.1-3 – BRR Package Basket and Fuel Weights

Design	Weight (lb)			
	Empty Basket	Fuel Element × Quan.	Combined Fuel	Total
MURR	650	15 × 8	120	770
MITR-II	560	10 × 8	80	640
ATR	450	25 × 8	200	650
TRIGA	290	10 × 19	190	480

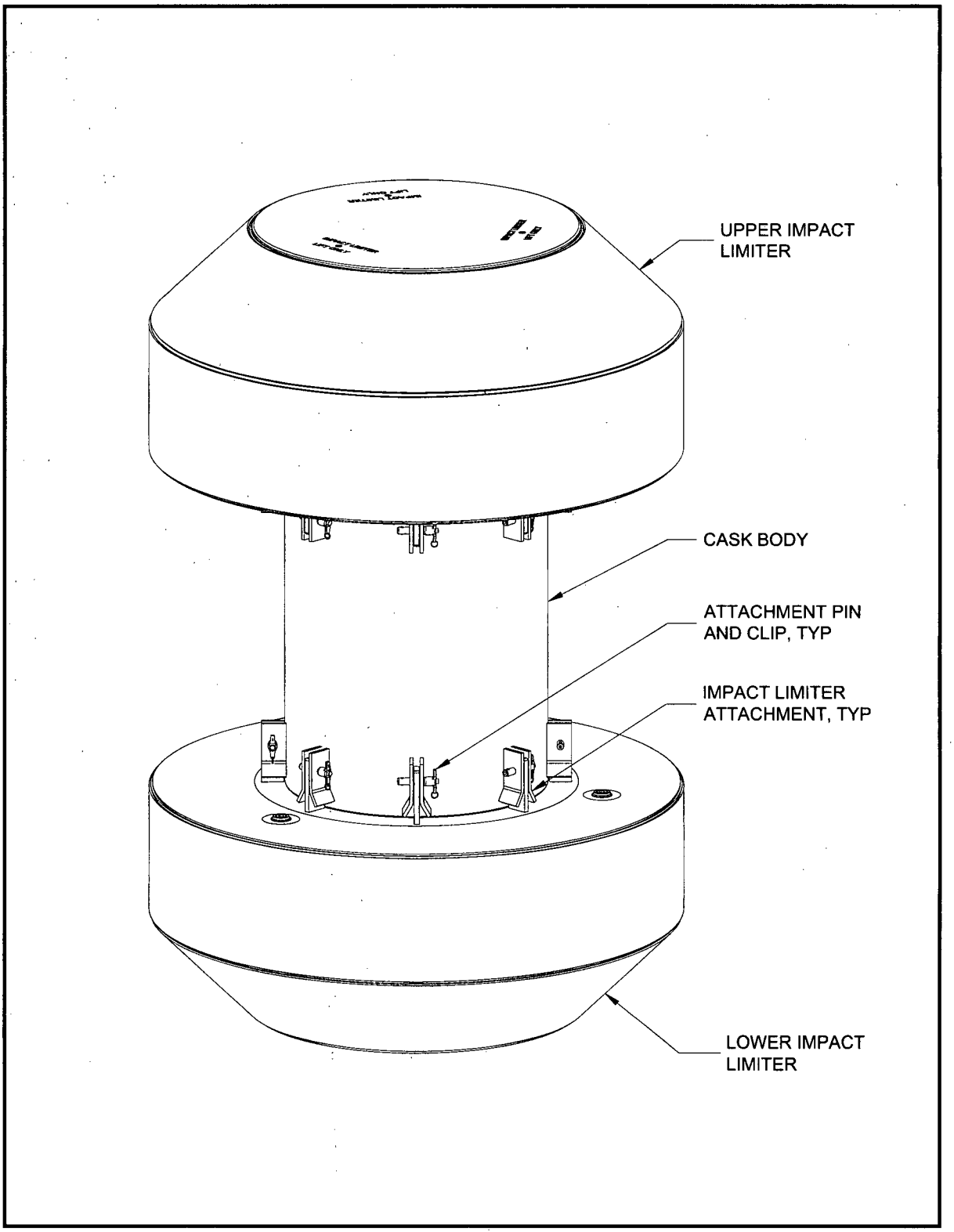

Figure 2.1-1 – BRR Packaging Components

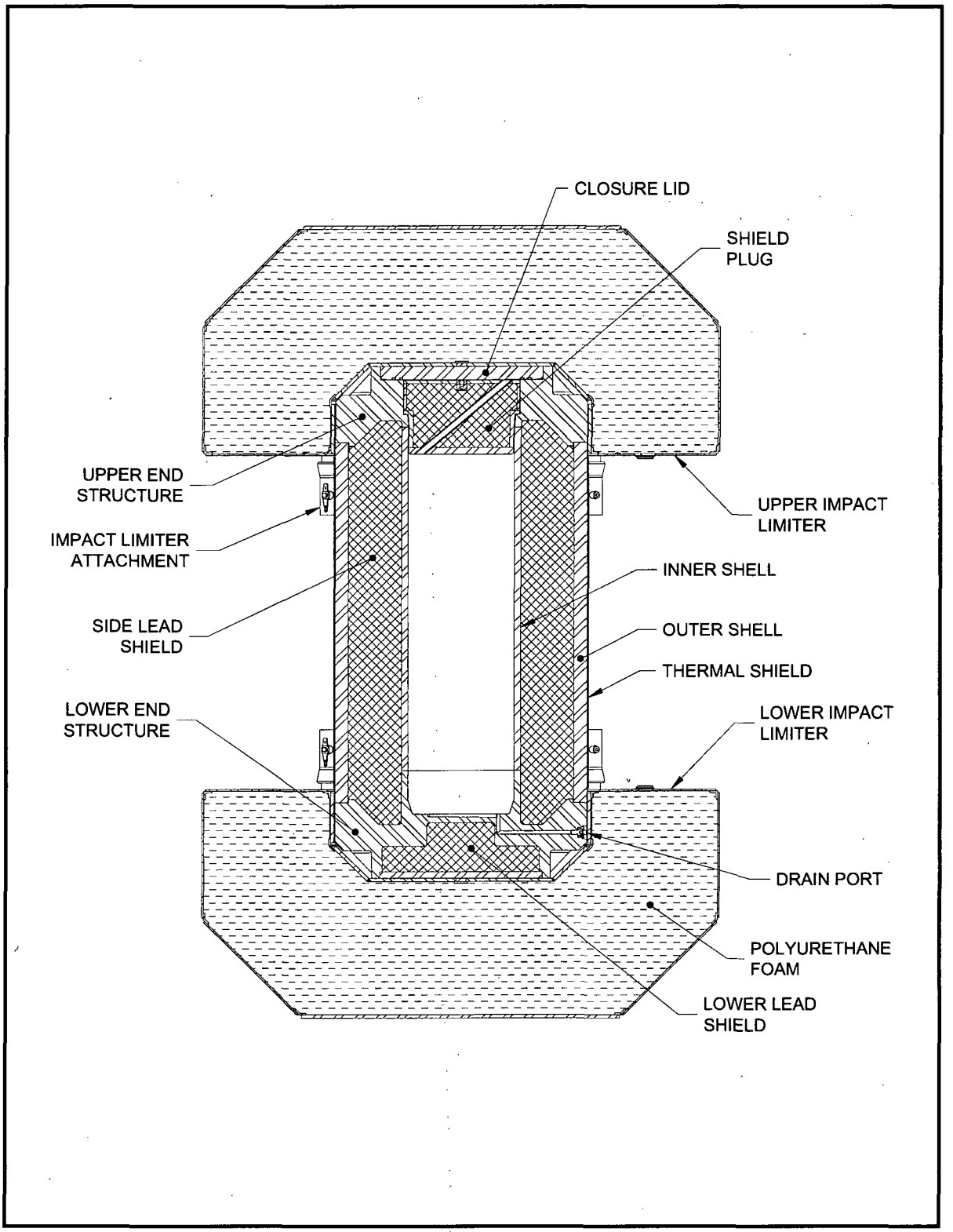

Figure 2.1-2 – BRR Package Cross Section

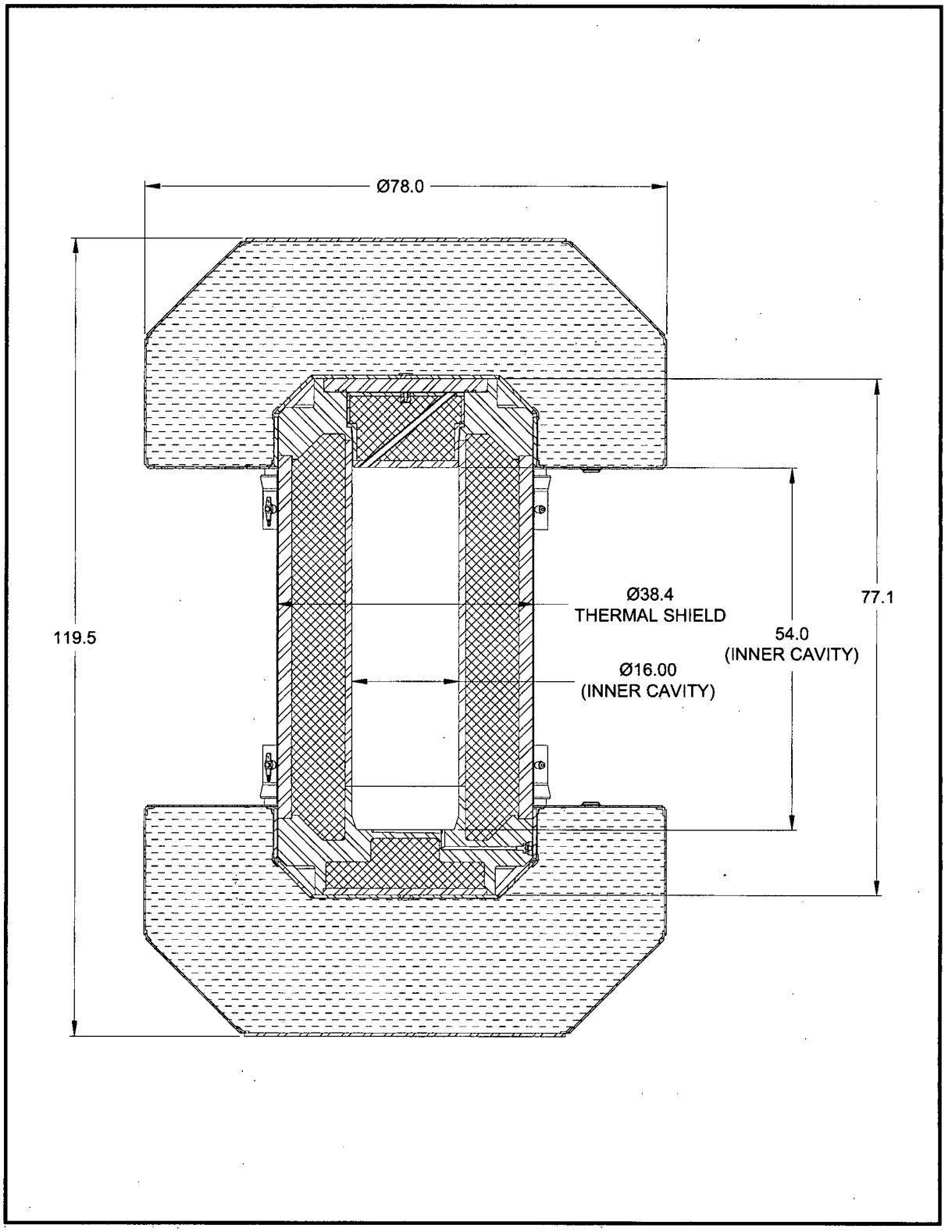

Figure 2.1-3 – BRR Package Dimensions

2.2 Materials

The BRR package structural components, including the impact limiter shells, are fabricated primarily from Type 304 stainless steel in various product forms. The gamma shielding is made from ASTM B29, Chemical Lead, or equivalent lead. Polyurethane foam is used for impact energy absorption. Other materials performing a structural function are ASTM B16 UNS C36000 brass alloy (for the test, vent, and drain port plugs), and ASTM A320, L43, alloy steel for the closure lid bolts. Austenitic stainless steel is used for the heavy duty thread inserts used for the closure bolt holes and lifting holes in the upper end structure. The ball lock pins that attach the impact limiters to the cask are made from 17-4PH stainless steel. The containment O-ring seal is made from butyl rubber. Plastic is used for the fire-consumable vent plugs in the foam cavities. The drawings presented in Appendix 1.3.3, *Packaging General Arrangement Drawings*, delineate the specific materials used for each BRR package component.

2.2.1 Material Properties and Specifications

Table 2.2-1 through Table 2.2-6 present the mechanical properties for the structural materials used in the BRR package. The density of stainless steel is 0.29 lb/in^3, and Poisson's ratio is 0.3. The density of lead is 0.41 lb/in^3 and Poisson's ratio is 0.45. Data is interpolated or extrapolated from the available data, as necessary, as noted in the tables.

The performance of the BRR package in free drop and puncture events is partially dependent on the energy-absorbing performance of polyurethane foam. The foam is poured in place within the impact limiter steel shells. Nominally 9 lb/ft^3 polyurethane foam is used. Section 8.1.5.1, *Polyurethane Foam* presents the details of acceptance tests for this material. The nominal, room-temperature crush properties of the polyurethane foam component are given in Table 2.2-6. Properties for both "parallel to rise" and "perpendicular to rise" are given. The "rise" direction is parallel to the force of gravity during solidification, and is oriented to be parallel to the cylindrical axis of the impact limiters.

2.2.2 Chemical, Galvanic, or Other Reactions

The materials of construction of the BRR package will not have significant chemical, galvanic or other reactions in air or water environments. These materials have been previously used, without incident, in radioactive material packages for transport of similar payload materials such as the RH-TRU 72-B (NRC Docket 9212) and the NAC LWT (NRC Docket 9225). The polyurethane foam is fully enveloped by sheets of stainless steel and welded closed. The foam is a rigid, closed-cell (non-water absorbent) material that is free of halogens and chlorides, as discussed in Section 8.1.5.1, *Polyurethane Foam*. The lead gamma shielding is fully encased in a stainless steel weldment and cannot be affected by water or atmospheric moisture.

The brass alloy vent port plug used in the closure lid is very corrosion resistant. Any damage that could occur to the material is easily detectable since the fitting is handled each time the BRR package is loaded and unloaded. Similarly, the alloy steel closure bolts, which are plated with corrosion-resistant nickel plating, can be readily inspected at each use for the presence of corrosion.

The butyl elastomer that is used for the containment O-ring seals contains no corrosives that would react with or adversely affect the BRR package. This material is organic in nature and noncorrosive to the stainless steel containment boundary of the BRR package.

A successful RAM packaging history combined with successful use of these fabrication materials in similar industrial environments ensures that the integrity of the BRR package will not be compromised by any chemical, galvanic or other reactions.

2.2.3 Effects of Radiation on Materials

The radiation associated with the decay of spent fuel will have no effect on the austenitic stainless steel comprising the structural components of the BRR package. Since the payload of the BRR package is heavily shielded, the radiation exposure of the overpack materials (including the polyurethane foam) is negligible. The butyl rubber containment seal, which is also located outside of the gamma shielding, likewise receives a negligible exposure. For these reasons, there will be no deleterious radiation effects on the packaging, and the requirements of 10 CFR §71.43(d) are met.

Table 2.2-1 – Mechanical Properties of Wrought Type 304 Stainless Steel

Material Specification	Temperature (°F)	① Yield Strength, S_y (psi)	② Ultimate Strength, S_u (psi)	③ Allowable Strength, S_m (psi)	④ Elastic Modulus, E ($\times 10^6$ psi)	⑤ Thermal Expansion Coefficient, α ($\times 10^{-6}$ /°F)
ASTM A240 ASTM A249 ASTM A276 ASTM A479 Type 304	-40	**30,000**	**75,000**	**20,000**	**28.9**	**8.2**
	-20	30,000	75,000	20,000	**28.8**	**8.2**
	70	30,000	75,000	20,000	28.3	8.5
	100	30,000	75,000	20,000	**28.1**	8.6
	200	25,000	71,000	20,000	27.5	8.9
	300	22,400	66,200	20,000	27.0	9.2
	400	20,700	64,000	18,600	26.4	9.5
	500	19,400	63,400	17,500	25.9	9.7
	600	18,400	63,400	16,600	25.3	9.8
	700	17,600	63,400	15,800	24.8	10.0
	800	16,900	62,800	15,200	24.1	10.1

Notes: ① ASME Code, Section II, Part D, Table Y-1.
② ASME Code, Section II, Part D, Table U.
③ ASME Code, Section II, Part D, Table 2A.
④ ASME Code, Section II, Part D, Table TM-1, Material Group G. Values for -40 °F and -20 °F interpolated from 70 °F and -100 °F.
⑤ ASME Code, Section II, Part D, Table TE-1, Material Group 3, Mean Coefficient. Values for -40 °F and -20 °F extrapolated from 70 °F and 100 °F.

Table 2.2-2 – Mechanical Properties of Forged and Cast Type 304 Stainless Steel

Material Specification	Temperature (°F)	① Yield Strength, S_y (psi)	② Ultimate Strength, S_u (psi)	③ Allowable Strength, S_m (psi)	④ Elastic Modulus, E ($\times 10^6$ psi)	⑤ Thermal Expansion Coefficient, α ($\times 10^{-6}$ /°F)
ASTM A182 Type F304, ASTM A351 Type CF8, and ASTM A451, Type CPF8 ⑥	-40	**30,000**	**70,000**	**20,000**	**28.9**	**8.2**
	-20	30,000	70,000	20,000	**28.8**	**8.2**
	70	30,000	70,000	20,000	28.3	8.5
	100	30,000	70,000	20,000	**28.1**	8.6
	200	25,000	66,300	20,000	27.5	8.9
	300	22,400	61,800	20,000	27.0	9.2
	400	20,700	59,700	18,600	26.4	9.5
	500	19,400	59,200	17,500	25.9	9.7
	600	18,400	59,200	16,600	25.3	9.8
	700	17,600	59,200	15,800	24.8	10.0
	800	16,900	58,600	15,200	24.1	10.1

Notes: ① ASME Code, Section II, Part D, Table Y-1.

② ASME Code, Section II, Part D, Table U.

③ ASME Code, Section II, Part D, Table 2A.

④ ASME Code, Section II, Part D, Table TM-1, Material Group G. Values for -40 °F and -20 °F interpolated from 70 °F and -100 °F.

⑤ ASME Code, Section II, Part D, Table TE-1, Material Group 3, Mean Coefficient. Values for -40 °F and -20 °F extrapolated from 70 °F and 100 °F.

⑥ Optional cast materials are ASTM A351 Type CF8A and ASTM A451 Type CPF8A. The yield, ultimate, and allowable strengths of these materials are higher than the values in this table at all temperatures with one exception: the allowable strength, S_m, is not given for a temperature of 800 °F. However, since the BRR package temperatures never exceed 700 °F, this limitation does not apply.

Table 2.2-3 – Mechanical Properties of ASTM A320, Grade L43 Alloy Bolting Material

Material Specification	Temperature (°F)	① Yield Strength, S_y (psi)	② Ultimate Strength, S_u (psi)	③ Allowable Strength, S_m (psi)	④ Elastic Modulus, E ($\times 10^6$ psi)	⑤ Thermal Expansion Coefficient, α ($\times 10^{-6}$ /°F)
ASTM A320 Grade L43	-40	**105,000**	**125,000**	**35,000**	**28.3**	**6.2**
	-20	105,000	125,000	35,000	**28.2**	**6.3**
	70	105,000	125,000	35,000	27.8	6.4
	100	105,000	125,000	35,000	**27.6**	6.5
	200	99,000	125,000	33,000	27.1	6.7
	300	95,700	125,000	31,900	26.7	6.9
	400	91,800	125,000	30,600	26.2	7.1
	500	88,500	125,000	29,500	25.7	7.3
	600	84,300	125,000	28,100	25.1	7.4
	700	79,200	125,000	26,400	24.6	7.6

Notes: ① ASME Code, Section II, Part D, Table Y-1.

② ASME Code, Section II, Part D, Table Y-1.

③ ASME Code, Section II, Part D, Table 4.

④ ASME Code, Section II, Part D, Table TM-1, Material Group B. Values for -40 °F and -20 °F interpolated from 70 °F and -100 °F.

⑤ ASME Code, Section II, Part D, Table TE-1, Material Group 1, Mean Coefficient. Values for -40 °F and -20 °F extrapolated from 70 °F and 100 °F.

Table 2.2-4 – Mechanical Properties of Lead Shielding

Material Specification	Temperature (°F)	① Tensile Yield Strength, S_y (psi)	① Tensile Ultimate Strength, S_u (psi)	① Tensile Proportional Limit (psi)	② Elastic Modulus, E ($\times 10^6$ psi)	② Thermal Expansion Coefficient, α ($\times 10^{-6}$ /°F)
ASTM B29 Chemical Lead or Fed Spec QQ-L-121E, Gr. A or C	-99	---	---	---	2.50	15.3
	70	---	---	---	2.34	16.1
	100	584	1,585	276	2.30	16.2
	175	509	1,158	293	2.20	16.6
	250	498	839	277	2.09	17.0
	325	311	639	189	1.96	17.5
	440	---	---	---	1.74	18.5
	620	---	---	---	1.36	20.4

Notes: ① WADC Technical Report 57-695, ASTIA Document No. 151165, "Determination of the Mechanical Properties of a High Purity Lead and a 0.05% Copper-Lead Alloy," April 1958, by Thomas Tietz, Stanford Research Center, pp. 14, 21, for copperized lead.

② NUREG/CR-0481, SAND77-1872, "An Assessment of Stress-Strain Data Suitable for Finite Element Elastic-Plastic Analysis of Shipping Containers," H. J. Rack and G. A. Knorovsky, Sept. 1978, p. 66.

Table 2.2-5 – Mechanical Properties of Brass Material

Material	Minimum Mechanical Properties
ASTM B16, UNS C36000, Temper H02	Yield Strength, σ_y = 25,000 psi Ultimate Strength, σ_u = 55,000 psi

Table 2.2-6 – Nominal Material Properties of 9 lb/ft^3 Polyurethane Foam

Property	Direction	Room Temperature Value
Compressive Strength, S	Axial (Parallel-to-Rise)	280 psi @ 10% Strain 306 psi @ 40% Strain 758 psi @ 70% Strain
	Radial (Perpendicular-to-Rise)	278 psi @ 10% Strain 303 psi @ 40% Strain 767 psi @ 70% Strain

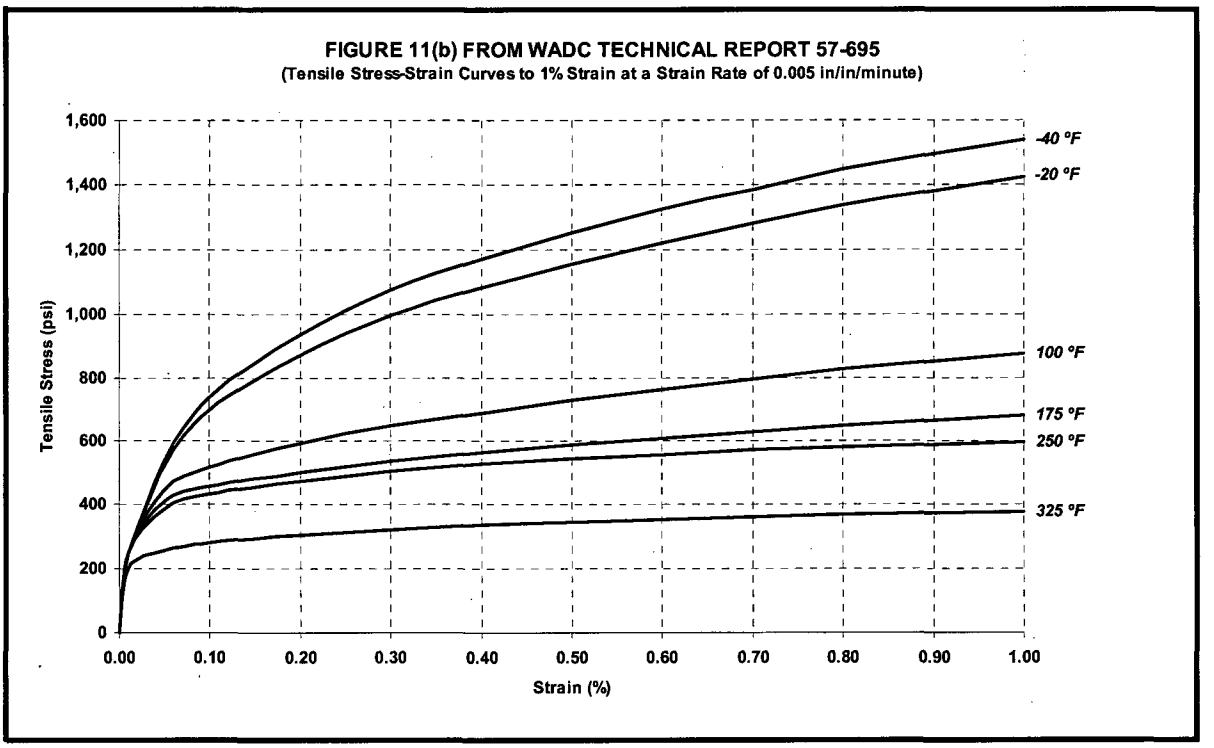

Figure 2.2-1 – Tensile Stress-Strain Curves for Lead Shielding (Source: see note 1 of Table 2.2-4)

2.3 Fabrication and Examination

2.3.1 Fabrication

The BRR package is fabricated using conventional metal forming and joining techniques. All welding procedures and welding personnel must be qualified in accordance with Section IX of the ASME Boiler and Pressure Vessel Code [14]. Containment boundary welds, as well as the welds at each end of the outer shell, are full penetration joints. All non-containment joints are fabricated in accordance with the requirements delineated on the drawings in Appendix 1.3.3, *Packaging General Arrangement Drawings*. The containment shell and outer shell fabrications shall comply with the tolerance requirements of the ASME Code, Subsection NE, Article NE-4220 [15]. Article NE-4220 is selected because the package cylindrical shells are verified for buckling performance using the ASME Code Case N-284-2. This Code Case is for Section III, Division 1, Class MC construction, and is based on the fabrication requirements of NE-4222, as stated in Section 1120 of the Code Case. Therefore, it is appropriate to fabricate the BRR package using shell tolerances from NE-4220, rather than NB-4220.

The polyurethane foam and butyl rubber O-rings are procured using written procedures. See Section 8.1.5, *Component Tests*, for details of the fabrication and performance requirements of these components.

2.3.2 Examination

Each of the materials performing a significant safety function must meet the ASTM specifications delineated on the drawings in Appendix 1.3.3, *Packaging General Arrangement Drawings*. Safety-significant materials not having an ASTM designation are controlled by means of written procedures whose requirements are summarized in Section 8.1.5, *Component Tests*.

Forgings are subject to ultrasonic and liquid penetrant inspection per the ASME Code, Subsection NB, Article NB-2540 [16]. Castings are subject to radiographic and liquid penetrant inspection per the ASME Code, Subsection NB, Article NB-2570 [17].

All welds are subject to visual examination per AWS D1.6 [18]. The welds between the inner containment shell and either end structure, the welds between the outer shell and either end structure, and the longitudinal weld(s) in the outer shell, if any, are examined by ultrasonic inspection in accordance with the ASME Code, Subsection NB, Article NB-5000, and Section V, Article 4 [20]. Optionally, the weld between the inner containment shell and the lower end structure may be examined by radiographic inspection in accordance with the ASME Code, Subsection NB, Article NB-5000, and Section V, Article 2 [19]. All welds on the BRR package, except seal welds, are liquid penetrant inspected on the final pass in accordance with the ASME Code, Subsection N*x*, Article N*x*-5000, and Section V, Article 6 [21]. The appropriate Subsection for the containment welds and outer shell welds is NB; for other cask body welds and the impact limiter shells, NF; and for the fuel baskets, NG.

Each BRR package will also be subjected to the following tests:

- An internal pressure test, in which the containment boundary is pressurized to 125% of the design pressure per the ASME Code [22], or 150% of the MNOP, per 10 CFR §71.85(b),

whichever is greater. The pressure test requirements are described in Section 8.1.3.2, *Containment Boundary Pressure Testing.*

- Containment boundary leakage rate test, which includes helium leakage rate tests of the containment boundary, the closure lid containment O-ring seal, the vent port containment O-ring seal, and the drain port containment O-ring seal. The leakage rate test requirements are described in Section 8.1.4, *Fabrication Leakage Rate Tests.*
- A test to ensure the integrity of the lead gamma shielding. The gamma test requirements are described in Section 8.1.6, *Shielding Integrity Test.*

2.4 General Standards for All Packages

This section defines the general standards for all packages. The BRR package meets all requirements delineated for this section.

2.4.1 Minimum Package Size

The minimum dimension of the BRR package is approximately 38.5 inches (the package diameter). Thus, the 4-in. minimum requirement of 10 CFR §71.43(a) is satisfied.

2.4.2 Tamper-Indicating Feature

A tamper-indicating seal is made by passing a lock wire through a hole in one of the upper impact limiter attachments. The wire passes through both the blade (impact limiter) and receptacle (cask body) components comprising the attachment. The upper impact limiter covers the closure lid and vent port. The wire must be destroyed in order to remove the impact limiter, thus providing evidence of possible tampering. Thus, the requirement of 10 CFR §71.43(b) is satisfied.

2.4.3 Positive Closure

The BRR package cannot be opened unintentionally. The impact limiters, which are each secured with eight, 1-inch diameter ball lock pins, fully conceal all cask openings. Thus, the requirements of 10 CFR §71.43(c) are satisfied.

2.4.4 Valves

The containment boundary of the BRR package does not contain any valves. The closure lid contains one vent port, and the lower end structure contains one drain port, which penetrate the containment boundary and which are closed with brass port plugs. Both ports are closed and tested during pre-shipment leak testing of the BRR package. The ports are protected from inadvertent use or from tampering by the impact limiters as described above. Thus, the requirements of 10 CFR §71.43(e) are satisfied.

2.4.5 Package Design

As shown in Chapter 2.0, *Structural Evaluation*, Chapter 3.0, *Thermal Evaluation*, and Chapter 5.0, *Shielding Evaluation*, the structural, thermal, and shielding requirements, respectively, of 10 CFR §71.43(f) are satisfied for the BRR package.

2.4.6 External Temperatures

As shown in Table 3.3-1 from Section 3.3, *Thermal Evaluation for Normal Conditions of Transport*, the maximum accessible surface temperature with maximum internal decay heat load and no insolation is bounded by 185 °F. This satisfies the limit of 10 CFR §71.43(g) for exclusive use shipments.

2.4.7 Venting

The BRR package does not include any features intended to allow continuous venting of the containment boundary during transport. Thus, the requirements of 10 CFR §71.43(h) are satisfied.

2.5 Lifting and Tie-down Standards for All Packages

2.5.1 Lifting Devices

The BRR package is lifted from four lift points located in the upper massive end structure. Lifting devices are installed in threaded holes containing optional alloy steel inserts. The failure mode of the lifting device is via shear tearout of the threads. Since the parent material is Type 304 stainless steel, it is conservative to consider the case in which the alloy steel inserts are not used.

The cask will be lifted using two cables, each attached to two lifting devices on the same side of the cask to preclude any crossing of the cables. In this way, both cables will have the same seating in the crane hook, and carry the same load. Consequently, all four lift points will experience the same lifting load. Although normal operating procedures call for the cask to be lifted without the lower impact limiter, it is conservatively assumed for the purpose of this analysis that it is in place during lifting. Since the upper impact limiter must be removed prior to installation of the lifting devices, lifting the cask with the upper limiter in place is impossible. The weight of the loaded cask with bottom impact limiter is:

$$W = 32{,}000 - 2{,}300 = 29{,}700 \text{ lb}$$

where the maximum package weight is 32,000 lb, and the upper impact limiter weight is 2,300 lb, from Table 2.1-2. For this calculation, a bounding weight of 30,000 lb is used. Since the weight will be evenly distributed among the four lifting devices, the load on each cask lift point is F = 30,000/4 = 7,500 lb.

The governing shear area is based on the hole thread specification, which is 1-8 UNC-2B. From [23], $A_i = 2.3256$ in^2/in. The shear stress in the inner threads is

$$\tau_i = \frac{F}{A_i L} = 2{,}150 \text{ psi}$$

where the minimum thread length, L = 1.5 inches. At the NCT hot bounding temperature of 250 °F, the yield strength of the Type 304 parent material from Table 2.6-1 is 23,700 psi. The margin of safety is

$$MS = \frac{23{,}700(0.6)}{2{,}150(3)} - 1 = +1.20$$

where the factor of 0.6 in the numerator accounts for the shear failure mode and the factor of 3 in the denominator ensures that a minimum factor of safety of 3 is present. In the case of lifting overload, the device will strip out of the parent material without damage to the cask. Therefore, the requirements of 10 CFR §71.45(a) are met.

2.5.2 Tie-down Devices

During transport, the BRR package rests on a steel pallet, and is held down to the pallet by means of a steel frame which rests on top of the upper impact limiter. The upper impact limiter covers the lifting holes described in the section just above, and the steel tiedown frame covers

the threaded holes in the upper impact limiter, thus these holes could not be erroneously used for tiedown. The steel tiedown frame is attached by wire ropes or equivalent to the conveyance, so that a nominal downward load is applied to keep the BRR package in place. In this configuration, the package contacts only the pallet on the bottom and the steel frame on the top, and therefore has no integral tie–down devices which are a structural part of the package. Therefore, per 10 CFR §71.45(b)(1), no evaluation of tie–down devices is required.

2.6 Normal Conditions of Transport

When subjected to normal conditions of transport (NCT) as specified in 10 CFR §71.71, the BRR package meets the performance requirements specified in Subpart E of 10 CFR 71. This is demonstrated in the following subsections where each NCT condition is addressed and shown to meet the applicable design criteria. Load combinations used in this section are consistent with Regulatory Guide 7.8.

2.6.1 Heat

The normal heat condition, as defined in 10 CFR §71.71(c)(1), is evaluated in Section 3.0, *Thermal Evaluation.* The bounding temperatures and pressures for use in structural analyses are summarized in the following section. Material properties and stress limits, consistent with the design criteria shown in Table 2.1-1, are summarized for the relevant bounding temperatures in Table 2.6-1.

2.6.1.1 Summary of Pressures and Temperatures

The bounding maximum temperatures for the 100 °F ambient NCT condition of the BRR package are presented in Table 3.1-1 of Chapter 3, *Thermal Evaluation.* For purposes of structural evaluation, the bounding fuel basket temperature is 400 °F. All components of the cask body, including the end structures, shells, shield plug, lead, closure lid and bolts, and elastomer seals, are bounded by a temperature of 250 °F. The bulk average polyurethane foam in both limiters is bounded by a temperature of 150 °F.

The initial pressure in the package at assembly is ambient, i.e., 14.7 psia. As determined in Section 3.3.2, *Maximum Normal Operating Pressure*, the maximum normal operating pressure (MNOP) can be conservatively defined to be 10 psig. The design pressure of the BRR package is 25 psig, which is significantly higher than the MNOP.

2.6.1.2 Differential Thermal Expansion

Acceptable minimum clearances are maintained, including consideration of worst-case tolerances, between the cask, the fuel baskets, and the fuel.

2.6.1.2.1 Baskets

The baskets for each fuel type have a nominal length of 53.45 inches with a tolerance of ± 0.12 inches, giving a maximum length of 53.57 inches. The cask cavity, with the shield plug installed, has a nominal length of 54.0 inches, with a tolerance of ± 0.1 inches, for a minimum length of $L_{Cask\text{-}min}$ = 53.9 inches. The length of the basket at a bounding temperature of 400 °F is:

$$L_{Bsk} = 53.57[1 + \alpha(400 - 70)] = 53.74 \text{ inches}$$

where the coefficient of thermal expansion, α, is taken from Table 2.6-1 for Type 304 stainless steel at 400 °F as $9.5(10^{-6})$ in/in/°F, and the reference temperature is 70 °F. The cask cavity thermal expansion is conservatively ignored. The minimum axial clearance at the NCT hot temperature is:

$$CLR_{Bsk-Axi} = L_{Cask-min} - L_{Bsk} = 0.16 \text{ inches}$$

All baskets have a nominal outer diameter of 15.63 inches with a tolerance of ± 0.12 inches, giving a maximum diameter of 15.75 inches. The cask cavity has a diameter of 16.0 inches, with a tolerance of ± 0.1 inches, for a minimum diameter of $D_{Cask-min}$ = 15.9 inches. The diameter of the basket at a bounding temperature of 400 °F is:

$$D_{Bsk} = 15.75[1 + \alpha(400 - 70)] = 15.80 \text{ inches}$$

where the coefficient of thermal expansion is the same as above. Again, the cask cavity thermal expansion is ignored. The minimum diametral clearance at the NCT hot temperature is:

$$CLR_{Bsk-Dia} = D_{Cask-min} - D_{Bsk} = 0.10 \text{ inches}$$

Therefore, the thermal expansion of the baskets is not of concern.

2.6.1.2.2 Fuel

The fuel types transported in the BRR Package are made primarily of aluminum. The TRIGA type also includes a stainless steel clad version, but its thermal expansion behavior will be governed by the aluminum clad configuration. At the bounding fuel temperature of 400 °F, the thermal expansion coefficient of 6061 aluminum alloy, α_{Al-400} = 13.6(10^{-6}) in/in/°F, per Table TE-3 of the ASME Code, Section II, Part D. As an example of the minimum clearance calculation, the MITR-II fuel type case is shown in detail.

From Section 1.2.2.2, *MITR-II*, the maximum length of the MITR-II fuel element (including variation, irradiation growth, and margin) is 26.52 inches. At 400 °F, the fuel length is:

$$L_{MIT-Fuel} = 26.52[1 + \alpha_{Al-400}(400 - 70)] = 26.64 \text{ inches}$$

The basket fuel cavity length is 26.88 inches, with a tolerance of ± 0.12, giving a minimum length of 26.76 inches at 70 °F. At a bounding temperature of 400 °F, the cavity length is:

$$L_{MIT-Cav} = 26.76[1 + \alpha(400 - 70)] = 26.84 \text{ inches}$$

where the thermal expansion coefficient for Type 304 stainless steel is the same as used above. The minimum axial clearance between the MITR-II fuel assembly and the basket cavity at the NCT hot temperature is:

$$CLR_{Fuel-Axi} = L_{MIT-Cav} - L_{MIT-Fuel} = 0.20 \text{ inches}$$

The minimum axial clearances of each fuel type are shown in Table 2.6-2.

2.6.1.2.3 Lead

Due to different thermal expansion coefficients, the lead gamma shielding creates a stress in the inner shell under NCT hot conditions. An upper bound interface pressure between the lead and the inner shell is now determined, and applied as a pressure load to the finite element model and to the buckling analysis. First, note that the lead and the cask inner and outer shells are all in contact, and are stress-free, at the point of solidification of the lead at 620 °F. As the cask and lead cool, the lead contracts more than the stainless steel, and an interface pressure develops between the lead and the inner shell. This interface pressure is a function of the amount of

interference between the lead and inner shell, and of the yield point of the lead at the NCT temperature. Due to the effects of material creep, the interface pressure will diminish over a relatively short period of time, thus reducing the resulting inner shell stresses. However, the effects of lead creep are conservatively neglected. The amount of interference between the lead and the inner shell depends upon the free state radii of these components, both at their respective NCT temperatures. The free state outer radius of the inner shell at the NCT hot temperature is

$$r_{ioh} = r_{io}[1 + \alpha_{s200}(T_{sh} - 70)] = 9.010 \text{ inches}$$

where the outer free state radius of the inner shell at room temperature, r_{io} = 9 inches, the lower bound NCT hot case temperature of the shell, T_{sh} = 200 °F, and the coefficient of thermal expansion of the inner shell material at 200 °F is $\alpha_{s200} = 8.9(10^{-6})$ /°F from Table 2.2-1. Note that the interface pressure calculation is conservative for lower bound temperatures, since the lead will contract more and apply a larger pressure.

To determine the free state radii of the lead under NCT temperatures, it is necessary to start with the radii of the steel shells at the lead solidification point at 620 °F, at which point all of the components are in stress free contact. The radii of the lead/steel interfaces at 620 °F are

$$r_{Li620} = r_{io620} = r_{io}[1 + \alpha_{s620}(620 - 70)] = 9.049 \text{ inches}$$

$$r_{Lo620} = r_{oi620} = r_{oi}[1 + \alpha_{s620}(620 - 70)] = 17.092 \text{ inches}$$

where r_{Li620}/r_{io620} represent the inner lead/steel interface radius, and r_{Lo620}/r_{oi620} represents the outer lead/steel interface radius at 620 °F. In these equations, the room temperature outer radius of the inner shell, r_{io} = 9 inches, the inner radius of the outer shell, r_{oi} = 17 inches, and the thermal expansion coefficient of the shells at 620 °F, $\alpha_{s620} = 9.84(10^{-6})$ /°F. These values are then used to find the free state lead dimensions at the NCT temperature of lead as follows. Note that two thermal expansion terms are used (first contracting the lead from 620 °F to 70 °F, then expanding it from 70 °F to the hot lead temperature), since the thermal expansion coefficients given in Table 2.2-4 are based on 70 °F. The NCT hot case temperature of the lead is given a conservative lower bound of T_{Lh} = 200 °F as discussed above.

$$r_{Lih} = r_{Li620}[1 - \alpha_{L620}(620 - 70) + \alpha_{L200}(T_{Lh} - 70)] = 8.967 \text{ inches}$$

$$r_{Loh} = r_{Lo620}[1 - \alpha_{L620}(620 - 70) + \alpha_{L200}(T_{Lh} - 70)] = 16.937 \text{ inches}$$

where r_{Lih} is the free state inner radius of the lead, and r_{Loh} is the outer radius, at NCT. From Table 2.2-4, the thermal expansion coefficient of the lead from 620 °F to 70 °F, $\alpha_{L620} = 20.4(10^{-6})$/°F, and from 70 °F to T_{Lh}, the corresponding coefficient is $\alpha_{L200} = 16.7(10^{-6})$/°F. Next, the interference between the inner shell and the lead will be found. Since the lead has a relatively low yield stress, the interface pressure between the inner shell and the lead will be governed by the lead yield stress, which in turn depends on the location of the lead stress state on the lead stress-strain curve. The hoop strain in the lead is equal to u/r, where u represents the radial displacement of the inner surface, and r is the inner radius, of the lead. The interface pressure can be conservatively maximized by assuming that the cask inner shell is rigid, and that therefore all of the radial interference is taken by the lead. The radial interference is

$$u = r_{ioh} - r_{Lih} = 0.043 \text{ inches}$$

The maximum lead strain is then

$$\varepsilon_{Lh} = \frac{u}{r_{Lih}}(100) = 0.480\ \%$$

Stress-strain curves for lead at various temperatures are reproduced in Figure 2.2-1. The hoop stress at a temperature of 200 °F, corresponding to a maximum strain of 0.480% may be conservatively bounded by a value of σ_{Lh} = 600 psi. It may be observed from the figure that the actual stress would be somewhat lower. The maximum sustainable interface pressure can be backed out of the equation for hoop stress in a thick walled cylinder, Table 32, Case 1a [25], as

$$p_h = \frac{\sigma_{Lh}}{\frac{r_{Loh}^2 + r_{Lih}^2}{r_{Loh}^2 - r_{Lih}^2}} = 337\ \text{psi}$$

In the finite element thermal stress analysis discussed in Section 2.6.1.3.2, a conservative upper bound external pressure of 350 psi is applied to the inner shell to represent the worst case lead contraction loading.

2.6.1.3 Stress Calculations

2.6.1.3.1 Stresses Due to Pressure Loading

The finite element model described in Appendix 2.12.4, *Stress Analysis Finite Element Models,* is loaded with the internal maximum design pressure of 25 psi, without thermal loading, and gives the result discussed in Section 2.12.4.4.1, *Case No. 1, Design Pressure Only*, and shown in Figure 2.12.4-5. The maximum overall stress intensity which results from the model, which bounds both the primary membrane and membrane plus bending stress, is 281 psi, located at the midpoint of the cavity bottom. Since this value is less than the lowest (primary membrane) stress allowable, as shown in Section 2.6.1.4, *Comparison with Allowable Stresses*, it is not necessary to identify the individual stress components.

Since the FEA model does not include the closure lid, the stress due to pressure on the lid is computed manually. From [25], Table 24, Case 10a for a simply supported, uniformly loaded plate, the bending moment is:

$$M = \frac{qa^2(3+\upsilon)}{16} = 668\ \text{in} - \text{lb/in}$$

where the radius, a = 22.75/2 = 11.38 inches, the design pressure, q = 25 psig, conservatively applied over the entire area within the bolt circle, and ν = 0.3. The stress in the closure lid is:

$$\sigma = \frac{6M}{t^2} = 1{,}002\ \text{psi}$$

where the lid thickness, t = 2.0 inches. As shown, the stress in the closure lid is bounding over the stress in the cavity bottom.

2.6.1.3.2 Stresses Due to Thermal Loading

The same finite element model is loaded with 25 psi internal pressure, as well as with the structural temperatures shown in Figure 2.12.4-3 and the lead contraction pressure determined in Section 2.6.1.2.3, *Lead*, and gives the result discussed in Section 2.12.4.4.2, *Case No. 2, Lead Shrinkage Pressure With Thermal*, and shown in Figure 2.12.4-6. The structural temperatures are originally obtained from the SINDA® thermal model described in Chapter 3, *Thermal Evaluation*, and are imported into the stress analysis as described in Appendix 2.12.4.2.1, *Thermal Loads*. The maximum overall stress intensity due to pressure and thermal gradient loading is 6,933 psi and occurs at the top of the inner shell cross section. Since this value is less than the lowest (primary membrane) stress allowable, as shown in Section 2.6.1.4, *Comparison with Allowable Stresses*, it is not necessary to identify the individual stress components.

2.6.1.4 Comparison with Allowable Stresses

From Table 2.1-1, the limit on primary membrane plus bending stress is $1.5S_m$. At the bounding temperature of 250 °F given in Section 2.6.1.1, *Summary of Pressures and Temperatures*, the value of $1.5S_m$ for Type 304 is 30,000 psi from Table 2.6-1. Applying this limit limit to the bounding stress intensity of 1,002 psi given in Section 2.6.1.3.1, *Stresses Due to Pressure Loading*, the margin of safety is:

$$MS = \frac{30{,}000}{1{,}002} - 1 = \underline{+28.9}$$

From Table 2.1-1, the limit on the range of primary plus secondary stress intensity is $3S_m$. For the range of stress intensity of 6,933 psi given in Section 2.6.1.3.2, *Stresses Due to Thermal Loading*, the margin of safety is:

$$MS = \frac{(3.0)20{,}000}{6{,}933} - 1 = \underline{+7.65}$$

As shown, all margins of safety for the NCT warm condition are positive.

2.6.1.5 Closure Bolts

Twelve closure bolts attach the closure lid to the cask opening. The closure lid is sized such that support against lateral loads (in the plane of the lid) is obtained from the fit between the lid and the cask opening, thus preventing any shear loading of the closure bolts. In addition, the lid is prepared with a 1/16-inch deep step located on the bolt circle which extends to the outer edge of the lid. The step prevents any bolt prying or significant bolt bending from occurring as a result of lid deformation.

The closure bolts are tightened to 220 ± 20 ft-lb of torque, or a maximum of 240 ft-lb. From Section 4.2 of [10], the maximum non-prying tensile force per bolt due to the preload, Fa_max, is found from:

$$Fa\_max = \frac{Q\,max}{(K)(Db)} = 19{,}200\ lb$$

where Qmax = 240 × 12 = 2,880 in-lb is the maximum bolt torque, K = 0.15 is the nut factor for a lubricated bolt (approximately equal to the average of the values for lubricated surfaces in

Table 4.1 of [10]), and Db = 1.0 inches is the nominal diameter of the closure bolt. The maximum residual torsion is 50% of the applied torsion, or:

$$Mtr = 0.5(Q\max) = 1{,}440 \text{ in} - \text{lb}$$

From Section 4.4 of [10], the maximum non-prying tensile force per bolt, Fa_max, due to pressure loads are:

$$Fa\_max = \frac{\pi D lg^2 (Pli - Plo)}{4Nb} = 789 \text{ lb}$$

where Dlg = 18.25 inches is the diameter of the pressure boundary, i.e., the inner (containment) O-ring seal, Pli = 25 psig + 14.7 psia = 39.7 psia is the internal pressure, Plo = 3.5 psia is the NCT cold external reduced pressure from Section 2.6.3, *Reduced External Pressure*, and Nb = 12 is the quantity of closure bolts. From this it is clear that the preload force is governing over the pressure force.

Even though the temperatures of the closure lid and bolts are the same, a thermally induced loading is applied to the closure bolts due to the difference in thermal expansion coefficient between the ASTM A320 L43 alloy steel closure bolts and the Type 304 stainless steel closure lid. From Section 4.5 of [10], the maximum non-prying tensile force due to thermal expansion effects is:

$$Fa = \frac{\pi}{4} Db^2 (Eb)[al(Tl) - ab(Tb)] = 8{,}747 \text{ lb}$$

where the modulus of elasticity of the bolt, Eb = 26.9(10^6) psi, the thermal expansion coefficient of the closure lid, al = 9.1(10^{-6}) in/in/°F, and the thermal expansion coefficient of the bolt, ab = 6.8(10^{-6}) in/in/°F, all from Table 2.6-1. The change in temperature of both components, Tl = Tb = (250 – 70) = 180 °F, where the bounding temperature of the components is 250 °F, and the ambient temperature is 70 °F.

The average axial bolt stress corresponding to these loadings is:

$$Sba = 1.2732 \frac{(19{,}200 + 8{,}747)}{Dba^2} = 46{,}158 \text{ psi}$$

where the load term in the numerator is the sum of the preload and thermal loads, and the stress diameter, Dba = Db – 0.9743(p) = 0.878 inches, where Db is 1.0 inches and the pitch, p, is 0.125 for the 1-8 UNC bolt. The residual torsional stress is:

$$Sbt = \frac{5.093(Mtr)}{Dba^2} = 9{,}514 \text{ psi}$$

From Table 2.1-1, for NCT the allowable average tensile stress is $S_m = (2/3)S_y$, which from Table 2.6-1 is equal to 64,900 psi at the NCT hot temperature of 250 °F. The margin of safety is:

$$MS_{Sba} = \frac{64{,}900}{Sba} - 1 = +0.41$$

Combining the axial and residual torsional shear stresses, the maximum closure bolt stress intensity is:

$$Sbi = \sqrt{Sba^2 + 4Sbt^2} = 49{,}926 \text{ psi}$$

As noted at the beginning of this section, bolt shear or prying loads are precluded by the design of the closure lid. From Table 2.1-1, the allowable stress intensity is $1.35S_m$ for cases where S_y is greater than 100 ksi. The margin of safety is:

$$MS_{Sbi} = \frac{1.35(64,900)}{49,926} - 1 = +0.75$$

Thus the closure bolts are not of concern for the NCT hot condition, including the reduced external pressure load case.

2.6.2 Cold

For the cold condition, a -40 °F steady state ambient temperature is utilized per Regulatory Guide 7.8 [3], with zero insolation and zero decay heat. This results in a uniform temperature of -40 °F throughout the cask. The materials of construction for the SEC transportation cask are not adversely affected by the -40 °F condition, including brittle fracture, which is evaluated in Section 2.1.2.3.1, *Brittle Fracture*.

In Section 2.6.1.2, *Differential Thermal Expansion*, the interface pressure between the cask inner shell and the lead gamma shielding was evaluated at the NCT maximum temperature. Since the lead will contract further at lower temperatures, that analysis is now repeated for the NCT cold condition. As discussed in Section 2.6.1.2, the lead and the cask inner and outer shells are all in contact, and stress free, at the point of solidification of the lead at 620 °F. As the cask and lead cool, the lead contracts more than the stainless steel, and an interface pressure develops between the lead and the inner shell. This interface pressure is a function of the amount of interference between the lead and inner shell, and of the yield point of the lead at the cold temperature. As stated in Section 2.6.1.2, material creep in the lead will reduce the interface pressure over time, but the effect is conservatively neglected. In addition, the entire strain history of the lead is assumed to occur at a temperature of -40 °F, which further maximizes the lead interface pressure. The amount of interference between the lead and the inner shell depends upon the free state radii of these components, both at -40 °F. The free state outer radius of the inner shell at -40 °F is:

$$r_{ioc} = r_{io}[1 + \alpha_{s-40}(-40 - 70)] = 8.992 \text{ inches}$$

where the outer free state radius of the inner shell at room temperature, r_{io} = 9 inches, and the coefficient of thermal expansion of the shell at -40 °F, $\alpha_{s-40} = 8.2(10^{-6})/°F$ from Table 2.6-1.

To determine the free state radii of the lead at -40 °F, it is necessary to start with the radii of the steel shells at the lead solidification point at 620 °F, at which point all of the components are in stress free contact. The radii of the lead/steel interfaces at 620 °F were found in Section 2.6.1.2. The value r_{Li620} = 9.049 inches represents the inner radius of the lead and r_{Lo620} = 17.092 inches represents the outer lead radius. These values are then used to find the free state lead dimensions at the cold temperature of -40 °F as follows. Note that two thermal expansion terms are used (first contracting the lead from 620 °F to 70 °F, then contracting it further from 70 °F to -40 °F), since the thermal expansion coefficients given in Table 2.2-4 are based on 70 °F.

$$r_{Lic} = r_{Li620}[1 - \alpha_{L620}(620 - 70) + \alpha_{L-40}(-40 - 70)] = 8.932 \text{ inches}$$

$$r_{Loc} = r_{Lo620}[1 - \alpha_{L620}(620 - 70) + \alpha_{L-40}(-40 - 70)] = 16.871 \text{ inches}$$

where r_{Lic} is the free state inner radius of the lead, and r_{Loc} is the outer radius, at -40 °F. From Table 2.2-4, the thermal expansion coefficient of the lead from 620 °F to 70 °F, α_{L620} = $20.4(10^{-6})$/°F, and from 70 °F to -40 °F, $\alpha_{L-40} = 15.6(10^{-6})$/°F. Since the lead has a relatively low yield stress, the interface pressure between the inner shell and the lead will be governed by the lead yield stress, which in turn depends on the location of the lead stress state on the lead stress-strain curve. The hoop strain in the lead is equal to u/r, where u represents the radial displacement of the inner surface, and r is the inner radius of the lead. The interface pressure can be conservatively maximized by assuming that the inner shell is rigid, and therefore all of the radial interference is taken by the lead. The radial interference is

$$u = r_{ioc} - r_{Lic} = 0.060 \text{ inches}$$

The maximum lead strain is then

$$\varepsilon_{Lh} = \frac{u}{r_{Lic}}(100) = 0.671\,\%$$

Stress-strain curves for lead at various temperatures are reproduced in Figure 2.2-1. From the curve representing a lead temperature of -40 °F, the maximum lead stress corresponding to a strain of 0.671% is bounded by σ_{Lc} = 1,400 psi. The maximum sustainable interface pressure can be backed out of the equation for hoop stress in a thick walled cylinder, Table 32, Case 1a [25], as

$$p_c = \frac{\sigma_{Lc}}{\frac{r_{Loc}^2 + r_{Lic}^2}{r_{Loc}^2 - r_{Lic}^2}} = 787 \text{ psi}$$

Using this external pressure, the inner shell membrane stress is

$$\sigma_i = \frac{p_c r_{avg}}{t} = 6{,}690 \text{ psi}$$

where r_{avg} is the minimum average inner shell radius, 8.5 inches, and t is the wall thickness of 1 inch. From Table 2.6-1, the allowable primary membrane stress intensity (S_m) is 20,000 psi. The margin of safety is

$$MS = \frac{20{,}000}{6{,}690} - 1 = +1.99$$

Therefore, the NCT cold condition is not of concern.

Since the coefficient of thermal expansion of the closure lid material is slightly larger than that of the bolting material, a reduction in closure bolt preload will occur at the NCT cold condition. Using the terminology of [10], the reduction in preload is:

$$Fa = \frac{\pi}{4} Db^2 (Eb)[al(Tl) - ab(Tb)] = -4{,}890 \text{ lb}$$

where the bolt nominal diameter, Db = 1.0 inches, the bolt modulus of elasticity, Eb = $28.3(10^6)$ psi, the coefficient of thermal expansion of the lid material, al = $8.2(10^{-6})$ in/in/°F for Type 304 stainless steel, the coefficient of thermal expansion of the bolt material, ab = $6.2(10^{-6})$ in/in/°F for A320 L43 alloy steel, and Tl = Tb = –40 – 70 = –110 °F. The material properties are taken from

Table 2.6-1. The minimum bolt preload torque is 220 ft-lb minus 20 ft-lb, or Qmin = 2,400 in-lb. The minimum bolt preload force is:

$$Fa\_min = \frac{Q\,min}{K(Db)} = 16{,}000\ lb$$

where Db is defined above and K = 0.15, consistent with the definition in Section 2.6.1.5, *Closure Bolts*. Thus, the reduction in preload due to differential thermal expansion is only 4,890/16,000 × 100 = 31%, and a large positive preload force remains at the NCT minimum temperature of -40 °F.

2.6.3 Reduced External Pressure

The effect of reduced external pressure of 3.5 psia, per 10 CFR §71.71(c)(3), is considered negligible for the BRR package compared to other design loadings. This conclusion is based on the NCT structural analyses presented in Section 2.6.1, *Heat*, demonstrating the structural integrity for a 25 psig internal design pressure. Based on the Maximum Normal Operating Pressure (MNOP) of 10 psig, the reduced external pressure conditions would cause a pressure of 21.2 psig. Therefore, the 25 psig internal design pressure analysis is conservatively bounding for the reduced external pressure case.

2.6.4 Increased External Pressure

The effect of an increased external pressure of 20 psia, per 10 CFR §71.71(c)(4), is acceptable for the BRR package. Consistent with Regulatory Guide 7.8, this loading corresponds to an ambient temperature of -20 °F, no insolation, no decay heat, and minimum internal pressure. Additionally, the fabrication stress resulting from the shrinking of the radial lead shield of p_c = 787 psi (see Section 2.6. 2, *Cold*) is included as a radial pressure on the outside of the inner shell. Note that the lead shrinkage stress corresponds to a temperature of -40 °F, which results in a conservatively higher shrinkage stress than would occur at the required ambient temperature of -20 °F. Conservatively, the inner shell is evaluated neglecting the outer shell, even though the external pressure would be applied to the much stronger outer shell rather than the inner shell.

Since the cask is closed under ambient conditions, the internal pressure in the cask at a temperature of -20 °F is

$$p_i = p_{amb}\frac{(-20 + 460)}{(70 + 460)} = 12.2\ psia$$

where p_{amb} is 14.7 psia. Therefore the net external differential gas pressure p_o = 20 - 12.2 = 7.8 psi. The combined external pressure on the inner shell is $p_{ext} = p_c + p_o$ = 794.8 psi. An upper bound value of p_{ext} = 800 psi is used. The compressive hoop stress is:

$$\sigma_\theta = p_{ext}\frac{r_{avg}}{t} = 6{,}800\ psi$$

where the mean inner shell radius, r_{avg} = 8.5 inches, and the thickness, t = one inch. The compressive axial stress, obtained by supporting the pressure load from the entire cask cross section over the inner shell cross section, is:

$$\sigma_\phi = \frac{p_o \pi r_{cask}^2}{2\pi r_{avg} t} = 169 \text{ psi}$$

where r_{cask} = 38.4/2 = 19.2 inches. Using Mohr's circle, the maximum shear stress is:

$$\sigma_{\phi\theta} = \frac{1}{2}(\sigma_\theta - \sigma_\phi) = 3{,}316 \text{ psi}$$

The maximum stress intensity is twice this value, or SI = 6,632 psi. From Table 2.6-1, the allowable membrane stress intensity for the inner shell is 20,000 psi. The margin of safety is:

$$MS = \frac{20{,}000}{6{,}632} - 1 = +2.02$$

The possibility of buckling of the inner shell is evaluated using [13]. Consistent with Regulatory Guide 7.6, a factor of safety corresponding to ASME Code, Service Level A is employed. In this case, the applicable factor of safety is 2.00 for normal conditions, as specified in [13]. The analysis used a modulus of elasticity of $28.8(10^6)$ psi, corresponding to -20 °F. Buckling analysis geometry and loading parameters are listed in Table 2.6-3 and results of the analysis in Table 2.6-4. As shown, all interaction check values, including the maximum value of 0.5974, are less than unity, as required. Thus, the increased external pressure load case is not of concern for the BRR package.

2.6.5 Vibration

The effects of vibration normally incident to transport are shown to be insignificant. Draft ANSI Standard N14.23 [24] identifies peak truck trailer vibration inputs. Table 2 of [24] shows peak vibration accelerations of a trailer bed as a function of package and tiedown system natural frequency. For the frequency range 0 to 5 Hz, and conservatively assuming a light package, Table 2 gives peak accelerations (99% level) of 2*g* in the vertical direction, and 0.1*g* in both the lateral and longitudinal directions. All other frequency ranges give significantly lower acceleration levels. Due to cask symmetry, the vertical load of ±2*g* governs the ±0.1*g* in the lateral and longitudinal directions.

Design fatigue curves are taken from Figure I-9.2.1 and Table I-9.2.2 of [12] for the Type 304 stainless steel cask material, from which the allowable amplitude, S_a, of the alternating stress component (1/2 of the alternating stress range) as a function of number of loading cycles may be obtained. Table I-9.2.2 extends the fatigue allowable data to the endurance limit, which is used in the fatigue assessment of transportation vibration. The allowable amplitude, S_a, from Table I-9.2.2 for Type 304 stainless steel cask material at 10^{11} cycles is 13,600 psi. This value is adjusted based on the ratio of room temperature elastic modulus of $28.3(10)^6$ psi, which is the basis for Table I-9.2.2, and the elastic modulus at NCT maximum temperature, as follows:

$$S_a = 13{,}600\left[\frac{27.3(10^6)}{28.3(10^6)}\right] = 13{,}119 \text{ psi}$$

where 27.3 (10^6) psi is the elastic modulus at the bounding temperature of all cask components of 250 °F from Table 2.2-1.

The BRR package is transported vertically. In this orientation, the closure lid experiences the ±2g loading transverse to the plane of the lid. The weight of the shield plug is conservatively assumed to act with the weight of the lid in responding to the vibratory input. From Table 2.1-2, the weight of the shield plug is 950 lb, and the weight of the lid is 280 lb, for a total of W = 1,230 lb. The lid is modeled as a simply supported plate with an effective outer radius equal to the bolt circle of 22.75 inches. Under a load of 2g, the maximum bending moment in the plate (at the center) is found from Table 24, Case 10a of [25], and is:

$$M = 2K_M qa^2 = 161.7 \text{ in} - \text{lb/in}$$

where the factor 2 is the vibrational load, $K_M = 0.20625$ for $r_o = 0$ from [25], the bolt circle radius, a = 22.75/2 = 11.375 inches, and q is the 1-g plate loading, equivalent to a pressure, found from:

$$q = \frac{W}{A} = 3.03 \text{ psi}$$

where W is defined above and A is the area defined by the bolt circle, equal to 406.5 in^2. The stress in the closure lid is:

$$\sigma = \frac{6M}{t^2} = 242.6 \text{ psi}$$

where the thickness of the closure lid, t = 2 inches. For the allowable amplitude, S_a, found above, equal to 13,119 psi, the margin of safety against fatigue of the closure lid due to vibration is:

$$MS = \frac{13{,}119}{242.6} - 1 = +53.1$$

Therefore, fatigue of the BRR package due to transportation vibration is not of concern.

2.6.6 Water Spray

The materials of construction used in the BRR package are not affected by the water spray test identified in 10 CFR §71.71(c)(6).

2.6.7 Free Drop

Section 10 CFR §71.71(c)(7) specifies a free drop from a height of 2 ft for a package weight between 22,000 and 33,100 lb. The governing orientations of end and side are evaluated for the NCT free drop event. The choice of governing orientations is discussed in further detail in Appendix 2.12.2, *Certification Test Plan*. NCT free drop impacts are developed in Appendix 2.12.5, *Impact Limiter Performance Evaluation*. A value of 40g is chosen to bound the calculated impact magnitude for all NCT drop orientations.

Cask body stresses are analyzed for the NCT free drop using the same finite element model identified in Section 2.6.1.3, *Stress Calculations*, and which is also used for evaluation of the HAC free drop event. The model is loaded by a global, quasi-static acceleration field consistent with an impact of 40g. The cask stress analysis for NCT is identical with the analysis for HAC, with the following exceptions:

- Thermal stresses are included in the NCT stress analyses
- The applied quasi-static acceleration field corresponds to the NCT free drop impact of 40g
- Allowable stresses are lower, in accordance with Regulatory Guide 7.6 recommendations.

As discussed in Section 2.7.1.4, *Oblique Drop*, cask stresses are governed by those resulting from the end and side drop orientations. The stress analyses for NCT free drop are given in Sections 2.6.7.1, *NCT End Free Drop*, and 2.6.7.2, *NCT Side Free Drop*.

2.6.7.1 NCT End Free Drop

The construction of the finite element model is discussed in Appendix 2.12.4, *Stress Analysis Finite Element Models*. Temperature loading is applied as discussed in that appendix. The end drop case is evaluated for both top down and bottom down orientations by applying a quasi-static acceleration of 40g. Five analyses are performed:

- Cask body stress
- Closure bolt stress
- Closure lid stress
- Lower closure plate weld stress
- End drop buckling evaluation

Cask Body Stress. From Section 2.12.4.4.3, *Case No. 3, NCT Bottom-down End Drop*, the maximum stress intensity resulting from the bottom-down impact of 40g is 15,202 psi, located at the outside surface of the bottom end structure, as shown in Figure 2.12.4-8. From Table 2.1-1, the limit on primary membrane stress is S_m. At the bounding temperature of 250 °F, the value of S_m for Type 304 is 20,000 psi from Table 2.6-1. Conservatively applying the membrane stress limit to the maximum stress intensity of 15,202 psi, the margin of safety is:

$$MS = \frac{20{,}000}{15{,}202} - 1 = \underline{+0.32}$$

From Section 2.12.4.4.4, *Case No. 4, NCT Bottom-down End Drop With Thermal*, the maximum stress intensity resulting from the bottom-down impact of 40g with thermal loads included is 14,586 psi, located at the top of the inner shell cross section, as shown in Figure 2.12.4-9. From Table 2.1-1, the limit on the range of primary plus secondary stress intensity is $3S_m$. The margin of safety is:

$$MS = \frac{(3.0)20{,}000}{14{,}586} - 1 = \underline{+3.11}$$

From Section 2.12.4.4.6, *Case No. 6, NCT Top-down End Drop*, the maximum stress intensity resulting from the top-down impact of 40g is 13,248 psi, located at the top of the inner shell, as shown in Figure 2.12.4-13. From Table 2.1-1, the limit on primary membrane stress is S_m. Conservatively applying the membrane stress limit to the maximum stress intensity of 13,248 psi, the margin of safety is:

$$MS = \frac{20{,}000}{13{,}248} - 1 = \underline{+0.51}$$

From Section 2.12.4.4.7, *Case No. 7, NCT Top-down End Drop With Thermal*, the maximum stress intensity resulting from the top-down impact of 40g with thermal loads included is 13,258 psi, located at the top of the inner shell, as shown in Figure 2.12.4-14. From Table 2.1-1, the limit on the range of primary plus secondary stress intensity is $3S_m$. The margin of safety is:

$$MS = \frac{(3.0)20{,}000}{13{,}258} - 1 = \underline{+3.53}$$

As shown, all cask body margins of safety for the NCT end free drop condition are positive.

Closure bolt stress. In the top-down orientation, the non-prying closure bolt load is calculated according to Section 4.6 of [10] using:

$$Fa = \frac{1.34\sin(xi)(DLF)(ai)(Wl + Wc)}{Nb} = 9{,}380 \text{ lb}$$

where the impact angle, xi = 90° for the end drop impact, the dynamic load factor, DLF = 1.05 as discussed in Section 2.7.1.2, *End Drop*, the impact magnitude, ai = 40g as discussed above, the weight of the lid, Wl = 280 lb, and the weight of the contents, Wc = 1,720 lb[1] from Table 2.1-2, and the quantity of bolts, Nb = 12. Note that no support for the lid is assumed from the inner surface of the impact limiter.

The sum of all applied loads (the NCT free drop load plus the load due to the design pressure, equal to 789 lb as determined in Section 2.6.1.5, *Closure Bolts*) is equal to 9,380 + 789 = 10,169 lb. This value is however much less than the sum of preload (19,200 lb) and thermal expansion load (8,747 lb). Therefore, the bolt load in the NCT free drop event is governed by the preload plus thermal load, and the margins of safety calculated in Section 2.6.1.5, *Closure Bolts*, are not affected by the free drop event.

Closure lid stress. In Section 2.7.1.2, *Free Drop*, the bending stress in the closure lid is calculated for the top-down HAC free drop under an impact load of 120g. The only difference in the case of the NCT free drop is that the impact is one-third as large, i.e., 40g. The following calculations rely on data given in Section 2.7.1.2. Since the total weight in the end drop is 2,000 lb, the applied load is 2,000 × 40 = 80,000 lb. Since the area of the lid is A_{lid} = 406.9 in^2, the uniform load on the lid is:

$$q = \frac{80{,}000}{A_{lid}} + 25 = 221.6 \text{ psi}$$

where the second term accounts for the design pressure of 25 psig. The uniform load in the HAC case is 614.8 psi, and the resulting stress is 25,865 psi. Using a ratio, the stress under the NCT free end drop is

$$\sigma_{NCT} = \frac{221.6}{614.8} 25{,}865 = 9{,}323 \text{ psi}$$

[1] This weight consists of the shield plug plus the heaviest basket/fuel combination.

From Table 2.1-1, the allowable membrane plus bending stress is equal to $1.5S_m$. From Table 2.6-1, $1.5S_m$ is equal to 30,000 psi at the NCT hot temperature of 250 °F. The margin of safety on the closure lid is:

$$MS = \frac{30,000}{9,323} - 1 = +2.22$$

Thus, the allowable stress is satisfied for the closure lid in the NCT end drop.

Lower closure plate weld stress. In Section 2.7.1.2, *Free Drop*, the combined stress in the lower closure plate weld is calculated for the top-down HAC free drop under an impact load of 120g. The resulting stress is 49,165 psi. This stress includes both fixed-edge bending effects as well as shear loading. Since the NCT impact is 40g and the HAC impact is 120g, the stress corresponding to the NCT free drop is:

$$\sigma_{NCT} = \sigma_{HAC} \frac{40}{120} = 16,388 \text{ psi}$$

From Table 2.1-1, the membrane plus bending stress allowable is $1.5S_m$, which from Table 2.6-1 is equal to 30,000 psi for Type 304 at 250 °F. The margin of safety is:

$$MS = \frac{30,000}{16,388} - 1 = +0.83$$

Thus, the allowable stress is satisfied for the lower closure plate weld stress in the NCT end drop.

End drop buckling evaluation. The cask shells are subject to buckling loads in the end drop orientation. Due to its much greater stiffness compared to the inner shell, the cask outer shell will carry most of the axial loading. The NCT case is essentially the same as the HAC case evaluated in Section 2.7.1.2, *End Drop*, except for the different impact load and factor of safety required by Code Case N-284-2 [13]. Since the HAC end drop is evaluated for an impact of 120g and the NCT for 40g, the axial stress in the NCT buckling evaluation is:

$$\sigma_{\phi-NCT} = \sigma_{\phi-HAC} \times \frac{40}{120} = 2,372 \text{ psi}$$

where $\sigma_{\phi-HAC}$ = 7,117 psi from Section 2.7.1.2, *End Drop*. No other stresses are applied for the end drop buckling evaluation. The outer shell is conservatively assumed to carry the entire axial load without assistance from the inner shell. Thermal stress, which is tensile in the outer shell, is conservatively ignored. Shell dimensions are taken from Table 2.6-5. The factor of safety is equal to 2.00, consistent with Code Case N-284-2 for NCT. The results are shown in Table 2.6-6. As shown, all interaction parameters are less than unity, as required. Therefore, buckling of the cask shells in the NCT free drop will not occur.

2.6.7.2 NCT Side Free Drop

The NCT side free drop is evaluated using the same finite element model which was used for the end drop case. The quasi-static acceleration of 40g also applies to the side drop, since it bounds the calculated side drop impact as discussed in Appendix 2.12.5, *Impact Limiter Performance*

Evaluation. The side drop orientation is governing over the slapdown orientation as discussed in Section 2.7.1.4, *Oblique Drop.*

From Section 2.12.4.4.9, *Case No. 9, NCT Side Drop*, the maximum stress intensity resulting from the side drop impact of 40g is 18,935 psi, located at the bottom outside edge of the lower lead cavity, as shown in Figure 2.12.4-19. From Table 2.1-1, the limit on primary membrane stress is S_m. At the bounding temperature of 250 °F, the value of S_m for Type 304 is 20,000 psi from Table 2.6-1. Conservatively applying the membrane stress limit to the maximum stress intensity of 18,935 psi, the margin of safety is:

$$MS = \frac{20{,}000}{18{,}935} - 1 = \underline{+0.06}$$

From Section 2.12.4.4.10, *Case No. 10, NCT Side Drop With Thermal*, the maximum stress intensity resulting from the side drop impact of 40g with thermal loads included is 22,704 psi, located at the shield plug shelf, as shown in Figure 2.12.4-20. From Table 2.1-1, the limit on the range of primary plus secondary stress intensity is $3S_m$. Conservatively applying the membrane stress limit to the maximum stress intensity of 22,704 psi, the margin of safety is:

$$MS = \frac{(3.0)20{,}000}{22{,}704} - 1 = \underline{+1.64}$$

As shown, all cask body margins of safety for the NCT side free drop condition are positive.

2.6.8 Corner Drop

The BRR package is not required to be evaluated for the corner drop condition, since 10 CFR §71.71(c)(8) applies only to rectangular fiberboard or wood packages weighing less than 110 lb or to cylindrical fiberboard or wood packages weighing less than 220 lb. The weight of the BRR package exceeds these limits and therefore does not need to be evaluated for the NCT corner drop.

2.6.9 Compression

The BRR package is not required to be evaluated for the compression condition, since 10 CFR §71.71(c)(9) applies only to packages weighing less than 11,000 lb. The weight of the BRR package exceeds this limit, and therefore does not need to be evaluated for compression.

2.6.10 Penetration

The impact of a 1.25–inch diameter, hemispherically ended, 13–lb steel bar, per 10 CFR §71.71(c)(10), dropped vertically from a height of 40 inches, has no significant effect on the BRR package. Slight denting of the thermal shield on the outside of the cask can occur, but the bar cannot penetrate or rip into the shield, and cannot harm the impact limiters or impact limiter attachments. Therefore, this test has no significant effect on the package.

Table 2.6-1 – Summary of NCT Design Parameters

Parameter	Body, Closure Lid (Type 304)	Closure Bolts (A320, Grade L43)	Baskets (all Type 304)
NCT Hot Bounding Temperature, °F	250	250	400
Coefficient of Thermal Expansion, α,(in/in/°F)	9.1×10^{-6}	6.8×10^{-6}	9.5×10^{-6}
Elastic Modulus, psi	27.3×10^{6}	26.9×10^{6}	26.4×10^{6}
Design Stress, S_m, psi	20,000	64,900	18,600
Yield Stress, S_y, psi	23,700	97,350	20,700
Primary Membrane Stress Intensity (P_m), psi	$S_m = 20,000$	n/a*	$S_m = 18,600$
Primary Membrane + Bending Stress Intensity ($P_m + P_b$), psi	$1.5S_m = 30,000$	n/a*	$1.5S_m = 27,900$
Primary Membrane + Bending + Secondary Stress Intensity ($P_m + P_b + Q$), psi	$3.0S_m = 60,000$	n/a*	$3.0S_m = 55,800$
NCT Cold Bounding Temperature, °F	-40	-40	-40
Coefficient of Thermal Expansion, α,(in/in/°F)	8.2×10^{-6}	6.2×10^{-6}	8.2×10^{-6}
Elastic Modulus, psi	28.9×10^{6}	28.3×10^{6}	28.9×10^{6}

* Bolting allowable stresses are discussed in the sections where they are used.

Table 2.6-2 – Axial Clearance of Fuel

Type	Max. fuel len., 70°F, in.	Max. fuel len., 400 °F, in.	Basket cavity len., 70 °F, in.	Basket cavity, less 0.12 in. tol.	Min basket cavity len., 400 °F, in.	Axial clearance, min, in.*
MURR	32.75	32.90	33.13	33.01	33.13	0.21
MITR-II	26.52	26.64	26.88	26.76	26.86	0.20
ATR	51.00	51.23	51.38	51.26	51.44	0.19
TRIGA	45.50	45.70	45.88**	45.76	45.90	0.20

* Axial clearance is equal to column 6 (min basket cavity length at 400 °F) minus column 3 (max fuel length at 400 °F).

**Total cavity length of 48.00 inches, minus a 2.12-inch long, short spacer.

Table 2.6-3 – Increased External Pressure Buckling Evaluation: Geometry and Loads

	Inner shell dimensions, inches	Applied stress, psi	
Inner Dia.	16.0	σ_φ	169
Outer Dia.	18.0	σ_θ	6,800
Length*	62.0	$\sigma_{\varphi\theta}$	3,316

* Bounding length used.

Table 2.6-4 – Increased External Pressure: N-284-2 Results

Parameter	Value	Remarks
Capacity Reduction Factors (-1511)		
$\alpha_{\phi L}$ =	0.2795	
$\alpha_{\theta L}$ =	0.8000	
$\alpha_{\phi\theta L}$ =	0.8000	
Plasticity Reduction Factors (-1610)		
η_{ϕ} =	0.0524	
η_{0} =	0.2811	
$\eta_{\phi\theta}$ =	0.0410	
Theoretical Buckling Values (-1712.1.1)		
C_{ϕ} =	0.6050	
$\sigma_{\phi eL}$ =	2,049,882 psi	
$C_{\theta r}$ =	0.0387	
$\sigma_{\theta eL} = \sigma_{reL}$ =	133,985 psi	
$C_{\theta h}$ =	0.0387	
$\sigma_{\theta eL} = \sigma_{heL}$ =	133,985 psi	
$C_{\phi\theta}$ =	0.1619	
$\sigma_{\phi\theta eL}$ =	548,683 psi	
Elastic Interaction Equations (-1713.1.1)		
σ_{xa} =	286,471 psi	
σ_{ha} =	52,394 psi	
σ_{ra} =	52,394 psi	
$\sigma_{\tau a}$ =	219,473 psi	
Axial + Shear ⇨ Check (c):	0.0008	<1 ∴ OK (see note*)
Hoop + Shear ⇨ Check (d):	0.1300	<1 ∴ OK
Inelastic Interaction Equations (-1714.2.1)		
σ_{xc} =	15,000 psi	
σ_{rc} =	14,730 psi	
$\sigma_{\tau c}$ =	9,000 psi	
Max(Axial,Hoop) ⇨ Check (a):	0.4616	<1 ∴ OK
Axial + Shear ⇨ Check (b):	0.1470	<1 ∴ OK
Hoop + Shear ⇨ Check (c):	0.5974	<1 ∴ OK

*Note: Elastic interaction checks (a), (b), (e), and (f) are not applicable.

Table 2.6-5 – NCT Free Drop Buckling Evaluation: Geometry and Loads

	Outer shell dimensions, inches	Applied stress, psi	
Inner Dia.	34.0	σ_φ	2,372
Outer Dia.	38.0	σ_θ	0
Length*	55.0	$\sigma_{\varphi\theta}$	0

* Bounding length used.

Table 2.6-6 – NCT Free Drop: N-284-2 Results

Parameter	Value	Remarks
Capacity Reduction Factors (-1511)		
$\alpha_{\phi L}$ =	0.2279	
$\alpha_{\theta L}$ =	0.8000	
$\alpha_{\phi\theta L}$ =	0.8000	
Plasticity Reduction Factors (-1610)		
η_{ϕ} =	0.0568	
η_{θ} =	0.0850	
$\eta_{\phi\theta}$ =	0.0232	
Theoretical Buckling Values (-1712.1.1)		
C_{ϕ} =	0.6050	
$\sigma_{\phi eL}$ =	1,831,806 psi	
$C_{\theta r}$ =	0.1150	
$\sigma_{\theta eL} = \sigma_{reL}$ =	348,340 psi	
$C_{\theta h}$ =	0.1078	
$\sigma_{\theta eL} = \sigma_{heL}$ =	326,534 psi	
$C_{\phi 0}$ =	0.2527	
$\sigma_{\phi\theta eL}$ =	765,157 psi	
Elastic Interaction Equations (-1713.1.1)		
σ_{xa} =	208,750 psi	
σ_{ha} =	130,614 psi	
σ_{ra} =	139,336 psi	
$\sigma_{\tau a}$ =	306,063 psi	
Axial + Shear ⇨ Check (c):	0.0114	<1 ∴ OK (see note*)
Hoop + Shear ⇨ Check (d):	0.0000	<1 ∴ OK
Inelastic Interaction Equations (-1714.2.1)		
σ_{xc} =	11,850 psi	
σ_{rc} =	11,850 psi	
$\sigma_{\tau c}$ =	7,110 psi	
Max(Axial,Hoop) ⇨ Check (a):	0.2002	<1 ∴ OK
Axial + Shear ⇨ Check (b):	0.2002	<1 ∴ OK
Hoop + Shear ⇨ Check (c):	0.0000	<1 ∴ OK

*Note: Elastic interaction checks (a), (b), (e), and (f) are not applicable.

2.7 Hypothetical Accident Conditions

When subjected to the hypothetical accident conditions (HAC) as specified in 10 CFR §71.73 [1], the BRR package meets the performance requirements specified in Subpart E of 10 CFR 71. This is demonstrated in the following subsections, where each accident condition is addressed and the cask shown to meet the applicable design criteria. The method of demonstration is primarily by analysis. The loads specified in 10 CFR §71.73 are applied sequentially, per Regulatory Guide 7.8 [3]. Resulting stresses are maintained below the limits established by Regulatory Guide 7.6 [2]. Dynamic testing of impact limiter performance is discussed in Section 2.12.3, *Certification Test Results*. A summary of cumulative damage is provided in Section 2.7.8, *Summary of Damage*.

2.7.1 Free Drop

Subpart F of 10 CFR 71 requires that a 30 ft free drop be considered. The free drop is to occur onto a flat, essentially unyielding, horizontal surface, and the cask is to strike the surface in an orientation for which maximum damage is expected. Several impact orientations and bounding ambient environments are considered. In order to minimize the number of specific analyses that must be performed, the worst case maximum cold drop impact loads are conservatively applied to the cask using material properties and allowables corresponding to maximum (warm) Normal Conditions of Transport (NCT) temperatures.

2.7.1.1 Impact Forces and Deformations

In Section 2.1.2.2, *Other Structures*, the design criteria of the impact limiters of the BRR Package includes the requirement to limit the free drop impact such that cask component stress and deflection criteria are met. The impact and deformation response of the impact limiters is evaluated and discussed in Appendix 2.12.5, *Impact Limiter Performance Evaluation*. This appendix also includes a comparison of the analysis results to the results obtained from the half-scale certification testing of the impact limiters. The tests are described in Appendix 2.12.2, *Certification Test Plan*, and in Appendix 2.12.3, *Certification Test Results*. The analysis results contributed to informing the choice of physical test orientations. The half-scale test impacts (tests D1, D2R, and D3) were all lower than predicted. The maximum predicted impact in full-scale is 86.8g for the secondary impact in the 15° oblique slapdown orientation. All of the calculations in this section utilize a bounding HAC impact of 120g, which is nearly 40% higher than the maximum result obtained from either test or analysis. Although no NCT tests were performed, the same conservative prediction techniques were used to set the bounding NCT impact at 40g, as described in Appendix 2.12.5, *Impact Limiter Performance Evaluation*.

The second design criterion of the impact limiters is to prevent "hard" contact of a rigid part of the cask with the ground due to excessive deformation of the foam. Since all of the certification testing was performed at the cold condition in order to obtain the maximum impact, the maximum crush deformation, which occurs at the maximum NCT hot temperature, could not be obtained directly from the testing. However, as the crush distances obtained from the half-scale test were found to be below the predicted cold case values, it is conservative not to adjust the predicted hot case crush distances downward. The maximum predicted hot case crush distance

occurs in the 15° oblique secondary impact event, and amounts to 15.9 inches, or 83.2% of the available crush distance. Not only is the majority of the foam in the limiter at a lower value of strain than this maximum value, the value is well within the range in which strain energy absorption is effective. The bounding bulk average foam temperature used for the analysis of 150 °F conservatively bounds the temperature predicted in the thermal analysis.

The final requirement is that the impact limiter structures and attachments to the cask maintain sufficient integrity subsequent to the HAC free drop and puncture drop events so that the containment O–ring seal is protected from excessive temperature in the subsequent HAC fire event. As documented in Appendix 2.12.3, *Certification Test Results*, while the original design did not meet this requirement, the final design of the attachment structures did meet it, as demonstrated by half-scale test. Section 2.7.1.7, *Impact Limiter Attachments*, shows that the final design is stronger than the successfully tested design. In addition, the worst–case damage to the impact limiter shells as a result of the puncture tests is fully accounted for in the thermal model, as discussed in Chapter 3, *Thermal Evaluation.*

For these reasons, the performance of the impact limiters is considered acceptable.

2.7.1.2 End Drop

The HAC end orientation free drop is evaluated using a combination of computer and manual calculations using an acceleration of 120g as discussed in Section 2.7.1.1, *Impact Forces and Deformations*. Stresses in the cask body are evaluated using the finite element model described in Appendix 2.12.4, *Stress Analysis Finite Element Models*. Both bottom down and top down impact orientations are considered. Including manual calculations, eight analyses of the HAC end drop are performed:

- Cask body stress
- Closure bolt stress
- Closure lid stress
- Lower closure plate weld stress
- Shield plug shell stress
- Buckling evaluation
- Lead slump evaluation
- Fuel basket stress is discussed in Section 2.7.1.5, *Basket Stress Analysis*.

Cask body stress. From Section 2.12.4.4.5, *Case No. 5, HAC Bottom-down End Drop*, the maximum stress intensity resulting from the bottom-down impact of 120g is 45,681 psi, located at the outside surface of the bottom end structure, as shown in Figure 2.12.4-10. The stress is linearized through the lower massive end structure cross section, Figure 2.12.4-11, and the maximum primary membrane stress is 22,680 psi. From Table 2.1-1, the limit on primary membrane stress is the lesser of $2.4S_m$ and $0.7S_u$, which for Type 304 cast or forged material (see Table 2.2-2) is $0.7S_u = 44,835$ psi at 250 °F. The margin of safety is:

$$MS = \frac{44{,}835}{22{,}680} - 1 = +0.98$$

The maximum membrane plus bending stress through the lower massive end structure cross section is 43,080 psi. The allowable membrane plus bending stress, from Table 2.1-1, is the lesser of $3.6S_m$ or S_u, which for Type 304 cast or forged material is S_u = 64,050 psi at 250 °F. The margin of safety is:

$$MS = \frac{64{,}050}{43{,}080} - 1 = +0.49$$

From Section 2.12.4.4.8, *Case No. 8, HAC Top-down End Drop*, the maximum stress intensity resulting from the bottom-down impact of 120g is 40,140 psi, located at the top of the inner shell, as shown in Figure 2.12.4-15. The stress is linearized through the inner shell cross section, Figure 2.12.4-16, and the maximum primary membrane stress is 22,720 psi. From Table 2.1-1, the limit on primary membrane stress is the lesser of $2.4S_m$ and $0.7S_u$, which for Type 304 cast or forged material (see Table 2.2-2) is $0.7S_u$ = 44,835 psi at 250 °F. The margin of safety is:

$$MS = \frac{44{,}835}{22{,}720} - 1 = +0.97$$

The maximum membrane plus bending stress through the inner shell cross section is 33,400 psi. The allowable membrane plus bending stress, from Table 2.1-1, is the lesser of $3.6S_m$ or S_u, which for Type 304 cast or forged material is S_u = 64,050 psi at 250 °F. The margin of safety is:

$$MS = \frac{64{,}050}{33{,}400} - 1 = +0.92$$

As shown, all cask body margins of safety for the HAC end free drop condition are positive.

Closure bolt stress. In the top–down orientation, the non–prying closure bolt load is calculated according to Section 4.6 of [10] using:

$$Fa = \frac{1.34\sin(xi)(DLF)(ai)(Wl + Wc)}{Nb} = 28{,}140 \text{ lb}$$

where the impact angle, xi = 90° for the end drop impact, the dynamic load factor, DLF = 1.05 as discussed below, the impact magnitude, ai = 120g for the HAC impact, the weight of the lid, Wl = 280 lb, and the weight of the contents, Wc = 1,720 lb[1] from Table 2.1-2, and the quantity of bolts, Nb = 12. Note that no support for the lid is assumed from the inner surface of the impact limiter.

The sum of all applied loads (the HAC free drop load of 28,140 lb plus the load due to the design pressure, equal to 789 lb as determined in Section 2.6.1.5, *Closure Bolts*) is equal to 28,140 + 789 = 28,929 lb. This value exceeds the preload of 19,200 lb. The average tensile stress is:

$$Sba = 1.2732\frac{Fa}{Dba^2} = 47{,}779 \text{ psi}$$

[1] This weight consists of the shield plug plus the heaviest basket/fuel combination.

where the value of Dba was computed as 0.878 inches in Section 2.6.1.5, *Closure Bolts*. From Table 2.1-1, the allowable average tensile stress intensity for HAC is the lesser of $0.7S_u$ or S_y, which for the ASTM A320 L43 bolting material is $0.7S_u = 87{,}500$ psi at 250 °F. The margin of safety is:

$$MS = \frac{87{,}500}{47{,}779} - 1 = +0.83$$

The dynamic load factor (DLF) used in this section and in Section 2.6.7.1, *NCT End Free Drop*, is calculated using NUREG/CR–3966 [26] (this quantity is called the DAF in that document). In Section 2.2.3 of [26], an estimated impact pulse duration is developed assuming a constant impact acceleration:

$$t_1 = \frac{Mv_o}{F_{max}}$$

This equation, however, underestimates the duration of a varying pulse such as a sinusoidal pulse, which is the closest shape to an actual, measured pulse. For a sinusoidal pulse, from Newton's Second Law:

$$F = Ma = MA\sin\omega t$$

The area under the pulse is the total change in velocity. Since the impact velocity is v_o, and the package comes to a complete stop during impact, the change in velocity is simply v_o. This can be written:

$$v_o = A\int_0^{\pi}\sin\omega t dt = -\frac{A}{\omega}\cos\omega t\Big|_0^{\pi} = \frac{2A}{\omega}$$

From this,

$$\omega = \frac{2A}{v_o}$$

Since the pseudo–frequency of the pulse is a full sine wave (two pulse lengths), the pulse length is equal to:

$$t_1 = \frac{T_1}{2} = \frac{1/f}{2} = \frac{2\pi/\omega}{2} = \frac{\pi}{\omega}$$

Substituting from above,

$$t_{1\text{-HAC}} = \frac{\pi v_o}{2A} = \frac{828.6}{A}$$

where v_o is the impact speed for a 30–foot free drop of 527.5 in/s. Parameter A is the acceleration, in/s^2. For the bounding impact acceleration of 120g, equivalent to A = 46,368 in/s^2, the pulse length of the sinusoidal impact time history is $t_{1\text{-HAC}} = 0.018$ s, which compares well with the duration of the end drop impact pulse accelerometer traces shown in Section 2.12.3.7, *Accelerometer Plots*.

For the NCT impact, the impact velocity for the two foot free drop is 136.2 in/s, and the bounding impact is 40g. The corresponding impact pulse length is:

$$t_{1\text{-NCT}} = \frac{\pi v_o}{2A} = 0.014\text{ s}$$

The frequency of the closure lid is found using [25], Table 36, Case 11a. The lowest mode frequency for a flat circular plate, assuming a simply supported edge, is found from:

$$f = \frac{K_n}{2\pi}\sqrt{\frac{Dg}{wr^4}} = 650 \text{ Hz}$$

where $K_1 = 4.99$, $g = 386.4$ in/s^2, and the lid bolt radius, $r = 11.38$ inches. Since from Table 2.1-2, the weight of the lid, $W = 280$ lb and the area, $A_{lid} = \pi r^2 = 406.9$ in^2, the weight per unit area, $w = W/A_{lid} = 0.688$ psi. Parameter D is found from:

$$D = \frac{Et^3}{12(1-\upsilon^2)} = 20.0(10^6)\text{in} - \text{lb}$$

where $E = 27.3(10^6)$ psi for Type 304 steel at 250 °F, $\nu = 0.3$, and the thickness, $t = 2.0$ inches. The period of the lid is equal to 1/f, or $T = 1/650 = 0.00154$ s. The amplification factor for a half sine wave is given in Figure 2-15 of [26]. The abscissa of the figure is the ratio t_1/T. The smallest value of the ratio occurs in the NCT impact, where $t_{1\text{-NCT}} = 0.014$ s:

$$\frac{t_{1-NCT}}{T} = 9.09$$

This value exceeds the range shown in the figure. The corresponding ratio for HAC, where t_1 equals 0.018 s, is even larger. As the curve is clearly tending toward unity, it is concluded that the DLF may be conservatively bounded by a value of 1.05 for both NCT and HAC.

Closure lid stress. In the top–down drop orientation, the closure lid supports both the contents weight and its self–weight against the impact load of 120g. The lid is a solid, 2–inch thick plate made of Type 304 stainless steel. The outer diameter of the lid will be taken as the bolt circle, since that is the location of the step (see Section 2.6.1.5, *Closure Bolts*, for a discussion of the lid step). The bolt circle diameter is 22.75 inches. The self–weight of the lid is 280 lb, and the maximum contents weight is 1,720 lb (including the shield plug and the maximum basket/fuel weight), from Table 2.1-2. The total weight is 1,720 + 280 = 2,000 lb. For an impact of 120g, the total force applied to the lid is 2,000 × 120 = 240,000 lb. From above, the area of the lid, $A_{lid} = 406.9$ in^2.

The lid will be considered as uniformly loaded. This is somewhat conservative, since the shield plug is very stiff, and will consequently shift some of the load toward the edges of the lid, lessening the bending stress. In addition, the internal design pressure is 25 psig. The uniform load is:

$$q = \frac{240{,}000}{A_{lid}} + 25 = 614.8 \text{ psi}$$

From [25], Table 24, Case 10a for a simply supported, uniformly loaded plate, the bending moment is:

$$M = \frac{qa^2(3+\upsilon)}{16}\text{DLF} = 17{,}243 \text{ in} - \text{lb/in}$$

where the radius, $a = 22.75/2 = 11.38$ inches, $\nu = 0.3$, and the dynamic load factor, DLF = 1.05 as discussed above. The stress is:

$$\sigma = \frac{6M}{t^2} = 25{,}865 \text{ psi}$$

where the plate thickness, t = 2.0 inches. The allowable membrane plus bending stress, from Table 2.1-1, is the lesser of $3.6S_m$ or S_u, which, from Table 2.2-1, is equal to 68,600 psi for ASTM A240, Type 304 at 250 °F. The margin of safety is:

$$MS = \frac{68{,}600}{25{,}865} - 1 = +1.65$$

Thus, the allowable stress is satisfied for the closure lid in the HAC end drop.

As noted in Section 2.1.2.1, *Containment and Criticality Control Structures*, a stress intensity in the cask closure region (such as the closure lid) which could affect compression of the containment O-ring seal is limited to the lesser of the Table 2.1-1 allowable, or the yield strength. For ASTM A240, Type 304 at 250 °F, the yield strength from Table 2.6-1 is 23,700 psi. The calculated value of stress exceeds the yield stress by approximately 5%. However, as noted above, the calculation is conservative, and the impact magnitude of 120g is very conservative. As found in Table 2.12.5-11, the actual calculated end drop impact is 74.4g, which bounds an even lower actual impact recorded in the certification testing. Therefore it is evident that the actual stress in the closure lid is well below the yield stress of the lid material.

Lower closure plate weld stress. In the bottom–down drop orientation, the lower closure plate supports both the lower lead shield hydrostatic pressure and its self–weight against the impact load of 120g. The closure plate is a solid, 1–inch thick plate made of Type 304 stainless steel. The outer diameter of the plate is d = 24.5 inches and connected by a full penetration weld to the adjacent massive end structure. The area of the closure plate is:

$$A_{cp} = \frac{\pi}{4} d^2 = 471.4 \text{ in}^2$$

The self–weight of the closure plate is:

$$W_{cp} = A_{cp} \rho_{ss} = 136.7 \text{ lb}$$

where the density of steel is $\rho_{ss} = 0.29$ lb/in^3. The weight of the lower lead is modeled as two separate hydrostatic loads based the inner and outer lead depths above the upper surface of the closure plate (see Section 2.12.4.2.2, *Free Drop Impact Loads*). The maximum hydrostatic pressure will be conservatively applied to the entire plate. The hydrostatic force is:

$$F = \rho \cdot h \cdot A_{cp} = 1{,}488.2 \text{ lb}$$

where the maximum depth of the lead column, h = 7.7 inches and the density of lead is 0.41. The total weight is 1,488.2 lb + 136.7 lb = 1,624.9 lb. For an impact of 120g, the total force applied to the closure plate is 1,624.9 × 120 = 194,988 lb.

Conservatively the closure plate will be considered as uniformly loaded. The uniform load is:

$$q = \frac{194{,}988}{A_{cp}} = 413.6 \text{ psi}$$

From [25], Table 24, Case 10b for a fixed edge, uniformly loaded plate, the maximum bending moment at the edge of the plate is:

$$M = \frac{qa^2}{8} DLF = 8{,}146 \text{ in} - \text{lb/in}$$

where the radius, a = 24.5/2 = 12.25 inches and the dynamic load factor, DLF = 1.05 as discussed above. The stress is:

$$\sigma = \frac{6M}{t^2} = 48{,}876 \text{ psi}$$

where the plate thickness, t = 1.0 inches. The shear stress at the fixed end of the closure plate is:

$$\tau = \frac{194{,}988}{24.5\pi t} DLF = 2{,}660 \text{ psi}$$

The maximum stress intensity is determined by combining the component stresses using Mohr's circle as follows:

$$SI = \sqrt{\sigma^2 + 4\tau^2} = 49{,}165 \text{ psi}$$

The allowable membrane plus bending stress found above is equal to 68,600 psi for ASTM A240, Type 304 at 250 °F. The margin of safety is:

$$MS = \frac{68{,}600}{49{,}165} - 1 = +0.40$$

Thus, the allowable stress is satisfied for the closure plate in the HAC end drop.

Shield plug shell stress. In a bottom–down end drop, the shield plug lead will be supported by the lower plate of the shield plug shell. The one–inch thick plate is 15.8 inches in diameter and connected by a complete joint penetration weld to the adjacent cylindrical shell. The weight of the lead in the shield plug, plus the self–weight of the lower steel plate, will be conservatively bounded by utilizing the weight of the full shield plug, from Table 2.1-2, of 950 lb. To simplify the calculation, the lead will be treated very conservatively as a liquid. The entire weight of 950 lb will therefore be applied as a pressure to the plate inner surface.

The area of the plate is:

$$A_p = \frac{\pi}{4} 15.8^2 = 196.1 \text{ in}^2$$

For the end drop impact of 120g, the total loading per unit area of the plate is:

$$q = \frac{950 \times 120}{A_p} = 581.3 \text{ psi}$$

It will be further conservatively assumed that the plate has a simply supported edge. From [25], Table 24, Case 10a, the maximum moment at the center of the plate is:

$$M_c = \frac{qa^2(3+\upsilon)}{16} DLF = 7{,}856.7 \text{ in} - \text{lb/in}$$

where the plate radius, a = 15.8/2 = 7.9 inches and the DLF is defined as equal to 1.05 above. The maximum stress is:

$$\sigma_c = \frac{6M_c}{t^2} = 47{,}140 \text{ psi}$$

where the thickness, t = 1 inch. The allowable membrane plus bending stress found above is equal to 68,600 psi for ASTM A240, Type 304 at 250 °F. The margin of safety is:

$$MS = \frac{68{,}600}{47{,}140} - 1 = +0.46$$

The side wall and weld are checked by establishing moment equilibrium between the bottom plate and cylindrical shell, solving for the common moment, and calculating the stress. The direct tension stress is also added.

The slope at the outer edge of the bottom plate is the sum of the slope of a simply supported plate with a pressure load q, and the slope from a restoring moment, M_o, applied in the opposite direction by the cylindrical shell. The pressure load causes the plate to deflect downward, and the moment causes it to deflect upward. The slope due to the pressure load, θ_d (see [25], Table 24, Case 10a) is:

$$\theta_d = \frac{qa^3}{8D_p(1+\upsilon)}$$

The slope due to the moment load (see [25], Table 24, Case 13a, for $r_o = a$) is:

$$\theta_m = K_\theta \frac{M_o a}{D_p}$$

The parameter D_p is:

$$D_p = \frac{Et_p^3}{12(1-\upsilon^2)} = 2.5(10^6) \text{ in} - \text{lb}$$

where $E = 27.3(10^6)$ psi, $\nu = 0.3$, and the plate thickness, $t_p = 1.0$ inches. The sum of these two slopes is:

$$\theta_d + \theta_m = 0.0098 - 2.338(10^{-6})M_o$$

where the lead hydrostatic pressure, q = 581.3 psi, the radius to the meridion of the cylindrical shell, a = 7.6 inches, and $K_\theta = -0.76923$.

The corresponding slope of a cylindrical shell under the action of an end moment is found from [25], Table 29, Case 3, as:

$$\theta_w = \frac{M_o}{D_w \lambda} \frac{C_{12}}{C_{11}}$$

Note that the notation for the slope has substituted θ for ψ for consistency. In addition, the sign value of the slope has been redefined to be opposite to that given in the introduction to Table 29 [25], thus, the negative sign has been omitted from the equation. The parameter λ is:

$$\lambda = \left[\frac{3(1-\upsilon^2)}{R^2 t_w^2}\right]^{1/4} = 0.602$$

where R = a = 7.6 inches, and the thickness of the cylindrical wall, t_w = 0.6 inches. The parameter D_w is:

$$D_w = \frac{Et_w^3}{12(1-\upsilon^2)} = 5.4(10^5)\text{in} - \text{lb}$$

Since the length of the lower cylindrical shell is L = 5 inches, the parameter λL is 3.01 inches. Parameters C_{12} and C_{11} are essentially identical, so their ratio is unity. The slope of the shell can now be evaluated as:

$$\theta_w = \frac{M_o}{D_w\lambda}\frac{C_{12}}{C_{11}} = 3.076(10^{-6})M_o$$

Setting $\theta_w = \theta_d + \theta_m$,

$$3.076(10^{-6})M_o = 0.0098 - 2.338(10^{-6})M_o$$

Solving, M_o = 1,810.1 in–lb/in. The stress in the cylindrical shell is:

$$\sigma_m = \frac{6M_o}{t_w^2}\text{DLF} = 31{,}677\text{ psi}$$

To this stress, the direct tension stress is added. The area of the weld to the cylindrical shell is:

$$A_s = \frac{\pi}{4}(\text{OD}^2 - \text{ID}^2) = 28.65\text{ in}^2$$

where the shell outer diameter, OD = 15.8 inches and the inner diameter, ID = 14.6 inches. The direct stress is therefore:

$$\sigma_D = \frac{950\times120}{A_s}\text{DLF} = 4{,}178\text{ psi}$$

The stress sum in the weld is:

$$\sigma_{Sum} = \sigma_m + \sigma_D = 35{,}855\text{ psi}$$

For a full penetration weld, the allowable stress is the same as determined above. The margin of safety is:

$$\text{MS} = \frac{68{,}600}{35{,}855} - 1 = +0.91$$

Thus, the allowable stress is satisfied for the shield plug lower plate stress and lower plate weld stress in the HAC end drop.

Buckling evaluation. In the end drop orientation, the outer shell will carry most of the axial loads due to its much greater stiffness compared to the inner shell. Therefore, end drop buckling analysis may be conservatively performed by considering only the outer shell. The outer shell, which is cooler than the inner shell, is subject to tensile thermal stress, but for the buckling evaluation, the thermal stress on the outer shell is conservatively neglected. Since the inner shell is neglected, lead shrinkage pressure, which only affects the inner shell, is not considered. The maximum cold HAC impact of 120g is conservatively applied along with the bounding hot temperature case of 250 °F.

The only applied stress is axial, and assumes a bottom–down end drop configuration, for which the weight supported by the outer shell is larger than for the top–down case. The total weight

supported by the outer shell is the sum of the total cask body (25,400 lb), less the side lead and bottom lead (see below), the closure lid (280 lb), the shield plug (950 lb), and the upper impact limiter (2,300 lb). Weight values are taken from Table 2.1-2.

The weights for the side and bottom lead are calculated using a lead density of 0.41 lb/in^3. The side lead has an outer diameter of 34.0 inches (outer shell ID), an inner diameter of 18.0 inches (inner shell OD), and a lower–bound length (cylindrical length only) of 55.0 inches. The conservatively underestimated weight of the side lead is:

$$W_{PbS} = \frac{\pi}{4}\left(34.0^2 - 18.0^2\right)(55.0)(0.41) = 14{,}735 \text{ lb}$$

The bottom lead has a large diameter of 23.7 inches and a length of 4.2 inches, and a small diameter of 10.3 inches and a length of 3.5 inches. The weight of the bottom lead is:

$$W_{PbB} = \frac{\pi}{4}\left[\left(23.7^2\right)(4.2) + \left(10.3^2\right)(3.5)\right](0.41) = 879 \text{ lb}$$

Conservatively, the bottom lead weight will be underestimated by 100 lb, so that W_{PbB} = 779 lb. The total weight supported by the outer shell is therefore:

$$W_{tot} = 25{,}400 - 14{,}735 - 779 + 280 + 950 + 2{,}300 = 13{,}416 \text{ lb}$$

The weight used is conservative, since it underestimates the removed weight of the side lead and bottom lead, and includes the lower end structure as part of the cask body weight, even though it is not supported by the outer shell. The cross sectional area of the outer shell is:

$$A_{OS} = \frac{\pi}{4}\left(38.0^2 - 34.0^2\right) = 226.2 \text{ in}^2$$

The axial stress is:

$$\sigma_\phi = \frac{W_{tot}}{A_{OS}}(120) = 7{,}117 \text{ psi}$$

No other stresses are applied in the end drop. Shell dimensions are taken from Table 2.7-1. The factor of safety is equal to 1.34, consistent with Code Case N–284–2 for HAC. The results are shown in Table 2.7-2. As shown, all interaction parameters, including the maximum value of 0.4024 are less than unity, as required. Therefore, buckling of the cask shells in the HAC free drop will not occur.

Lead Slump. In the end drop, impact forces act on the lead gamma shield which could cause a reconfiguration of the lead in the direction of impact. As shown in the evaluation of the cask body stress above, the steel shells which enclose the lead will not significantly deform, but the lead could experience flow strains causing a gap to appear at the upper surface of the lead. In the following analysis, the lead is conservatively treated as a fluid, having no resistance to flow from impact forces. The lead will therefore occupy the lower portion of the volume available within the lead cavity. The difference between the cavity volume and the lead volume defines the maximum possible gap at the top of the lead. Of note, since the shield plug and bottom lead shield are installed manually, using small scraps and lead wool hammered into place to fill all cavities, lead slump cannot occur. The following analysis applies only to the side cavity in which lead is poured in the molten state.

The amount of lead installed in the side cavity of the BRR cask body is assumed to correspond to the volume of the cavity at the point of solidification of the lead of 620 °F. At this point, there is no difference between the volume of the cavity and the volume of the lead. As the cask cools to the minimum HAC temperature of -20 °F, the lead will shrink more than the cavity due to the greater thermal expansion coefficient of lead than steel, generating a volume difference. Assuming the lead behaves as a fluid in the end drop concentrates this volume difference at one end or the other of the cask cavity, which constitutes the lead slump gap. This gap is further evaluated in Chapter 5, *Shielding Evaluation.*

To simplify calculations, the side lead shield is assumed to have a fully rectangular cross section, i.e., the lead cavity is assumed to have square corners at the full length. This simplification does not have a significant affect on the calculation. The lead cavity at the assumed fabrication temperature of 70 °F has an inner diameter of 18 inches (the inner shell OD), an outer diameter of 34 inches (the outer shell ID), and a length of 60.9 inches. The volume therefore is:

$$V_{CAV-RT} = \frac{\pi}{4}\left(34^2 - 18^2\right)60.9 = 39{,}795\ \text{in}^3$$

It will be convenient to define a volumetric expansion relation. Note that, for a general case:

$$V_C = L_C^3$$

$$L_H = L_C(1 + \alpha\Delta T)$$

where V_C and L_C are the original (cold state) volume and length, respectively, L_H is the expanded (hot) length, and α and ΔT are the thermal expansion coefficient and the change in temperature, respectively. Since the expanded (hot) volume is:

$$V_H = L_H^3 = L_C^3(1 + \alpha\Delta T)^3,$$

Then:

$$V_H = V_C(1 + \alpha\Delta T)^3$$

From Table 2.2-4, the thermal expansion coefficient of steel between 70 °F and 620 °F is $\alpha_{s620} = 9.84(10^{-6})$in/in/°F. The lead cavity and lead volumes at the lead solidification temperature are then:

$$V_{CAV620} = V_{L620} = V_{CAV-RT}\left(1 + \alpha_{s620}\Delta T_{70-620}\right)^3 = 40{,}445\ \text{in}^3$$

Next, calculate the volume of the lead at 70 °F and at -20 °F. This must be done in two steps because the thermal expansion coefficients are referenced to 70 °F. The thermal expansion of lead between 620 °F and 70 °F is $\alpha_{L620} = 20.4(10^{-6})$in/in/°F, and between 70 °F and -20 °F is $\alpha_{L\text{-}20} = 15.7(10^{-6})$in/in/°F, as shown in Table 2.2-4.

$$V_{L-RT} = V_{L620}\left(1 - \alpha_{L620}\Delta T_{620-70}\right)^3 = 39{,}099\ \text{in}^3$$

$$V_{L-20} = V_{L-RT}\left(1 - \alpha_{L-20}\Delta T_{70--20}\right)^3 = 38{,}933\ \text{in}^3$$

The volume of the cavity at -20 °F, utilizing the thermal expansion coefficient between 70 °F and -20 °F of $\alpha_{s\text{-}20} = 8.2(10^{-6})$in/in/°F, is:

$$V_{CAV-20} = V_{CAV-RT}\left(1-\alpha_{s-20}\Delta T_{70--20}\right)^3 = 39{,}707\ \text{in}^3$$

The difference in volume between the cavity and the lead at the HAC free drop temperature of -20 °F is:

$$\Delta V_{-20} = V_{CAV-20} - V_{L-20} = 774\ \text{in}^3$$

The volume of the cavity per inch of length is:

$$\Delta V_{/in} = \frac{\pi}{4}\left(34^2 - 18^2\right) = 653\ \text{in}^3/\text{in}$$

The lead slump dimension (the gap between the top of the lead cavity and the top of the lead) therefore has a bounding value of:

$$x_{slump} = \frac{\Delta V_{-20}}{\Delta V_{/in}} = 1.185\ \text{in}$$

This value is conservative since it takes no credit for any resistance to flow of the lead material. The effect of this gap is evaluated in Chapter 5, *Shielding Evaluation.*

2.7.1.3 Side Drop

The HAC side orientation free drop is evaluated using the finite element model described in Appendix 2.12.4, *Stress Analysis Finite Element Models*, and an acceleration of 120g as discussed in Section 2.7.1.1, *Impact Forces and Deformations.*

From Section 2.12.4.4.11, *Case No. 11, HAC Side Drop*, the maximum stress intensity resulting from the side drop impact of 120g is located at the bottom outside edge of the lower lead cavity as shown in Figure 2.12.4-21. The stress is linearized through the lower closure plate cross section, Figure 2.12.4-22, and the maximum primary membrane stress is 16,330 psi. From Table 2.1-1, the limit on primary membrane stress is the lesser of $2.4S_m$ and $0.7S_u$, which for Type 304 cast or forged material is $0.7S_u$ = 44,835 psi at 250 °F. The margin of safety is:

$$MS = \frac{44{,}835}{16{,}330} - 1 = +1.75$$

The maximum membrane plus bending stress resulting through the lower closure plate cross section is 51,990 psi. The allowable membrane plus bending stress, from Table 2.1-1, is the lesser of $3.6S_m$ or S_u, which for Type 304 cast or forged material is S_u = 64,050 psi at 250 °F. The margin of safety is:

$$MS = \frac{64{,}050}{51{,}990} - 1 = +0.23$$

As shown, all cask body margins of safety for the HAC side drop condition are positive.

2.7.1.4 Oblique Drop

For the HAC free drop, the BRR package can strike the ground in any primary orientation. As shown in the following discussion, the cask stresses for all oblique drop orientations are conservatively bounded by the side drop (horizontal) orientation when performed using an impact of 120g. This evaluation is based on the axial, shear, and moment forces in the cask

shells as derived in NUREG/CR–3966 [26]. It is shown that, for the specific impact forces developed in the HAC oblique free drops, the cask shell stress intensity is governed by the side drop case.

In Section 2.2 of [26], the maximum axial force, R, shear force, V, and bending moment, M, in the cask shells are given for the primary oblique impact as:

$$R_p = F_p \sin(\theta)$$

$$V_p = F_p \cos(\theta)$$

$$M_p = (4/27)\, F_p L \cos(\theta)$$

where the subscript p indicates the primary impact event, L is the overall length of the cask, θ is the primary impact angle with respect to the horizontal, and F_p is the maximum primary impact limiter force. For the subsequent secondary (slapdown) impact, the maximum values of the above parameters are:

$$R_s = 0$$

$$V_s = F_s$$

$$M_s = (4/27)\, F_s L$$

where the subscript s indicates the secondary impact event, and F_s is the maximum secondary impact limiter force. In the horizontal side drop impact, the maximum values of the above parameters are:

$$R_h = 0$$

$$V_h = F_h$$

$$M_h = (1/4)\, F_h L$$

where the subscript h indicates the horizontal case, and F_h is the maximum impact limiter force in the side drop. The cask shell stresses resulting from these applied forces and moments can be calculated as follows:

$$\sigma_a = \frac{R_i}{A}$$

$$\tau = \frac{V_i}{A}$$

$$\sigma_b = \frac{M_i c}{I}$$

where σ_a is the axial stress, τ the shear stress, and σ_b the bending stress in the cask shells, and where A is the cross sectional area of the cask shells, and I is the moment of inertia. The maximum stress intensity in the cask shells is determined by combining the component stresses using Mohr's circle as follows:

$$SI = \frac{\sigma_a + \sigma_b}{2} \pm \sqrt{\left(\frac{\sigma_a + \sigma_b}{2}\right)^2 + \tau^2}$$

For purposes of comparison, it is only necessary to consider one shell, for example, the inner shell. The cross sectional area of the inner shell is

$$A = (\pi/4)\left(d_o^2 - d_i^2\right) = 53.4\ \text{in}^2$$

and the moment of inertia is

$$I = (\pi/64)\left(d_o^4 - d_i^4\right) = 1{,}936\ \text{in}^4$$

where d_o = 18.0 inches and d_i = 16.0 inches. The parameter c = 18.0/2 = 9.0 inches, and the length between the center of the cylindrical portion of each impact limiter is L = 70 inches.

The maximum force on each impact limiter in the HAC 30 ft, horizontal side drop for the bounding impact value of g_h = 120g and an overall cask weight of W = 32,000 lb is:

$$F_h = \frac{Wg_h}{2} = 1.920(10^6)\text{lb}$$

The worst case oblique free drop is the shallow–angle side slapdown orientation at a primary impact angle of 15°, as discussed in Appendix 2.12.5, *Impact Limiter Performance Evaluation.* The primary and secondary impact limiter forces are found using the calculated maximum deformation at cold conditions and the force-deflection curves corresponding to the impact orientation. From Table 2.12.5-11, the maximum primary deformation for the 15° impact case is 10.7 inches, and from Table 2.12.5-12, the maximum secondary deformation is 12.1 inches. From Figure 2.12.5-4 (primary impact at 15°), the maximum crush force at the primary deformation of 10.7 inches is bounded by a value of 1,049,000 lb, and from Figure 2.12.5-3 (secondary impact, taken at 0°), the maximum crush force at the secondary deformation of 12.1 inches is bounded by a value of 1,220,000 lb.

The resulting cask shell forces and maximum combined stress intensities are shown in Table 2.7-3. Since only the inner shell properties are used, the stress intensity is relative, and is used for comparison between the different cases only. The stress values in the table therefore do not represent actual inner shell stress intensity. As shown, the stress intensity is greatest in the horizontal side drop case at the bounding value of 120g. Since, according to Section 2.7.1.1, *Impact Forces and Deformations*, the actual impacts are lower than the calculated values, the difference between the actual loading in the oblique impacts and the bounding side drop is even greater. Therefore, the side drop stress analyses, detailed in Section 2.7.1.3, *Side Drop*, are enveloping for all oblique drop orientations.

2.7.1.5 Fuel Basket Stress Analysis

Each of the four fuel baskets is evaluated for structural integrity in the governing free drop orientations of end and side. The maximum cold impact acceleration of 120g is used, but conservatively the material allowable stresses are evaluated at the maximum NCT temperature of 400 °F. Allowable stresses are taken from Table 2.1-1. Each basket is analyzed for several modes of failure which are applicable to its design, including bending, weld shear, and buckling. Bounding weights for the baskets and fuel are given in Table 2.1-3.

The smallest margin of safety of any of these evaluations is +0.12, for the shear load on the TRIGA basket spacer pedestal screw. All of the evaluations and corresponding margins of safety are summarized in Table 2.7-4. The analysis details are provided in Appendix 2.12.8, *Fuel Basket Stress Analysis*. Therefore, the BRR package fuel baskets are adequate to support the fuel in all HAC free drops.

In the HAC side drop impact orientation, the fuel baskets apply a load to the inside of the inner shell. The heaviest basket is for MURR fuel, but this basket has no ribs and the load is well distributed. The next-heaviest basket, for ATR fuel (650 lb), has four ribs. The top rib is a 0.5-inch thick plate with a 0.19-inch chamfer, for a land width of 0.31 inches. The middle two ribs are made from 0.38-inch thick plate with 0.19-inch chamfers, for a land width of 0.19 inches each. The lowest rib is made from 0.50-inch thick plate with a 0.13-inch step and a 0.19-inch chamfer, for a land width of 0.18 inches. The diameter of each rib is 15.63 inches. The projected bearing area of the ribs against the inner shell is:

$$A = 15.63(0.31 + 0.19 + 0.19 + 0.18) = 13.60 \text{ in}^2$$

The side load, using the bounding side drop impact of 120g, is:

$$P = 650(120) = 78{,}000 \text{ lb}$$

The bearing stress is:

$$\sigma = \frac{P}{A} = 5{,}735 \text{ psi}$$

The MITR-II basket, with a loaded weight of 640 lb, is nearly the same weight as the ATR. But, as in the case of the MURR basket, the weight of the basket is well distributed to the interior wall of the cask; primarily over the area of the massive weldment with the minor addition of the pedestal support ring.

The TRIGA basket is considerably lighter than the other three baskets and not bounding. At the bounding fuel basket temperature of 400 °F, the minimum yield strength of the inner shell material, from Table 2.2-2, is 20,700 psi. Since this stress is over three times larger than the bearing stress, bearing yield of the basket ribs or of the inner shell will not occur.

2.7.1.6 Fuel Impact Deformation

During the end drop, the fuel elements may experience a separate, internal impact with the cask or basket structures. This impact could occur if, during the period of package free fall, the fuel was in contact with the upper end of its cavity, which would be possible due to the zero–g environment of free fall. When the package strikes the ground, the velocity of the cask would begin to decrease, but the fuel would continue to fall freely until impact with the lower end occurred. When the gap between the fuel and the cask was traversed, the fuel would hit the cavity end. The fuel would have the full free drop velocity, v_o, but the cask cavity would be traveling in the same direction with a lower velocity. See Figure 2.7-1.

To simplify calculations, it will be conservatively assumed that, at the moment of impact with the fuel, the cask inner contact surface is motionless and unyielding. Further, it will be assumed that the deceleration of the package during the period of fuel traversing the gap is constant and equal to the maximum bounding deceleration of 120g. The fuel will therefore experience an equivalent free drop. This analysis will determine the magnitude of the free drop impact and determine the effect on the fuel elements.

At the moment of impact with the ground, both the cask and fuel have a velocity of v_o. The cask immediately begins to decelerate according to:

$$v(t) = at + v_o$$

The distance the cask travels until the moment of impact with the fuel is:

$$x_c = a\int_0^T t\,dt = \frac{1}{2}at^2 + v_o t\Big|_0^T = \frac{1}{2}aT^2 + v_o T$$

where T is the time of fuel impact, and $x_c = 0$ at $t = 0$ (the time of package impact). Note that during time T, the fuel has traveled the distance the cask has traveled, plus the initial gap between the fuel and cask. Alternately, it can be stated that the fuel has traveled $v_o T$, since its velocity is unchanged during this interval. Therefore:

$$x_c + GAP = v_o T, \quad \text{or}$$
$$x_c = v_o T - GAP$$

Substituting this into the formula for x_c above,

$$x_c = \frac{1}{2}aT^2 + v_o T = v_o T - GAP$$

Simplifying,

$$T = \left(\frac{-2GAP}{a}\right)^{1/2}$$

Since the difference in velocity between the fuel and the cask at time T is equal to the decay in velocity over the interval, equal to (aT), the difference can be written as:

$$\Delta v = aT = a\left(\frac{-2GAP}{a}\right)^{1/2} = (-2aGAP)^{1/2}$$

(Note that since the acceleration is negative (deceleration), the quantity under the square root will be positive.) The energy associated with a change in velocity, Δv, is equivalent to the energy of a free drop height, h. Since:

$$h = \frac{\Delta v^2}{2g_g}$$

then the equivalent free drop height of the fuel element in the BRR package impact is:

$$h = \bar{g}GAP$$

where g_g is the acceleration due to gravity, and the deceleration in g–units, $\bar{g} = a/g_g = 120g$. The energy to be dissipated during the impact of the fuel is equal to Wh, or:

$$E = W\bar{g}GAP$$

where W is the weight of a fuel element. If this energy is absorbed in the fuel structure by volumetric plastic flow, the energy absorbed is related to the volume of flow according to:

$$E = V\sigma_f$$

where σ_f is the flow stress of the material, equal to the average of the yield and ultimate tensile strengths. Solving this for the volume,

$$V = \frac{W\bar{g}GAP}{\sigma_f}$$

Since the material flow is assumed to occur on the fuel cross section, the deformation length is equal to the volume divided by the cross–sectional area of the fuel element, $L = V/A_{xc}$, or:

$$L = \frac{W\bar{g}GAP}{\sigma_f A_{xc}}$$

This formula will be evaluated for the bounding fuel case. The fuel is made from 6061–T6 aluminum material. From the ASME B&PV Code, Section II, Part D, Table Y–1, the yield strength at a temperature of 400 °F is equal to 13.3 ksi. Since this material does not appear in Table U, an ultimate tensile strength at temperature is not readily available. Conservatively, the yield strength will be used for the flow strength as defined above. Therefore, σ_f = 13,300 psi.

The total gap value, GAP, consists of a) the free space between the fuel element and the basket cavity length, plus b) the difference between the cask cavity and the basket length. Parameter a), denoted as L_{FB}, is calculated by subtracting the fuel length from the basket cavity length, and is listed in Table 2.7-5. Parameter b) is found by subtracting the basket length (equal to 53.45 inches in all cases) from the cask cavity length of 54.0 inches, and is equal to 0.55 inches. The total fuel gap is therefore:

$$GAP = L_{FB} + 0.55$$

Due primarily to its larger gap and weight, the ATR fuel is the governing case. The maximum deformation length of any fuel element is therefore:

$$L = \left(\frac{W}{A_{xc}}\right)\frac{\bar{g}GAP}{\sigma_f} = 0.096 \text{ inches}$$

The fuel bounding weights, cross–sectional areas, and W/A_{xc} ratios are presented in Table 2.7-5. The bounding fuel weights are taken from Table 2.1-3. The areas are calculated from CAD drawings of the fuel active region cross section, and do not consider the end structures. The end structures are considered sacrificial since a) they do not contain any fissile material and b) the criticality analysis discussed in Section 6.3.1 does not model the end structures, and determines the most reactive axial position of the active length of the fuel as if the end structures were absent. Since the fuel end structures do not serve a safety function, they are ignored in the axial deformation analysis.

This maximum deformation length, which is just below $1/10^{th}$ of an inch, is negligible from a structural, shielding, or criticality perspective. Therefore fuel behavior in the HAC end drop is acceptable.

2.7.1.7 Impact Limiter Attachments

As reported in Appendix 2.12.3, *Certification Test Results*, the initial design of the impact limiter attachments was not adequate, since they did not securely retain the primary impact limiter in the 15° oblique slapdown free drop impact. The redesigned attachments are shown in the drawings in Appendix 1.3.3, *Packaging General Arrangement Drawings*. One half-scale certification test limiter was refurbished, as far as possible, to incorporate the revised design and retested to

confirm its adequacy. The attachment load path of the refurbished test article, when converted to full-scale, was conservatively less strong than the revised design, as shown by the comparison shown in Table 2.7-6. Note: in the table, the blade is the attachment component integral to the impact limiter, and the receptacle is the pair of plates, attached to the cask, that accept the blade.

As detailed in Section 2.12.3.6, *Confirmatory Test of Attachments*, the 15° oblique slapdown free drop was repeated, followed by a puncture test. The attachments that experienced the greatest loads from the puncture test were the same ones that experienced the greatest loads in the free drop test. The result was that the impact limiter was securely retained on the test cask. The only measurable change to the refurbished attachment hardware was a negligible elongation of one of the blade holes by 0.07 inches (full-scale). Other than that slight deformation, there were no signs of distress or impending failure in any other feature located in the attachment load path. Of note, no other free drop or puncture drop test orientation caused any significant damage to the original, smaller design of the attachments. Therefore the impact limiter attachments are adequate to securely retain the impact limiter in the worst-case series of free drop and puncture events.

2.7.2 Crush

Since the weight of the BRR package exceeds 1,100 lb, the crush test specified in 10 CFR §71.73(c)(2) does not apply.

2.7.3 Puncture

The BRR package is evaluated for puncture resistance under HAC as defined in 10 CFR §71.73(c)(3). The puncture event is defined as a free drop from a height of 40 inches onto a vertical, cylindrical mild steel bar, 6 inches in diameter, in an orientation and in a location for which maximum damage is expected. Puncture performance of the BRR package is divided into two categories: puncture on the impact limiters, which was evaluated by half-scale certification test, and puncture of the package body, which is evaluated by analysis.

2.7.3.1 Puncture on the Impact Limiters

Appendix 2.12.2, *Certification Test Plan*, discusses the strategy used to evaluate the puncture performance of the impact limiters under the worst-case conditions, including the test objectives and success criteria. Section 2.12.2.4.1, *Test Sequence and Damage Accumulation*, identifies the five puncture tests that were performed on the half-scale certification test unit. The results of these tests is summarized below. Details are to be found in Appendix 2.12.3, *Certification Test Results*. The configuration of each test is shown schematically in Figure 2.12.3-2.

Test P1. This test was designed to show that the puncture bar would not penetrate beyond the impact limiter shell located on the flat bottom. This protects the closure lid from direct puncture bar loading, and prevents possible excessive loss of foam for protection in the HAC fire event. This test was performed subsequent to the end free drop test. The bar impacted the shell at an oblique angle through the cask c.g., which would enhance its ability to perforate the plate. The result shown in Figure 2.12.3-12 demonstrates that the impact limiter shell prevents perforation by the bar.

Test P2. This test was designed to show that the puncture bar would not create a significant exposure of foam adjacent to the cask (and containment seal) or dislodge the impact limiter from the end of the cask. Although Figure 2.12.3-2 shows the impact occurring on the same side as the slapdown free drop primary damage, it was found that it would be much more challenging to impact the side opposite to this damage, since that is the azimuth location where the attachments experienced the greatest loading in the free drop. This test was successfully repeated (test P2C) after the redesign of the impact limiter attachments, and subsequent to the repeated 15° oblique slapdown free drop (test D2C). As shown in Figure 2.12.3-40, the impact with the bar did not perforate the shell or expose any foam, and the discussion in Section 2.12.3.6.4, *Examination of Attachments*, documents that the impact limiter was not dislodged by the impact.

Test P3. This test was designed to show that the puncture bar would not enter the impact limiter through a side impact on the limiter shell (in this case, the secondary slapdown damage area caused by the 15° oblique slapdown free drop) and rip open a large area that could compromise the performance in the subsequent HAC fire event. As shown in Figure 2.12.3-34, no perforation of the shell occurred.

Test P4. This test was designed to show that the puncture bar damage from impact on the c.g.-over-corner free drop damage would be acceptable. The bar impacted the thinner shell material (formerly the conical portion of the limiter shell, before the free drop deformation occurred), adjacent to the thicker bottom plate material. As shown in Figure 2.12.3-29, the exposure of foam from this test was modest, and is bounded by a large margin by the exposure of foam from test P5.

Test P5. This test was originally designed to apply an oblique impact on a damaged portion of the shell to determine that the exposure of foam would be acceptable. When it was determined that the limiter shell corner joint between the top flat annular portion and the cylindrical side had developed a crack in the secondary 15° oblique slapdown free drop, this test was used to accumulate the maximum amount of damage in that area. The orientation of the test is shown in Figure 2.12.3-30. The impact with the bar opened up the cracked region and peeled back part of the annular plate, exposing the underlying foam. The final configuration is shown in Figure 2.12.3-31 and Figure 2.12.3-32. Since this test is clearly governing above the other puncture tests regarding the HAC fire event, it is used in modeling the fire event as discussed in Section 3.4, *Thermal Evaluation for Hypothetical Accident Conditions*. It is worth noting that a design change was made subsequent to this test, aimed at preventing this breach of the joint from recurring. The design shown in Appendix 1.3.3, *Packaging General Arrangement Drawings*, includes the stronger joint. The details of the change are discussed in Section 2.12.3.3, *Test Unit Configuration*. However, as just noted, in spite of the design change, the result from the half-scale puncture test P5 was conservatively used for the HAC fire event analysis.

2.7.3.2 Puncture on the Cask Body

The puncture resistance of the outer surface of the cask body is evaluated using Nelms' Equation [27], which is used to determine the resistance to puncture of lead–backed stainless steel shells. For the NCT hot case temperature of 250 °F, the ultimate strength of the Type 304 outer shell (assuming the lower strength cast or forged option) is S_u = 64,050 psi from Table 2.2-2. The bounding weight of the BRR package, including impact limiters, is W = 32,000 lb. The required thickness of the outer shell to resist puncture is:

$$t = \left(\frac{W}{S_u}\right)^{0.71} = 0.61 \text{ inches}$$

The thickness of the outer shell is 2 inches. The margin of safety on the cask outer shell thickness is:

$$MS = \frac{2.0}{0.61} - 1 = +2.28$$

Therefore, puncture of the BRR package is not of concern.

2.7.4 Thermal

The BRR package is designed to withstand the HAC 30 minute fire specified in 10 CFR §71.73(c)(4). The thermal evaluation is presented in Section 3.4, *Thermal Evaluation under Hypothetical Accident Conditions*.

2.7.4.1 Summary of Pressures and Temperatures

As shown in Table 3.1-2, the maximum internal cask pressure as a result of the HAC fire event is 8.8 psig. This is lower than the bounding value of MNOP of 10 psig, and significantly lower than the design pressure of 25 psig stated in Section 2.6.1.1, *Summary of Temperatures and Pressures*. Package component stresses were calculated for an internal pressure of 25 psig in Section 2.6.1.3, *Stress Calculations*, and are compared to allowable stress at the higher HAC temperature in Section 2.7.4.3, *Stress Calculations*.

From Table 3.1-1, as a result of the HAC fire event, the maximum temperature of any part of the cask (except closure bolts) may be bounded by a temperature of 710 °F. The maximum temperature of the closure bolts is considered to be the same as that of the closure lid, bounded by a temperature of 350 °F. Conservatively, all stainless steel components will be assumed to be made from cast or forged Type 304 material, which has a lower ultimate strength than plate material. From Table 2.2-2, S_u = 59,140 psi at 710 °F. The value of S_u for the closure bolts at 350 °F is equal to 125,000 psi, from Table 2.2-3.

2.7.4.2 Differential Thermal Expansion

Differential expansion under NCT is evaluated in Section 2.6.1.2.1, *Baskets*. In that case, the basket was given a uniform bounding temperature of 400 °F, and the thermal expansion of the cask was conservatively neglected. The resulting minimum axial clearance is shown as 0.16 inches, and the minimum diametral clearance is 0.10 inches. In the HAC fire event, from Table 3.1-1, the peak basket temperature is given as 437 °F. Since the basket temperature is locally only 37 °F hotter than the uniform NCT assumption, and in consideration of the significant thermal expansion of the cask cavity dimensions (for example, the inner shell peak temperature is 393 °F), the clearance between the basket and the cask will not be significantly affected by the cask temperatures resulting from the fire event.

Similarly, the fuel axial clearance was evaluated using a uniform bounding temperature of 400 °F in Section 2.6.1.2.2, *Fuel*, and found to have a minimum value of 0.19 inches. Given that the local peak fuel temperature, from Table 3.1-1 is only 451 °F, and that the NCT evaluation again

neglected the thermal expansion of the cask components, the clearance between the fuel and the basket will not be significantly affected by the cask temperatures resulting from the fire event.

2.7.4.3 Stress Calculations

Cask stress due to the internal design pressure of 25 psig is presented in Section 2.6.1.3.1, *Stresses Due to Pressure Loading*, as equal to 1,002 psi. This corresponds to the stress in the outer fiber of the closure lid, and is classified as a membrane plus bending stress. This stress clearly bounds the stress generated under an internal pressure in the HAC fire event of 8.8 psig, and the margin of safety may be conservatively calculated using this stress along with the lower fire case allowable stress determined in Section 2.7.4.1, *Summary of Temperatures and Pressures*. The margin of safety is:

$$MS = \frac{59{,}140}{1{,}002} - 1 = +58.0$$

The primary load on the closure bolts is governed by the preload force, calculated in Section 2.6.1.5, *Closure Bolts*, as equal to 19,200 lb. The stress is:

$$Sbs = 1.2732 \frac{19{,}200}{Dba^2} = 31{,}711 \text{ psi}$$

where the stress diameter, Dba = 0.878 inches from Section 2.6.1.5. From Table 2.1-1, the allowable average tensile stress intensity for HAC is the lesser of $0.7S_u$ or S_y, which for the ASTM A320 L43 bolting material is $0.7S_u$ = 87,500 psi at 350 °F. The margin of safety is:

$$MS = \frac{87{,}500}{31{,}711} - 1 = +1.76$$

Per Regulatory Guide 7.6, paragraph C.7, the extreme range of stress must be considered. Of all the various allowable stresses corresponding to the different conditions evaluated (including fabrication stresses and normal conditions of transport), the largest allowable stress is equal to the material ultimate strength, S_u. It is therefore conservative to assume that S_u bounds all stresses actually developed in the structure. For Type 304 stainless steel, S_u = 75,000 psi at 70 °F. The maximum possible stress intensity range is twice this value, or 150,000 psi. Applying a factor of four to account for possible stress concentrations at structural discontinuities gives a total elastic stress range of 600,000 psi. The alternating component is one-half of this value, or 300,000 psi. To account for temperature effects, this value of alternating stress is factored by the ratio of modulus of elasticity. This ratio is formed between the modulus of elasticity at room temperature (at which the test data applies directly) and the modulus of elasticity at the maximum temperature, conservatively bounded by a temperature of 710 °F for any structural part of the package. The adjusted stress is

$$S_{alt} = 300{,}000 \frac{E_{70°F}}{E_{710°F}} = 343{,}725 \text{ psi}$$

where $E_{70°F} = 28.3(10^6)$ psi and $E_{710°F} = 24.7(10^6)$ psi. Per Figure I-9.2.1 and Table I-9.1 of the ASME Code [9], the allowable value for S_{alt} at 10 cycles is 708,000 psi. The margin of safety is

$$MS = \frac{708{,}000}{343{,}725} - 1 = +1.06$$

Considering the significant conservatism used in the underlying assumptions (e.g., use of allowable stress rather than smaller actual stresses, assuming worst case stresses are fully reversing, use of the maximum factor of stress concentration), it is apparent that the actual margin of safety is larger than 1.06. Thus, the requirement of paragraph C.7 of Regulatory Guide 7.6 is met.

2.7.5 Immersion – Fissile

An immersion test for fissile material packages is required by 10 CFR §71.73(c)(5). The criticality evaluation presented in Chapter 6, *Criticality Evaluation*, assumes optimum hydrogenous moderation of the contents, thereby conservatively addressing the effects and consequences of water in–leakage.

2.7.6 Immersion – All Packages

An immersion test for all packages is required by 10 CFR §71.73(c)(6), in which a separate, undamaged specimen must be subjected an equivalent pressure of 21.7 psig. Since the BRR package is evaluated to the much greater hydrostatic pressure of the deep immersion test (see the next section), this test does not need to be evaluated.

2.7.7 Deep Water Immersion Test (for Type B Packages Containing More than 10^5 A_2)

For Type B packages containing an activity of more than 10^5 A_2, 10 CFR §71.61 requires that an undamaged containment system withstand an external pressure of p_o = 290 psig for a period of not less than one hour without collapse, buckling, or inleakage of water. This test will not have a significant effect on the BRR package. Although a temperature is not specified for this test, a lead shrinkage (fabrication) stress corresponding to a temperature of -40 °F, taken from Section 2.6.2, *Cold*, will be conservatively applied in addition to the specified hydrostatic pressure. The lead shrinkage pressure is p_c = 787 psi. Conservatively, the inner shell is evaluated neglecting the outer shell, even though the external pressure would be applied to the much stronger outer shell.

The internal pressure in the cask is assumed to be ambient, thus the net external pressure across the inner shell on its outer cylindrical surface is equal to a sum of the applied hydrostatic pressure of 290 psig and the lead shrinkage pressure of 787 psi, or a total of:

$$p_{cyl} = 290 + 787 = 1{,}077 \text{ psi}$$

The compressive hoop stress is:

$$\sigma_\theta = p_{cyl}\frac{r_{avg}}{t} = 9{,}155 \text{ psi}$$

where the mean inner shell radius, r_{avg} = 8.5 inches, and the thickness, t = one inch. The compressive axial stress, obtained by supporting the hydrostatic pressure load, p_o, from the entire cask end cross section over the inner shell cross section, is:

$$\sigma_\phi = \frac{p_o \pi r_{cask}^2}{2\pi r_{avg} t} = 6{,}289 \text{ psi}$$

where r_{cask} = 38.4/2 = 19.2 inches. Using Mohr's circle, the maximum shear stress is:

$$\sigma_{\phi\theta} = \frac{1}{2}(\sigma_\theta - \sigma_\phi) = 1{,}433 \text{ psi}$$

The possibility of buckling of the inner shell is evaluated using [13]. Consistent with Regulatory Guide 7.6, a factor of safety corresponding to ASME Code, Service Level D is employed. In this case, the applicable factor of safety is 1.34 for hypothetical accident conditions, as specified in [13]. The analysis used a modulus of elasticity of 28.3(10^6) psi, corresponding to 70 °F. Buckling analysis geometry and loading parameters are listed in Table 2.7-7 and results of the analysis in Table 2.7-8. As shown, all interaction parameters, including the maximum value of 0.4286, are less than unity, as required. Thus, the deep water immersion test is not of concern for the BRR package.

2.7.8 Summary of Damage

From the analyses presented, it is shown that the HAC sequence does not result in significant damage to the BRR package, and that all stress criteria established for HAC in Section 2.1.2, *Design Criteria*, are satisfied. The margins of safety resulting from the analyses performed in this section are shown in Table 2.7-9.

The BRR cask body and internal components were evaluated primarily by analysis, and the impact limiters and attachments were evaluated by test. The test results confirmed that the impact acceleration of 120g used in the analyses was bounding for all free drop orientations. The tests are summarized below.

The analysis of the cask body and internal components under free drop impact included the cask body structure, the closure lid, the closure bolts, and the shield plug shell. Bounding orientations of end and side drop were evaluated. A demonstration that the side drop governs over the worst-case slapdown is provided in Section 2.7.1.4, *Oblique Drop*. The cask body was analyzed using finite element analysis, in which the cask was loaded by self-weight and contents weight, and supported by the impact limiters. Conservatively, the lead shielding was considered to act as a fluid, having no structural strength. The minimum margin of safety from the finite element analysis, which corresponded to the side drop impact case, was +0.23. All of the manual evaluations resulted in larger margins of safety, as shown in Table 2.7-9. The end drop buckling analysis of the package shells, performed using ASME Code Case N-284-2, resulted in a maximum check value of 0.4024, which is well below the limit of unity, as required by the Code Case. An evaluation of lead slump in the end drop orientation was performed, and resulted in a bounding value of 1.185 inches. This value was used in the shielding evaluation documented in Chapter 5.0, *Shielding Evaluation*. An analysis of the fuel baskets was performed as documented in Appendix 2.12.8, *Fuel Basket Stress Analysis*. Each basket was evaluated for governing modes of failure, with a minimum margin of safety of +0.12. A summary of the margins of safety for the fuel baskets is provided in Table 2.7-4. An analysis of the puncture test on the cask body was performed using Nelms' equation, and resulted in a margin of safety of +2.28. Therefore, since all margins of safety are positive, the criteria of Section 2.1.2, *Design Criteria*, are satisfied for the BRR package.

The impact limiter design was tested using half-scale, prototypic certification test units and a dummy cask body. The impact limiters successfully performed their role in limiting the impact acceleration to a value considerably lower than the value of 120g used for stress analysis. In addition, the test showed that the calculated maximum strain in the energy-absorbing polyurethane foam of 83.2% was conservative. Some exposure of the foam was produced by the worst-case sequence of free drop and puncture tests. The final configuration of the impact limiter shell and of the exposed foam was included in the HAC fire event thermal model as described in Section 3.5.3.7, *Description of Thermal Model for HAC Conditions*. The impact limiter attachments, subsequent to a redesign and retest under the worst-case free drop and puncture conditions, successfully retained the impact limiters on the cask. Therefore the impact limiters satisfy their design criteria established in Section 2.1.2.2, *Other Structures*.

Table 2.7-1 – HAC Free Drop Buckling Evaluation: Geometry and Loads

	Outer shell dimensions, inches	**Applied stress, psi**	
Inner Dia.	34.0	σ_φ	7,117
Outer Dia.	38.0	σ_θ	0
Length (bounding)	55.0	$\sigma_{\varphi\theta}$	0

Table 2.7-2 – HAC Free Drop: N–284–2 Results

Parameter	Value	Remarks
Capacity Reduction Factors (-1511)		
$\alpha_{\phi L}$ =	0.2279	
$\alpha_{\theta L}$ =	0.8000	
$\alpha_{\phi\theta L}$ =	0.8000	
Plasticity Reduction Factors (-1610)		
η_{ϕ} =	0.0568	
η_{θ} =	0.0850	
$\eta_{\phi\theta}$ =	0.0232	
Theoretical Buckling Values (-1712.1.1)		
C_{ϕ} =	0.6050	
$\sigma_{\phi eL}$ =	1,831,806 psi	
$C_{\theta r}$ =	0.1150	
$\sigma_{\theta eL} = \sigma_{reL}$ =	348,340 psi	
$C_{\theta h}$ =	0.1078	
$\sigma_{\theta eL} = \sigma_{heL}$ =	326,534 psi	
$C_{\phi\theta}$ =	0.2527	
$\sigma_{\phi\theta eL}$ =	765,157 psi	
Elastic Interaction Equations (-1713.1.1)		
σ_{xa} =	311,567 psi	
σ_{ha} =	194,946 psi	
σ_{ra} =	207,964 psi	
$\sigma_{\tau a}$ =	456,810 psi	
Axial + Shear ⇨ Check (c):	0.0228	<1 ∴ OK (see note*)
Hoop + Shear ⇨ Check (d):	0.0000	<1 ∴ OK
Inelastic Interaction Equations (-1714.2.1)		
σ_{xc} =	17,687 psi	
σ_{rc} =	17,687 psi	
$\sigma_{\tau c}$ =	10,612 psi	
Max(Axial,Hoop) ⇨ Check (a):	0.4024	<1 ∴ OK
Axial + Shear ⇨ Check (b):	0.4024	<1 ∴ OK
Hoop + Shear ⇨ Check (c):	0.0000	<1 ∴ OK

*Note: Elastic interaction checks (a), (b), (e), and (f) are not applicable.

Table 2.7-3 – Cask Shell Force and Stress Comparison

Case	Impact Limiter Force, lb	Axial Force, R, lb	Shear Force, V, lb	Bending Moment, M, in–lb	Relative Stress Intensity, psi
Side Drop	$1.920(10^6)$	0	$1.920(10^6)$	$33.600(10^6)$	164,077*
15°, Primary	$1.049(10^6)$	271,501	$1.013(10^6)$	$10.508(10^6)$	59,940*
15°, Secondary	$1.220(10^6)$	0	$1.220(10^6)$	$12.652(10^6)$	66,647*

*Stress for comparison purposes only; not actual inner shell stress.

Table 2.7-4 – Fuel Basket Stress Analysis Results

Analysis Description	Reference Section①	Margin of Safety
MURR Basket		
Fuel Support Plate Bending		+8.32
Outer Shell Slot Welds		+3.00
Buckling of Lower Shell		Pass②
MITR–II Basket		
Buckling of Lower Shell		Pass②
ATR Basket		
Fuel Support Plate Bending		+10.2
Outer Shell Slot Welds		+1.02
Side Drop Bending		+4.16
TRIGA Basket		
Fuel Support Plate Bending		+0.65
Shear Load on Spacer Screw		+0.12
Bucking of Fuel Tubes		Pass②
Side Drop Bending		+1.81

Notes:
1. Calculational details are presented in Appendix 2.12.8, *Fuel Basket Stress Analysis*.
2. Interaction equation checks are less than unity, as required by [13].

Table 2.7-5 – Fuel Impact Deformation Results

Fuel Type	W, lb	L_{FB}	A_{xc}, in^2	W/A_{xc}, lb/in^2	GAP	L, in
MURR	15	0.38	4.584	3.27	1.18	0.035
MITR–II	10	0.36	3.814	2.62	1.17	0.028
ATR	25	0.38	3.961	6.31	1.68	0.096
TRIGA	10	0.37	1.72*	5.81	1.18	0.062

*TRIGA fuel has 0.03–inch thick cladding for aluminum clad and 0.02–inch thick cladding for stainless steel clad fuel. Since the entire fuel cross–section is made of a strong material (fuel pellet of UZrH), the area used is that of the entire pellet cross–section of 1.48 inches.

Table 2.7-6 – Impact Limiter Attachment Comparisons

Feature Description	Refurbished Test article (Full-scale Equiv.)	Final Production Design (per Appendix 1.3.3)	Remarks
Blade and receptacle material	ASTM Type 304	ASTM Type 304	Same
Blade thickness, in.	3/4	3/4	Same
Blade width, in.	3.0	3.3	Improved
Hole diameter in blade, in.	1.13	1.13	Same
Hole-to-blade edge, in.	0.94	1.06	Improved
Blade weld to limiter inner shell structure	3/8-in. fillet on both sides	3/8-in. fillet on both sides	Same
Receptacle plate thickness, in.	3/8	1/2	Improved
Ball lock pin diameter, in.	1.0	1.0	Same
Pin material	Carbon steel	Stainless steel	Improved
Pin rated double shear strength, lb	65,600	73,500	Improved
Attachment quantity per limiter	6	8	Improved

Table 2.7-7 – Deep Immersion Test: Geometry and Loads

	Inner shell dimensions, inches	Applied stress, psi	
Inner Dia.	16.0	σ_φ	6,289
Outer Dia.	18.0	σ_θ	9,155
Length (bounding)	62.0	$\sigma_{\varphi\theta}$	1,433

Table 2.7-8 – Deep Immersion Test: N–284–2 Results

Parameter	Value	Remarks
Capacity Reduction Factors (-1511)		
$\alpha_{\phi L}$ =	0.2850	
$\alpha_{\theta L}$ =	0.8000	
$\alpha_{\phi\theta L}$ =	0.8000	
Plasticity Reduction Factors (-1610)		
η_{ϕ} =	0.0523	
η_{θ} =	0.2856	
$\eta_{\phi\theta}$ =	0.0417	
Theoretical Buckling Values (-1712.1.1)		
C_{ϕ} =	0.6050	
$\sigma_{\phi eL}$ =	2,014,294 psi	
$C_{\theta r}$ =	0.0387	
$\sigma_{\theta eL} = \sigma_{reL}$ =	128,711 psi	
$C_{\theta h}$ =	0.0387	
$\sigma_{\theta eL} = \sigma_{heL}$ =	128,711 psi	
$C_{\phi\theta}$ =	0.1619	
$\sigma_{\phi\theta eL}$ =	539,157 psi	
Elastic Interaction Equations (-1713.1.1)		
σ_{xa} =	428,445 psi	
σ_{ha} =	76,843 psi	
σ_{ra} =	76,843 psi	
$\sigma_{\tau a}$ =	321,885 psi	
Axial + Shear ⇨ Check (c):	0.0147	<1 ∴ OK (see note*)
Hoop + Shear ⇨ Check (d):	0.1192	<1 ∴ OK
Inelastic Interaction Equations (-1714.2.1)		
σ_{xc} =	22,388 psi	
σ_{rc} =	21,943 psi	
$\sigma_{\tau c}$ =	13,433 psi	
Max(Axial,Hoop) ⇨ Check (a):	0.4172	<1 ∴ OK
Axial + Shear ⇨ Check (b):	0.2923	<1 ∴ OK
Hoop + Shear ⇨ Check (c):	0.4286	<1 ∴ OK

*Note: Elastic interaction checks (a), (b), (e), and (f) are not applicable.

Table 2.7-9 – Minimum Margins of Safety from HAC Evaluations

Component	Loading Condition	Minimum Margin of Safety
	Free Drop	
Cask body (FEA)	End drop, bottom down, membrane stress	+0.98
	End drop, bottom down, membrane + bending	+0.49
	End drop, top down, membrane stress	+0.97
	End drop, top down, membrane + bending stress	+0.92
	Side drop, membrane stress	+1.75
	Side drop, membrane + bending stress	+0.23
Lower closure plate	End drop, bottom down, membrane + bending	+0.40
Closure bolts	End drop, top down	+0.83
Closure lid	End drop, top down	+1.65
Shield plug shell lower plate	End drop, bottom down, assuming simple support, stress at center	+0.46
	End drop, bottom down, assuming fixed edge support, stress at edge (weld)	+0.91
Cask outer shell	End drop, buckling (Code Case N-284-2)	0.4024*
	Puncture	
Cask outer shell	Nelms' Equation	+2.28
	Thermal	
Containment boundary	Internal pressure, fire conditions	+58.0
Closure bolts	Internal pressure, fire conditions	+1.76
Cask	Range of stress	+1.06

*Maximum check value must be less than unity.

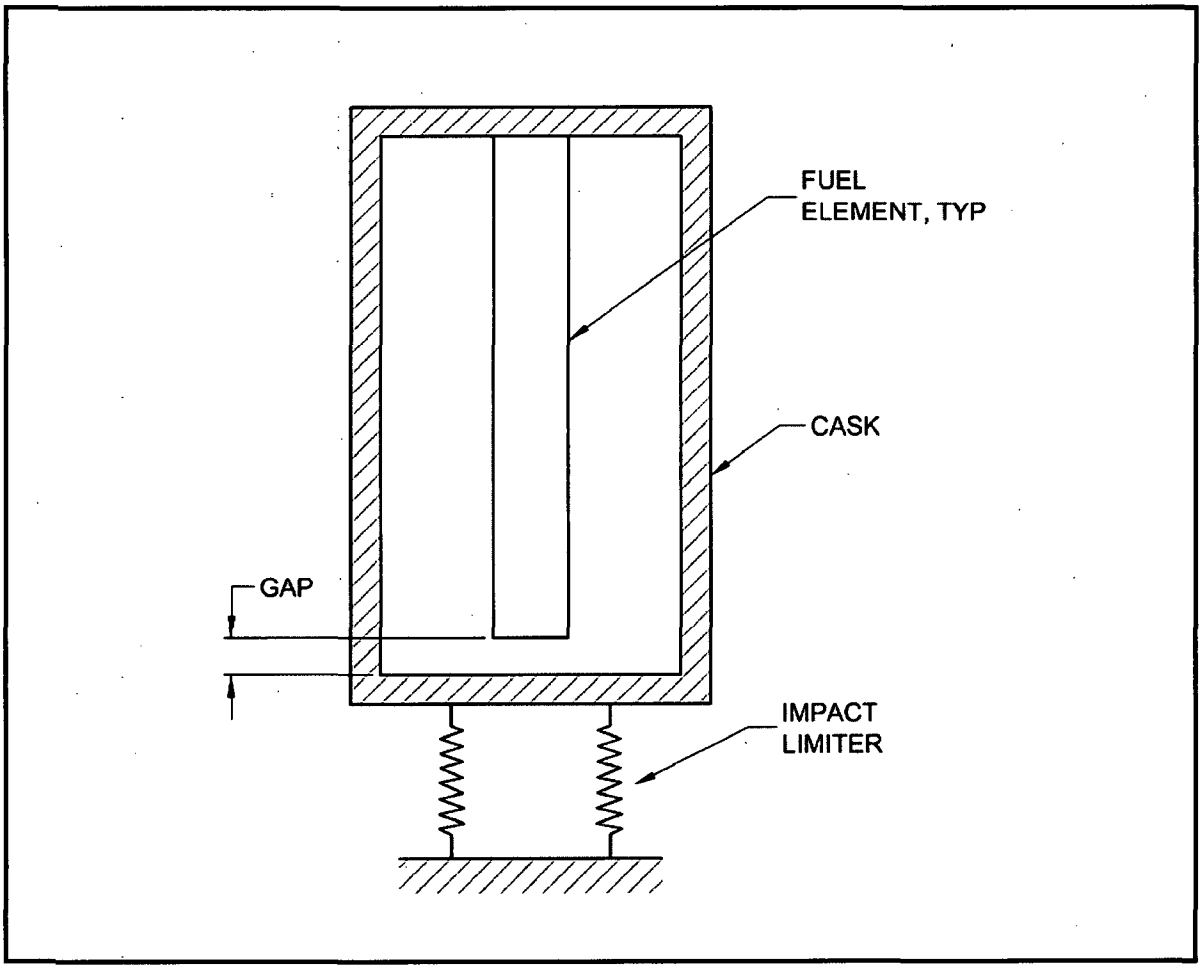

Figure 2.7-1 – Cask Cavity and Fuel During Free End Drop

2.8 Accident Conditions for Air Transport of Plutonium

This section does not apply, since air transport is not used for the BRR package.

2.9 Accident Conditions for Fissile Material Packages for Air Transport

This section does not apply, since air transport is not used for the BRR package.

2.10 Special Form

This section does not apply, since special form is not claimed for the BRR package.

2.11 Fuel Rods

This section does not apply, since fuel rod cladding is not credited with containment in the BRR package.

2.12 Appendices

2.12.1 References

2.12.2 Certification Test Plan

2.12.3 Certification Test Results

2.12.4 Stress Analysis Finite Element Models

2.12.5 Impact Limiter Performance Evaluation

2.12.6 Impact Analysis Software Descriptions

2.12.7 Seal Performance Tests

2.12.8 Fuel Basket Stress Analysis

2.12.1 References

1. Title 10, Code of Federal Regulations, Part 71 (10 CFR 71), *Packaging and Transportation of Radioactive Material*, 01–01–08 Edition.
2. U. S. Nuclear Regulatory Commission, Regulatory Guide 7.6, *Design Criteria for the Structural Analysis of Shipping Cask Containment Vessels*, Revision 1, March 1978.
3. U. S. Nuclear Regulatory Commission, Regulatory Guide 7.8, *Load Combinations for the Structural Analysis of Shipping Casks for Radioactive Material*, Revision 1, March 1989.
4. U. S. Nuclear Regulatory Commission, Regulatory Guide 7.11, *Fracture Toughness Criteria of Base Material for Ferritic Steel Shipping Cask Containment Vessels with a Maximum Wall Thickness of 4 Inches (0.1 m)*, June 1991.
5. R. E. Monroe, H. H. Woo, and R. G. Sears, *Recommended Welding Criteria for Use in the Fabrication of Shipping Containers for Radioactive Materials,* NUREG/CR–3019, UCRL–53044, March 1985.
6. L. E. Fischer, W. Lai, *Fabrication Criteria for Shipping Containers,* NUREG/CR–3854, UCRL–53544, U.S. Nuclear Regulatory Commission, March 1985.
7. American Society of Mechanical Engineers (ASME) Boiler and Pressure Vessel Code, Section III, *Rules for Construction of Nuclear Facility Components*, Division 1 – Subsection NB, *Class 1 Components*, 2007 Edition.
8. American Society of Mechanical Engineers (ASME) Boiler and Pressure Vessel Code, Section III, *Rules for Construction of Nuclear Facility Components*, Division 1 – Subsection NG, *Core Support Structures*, 2007 Edition.
9. American Society of Mechanical Engineers (ASME) Boiler and Pressure Vessel Code, Section III, *Rules for Construction of Nuclear Facility Components*, Division 1 – Subsection NF, *Supports,* 2007 Edition.
10. G.C. Mok, L.E. Fischer, S.T. Hsu, *Stress Analysis of Closure Bolts for Shipping Casks*, NUREG/CR–6007, UCRL–ID–110637, U.S. Nuclear Regulatory Commission, April 1992.
11. W.R. Holman, R. T. Langland, *Recommendations for Protecting Against Failure by Brittle Fracture in Ferritic Steel Shipping Containers Up to Four Inch Thick*, NUREG/CR–1815, UCRL–53013, August 1981.
12. American Society of Mechanical Engineers (ASME) Boiler and Pressure Vessel Code, Section III, *Rules for Construction of Nuclear Facility Components*, Appendix I, *Design Stress Intensity Values, Allowable Stresses, Material Properties, and Design Fatigue Curves*, 2007 Edition.
13. American Society of Mechanical Engineers (ASME) Boiler and Pressure Vessel Code, Section III, *Rules for Construction of Nuclear Power Plant Components*, Division 1, Class MC, Code Case N–284–2, *Metal Containment Shell Buckling Design Methods*, 2007 Edition.
14. American Society of Mechanical Engineers (ASME) Boiler and Pressure Vessel Code, Section IX, *Qualification Standard for Welding and Brazing Procedures, Welders, Brazers, and Welding and Brazing Operators*, 2007 Edition.

15. American Society of Mechanical Engineers (ASME) Boiler and Pressure Vessel Code, Section III, *Rules for Construction of Nuclear Facility Components*, Division 1 – Subsection NE, *Class MC Components,* Article NE–4220, 2007 Edition.

16. American Society of Mechanical Engineers (ASME) Boiler and Pressure Vessel Code, Section III, *Rules for Construction of Nuclear Facility Components*, Division 1 – Subsection NB, *Class 1 Components*, Article NB–2540, 2007 Edition.

17. American Society of Mechanical Engineers (ASME) Boiler and Pressure Vessel Code, Section III, *Rules for Construction of Nuclear Facility Components*, Division 1 – Subsection NB, *Class 1 Components*, Article NB–2570, 2007 Edition.

18. ANSI/AWS D1.6:2007, *Structural Welding Code–Stainless Steel*, American Welding Society (AWS).

19. American Society of Mechanical Engineers (ASME) Boiler and Pressure Vessel Code, Section III, *Rules for Construction of Nuclear Facility Components*, Division 1 – Subsection NB, *Class 1 Components*, and Section V, *Nondestructive Examination*, Article 2, *Radiographic Examination*, 2007 Edition.

20. American Society of Mechanical Engineers (ASME) Boiler and Pressure Vessel Code, Section III, *Rules for Construction of Nuclear Facility Components*, Division 1 – Subsection NB, *Class 1 Components*, and Section V, *Nondestructive Examination*, Article 4, *Ultrasonic Examination Methods for Welds*, 2007 Edition.

21. American Society of Mechanical Engineers (ASME) Boiler and Pressure Vessel Code, Section III, *Rules for Construction of Nuclear Facility Components*, Division 1 – Subsection NB, *Class 1 Components*, and Section V, *Nondestructive Examination*, Article 6, *Liquid Penetrant Examination*, 2007 Edition.

22. American Society of Mechanical Engineers (ASME) Boiler and Pressure Vessel Code, Section III, *Rules for Construction of Nuclear Facility Components*, Division 1 – Subsection NB, *Class 1 Components*, Article NB–6220, 2007 Edition.

23. Boucher, R. C., Strength of Threads, Product Engineering, November 27, 1961.

24. ANSI N14.23, *Design Basis for Resistance to Shock and Vibration of Radioactive Material Packages Greater Than One Ton in Truck Transport* (DRAFT), 1980, American National Standards Institute, Inc, New York.

25. Roark's Formulas for Stress and Strain, Sixth Edition, McGraw–Hill, New York, 1989.

26. T.A. Nelson and R. C. Chun, *Methods for Impact Analysis of Shipping Casks*, NUREG/CR–3966, UCID–20639, U.S. Nuclear Regulatory Commission, November 1987.

27. A. Nelms, *Structural Analysis of Shipping Casks, Effect of Jacket Physical Properties and Curvature on Puncture Resistance*, ORNL–TM–1312, Vol. 3, Oak Ridge National Laboratory, 1968.

28. General Plastics Manufacturing Company, *Design Guide for Use of Last–A–Foam® FR–3700 For Crash & Fire Protection of Radioactive Material Shipping Containers*, Issue 004.

29. NRC Docket No. 71–9295, Mixed Oxide Fresh fuel Package Safety Analysis Report, Revision 7, July 2008.

30. G. D. Sjaardema and G. W. Wellman, *Numerical and Analytical Methods for Approximating the Eccentric Impact Response (Slapdown) of Deformable Bodies*, SAND88–0616 (UC–71), Sandia National Laboratories.

31. ***SCANS** (**S**hipping **C**ask **AN**alysis **S**ystem), A Microcomputer Based Analysis System for Shipping Cask Design Review*, NUREG/CR–4554 (UCID–20674), Lawrence Livermore National Laboratory.

32. American Society of Mechanical Engineers (ASME) Boiler and Pressure Vessel Code, Section III, *Rules for Construction of Nuclear Facility Components*, Division 1 – Subsection NG, *Core Support Structures*, Article NG–3350, 2007 Edition.

33. American Society of Mechanical Engineers (ASME) Boiler and Pressure Vessel Code, Section III, *Rules for Construction of Nuclear Facility Components*, Appendix F, *Rules for Evaluation of Service Loadings with Level D Service Limits*, 2007 Edition.

34. General Plastics Manufacturing Company, *General Plastics Last-A-Foam® FR-3700 For Crash & Fire Protection of Radioactive Material Shipping Containers*, June 1997.

2.12.2 Certification Test Plan

This appendix describes the certification tests that were performed on the BEA Research Reactor package impact limiters. The justification for choosing the specific tests is presented and discussed. Since this material served for test planning purposes, the future tense is used. The results of the tests is provided in Appendix 2.12.3, *Certification Test Results*.

Because the BRR package includes a conventional, austenitic stainless steel cask shielded by lead and closed by a bolted lid, testing of the cask body is not necessary. The licensing basis for the cask body is by analysis. Physical testing will focus only on the impact limiters and attachments. The licensing basis for the impact limiters will be a combination of half-scale physical test and analysis. Free drop and puncture drop damage of steel-shell, polyurethane foam-filled impact limiters can be adequately modeled using scaled test specimens with appropriate scaling factors.

The test unit configuration will therefore consist of a half-scale dummy cask and half-scale prototypic impact limiters and attachments. Testing will consist of free drops and puncture drops. Test data will consist of measured accelerations and measurements of the damaged configuration.

2.12.2.1 Certification Objective

The objective of the certification test program is to demonstrate the adequacy of the BRR package impact limiter design. The impact limiters were designed using computer software to predict the impact (maximum at cold temperature) and the crush deformation (maximum at hot temperature). Refer to Appendix 2.12.5, *Impact Limiter Performance Evaluation*. The certification tests will demonstrate the performance of the limiters in both the hypothetical accident condition (HAC) free drop and puncture drop events. Free drop impact and crush deformation results will be used to benchmark the computer program for use in non-tested orientations or conditions. Puncture drop deformation results will be used to demonstrate impact limiter structural integrity and in the HAC thermal analysis as discussed below.

Several orientations will be tested to ensure that the worst-case series of free and puncture drop events has been considered. The maximum combination of free and puncture drop deformation will be used in the thermal analysis to show that under these worst-case conditions, the elastomer containment O-ring seal temperatures do not exceed safe limits during the HAC fire event.

Since a half-scale test unit will be used, a scaling of the various test parameters is necessary. All of the dimensions of the test unit will be one half of the full-scale design. Dimensional results from the half-scale model (e.g., crush distance) must be multiplied by a factor of two to obtain the full-scale equivalent result. Similarly, the measured accelerations must be divided by two to convert to full-scale. The test unit weight will be 1/8 the weight of the full-scale design, and the rotational moment of inertia will be 1/32 of the full-scale package.

2.12.2.2 Initial Test Conditions

2.12.2.2.1 Temperature

To confirm the maximum free drop impact accelerations that have been obtained from computer analysis, the free drops must occur at or near the minimum temperature of -20 °F, due to the increase in crush strength of the energy absorbing materials (polyurethane foam) with decreasing

temperature. The maximum crush, which occurs at the maximum NCT temperature, will be obtained by first benchmarking the computer code using the cold case impacts and deformations, and then performing runs with material properties at maximum temperature. Consequently, free drop impacts will occur with the foam material at a bulk average temperature at or near -20 °F. A temperature somewhat below -20 °F is desirable. However, to facilitate testing, a small deviation of as much as 10 °F (to -10 °F) is permissible, since the difference can be accounted for analytically.

Puncture damage depends on the perforation resistance of the shell and the compressive/shearing behavior of the foam subsequent to perforation. Perforation resistance is least at cold temperature, since the underlying foam is stronger and supports a greater shearing action of the edge of the puncture bar. Subsequent to perforation, if that occurs, the 9 lb/ft^3 (pcf) foam used for the BRR package impact limiters will not present a significant resistance to the puncture bar, regardless of strength. Therefore, the cold condition is worst-case when perforation resistance is of primary interest. However, since most puncture drop tests are expected to perforate the thinner shells regardless of temperature, only the puncture drop tests on the thicker shell (the flat, circular shell located at the end of the impact limiter, which is expected to resist perforation) needs to be performed at the cold, -20 °F temperature. As for the free drop, a small deviation up to a bulk foam temperature of -10 °F is acceptable.

2.12.2.2.2 Test Facilities and Instrumentation

The certification drop and puncture testing will be conducted using a drop pad having a mass of at least 10 times the weight of the certification test unit (CTU), or at least 40,000 lb. The top of the pad will be covered by an embedded steel plate of adequate thickness such that the drop pad will represent an essentially unyielding surface. The half-scale puncture bar will be a 3-in diameter bar of mild steel, mounted perpendicular to the drop pad, and having an edge radius not exceeding 1/8-inch. The bar will be reinforced by gussets at its base and fastened securely to the pad. The length of the bar will permit the bar to do maximum damage before the package becomes supported by the drop pad, and it will be at least 8 inches long. More than one length of bar may be used. Puncture bars will not be reinforced beyond what is necessary to provide rigidity at the baseplate joint.

CTU temperature will be measured by means of thermocouples embedded in the foam. As a minimum, the region of foam expected to undergo crush deformation will be monitored.

The primary means of recording the results of the certification testing will be physical measurements and observations of the CTU before and after testing. In addition, each free drop impact will be recorded using active accelerometers.

2.12.2.2.3 Certification Test Unit Configuration

The certification tests will be performed using a test unit consisting of a dummy cask assembled with prototypic, half-scale impact limiters. The impact limiter attachments, including the welds of the mating attachments to the dummy cask, will be prototypic. The dummy cask will be made of steel and lead, and possess a weight of 1/8 of the weight of the full-scale cask (consistent with half-scale). The dummy cask's impact limiter interface dimensions and features, and its overall length, will be in prototypic half-scale.

The impact limiters will be constructed using the same materials and details as the full-scale limiters, using half-scale dimensions. The polyurethane foam will use the same procurement specification,

including crush properties, as the full-scale components. Lifting features will be omitted from the half-scale components. Prior to testing, the impact limiters will receive a certificate of compliance with all fabrication drawing and specification requirements.

2.12.2.3 Identification of Worst-Case Test Orientations

The objectives of the certification test program are:

1. To confirm maximum free drop impact accelerations obtained from computer calculations.
2. To calibrate or benchmark the computer program, in order to validate calculations for orientations not tested.
3. To demonstrate the general structural integrity of the impact limiter during impact.
4. To demonstrate the effectiveness of the impact limiter attachments in both free drop and puncture drop events.
5. To demonstrate that the puncture bar will not penetrate the circular end plate of the upper impact limiter shell.
6. To quantify the worst-case puncture damage for the HAC fire event thermal analysis.

These objectives will now be discussed under the headings of free drop impact and puncture damage.

2.12.2.3.1 Free Drop Impact Objectives

The computer analysis documented in Appendix 2.12.5, *Impact Limiter Performance Evaluation*, shows that the governing free drop orientation for impact is the 15° slapdown secondary impact in the cold case, at 87g (full scale). Similarly, the governing crush damage occurs for the primary impact in the 15° slapdown orientation in the hot case, at a strain of 81%. The c.g.-over-corner impact is next closest in damage severity, having a maximum strain of 76% in the hot case. Therefore, the 15° slapdown and c.g.-over-corner orientations should be considered for the certification test. In addition, since the end drop orientation is of critical importance to the analysis of the cask body shells, the closure lid bolts, and lead slump, the end drop orientation should also be considered.

The 15° slapdown test in the cold condition will directly result in the worst-case impact occurring in the 30-foot free drop. The primary impact crush deformation will not be the worst-case, since the worst-case occurs at maximum temperature. However, the impact analysis will be benchmarked for the cold case, and by subsequently adjusting the foam and steel properties for hot temperatures, the maximum crush can be demonstrated using a computer calculation.

The end drop test will directly result in the maximum impact occurring in the 30-foot end drop. This data can be used to ensure that the impact used in the quasi-static finite element analysis for the end drop is adequately bounding.

The c.g.-over-corner free drop will not result in the worst-case deformation that could occur in that orientation, which occurs at hot temperature. However, using the same benchmarking technique as for the slapdown test, the maximum crush deformation for this orientation can be readily calculated. Of note, this test could be performed using hot temperature, but it is more convenient

to use the naturally occurring temperature, so long as it is adequately characterized to support the benchmarking procedure.

The finite element analysis which is documented in Chapter 2.0, *Structural Evaluation*, will include both the end drop orientation and the side drop orientation. From the data collected in other drop tests, the impact analysis software can adequately predict a bounding impact acceleration for the side drop. Therefore, a side drop orientation does not need to be performed.

The licensing strategy for demonstrating the adequacy of the impact limiter attachments depends upon test. The multiplicity of the free drops considered above (along with puncture drops, see below) ensures that this can be done solely by means of the test results. Furthermore, the general integrity of the impact limiter shells and joints, and the energy absorbing efficiency of the foam at cold temperatures, can also be clearly demonstrated with the proposed tests.

2.12.2.3.2 Puncture Drop Objectives

The circular plate on the end of the upper impact limiter is designed to prevent perforation by the puncture bar. This prevents concentrated puncture loads from occurring directly on the closure lid. Perforation of the conical or side cylindrical impact limiter shells is expected, however the possible orientation of the bar with respect to the closure lid would either be too oblique to be damaging to the lid, or would impact the relatively strong end structure. To demonstrate the puncture resistance of the plate, an end puncture should be considered. The angle should be somewhat oblique to enhance perforation. Per Section 10 CFR §71.73(a), the puncture should follow the free drops, and should occur on the surface impacted in the end drop, if determined to be the worst orientation.

As a part of achieving the worst-case damage to bound the fire event thermal analysis, a puncture on the c.g.-over-corner free drop damage should be considered. The bar should be oriented so that the potential penetration depth is not hindered by the resistance of the cask end structure. This would also examine the possibility that significant damage could occur from the cask rolling off of the bar, if the impact limiter becomes impaled on it. The resulting puncture damage measurements can be added to the hot case bounding free drop damage calculation to obtain the worst-case from this sequence of events.

Another possibility is that the puncture bar could penetrate the conical region from a side, or near-side orientation, and rip deeply into the limiter in a direction more or less parallel to the cask end surface, and either cause a chimney to occur, or rip out a large section of the limiter as the cask is rolling off of the bar, if the impact limiter becomes impaled on it. This action might be somewhat limited by the fact that the bar orientation would not be toward the c.g., allowing the package to rotate away from the damage site. This test could be located on the slapdown primary or secondary free drop damage.

The cask drain port, located in the cask lower end structure, is closed using an elastomer O-ring seal that may be damaged in the HAC fire event. Therefore, exposure of the end structure side could allow excessive temperatures in the drain port area. An attack from a puncture bar more or less parallel to the package axis, contacting the edge of the damaged area from the secondary slapdown event, could either cause a local exposure of the top end structure of the cask, or possibly substantially dislodge the upper impact limiter due to partial or complete failure of the attachments.

Significant puncture damage could also occur from an attack on the slapdown damage if the puncture bar is aimed at the massive cask end structure. The angle of the bar to the damaged surface will need to be a compromise between an angle that aims through the package c.g., without being so steep that it just bounces off. This test will also explore the maximum damage at the drain port.

2.12.2.3.3 NCT Free Drop

For the BRR package, which weighs just over 30,000 lb, the normal conditions of transport (NCT) free drop height required by 10 CFR §71.71(c)(7) is 2 feet. This represents only 6.7% of the energy of the HAC free drop height of 30 feet. The effect of the NCT free drop on the maximum impact and crush deformation can be found by increasing the free drop height from 30 feet to 32 feet. The governing impact (cold, 15° slapdown, secondary impact) increases by less than 4%, and the governing crush deformations (c.g.-over-corner, hot, and 15° slapdown, secondary, hot) increase by only 2%. These differences may be neglected, particularly considering that the bounding impact used in the finite element analysis is approximately 35% greater than that predicted by Appendix 2.12.5, *Impact Limiter Performance Evaluation.* Therefore, the NCT free drop does not need to be included in the certification test program.

2.12.2.4 Summary of Certification Tests

Based on the discussions in Section 2.12.2.3, *Identification of Worst-Case Test Orientations*, the planned certification tests for the BRR package are summarized below and in Table 2.12.2-1. Free drops are depicted in Figure 2.12.2-1 and puncture drops in Figure 2.12.2-2.

2.12.2.4.1 Test Sequence and Damage Accumulation

The order of free drops and punctures is given below. The order and sequence of free drop and puncture damage may be altered as long as the test objectives, as outlined above, are satisfied. If stated to be cold, the bulk average temperature of the foam must be per the discussion given in Section 2.12.2.2.1, *Temperature.* Interference of damage is expected to be negligible.

The test sequence envisions three separate prototypic impact limiter test articles. Package No. 1 consists of impact limiter nos. 1 and 2, and Package No. 2 consists of Impact Limiter nos. 2 and 3, each using the same dummy cask. The test series consists of three, 30-foot free drops, and five, 40-inch puncture drops.

Note that since all test articles are identical and include the thicker end plate, each end of the test package qualifies as the package "top", as necessary. No tests need to be performed on the package "bottom".

Test D1. Package No. 1, Limiter No. 1 will be tested in the end drop orientation at cold temperature. The purpose of this test is to quantify the maximum end drop impact acceleration, and to prepare a surface for the subsequent puncture on the thicker end plate (test P1).

Test P1. Package No. 1, Limiter No. 1 will be dropped on the puncture bar through the package c.g., onto the thicker end plate at cold temperature. The axis of the bar should pass approximately one bar diameter in from the plate edge. The axis of the bar should be oblique in order to enhance its ability to cut into the plate. The purpose of this test is to demonstrate that the thicker end plate does not perforate.

Test D2. Package No. 2, Limiter Nos. 2 (primary) and 3 (secondary) will be tested in the 15° slapdown orientation at cold temperature. The purpose of this test is to quantify the maximum impact acceleration (secondary impact) and, using analysis, to quantify the maximum crush strain (secondary impact). An additional purpose is to prepare a surface for subsequent puncture testing.

Test D3. Package No. 2, Limiter No. 3 will be tested in the c.g.-over-corner orientation. The temperature does not need to be controlled, but it must be well characterized for later analysis. The purpose of this test is to quantify the maximum crush strain in the c.g.-over-corner orientation (analytically using properties at maximum temperature); also to ensure the thicker end plate does not cause unexpected results or failure of the weld joints; and to prepare a surface for the subsequent puncture test (test P4). The impact point should be opposite from the slapdown damage.

Test P2. Package No. 2, Limiter No. 2 will be dropped such that the puncture bar strikes the inside edge of the slapdown primary-end damage from test D2. The cask axis will be as vertical as possible, given that the secondary impact limiter must clear the puncture bar. The purpose of this puncture test is to either expose a region next to the cask top end structure which could soak in heat in the HAC fire, or possibly dislodge the limiter by failing some or all attachments. The puncture bar will need to have adequate length; bending of the bar would not be an unexpected outcome of this test.

Test P3. Package No. 2, Limiter No. 2 will be dropped onto the puncture bar with an impact point on the primary-end impact damage from test D2. The exact impact point and orientation of the package axis may be chosen by the Test Engineer in light of the damage which occurs in test D2, but the package axis should be nearly horizontal (0° to 15° from the horizontal), and the impact point approximately halfway between the cask end surface and the limiter outside end surface. Therefore, the bar axis is not through the package c.g., but could do significant damage before the package has time to rotate.

Test P4. Package No. 2, Limiter No. 3 will be dropped on the damage from the c.g.-over-corner free drop, with impact on the thinner conical shell material. The puncture bar edge will align with the joint between the thick end plate and the thinner conical plate, and be aimed to miss significant support from the cask end structure, i.e., with the package axis inclined approximately 75° from the horizontal. This will miss the package c.g. by only a few inches, and the energy loss will be insignificant. The purpose of this test is to quantify a possible worst-case configuration for the HAC fire thermal analysis.

Test P5. Package No. 2, Limiter No. 3 will be dropped such that the puncture bar strikes the approximate center of the slapdown secondary damage, in order to create the smallest remaining foam thickness adjacent to the cask end structure (location of the drain port). The cask axis should be approximately 30° to the horizontal. The bar axis should be aimed directly at the cask end structure, but it will not be directly through the c.g. To aim through the c.g. would mean that impact with the damaged limiter would be too oblique, and the cask would be expected to only bounce off of the bar.

2.12.2.4.2 Measurements

Measurements of the certification test results will be made in explicit support of the test objectives identified in Section 2.12.2.3, *Identification of Worst-Case Test Orientations*, and will consist of configuration (dimensional) measurements of the damage, and acceleration

measurements of the free drops. Temperature measurements will be made on an ongoing basis to fully characterize the bulk average temperature of the foam.

Measurements of the free drop deformation damage will take springback of the limiter into account, and by use of crush gages or other techniques, attempt to obtain the maximum crush at the moment of impact. Puncture measurements should be made from the prevailing damage surface and record the depth and diameter, or other relevant information, of the puncture test damage. A conventional speed video and still photographic record of each drop and puncture should also be made.

Accelerometers should be redundant, and placed to adequately characterize the primary and secondary slapdown impacts. The data should be filtered to obtain the rigid body impact, using the guidance of a fast Fourier transform (FFT), or equivalent, of the time history data.

2.12.2.5 Acceptance Criteria

The following are the acceptance criteria for certification testing of the BRR package:

1. The impact limiter shells must retain their general integrity for all impacts and deformations. Ripped welds or other tears or fissures are acceptable as long as they are limited in extent and compatible with the HAC fire thermal analysis. Full puncture perforation of the impact limiter shells in regions of standard thickness is expected.
2. The impact limiter attachments must retain the limiters on the cask. A limited degree of distortion or dislodging of the limiters is acceptable, but must be compatible with the HAC fire thermal analysis.
3. The impact limiters must maintain package deceleration to acceptable levels. The safety analyses will utilize as inputs values which bound the results of the certification test.
4. The thicker end plate must not perforate in the puncture drop test.
5. The maximum damage to the limiter from the single worst-case free drop and puncture test sequence must fall within the bounding assumptions used in the HAC fire thermal analysis.

Table 2.12.2-1 - Summary of Certification Tests

No.	Test Description	Test Limiter	Temperature	Purpose of Test & Expected Damage
D1	End drop	#1	Cold (see note 2)	Maximum end impact
D2	Slapdown oblique drop, 15°	#2 & #3	Cold (see note 2)	Maximum slapdown secondary impact, obtain data to permit calculation of maximum strain
D3	C.G. over corner drop	#3	Not controlled	Obtain data to permit calculation of maximum strain
P1	Oblique through c.g. on thicker end plate on test D1 damage	#1	Cold (see note 2)	Demonstrate perforation resistance of thicker end plate
P2	Approx. parallel to package axis, on test D2 primary-end damage	#2	Not controlled	Quantifies possible maximum accumulation of free drop and puncture damage – local severe damage or dislodge limiter
P3	Approx. perpendicular to package axis, on test D2 primary-end damage	#2	Not controlled	Quantifies possible maximum accumulation of free drop and puncture damage – chimney or other severe damage
P4	On test D3 damage, on thick/thin joint, near c.g.	#3	Not controlled	Quantifies possible maximum accumulation of free drop and puncture damage – minimum foam thickness at cask corner
P5	Oblique to package axis, on test D3 secondary-end damage	#3	Not controlled	Quantifies possible maximum accumulation of free drop and puncture damage – minimum foam thickness at cask side

Notes:

1. All free drops (Dx) are from 30 feet, and all punctures (Px) are from 40 inches.
2. See Section 2.12.2.2.1, *Temperature*.

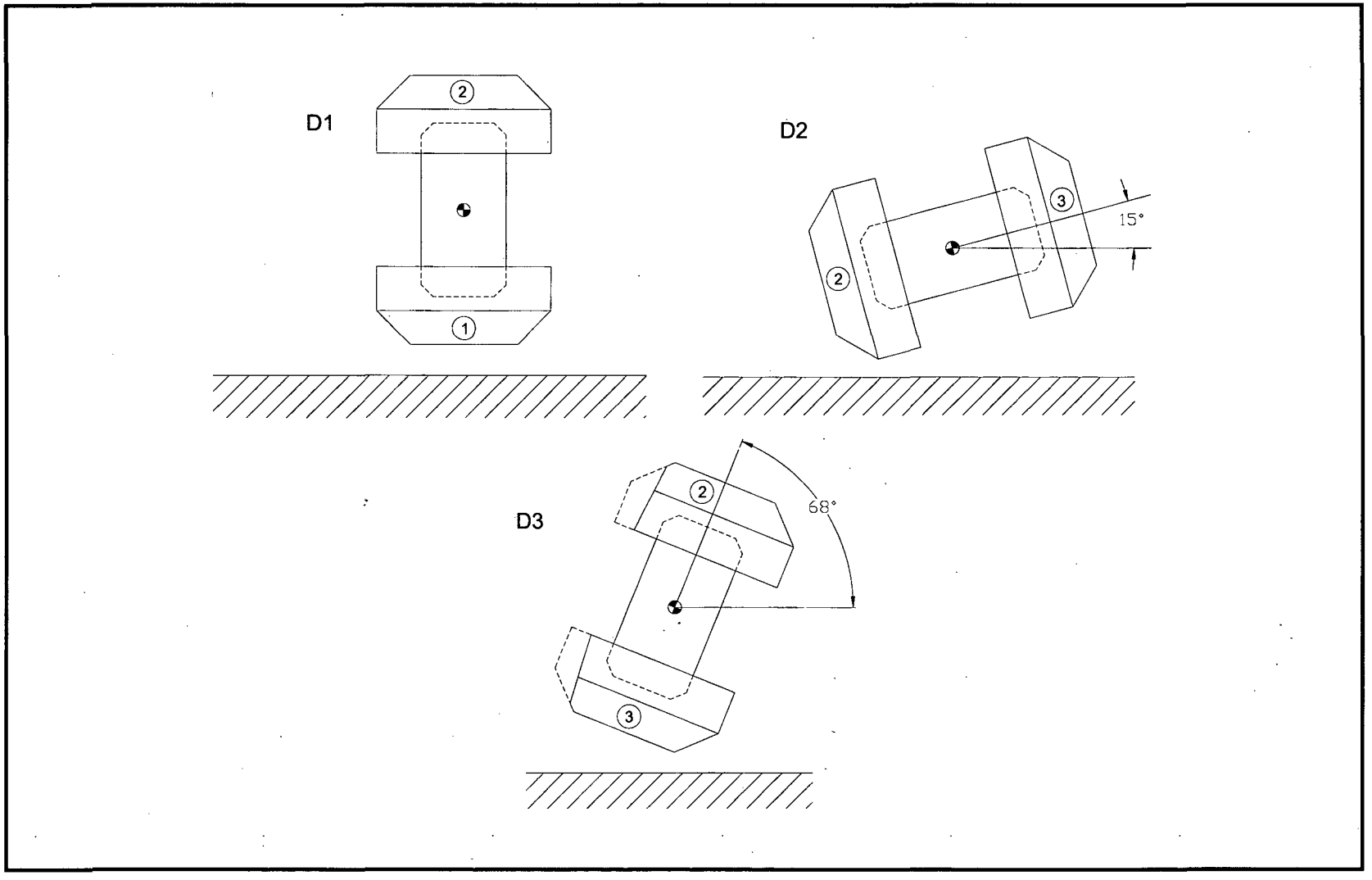

Figure 2.12.2-1 - BRR Package Free Drop Orientations

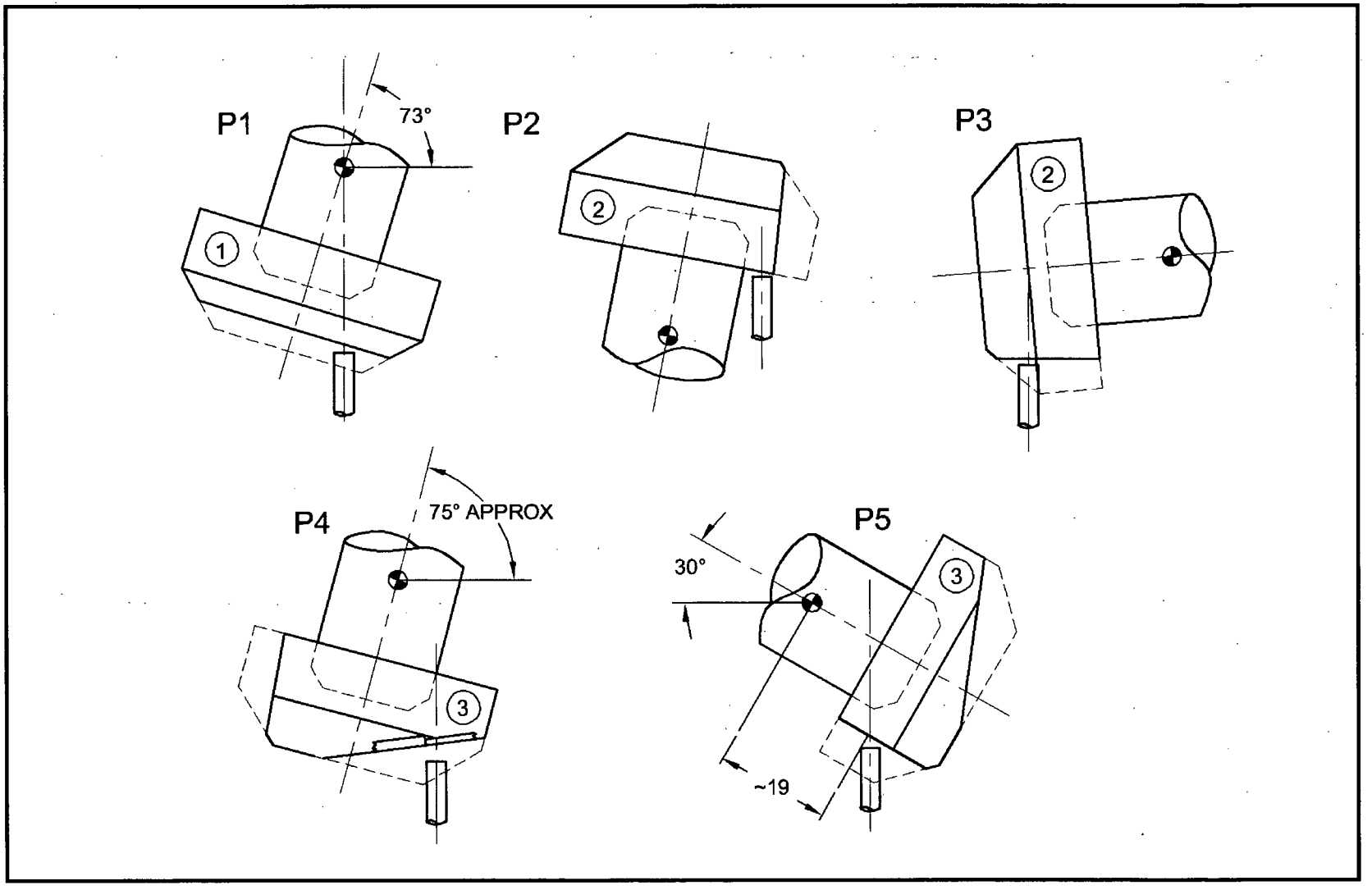

Figure 2.12.2-2 - BRR Package Puncture Drop Orientations

2.12.3 Certification Test Results

This appendix presents results of the certification tests that were performed on the BEA Research Reactor package impact limiters. The information contained in the certification test report is summarized.

2.12.3.1 Introduction

Demonstration of the compliance of the BRR package design with the requirements of 10 CFR §71.73 is achieved primarily by analysis. Certification testing is used to demonstrate the performance of the polyurethane foam-filled impact limiters. The tests reported in this appendix were performed using prototypic, half-scale test impact limiters and a dummy cask which had prototypically scaled weight. Both the impact limiters and the attachments (including the limiter attachment components and the cask attachment components) were of prototypic materials and construction. The impact limiter test specimens were in full compliance with the drawings in Section 1.3.3, *Packaging General Arrangement Drawings*, except for the scale factor of ½, and with the exceptions discussed below in Section 2.12.3.3, *Test Unit Configuration.*

The objectives of these tests were to demonstrate the general structural integrity of the impact limiters and attachments in free drop and puncture events, to confirm the maximum impact magnitudes, and to verify that the maximum damage to the impact limiters was bounded by the assumptions used in the thermal and criticality analyses. Further discussion of the tests, including a justification of the tests chosen, is provided in Appendix 2.12.2, *Certification Test Plan.* A comparison of the test results to the impact limiter calculations is given in Section 2.12.5.3, *Reconciliation with Certification Test Results.*

2.12.3.2 Test Facilities

Free drop and puncture testing was performed at Hiline Engineering in Richland, Washington. The drop pad had a total weight of approximately 50,000 lb. The embedded steel plate target had a thickness of 2½ inches. The pad therefore constituted an essentially unyielding surface for the test package, which weighed somewhat less than 4,000 lb.

In accordance with the requirements of 10 CFR §71.73(c)(3), the half-scale puncture bars were fabricated from solid, 3-inch diameter mild steel bars. Puncture bars of two lengths were used: 25 inches and 50 inches long, measured from the top of the baseplate. The length of each bar was designed to allow the puncture event to proceed to completion before the test package gained any support from the unyielding surface, but without excessive length. Each puncture bar was welded with gussets perpendicularly to a thick, mild steel plate. The top edge of each puncture bar was finished to a 1/8-inch maximum radius. Each puncture bar assembly was securely welded to the impact surface.

2.12.3.3 Test Unit Configuration

The certification test articles were essentially prototypic, half-scale models of the BRR package impact limiters. Three test articles were fabricated using drawings which were in compliance with the drawings in Section 1.3.3, *Packaging General Arrangement Drawings*, except for the differences enumerated and justified below.

The dummy cask was a steel cylinder which represented the BRR cask in half-scale. It consisted of a thick-walled carbon steel outer cylinder, having an outer diameter of 19 inches and an inner diameter of 12.3 inches. The inner cavity was occupied by a lead-filled pipe. The cask impact limiter attachments were prototypic and made of Type 304 stainless steel. The cask attachments were welded to stainless steel plates which were embedded in the surface of the dummy cask, thus ensuring that the entire impact limiter attachment load path was fully prototypic. The weights of the dummy cask and impact limiters are given in Table 2.12.3-1.

The following list summarizes the differences between the test articles and the full-scale production impact limiters:

1. The half-scale impact limiters had no lifting features, which consist of threaded lifting bosses located in the end sheet of the upper limiter. This omission had no effect on the test results.
2. The half-scale impact limiters had no paint. This omission had no effect on the test results.
3. The dummy cask, which modeled the cask, shield plug, closure lid, and maximum contents, weighed 3,181 lb. In full-scale, that weight would be eight times larger, or 25,448 lb. This is approximately 7% less than the estimated upper bound weight of the full-scale cask body, less impact limiters, of 27,400 lb. This difference is not significant.
4. Subsequent to testing, the impact limiter corner joint between the top surface and the cylindrical outer shell has been revised. This change came about as a result of the tests documented in Section 2.12.3.5.4, *Repeated Oblique Slapdown Free Drop Test D2R* and Section 2.12.3.5.8, *Puncture Drop Test P5*. In the secondary slapdown impact of free drop D2R, and exacerbated in the subsequent puncture drop P5, the outer shell seam split open, exposing the polyurethane foam. To prevent this seam failure from recurring, the outer shell joint has been redesigned to include two lap joints on the corner angle. The 'from' and 'to' configuration of the outer shell joint is shown in Figure 2.12.3-3. Since the outer joint can no longer be used as a final closure joint of the impact limiter shell during fabrication, a new seam has been introduced near the inner shell, as shown in Figure 2.12.3-4. Since the redesigned corner joint is stronger than the tested design, the change is conservative.
5. Subsequent to testing, the full-scale inner diameter of the impact limiter was reduced from 38.5 inches to 38.25 inches, which reduces the diametral clearance between the impact limiter and the cask OD from 0.5 inches to 0.25 inches. This change has the effect of reducing the attachment loads, since it will more closely couple the impact limiter to the cask. Thus the change is conservative.
6. The impact limiter attachment ball-lock pins used in testing were made of carbon steel. The full-scale production pins will be made of stainless steel. Since the stainless steel pins have a higher rated load than the carbon steel pins, this difference is conservative.
7. Subsequent to testing, the impact limiter attachment to the cask has been increased in size. This change came about as a result of the tests documented in Section 2.12.3.5.3, *Oblique Slapdown Free Drop Test D2* and Section 2.12.3.5.4, *Repeated Oblique Slapdown Free Drop Test D2R*. In the oblique slapdown drops D2 and D2R, a majority of the attachments of the primary impact limiter failed. To prevent this failure from recurring, the attachments have been increased in size and in quantity. The detail of the change, and the result of a confirmatory retest, are documented in Section 2.12.3.6, *Confirmatory Test of Attachments*.

2.12.3.4 Instrumentation

2.12.3.4.1 Accelerometers

Accelerometers were used to record the impact of each free drop, except drop D2C, which was a confirmatory test for the revised impact limiter attachments. Accelerations of the puncture drops were not recorded. For axial or near-axial drop orientations (D1 – end drop, and D3 – c.g.-over-corner drop), the measurement axis of the accelerometers was axial. For the near-horizontal, 15° slapdown drops (D2 and D2R), the measurement axis was transverse to the cask axis.

Four axial and four transverse mounting positions were provided at each end of the cask. The measurement axes were as close to the cask surface as possible, and the mounting blocks were rigidly welded to the cask. The transverse measurement axis was located 8.68 inches from the flat end of the cask. The mounting location and orientation of each accelerometer is shown in Figure 2.12.3-5 and Figure 2.12.3-6. The transverse accelerometers at each end were all mounted on the same axial plane with their axes parallel.

The raw data was conditioned and low-pass filtered at a level of 1019 Hz. As shown in Section 2.12.3.7, *Accelerometer Plots*, the filtered accelerometer time histories retain a significant vibrational component, indicating that a lower filter cutoff frequency could have been used, which would have lowered the peak values. The rigid body peak accelerations (i.e., without a vibrational component) are estimated by observation of the accelerometer time histories and are shown in Table 2.12.3-6 in Section 2.12.3.7, *Accelerometer Plots*.

The (1019 Hz) filtered peak acceleration values are adjusted using the accelerometer calibration constants listed in Table 2.12.3-5 below. The calibration constants were not entered into the signal conditioner, and therefore are applied manually only to the peak value of the accelerometer output, as shown in Section 2.12.3.5, and not to the entire output. Thus, the filtered accelerometer plots, in Section 2.12.3.7, do not show the effect of this adjustment. Since the calibration constants are all between 0.89 and 0.97 mV/g, the adjusted peak acceleration value is approximately 10% higher than the peak value shown on the plots in Section 2.12.3.7. Individual results are discussed in Section 2.12.3.5.

2.12.3.4.2 Thermocouples

A refrigerated trailer was present onsite to chill the certification test articles prior to assembly onto the dummy cask for testing. Thermocouples were inserted in 1/8-inch diameter holes in each test article, five inches deep, and approximately 6.75 inches from the flat annulus side of the test article. Two thermocouples were used for each test article, located 180° apart. Since the minimum temperature which could be set on the chiller unit was -20 °F, the test articles were generally between -10 °F and -20 °F at the time of test. The temperature of the foam in tests D3, P2, P2C, P3, P4, and P5 was not required to be cold. Temperature of the foam was recorded just prior to the test for the impact limiter(s) experiencing impact or puncture.

2.12.3.5 Test Results

Results for the initial series of four, 30-ft free drop tests and five puncture drop tests are given in the sections below. (Results for the confirmatory test of the attachments (tests D2C and P2C) are given in Section 2.12.3.6, *Confirmatory Test of Attachments*.) The tests were performed in the order D1, P1, D2, D2R, P2, D3, P4, P5, P3. A description of the tests is given in Table 2.12.3-2.

Figures of the tests are shown in Figure 2.12.3-1 and Figure 2.12.3-2. Peak accelerations given in tables below are taken from column B, 'From Plots, Calibration Adjusted' of Table 2.12.3-6, in Section 2.12.3.7, *Accelerometer Plots*. The average of the peak values is then resolved to a value which is perpendicular to the ground, when necessary. Since the data was collected orthogonal to the cask axes, the resolution of the data in the oblique impact cases is as follows.

For test D1, which was a vertical end drop, the accelerometers were mounted with their measurement axes parallel to the dummy cask axis. Therefore, the accelerometer readings require no adjustment.

For tests D2 and D2R, which were identical, 15° slapdown free drops, the accelerometers were mounted with their measurement axes transverse to the dummy cask axis. For the secondary impact, in which the cask axis is essentially parallel to the ground, the accelerometer readings require no adjustment. For the primary impact at 15°, the average accelerometer reading is divided by the cosine of the recorded impact angle to obtain the impact which occurred perpendicular to the ground.

For test D3, which was the c.g.-over-corner free drop, the accelerometers were mounted with their measurement axes parallel to the dummy cask axis. The average accelerometer reading is divided by the cosine of 23°, which corresponds to the recorded angle between the cask axis in the c.g.-over-corner drop and the ground, to obtain the impact perpendicular to the ground.

All puncture drop tests were performed from a height of 40 inches above the top of the puncture bar. All puncture tests except P2 and P2C were performed using a 25-inch long puncture bar. Tests P2 and P2C utilized the 50-inch long bar. The puncture bars remained securely attached to the steel drop pad in all cases.

For each test, the recorded temperature of the polyurethane foam was taken as described in Section 2.12.3.4.2, *Thermocouples*. Note that all data reported in this appendix applies to the half-scale test unless stated otherwise. According to the laws of scaling, the full-scale linear measurements are twice those recorded here, and the full-scale accelerations are half of those recorded here. The tests are documented in the order in which they were performed.

2.12.3.5.1 Free Drop, Vertical (D1)

Test D1 was performed using a drop height of 30 feet, oriented with the cask axis vertical, as shown in Figure 2.12.3-1 and Figure 2.12.3-7. The lower impact limiter was serial number 1. The two polyurethane foam temperature readings were -16.4 °F and -15.6 °F. Four accelerometers were used. Results are shown in the table below.

Free Drop Test D1 (End)					
Channel	**12**	**13**	**14**	**15**	**Avg.**
Peak Value	110g	121g	113g	118g	**116g**

The impact deformation was a combination of outside-in and inside-out. The outside-in crush depth is calculated from the diameter of the scuff mark (contact area) on the bottom of the limiter. Two orthogonal diameter measurements showed a scuff diameter of 27-1/2 and 27-5/8 inches, or an average of 27.6 inches. Since the original diameter of the bottom of the impact

limiter was 24.0 inches, and the tapered portion had an angle of 45°, the outside-in crush distance is:

$$(D_{scuff} - D_{orig})/2 = 1.8 \text{ inches}$$

The inside-out crush distance is calculated from the dimension from the top of the dummy cask (with the upper impact limiter removed) to the outside rim of the lower impact limiter. Since the outside rim of the limiter is undeformed, this measurement will reveal how far the dummy cask has "sunk" into the lower impact limiter. Measurements of this distance, taken in four quadrants, were 29-7/8, 29-7/8, 30-1/2, and 30-7/16 inches. The average value is 30.2 inches. In an undeformed limiter, the top surface of the cask would stand (38.6 – 6.8) = 31.8 inches above the outer rim of the lower limiter, given that the cask is 38.6 inches long, and the center pocket of the limiter is 6.8 inches deep. The inside-out crush is therefore (31.8 – 30.2) = 1.6 inches. The sum of the outside-in and inside-out crush distances is therefore 1.8 + 1.6 = 3.4 inches.

The impact limiter was securely attached following the test. Of the six impact limiter attachment pins, one failed by bending and shear, and others showed signs of bending without failure. At least two had no noticeable damage. The shells of the limiter deformed without any tearing or exposure of foam. The post-test configuration is depicted in Figure 2.12.3-8 and Figure 2.12.3-9.

2.12.3.5.2 Puncture Drop Test P1

Puncture test P1 was performed immediately after drop test D1. The test was a c.g.-over-corner impact on the thicker bottom plate of the impact limiter, near the outer edge of the thicker plate, as shown in Figure 2.12.3-2 and Figure 2.12.3-10. The impact took place on the crush damage from free drop test D1, on serial number 1. The angle of the cask axis was 73° ±3° to the horizontal. The two polyurethane foam temperature readings were -3.8 °F and -5.0 °F.

The bar impact was located approximately one inch from the outer edge of the thicker bottom plate (i.e., the center of the 3-inch bar was approximately 2-1/2 inches in from the edge). The impact created a dent approximately 1-3/4 inches deep. One or two rebound impacts having negligible deformation also occurred. There were no signs of cracking in the dent or in the nearby weld seam. The post-test configuration is depicted in Figure 2.12.3-11 and Figure 2.12.3-12.

2.12.3.5.3 Oblique Slapdown Free Drop Test D2

Test D2 was performed using a drop height of 30 feet, oriented with the cask axis at 16° to the horizontal, as shown in Figure 2.12.3-1 and Figure 2.12.3-13. The primary (lower) impact limiter was serial number 2, and the secondary (upper) impact limiter was serial number 3. The polyurethane foam temperature reading in the primary limiter was -15.6 °F (only one thermocouple was functioning), and in the secondary limiter, the readings were -13.8 °F and -16.4 °F. Four accelerometers were used at each end. Results are shown in the table below.

The general post-test configuration is shown in Figure 2.12.3-14. Comparing the measurements of the undeformed and deformed impact limiters, as shown in Figure 2.12.3-15, the crush distance, perpendicular to the ground, was 3.9 inches for the primary impact limiter and 4.0 inches for the secondary impact limiter.

Free Drop Test D2 (15° Oblique)					
Channel	**16**	**17**	**18**	**19**	**Avg., Primary End**
Peak Value, g	Severed wire	133g	137g	135g	**140g ⊥ to ground***
Channel	**12**	**13**	**14**	**15**	**Avg., Secondary End**
Peak Value, g	102g	108g	110g	108g	**107g**

*Equal to (133 + 137 + 135)/3/cos(16°).

In the test, all of the attachment pins on the primary impact limiter sheared off. The limiter remained attached to the cask, although after coming to rest, it was displaced approximately 1-1/2 inches at the top, as shown in Figure 2.12.3-16. None of the pins failed on the secondary impact limiter. There was some incipient cracking of the weld seam on the secondary limiter, but the cracks were of insignificant size and no foam was exposed. The impact surfaces of the impact limiters are shown in Figure 2.12.3-17.

2.12.3.5.4 Repeated Oblique Slapdown Free Drop Test D2R

Test D2R was designed as a repeat of test D2, made after increasing the size of the attachment pins from the original diameter of 1/4 inches to 1/2 inches. To accommodate this increase, the hole through the cask attachment lugs was increased to 1/2 inches and the hole in the impact limiter blade was increased to 5/8 inches. The effect of increasing the blade hole size was to reduce the ligament width on both sides of the hole, but especially on the inner side (toward the cask body). These changes were made to all three impact limiter test articles. Due to the small size of these ligaments, the inner ligament width on serial numbers 1 and 3 were enhanced after drilling by application of a Type 308 weld overlay. Serial number 2 ligaments were not enhanced after drilling. The average ligament widths of the three impact limiters are as follows:

- S/N 001: 0.306 inches (weld overlay enhanced)
- S/N 002: 0.243 inches (not welded)
- S/N 003: 0.320 inches (weld overlay enhanced)

The attachment pins were Carr-Lane part no. CL-8-BLPT-2.00, 1/2-inch diameter carbon steel ball lock pins, having a rated load of 16,000 lb, or four times that of the 1/4-inch pins.

Test D2R was performed using a drop height of 30 feet, oriented with the cask axis at 17° to the horizontal, as shown in Figure 2.12.3-1 and Figure 2.12.3-18. The primary (lower) impact limiter was serial number 2, rotated 180° from its orientation in test D2. The secondary (upper) impact limiter was serial number 1. The polyurethane foam temperature readings in the primary limiter were -13.4 °F and -12.8 °F, and in the secondary limiter, the readings were -13.0 °F and -13.4 °F. Four accelerometers were used at each end. Results are shown in the table below.

Free Drop Test D2R (15° Oblique)					
Channel	**16**	**17**	**18**	**19**	**Avg., Primary End**
Peak Value, g	111g	116g	106g	106g	**115g ⊥ to ground***
Channel	**12**	**13**	**14**	**15**	**Avg., Secondary End**
Peak Value, g	113g	111g	106g	124g	**114g**

*Equal to (111 + 116 + 106 + 106)/4/cos(17°).

The general post-test configuration is shown in Figure 2.12.3-19. Comparing the measurements of the undeformed and deformed impact limiters, as shown in Figure 2.12.3-20, the crush distance, perpendicular to the ground, was 4.0 inches for the primary impact limiter and 3.9 inches for the secondary impact limiter. Note that the measurements of the crush in test D2 are very similar to these (3.9 inches primary and 4.0 inches secondary). This is to be expected since the tests are essentially identical. However, since test D2 showed the apparent anomaly of the primary impact being significantly higher than the secondary impact (the opposite would be expected), then test D2R will be taken as the official crush results for this orientation.

In the test, none of the attachment pins failed, but four out of six of the blades of the primary limiter failed by tensile failure of the inner ligaments, as shown in Figure 2.12.3-21. The limiter remained attached to the cask, although after coming to rest, it was displaced approximately 2 inches at the top, as shown in Figure 2.12.3-19. None of the pins or ligaments failed on the secondary impact limiter, although the holes were elongated up to 0.854 inches.

In addition, the corner joint between the top annular plate and the outer cylindrical shell of the secondary impact limiter (serial number 1) failed in the impact region, as shown in Figure 2.12.3-22. This limiter had been tested in the 30-foot end drop (D1) and the subsequent puncture (P1), and the torn joint may have been the result of over-testing. The tear had a maximum opening of 1/2 inches. It appeared to start at the outer edges of the impact zone and travel inward. The length of the torn joint on one side was 7-1/2 inches, and on the other side 10-1/4 inches, with approximately 4-3/4 inches of sound material in the center. The tear appeared in both the weld as well as in the leg of the corner angle located on the top surface. However, the tear did not occur in the outer cylindrical shell side of the joint, where the thickness is double by virtue of the lap joint used in that position.

2.12.3.5.5 Puncture Drop Test P2

Puncture test P2 was performed immediately after drop test D2R. The longer puncture bar was used to impact the top annular surface of the damaged primary impact limiter (serial number 2), as shown in Figure 2.12.3-2 and Figure 2.12.3-23. The orientation could not be over the center of gravity due to the desired impact location. The impact occurred just to the inside of the bulge, in approximately the radial center of the annular plate. The two polyurethane foam temperature readings were -0.2 °F and -3.0 °F.

The impact dent on the annular plate was negligible, but the impact limiter became significantly dislodged from the cask end due to the failure of the impact limiter attachment blades, as shown in Figure 2.12.3-24. By inspection of the conventional-speed video record, the impact limiter was displaced by a greater amount than is shown in the figure, before it was driven partially back on by a secondary impact with the safety wall.

2.12.3.5.6 CG-Over-Corner Free Drop Test D3

Test D3 was performed from a drop height of 30 feet, with the cask axis oriented at 67° to the horizontal, or essentially center of gravity over corner, as shown in Figure 2.12.3-1 and Figure 2.12.3-25. The lower impact limiter was serial number 3, rotated 180° from its orientation in test D2. The polyurethane foam temperature reading in the lower limiter was -2.2 °F (the other thermocouple was not functioning). Four accelerometers were used at each end, oriented parallel

to the cask axis. Results are shown in the table below. Note, since channels 16 – 17 exhibited excess noise, only channels 12 – 15 are used.

Free Drop Test D3 (CG Over Corner)					
Channel	**12**	**13**	**14**	**15**	**Avg.**
Peak Value, g	106g	111g	110g	103g	**117g ⊥ to ground***

*Equal to (106 + 111 + 110 + 103)/4/cos(23°).

The general post-test configuration is shown in Figure 2.12.3-26. Comparing the measurements of the undeformed and deformed impact limiters, as shown in Figure 2.12.3-27, the crush distance perpendicular to the ground was 5.5 inches.

None of the pins or ligaments failed the test, although the holes were elongated up to 0.725 inches. There were no shell failures and no exposure of foam.

2.12.3.5.7 Puncture Drop Test P4

Puncture test P4 was performed on the damage incurred in free drop test D3, on serial number 3. The bar impacted just outside the thicker bottom plate, on the 0.12-inch thick material which once constituted the tapered region of the shell. The orientation is shown in Figure 2.12.3-2 and Figure 2.12.3-28. The cask axis was oriented at 74° to the horizontal. The line of action was nearly, but not completely, c.g.-over-corner. The polyurethane foam temperature readings in the lower limiter were 17.6 °F and 5.0 °F.

As expected, the puncture bar penetrated the shell, and entered the foam to a depth of 2-1/4 inches. The width of the hole was 4 inches, and the length of the hole/torn flap was 5 inches. The impact limiter attachments were not affected. A close-up view of the damage is shown in Figure 2.12.3-29.

2.12.3.5.8 Puncture Drop Test P5

Puncture test P5 was performed on the damaged corner joint created in free drop test D2R on serial number 1 (the secondary impact end). The orientation is shown in Figure 2.12.3-2 and Figure 2.12.3-30. The puncture bar was oriented at approximately 45° to the package axis, and contacted a fold which was adjacent to the damaged corner joint. Since the test was carried out shortly after puncture test P4, the polyurethane foam temperature is considered to be essentially the same as that recorded for test P4.

The bar caught the fold and tore the damaged joint open as shown in Figure 2.12.3-31 and Figure 2.12.3-32. The total length of the damage, measured as a chord, was approximately 26 inches. At the location of the bar (i.e., the center of the damage), the width was 5 inches. On either side the width of the opening was approximately 2-1/2 inches, tapering to zero at the ends. Only negligible amounts of foam were lost from the shells as shown in Figure 2.12.3-32.

2.12.3.5.9 Puncture Drop Test P3

Puncture test P3 was performed on the secondary slapdown damage incurred by serial number 3 in free drop test D2. The orientation is shown in Figure 2.12.3-2 and Figure 2.12.3-33. The bar struck the damaged area approximately in the center. The cask axis was at a small angle to the

horizontal. Since the test was carried out shortly after puncture tests P4 and P5, the polyurethane foam temperature is considered to be essentially the same as that recorded for test P4.

The depth of the impact dent was approximately one inch. There was no sign of cracking or tearing of the impact limiter shell, as shown in Figure 2.12.3-34.

2.12.3.6 Confirmatory Test of Attachments

The confirmatory tests were performed on February 17, 2009 at Hiline, in order to demonstrate the adequacy of the redesigned impact limiter attachments. The test used the existing dummy cask and impact limiters, which had been altered to enhance the strength of the attachments. The revisions made to the test articles resulted in attachments which, in full-scale, were not stronger than the attachment design used on the production hardware.

None of the other tests will be invalidated by the increase in the strength of the attachments. In all of the other tests, the attachments did not fail, therefore, making the attachments stronger had no effect on the prior tests.

The tests that were selected to demonstrate the attachments were the D2 free drop and P2 puncture drop configurations. The D2 drop was chosen since that is the orientation in which the primary impact limiter attachments consistently failed. Attachment failures did not occur in any other impacts. The P2 puncture was chosen since a) a puncture subsequent to free drop is required by 10 CFR 71, and b) it is the puncture test that places the greatest load on the attachments. The test article having the greatest remaining capacity for an additional impact was serial no. 2, which was the primary limiter in tests D2 and D2R. The secondary limiter in the confirmatory tests was serial no. 3, which was less damaged than serial no. 1. The confirmatory tests were designated D2C and P2C.

Prior damage required that the CTU be rotated 90° about its axis. Since the attachment pattern has only one plane of symmetry, this meant that instead of one worst-case loaded attachment at 12 o'clock (relative to the impact at 6 o'clock), there were two attachments at approximately 11 and 1 o'clock, which were loaded somewhat less than in the prior drops. However, since the production redesign now features eight attachments, the load developed in each of the two maximum-loaded attachments in this test was greater than the maximum load which would develop in the production design.

2.12.3.6.1 Description of Design Changes

The configuration of the attachments was increased in capacity as much as possible given the limitations of the existing hardware. In no case did the revised test hardware have a greater strength than the revised full-scale design. A detailed comparison of the test configuration and the full-scale design is given in Section 2.7.1.7, *Impact Limiter Attachments*. The revised CTU attachment is depicted in Figure 2.12.3-35. The nominal thickness of the blades, made of ASTM Type 304 material, was 3/8 inches. The width of the blades was increased to 1.5 inches, and their inner edge was set at 1/8 inches from the inner diameter of the impact limiter. The new blades were attached to the original blade roots using a full penetration weld, and the region between the top surface of the limiter and the new blade (approximately 1/2-inches) was buttered with weld metal to approximately the dimensions of the new blade. The hole in the blade was match-drilled from the existing hole in the cask attachments, and drilled out to 9/16 inches in diameter. The thickness, width, hole diameter, and hole-to-inner edge dimension for each blade

before testing are given in Table 2.12.3-3. Serial no. 2 was mated with end A of the dummy cask, at the existing orientation marks.

Since the secondary impact limiter attachments did not fail in either prior slapdown drop, the refurbishment to serial no. 3 was minimal. The existing 3/16-inch thick blade was cut off and replaced with the same thickness material by a full penetration weld, match drilled to the existing holes on cask end B, and drilled out to 9/16-inch diameter. Both limiters were attached using 1/2 inch diameter carbon steel ball lock pins (the same specification as used in test D2R).

Since the test articles had both received two prior 30-ft drop impacts, and since good data was collected in the same orientation in tests D2 and D2R, test D2C was not instrumented with accelerometers. Both impact limiters were cold for the free drop test. Foam temperature was not recorded for the secondary limiter since the purpose of this test was not related to the secondary impact event.

2.12.3.6.2 Oblique Slapdown Free Drop Test D2C Results

Test D2C was performed using a drop height of 30 feet, oriented with the cask axis at 17° to the horizontal, as shown in Figure 2.12.3-1 and Figure 2.12.3-36. The primary (lower) impact limiter was serial no. 2, and the secondary (upper) impact limiter was serial no. 3. The polyurethane foam temperature readings in the primary limiter were -8.8 °F and -5.6 °F. The primary limiter was oriented so that blade nos. 5 and 6 were directly opposite the impact, where experience showed that the attachment loads are the highest.

The crush deformations were very similar to those obtained in tests D2 and D2R on the same limiter. All of the attachments, both primary and secondary, remained completely intact. Figure 2.12.3-37 and Figure 2.12.3-38 show the post-test configuration of the two most highly loaded attachments, at locations #5 and #6, respectively. All welds attaching the blades to the impact limiter appeared in good condition without failure. The attachments were examined in further detail following the puncture test.

2.12.3.6.3 Puncture Drop P2C Results

Puncture test P2C was performed immediately after drop test D2C. The longer puncture bar was used to impact the top annular surface of the damaged primary impact limiter (serial no. 2), as shown in Figure 2.12.3-2 and Figure 2.12.3-39. The orientation could not be over the center of gravity due to the desired impact location. The impact occurred adjacent to the outside edge of the limiter, halfway between attachment locations #5 and #6, thus maximizing the moment arm and loading of those attachments. The polyurethane foam temperature reading closest to the impact was lower than -3.0 °F.

The impact caused the long puncture bar to bend somewhat, but the attachment to the steel drop pad plate remained intact. The impact dent on the annular plate was negligible, without any cracking or tearing of the steel shell, and no exposure of foam. The attachments all appeared to be in good shape following the test. Figure 2.12.3-40 shows the impact dent and the attachment at location #5.

2.12.3.6.4 Examination of Attachments

After removal of the impact limiters from the dummy cask, the attachments were examined in detail. There was very little evidence of plastic deformation in the attachments, except that the holes of the most highly loaded blades were very slightly elongated. There was no evidence of bearing yielding in the hole, and no evidence of bending or cracking in the attachment pins. There was no evidence of weld cracking or deformation, except in one case, part of the weld between the blade and the annular sheet showed some shear. This was due to deformation of the annular plate in the puncture test, and this weld has no role in the impact limiter attachment load path. Table 2.12.3-4 shows the measurements of the blade after test. Comparing Table 2.12.3-3 and Table 2.12.3-4, the largest increase in the hole dimension (measured in-line with the attachment loading direction, parallel to the cask axis) was 0.034 inches for blade no. 5, which is negligible. A comparison of the hole-to-edge dimension indicates that this distance appeared to increase slightly in several cases (ranging between a 0.016-inch decrease in width to a 0.010-inch increase), but as this goes against reason, it is assumed to be caused by measuring error on the rough surfaces. Figure 2.12.3-41 shows the blade configuration at location #5, and Figure 2.12.3-42 shows location #6, after all testing. Figure 2.12.3-43 shows a view of all of the pins used to retain the primary impact limiter. These photographs demonstrate that the attachments were essentially unchanged by the test loads.

The cask receptacle plate holes were somewhat elongated from prior testing (they were not refurbished). After the tests, the holes did not appear to have deteriorated any further.

Table 2.12.3-1 - CTU Weights

Component	Weight, lb
Dummy Cask	3,181
Impact Limiter Serial No. 1	278
Impact Limiter Serial No. 2	276
Impact Limiter Serial No. 3	276

Table 2.12.3-2 - Summary of Certification Tests

No.	Test Description	Test Limiter	Temperature
D1	End drop	#1	Cold per Section 4.3
D2	Slapdown oblique drop, 15°	#2 & #3	Cold per Section 4.3
D2R	Slapdown oblique drop, 15°	#2 & #1	Cold per Section 4.3
D2C	Slapdown oblique drop, 15°	#2 & #3	Cold per Section 4.3
D3	C.G.-over-corner drop	#3	Not controlled
P1	Oblique through c.g. on thicker end plate on test D1 damage	#1	Cold per Section 4.3
P2	Approx. parallel to package axis, on test D2 primary-end damage	#2	Not controlled
P2C	Approx. parallel to package axis, on test D2C primary-end damage	#2	Not controlled
P3	Approx. perpendicular to package axis, on test D2 primary-end damage	#2	Not controlled
P4	On test D3 damage, on thick/thin joint, near c.g.	#3	Not controlled
P5	Oblique to package axis, on test D3 secondary-end damage	#3	Not controlled

Notes:

1. All free drops (Dx) are from 30 feet, and all punctures (Px) are from 40 inches.
2. Figures of each orientation are provided in Figure 2.12.3-1 and Figure 2.12.3-2.
3. See Section 2.12.3.6, *Confirmatory Test of Attachments*, for a description of tests D2C and P2C.

Table 2.12.3-3 - Attachment Pretest Data (Serial No. 2 Before D2C), inches

No.	Blade Thick	Blade Width	Hole Dia.	Hole-to-Edge
1	0.376	1.515	0.565	0.376
2	0.375	1.517	0.565	0.353
3	0.375	1.520	0.563	0.375
4	0.377	1.519	0.565	0.471
5	0.376	1.519	0.565	0.420
6	0.377	1.519	0.565	0.396

Table 2.12.3-4 - Attachment Post-test Data (Serial No. 2 After D2C), inches

No.	Hole Axial* Diameter	Hole Lateral** Diameter	Hole-to-Edge
1	0.573	0.567	0.360
2	0.569	0.565	0.354
3	0.568	0.565	0.375
4	0.567	0.566	0.472
5	0.599	0.566	0.430
6	0.585	0.569	0.400

Note: Blade thickness and width were unchanged from the pre-test measurements.

*Parallel to cask axis

**Taken at right angle to axial diameter

Table 2.12.3-5 - Accelerometer Calibration Constants

Accelerometer Channel	Calibration Constant (mV/g)
12	0.935
13	0.926
14	0.930
15	0.941
16	0.916
17	0.889
18	0.905
19	0.973

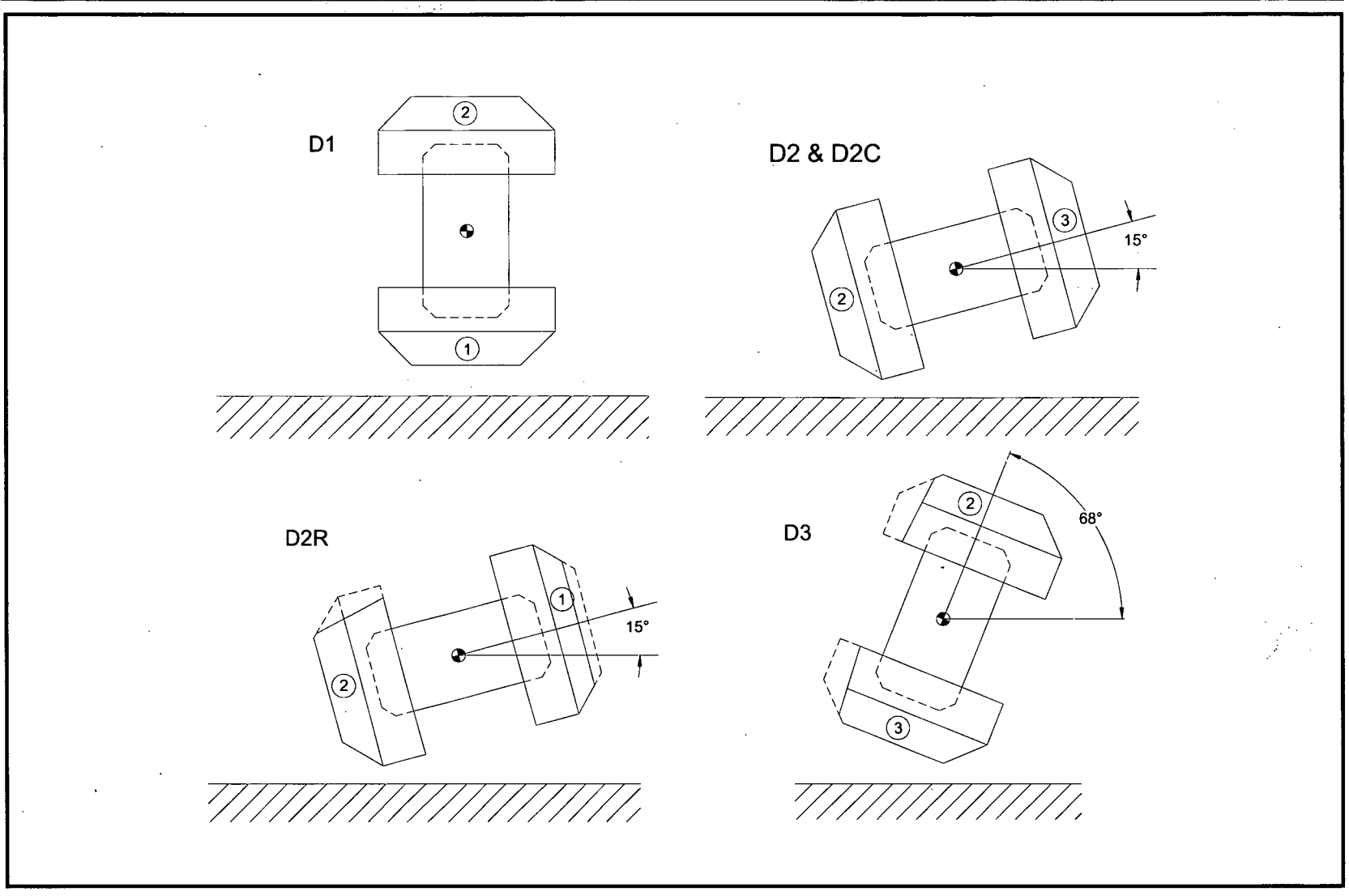

Figure 2.12.3-1 - BRR Package Free Drop Orientations

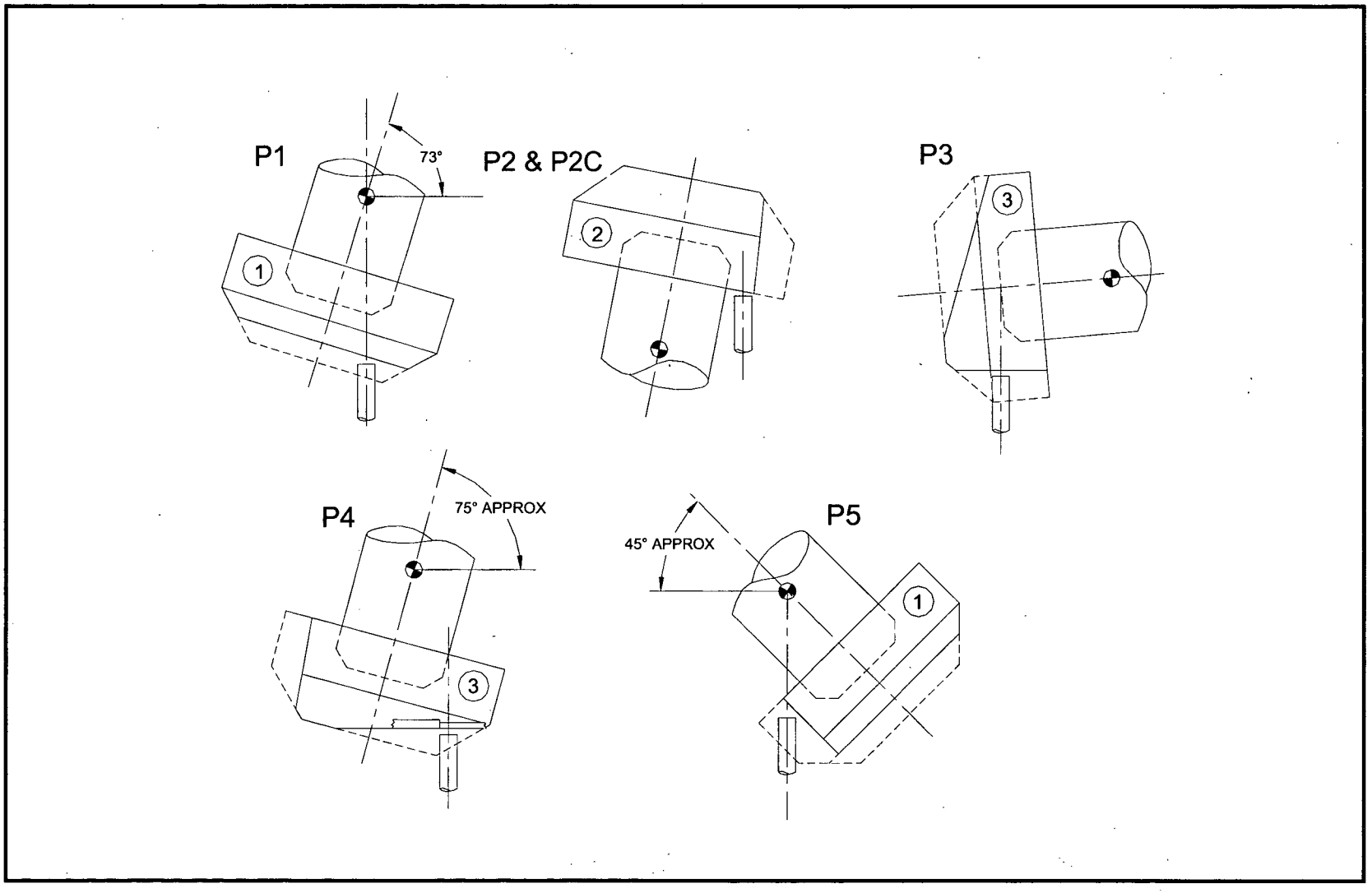

Figure 2.12.3-2 - BRR Package Puncture Drop Orientations

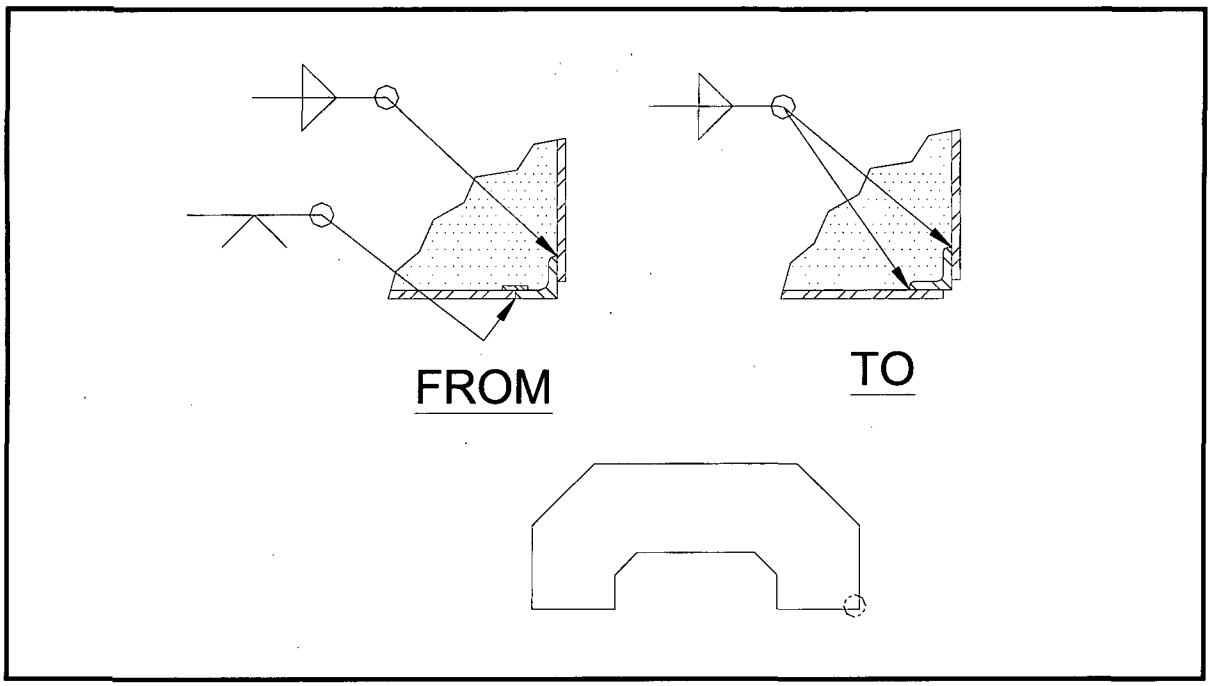

Figure 2.12.3-3 - Change to Outer Impact Limiter Joint

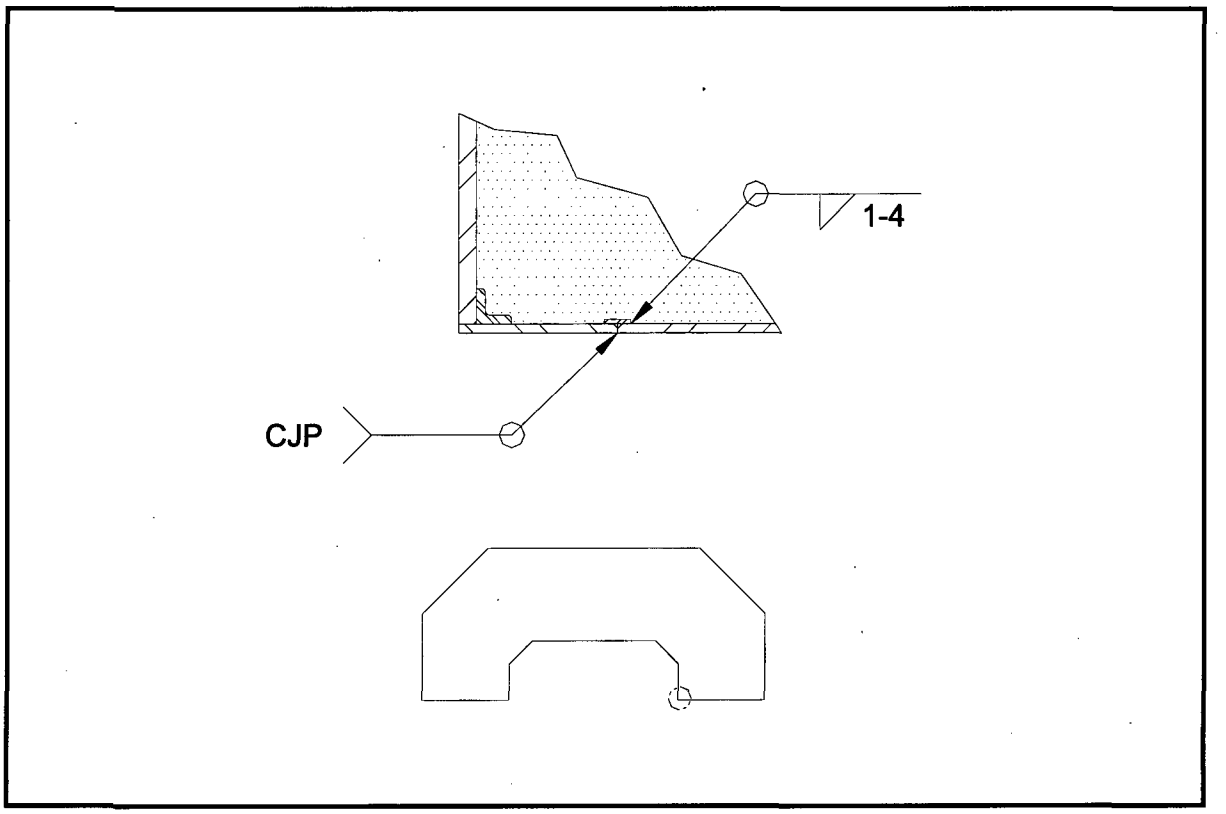

Figure 2.12.3-4 - Added Weld Seam Near Impact Limiter Inner Diameter

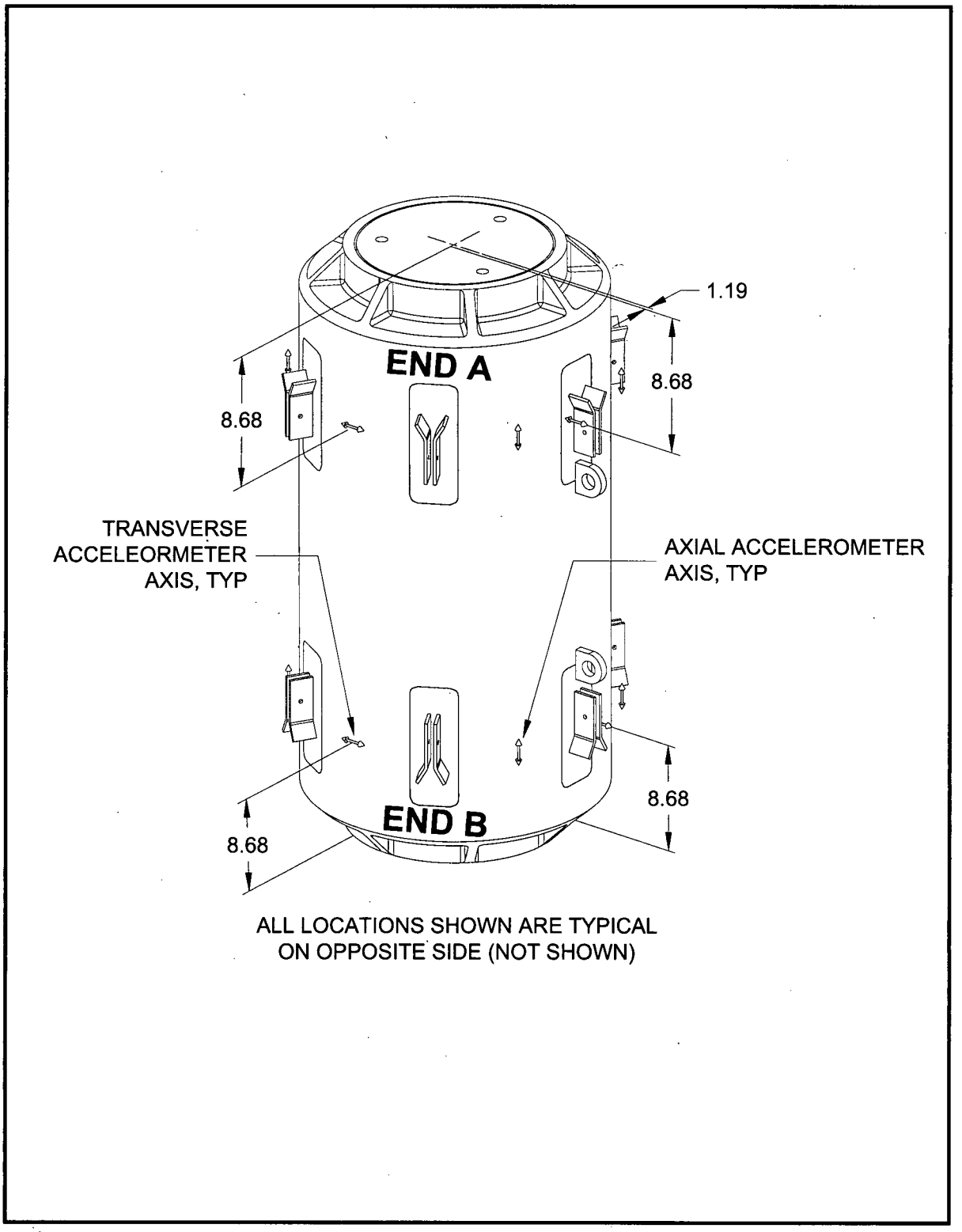

Figure 2.12.3-5 - Accelerometer Mounting

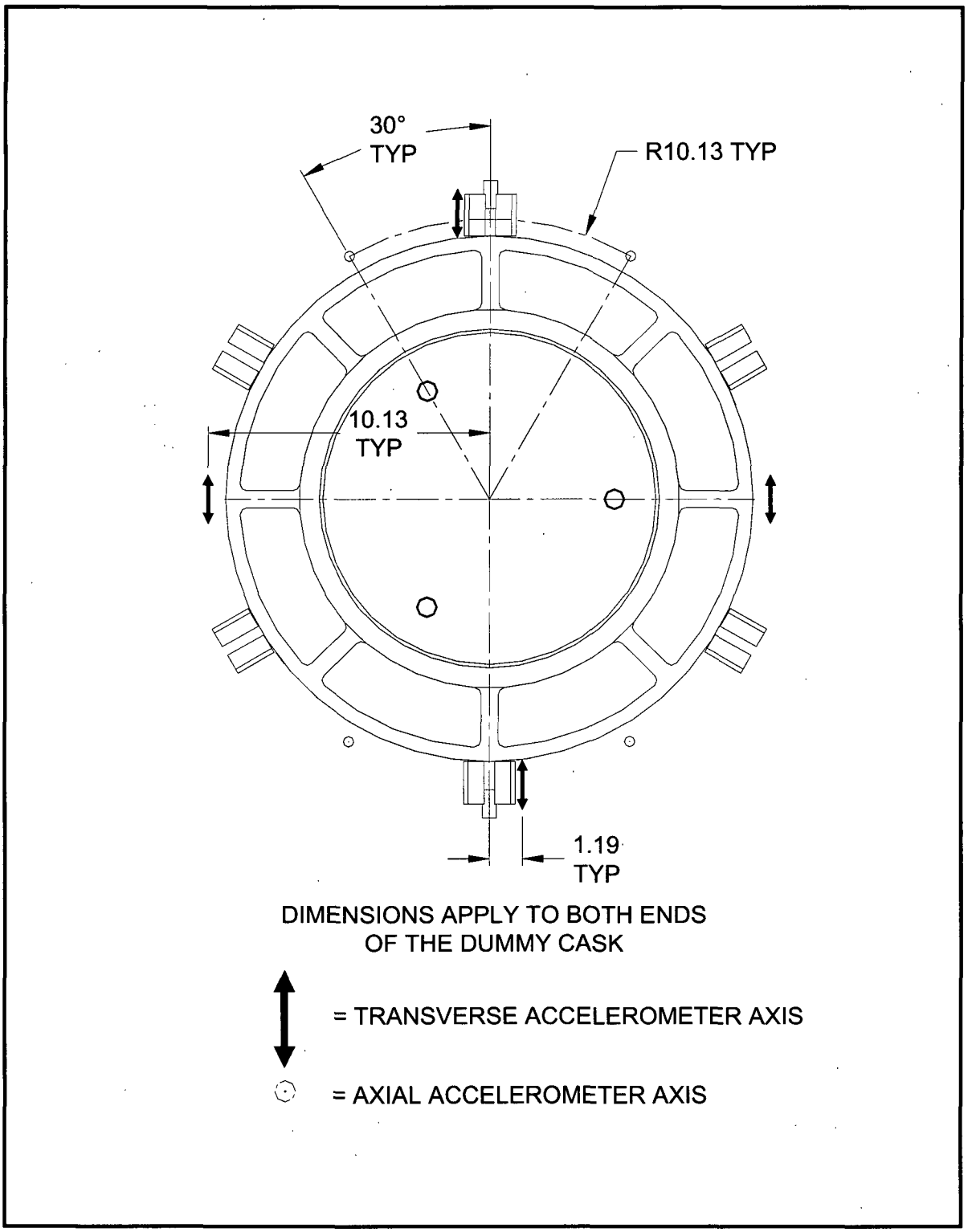

Figure 2.12.3-6 - Accelerometer Mounting, Top View

Figure 2.12.3-7 - Free Drop Test D1 Orientation

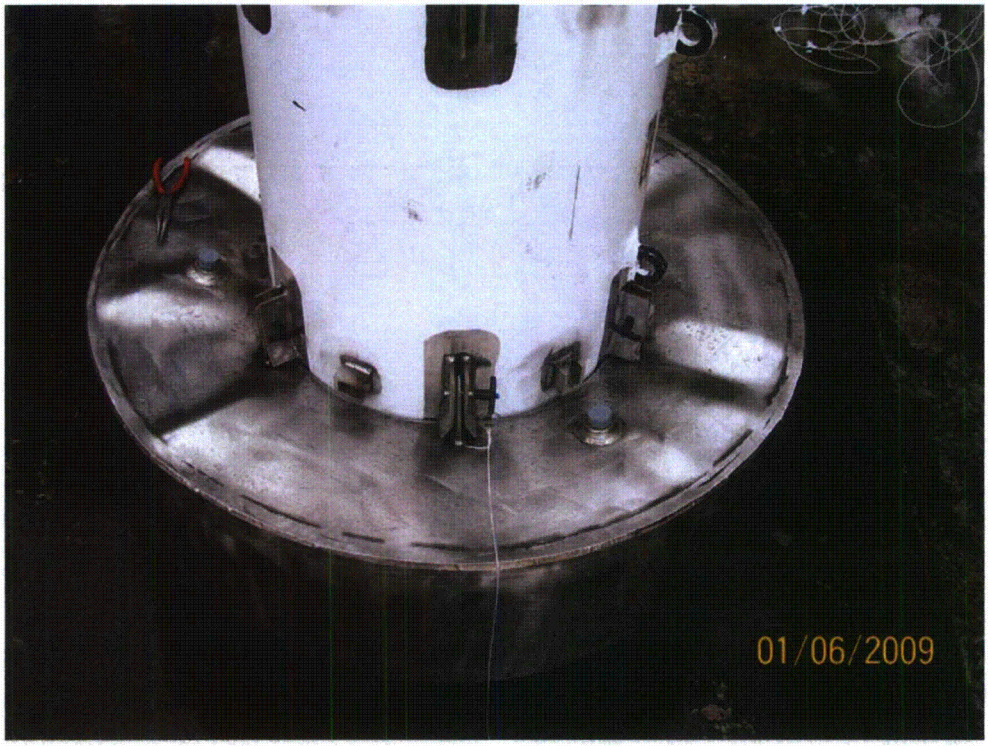

Figure 2.12.3-8 - Free Drop Test D1 Inside-Out Deformation

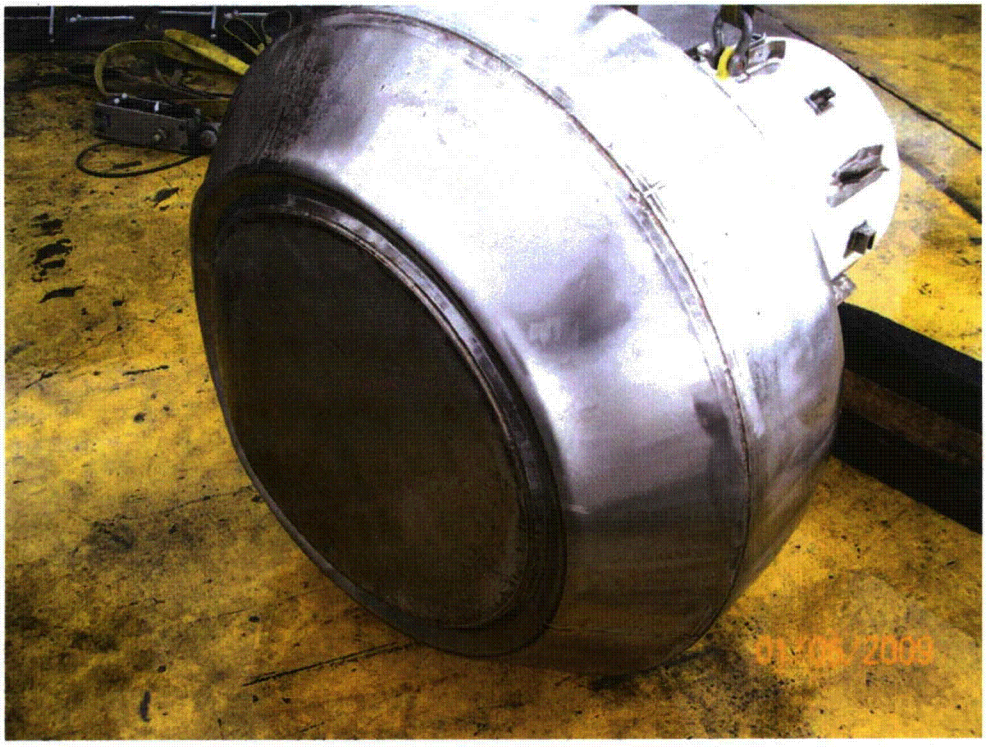

Figure 2.12.3-9 - Free Drop Test D1 Outside-In Deformation

Figure 2.12.3-10 - Puncture Test P1 Orientation

Figure 2.12.3-11 - Puncture Test P1 Deformation

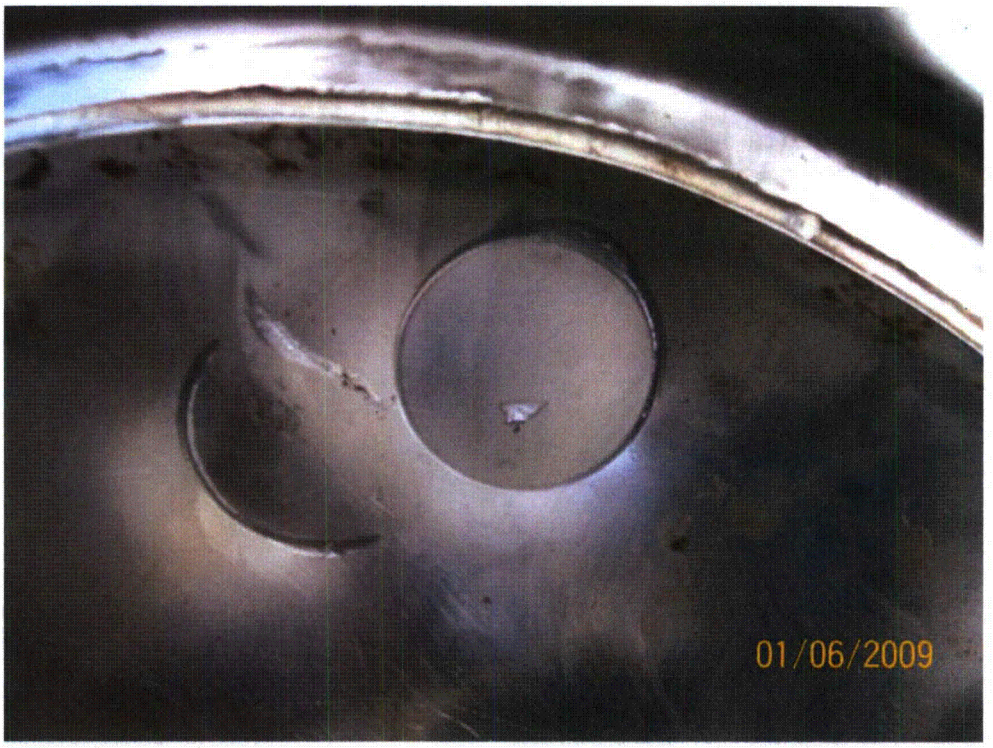

Figure 2.12.3-12 - Puncture Test P1 Deformation – Close-up View

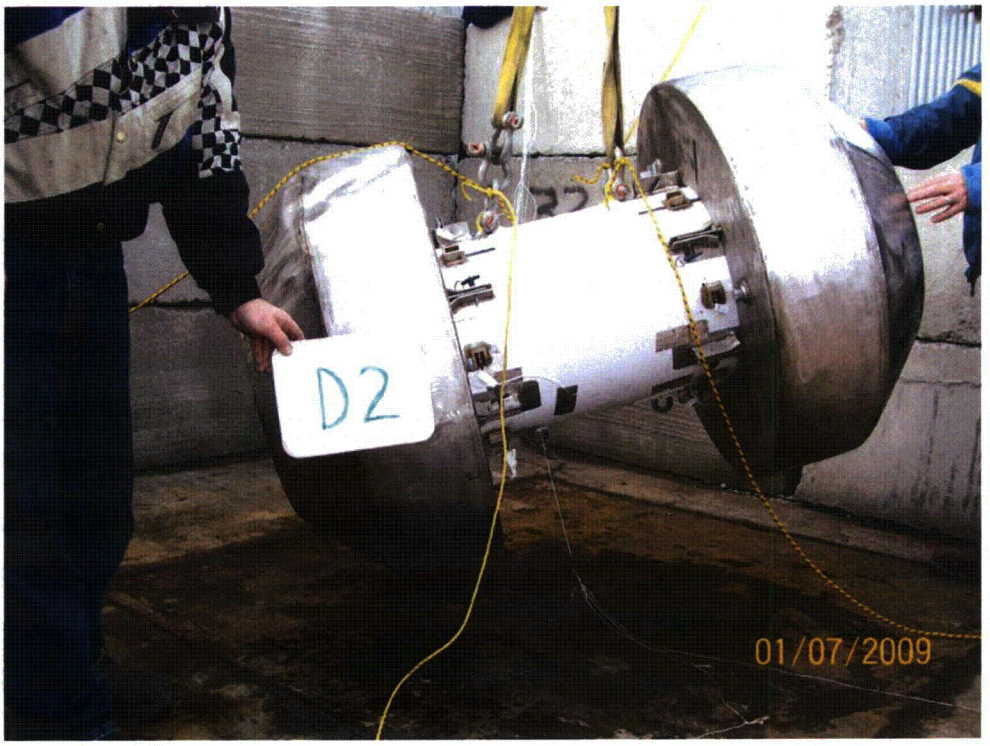

Figure 2.12.3-13 - Free Drop Test D2 Orientation

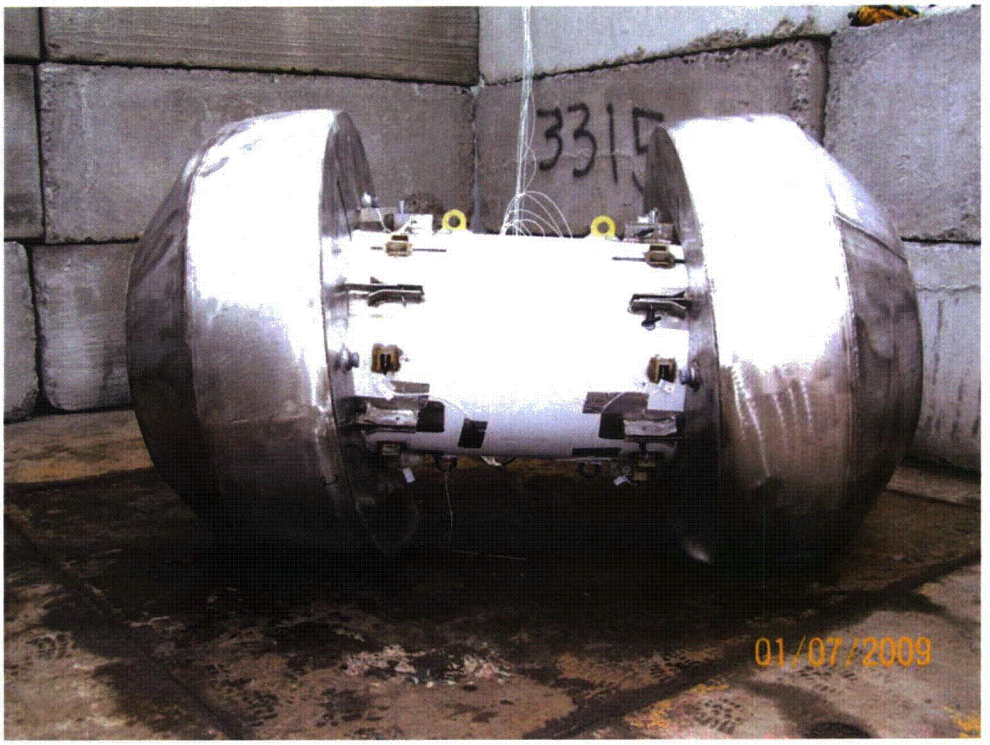

Figure 2.12.3-14 - Free Drop Test D2 Post-test Configuration

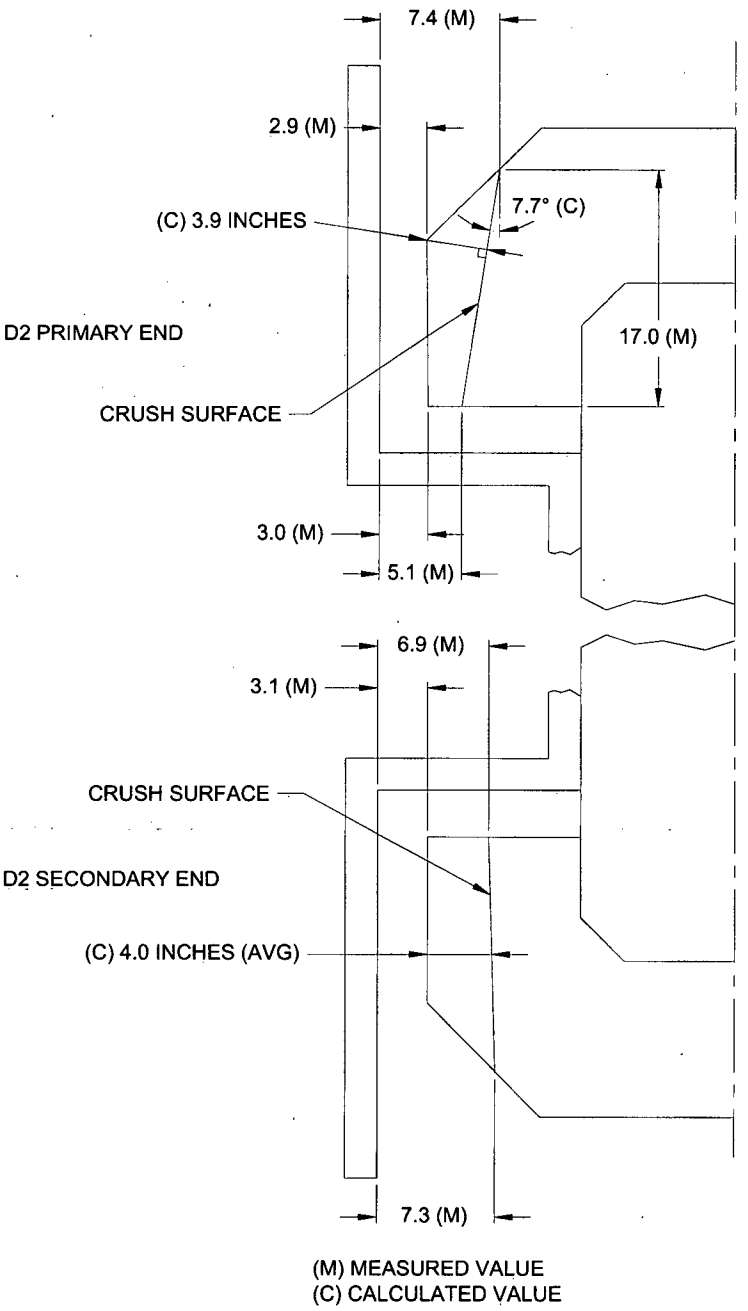

Figure 2.12.3-15 - Free Drop Test D2 Crush Measurements

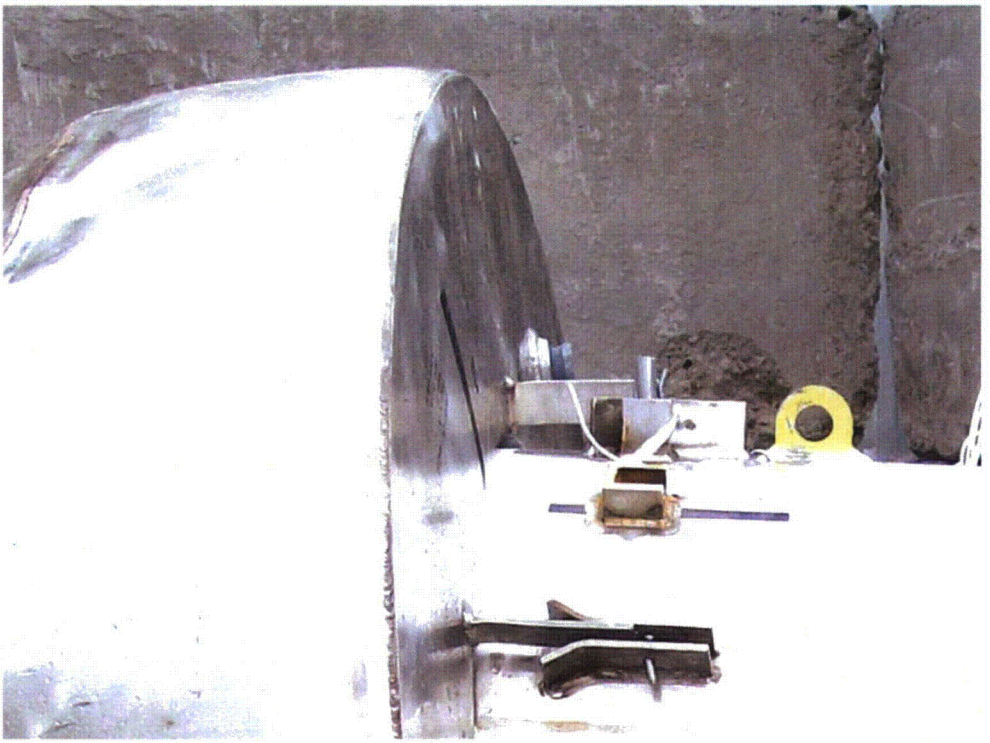

Figure 2.12.3-16 - Free Drop Test D2, Close-up View of Failed Attachments

Figure 2.12.3-17 - Free Drop Test D2 Impact Deformation Surfaces

Figure 2.12.3-18 - Free Drop Test D2R Orientation

Figure 2.12.3-19 - Free Drop Test D2R Post-test Configuration

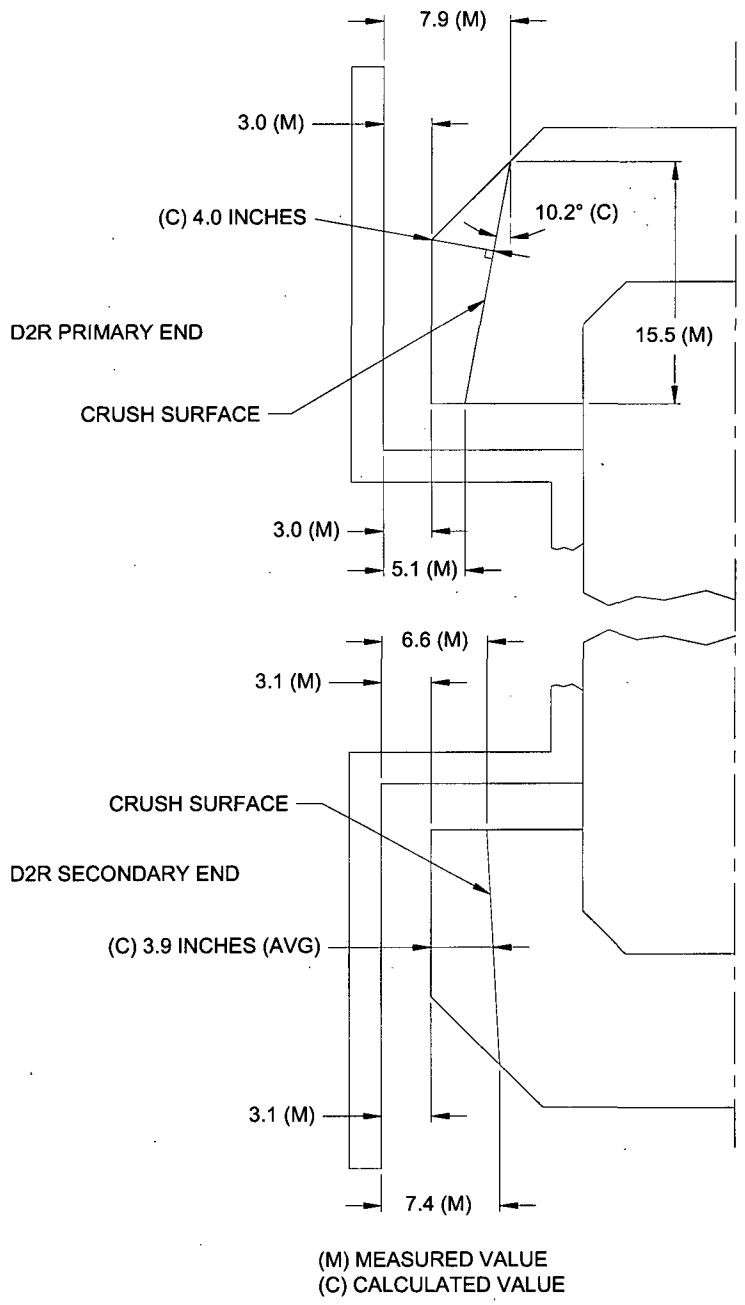

Figure 2.12.3-20 - Free Drop Test D2R Crush Measurements

Figure 2.12.3-21 - Free Drop Test D2R, Close-up View of Failed Attachments

Figure 2.12.3-22 - Free Drop Test D2R, View of Torn Corner Joint

Figure 2.12.3-23 - Puncture Test P2 Orientation

Figure 2.12.3-24 - Puncture Test P2 Result

Figure 2.12.3-25 - Free Drop Test D3 Orientation

Figure 2.12.3-26 - Free Drop Test D3 Deformation

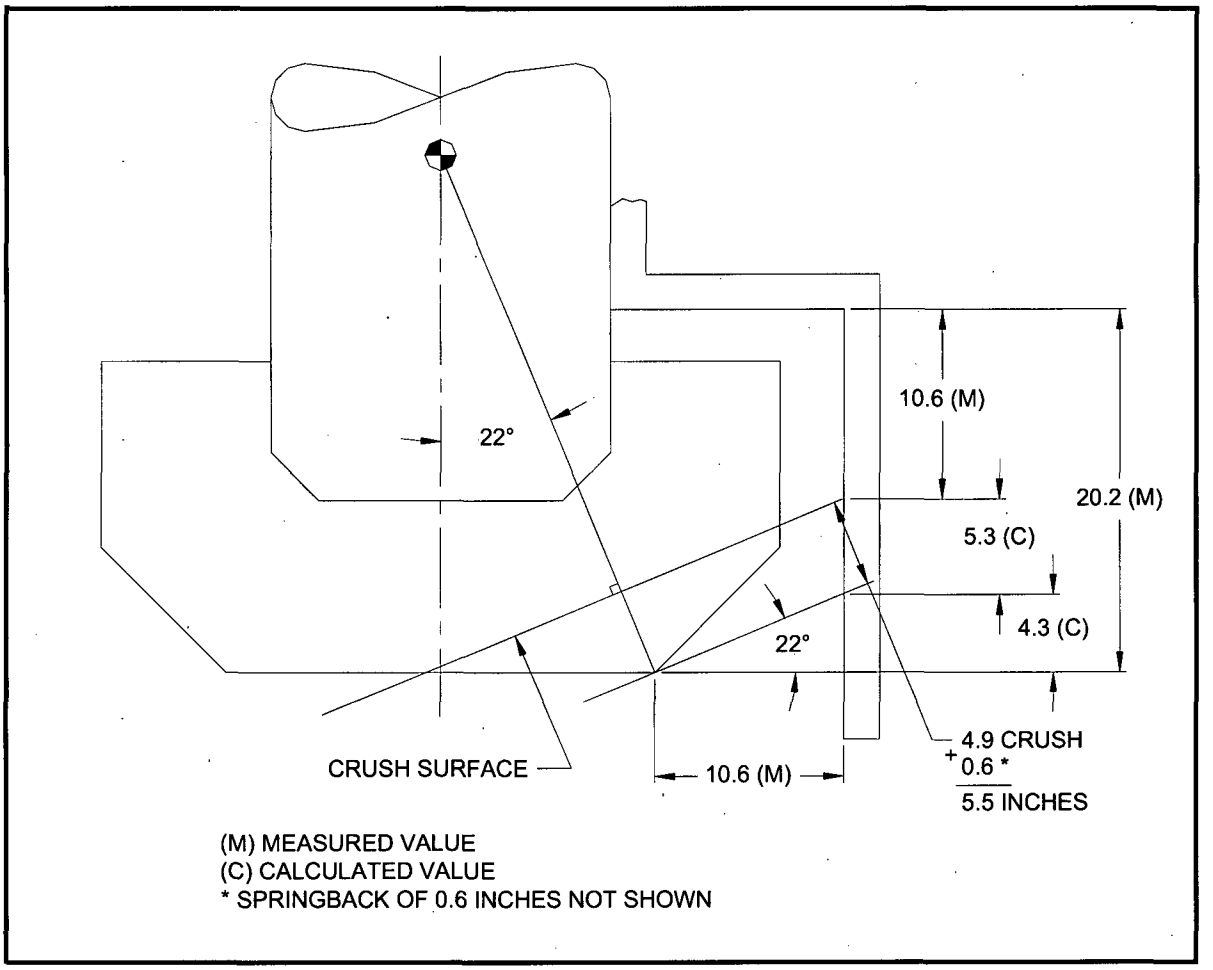

Figure 2.12.3-27 - Free Drop Test D3 Crush Measurements

Figure 2.12.3-28 - Puncture Test P4 Orientation

Figure 2.12.3-29 - Puncture Test P4 Damage

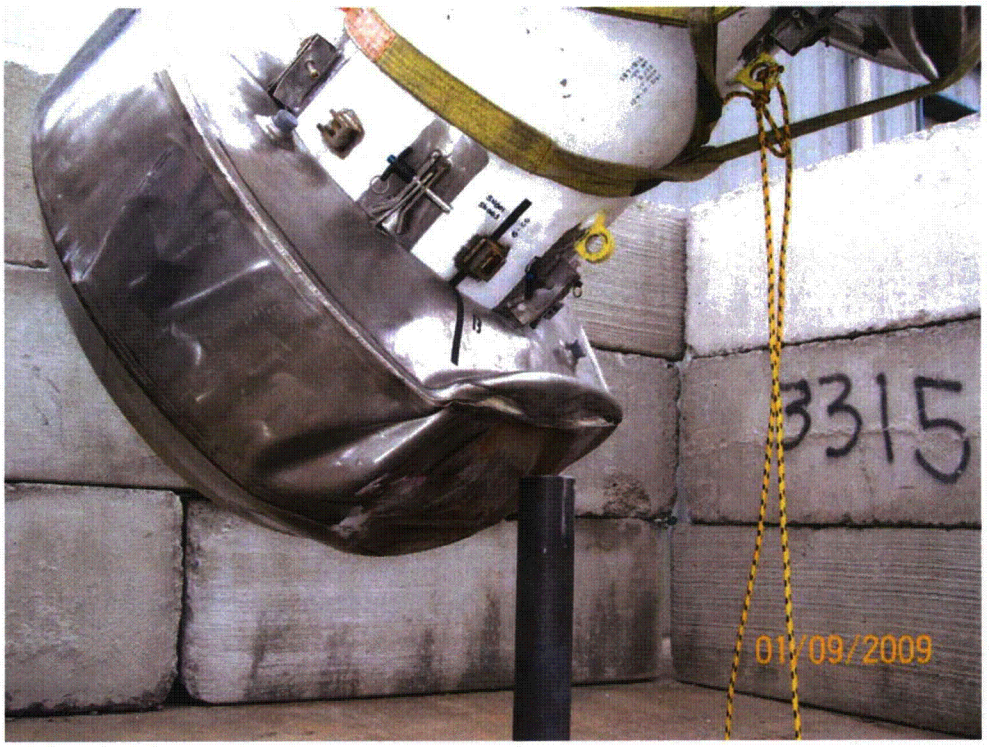

Figure 2.12.3-30 - Puncture Test P5 Orientation

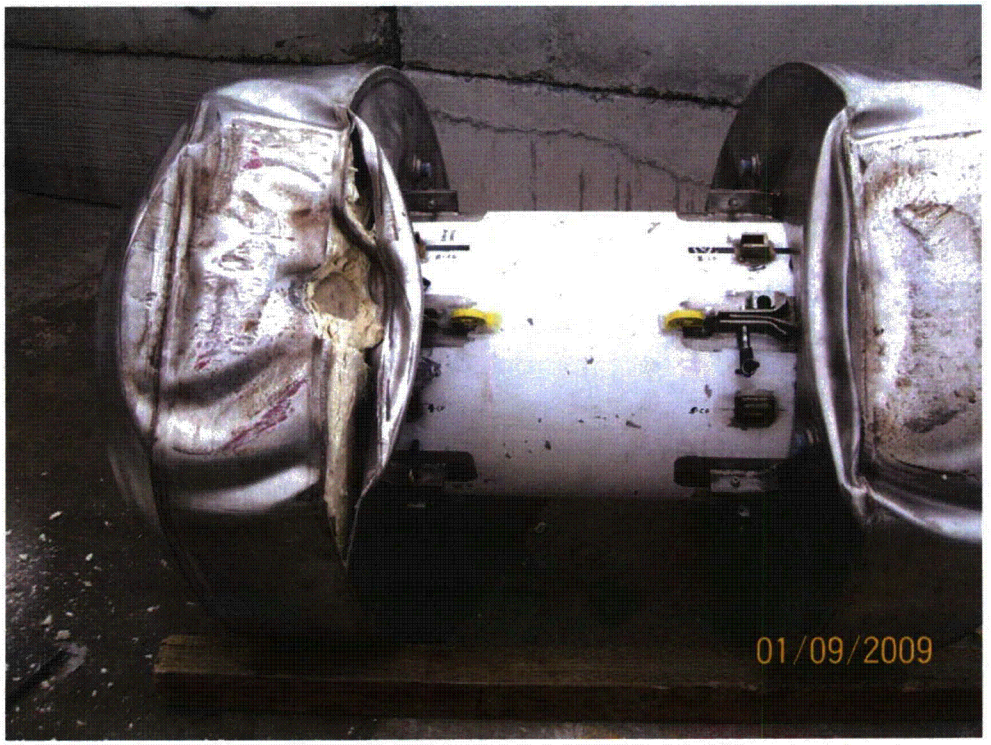

Figure 2.12.3-31 - Puncture Test P5 Damage

Figure 2.12.3-32 - Puncture Test P5 Damage

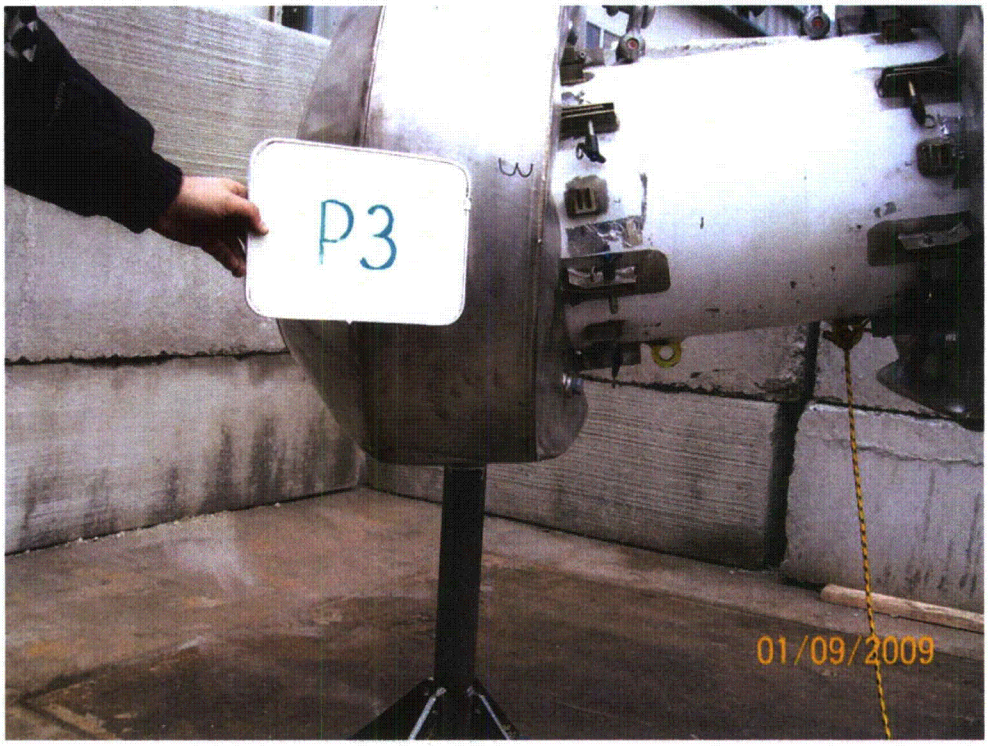

Figure 2.12.3-33 - Puncture Test P3 Orientation

Figure 2.12.3-34 - Puncture Test P3 Damage

Figure Withheld Under 10 CFR 2.390

Figure 2.12.3-35 - Revised Half-Scale Attachment Configuration

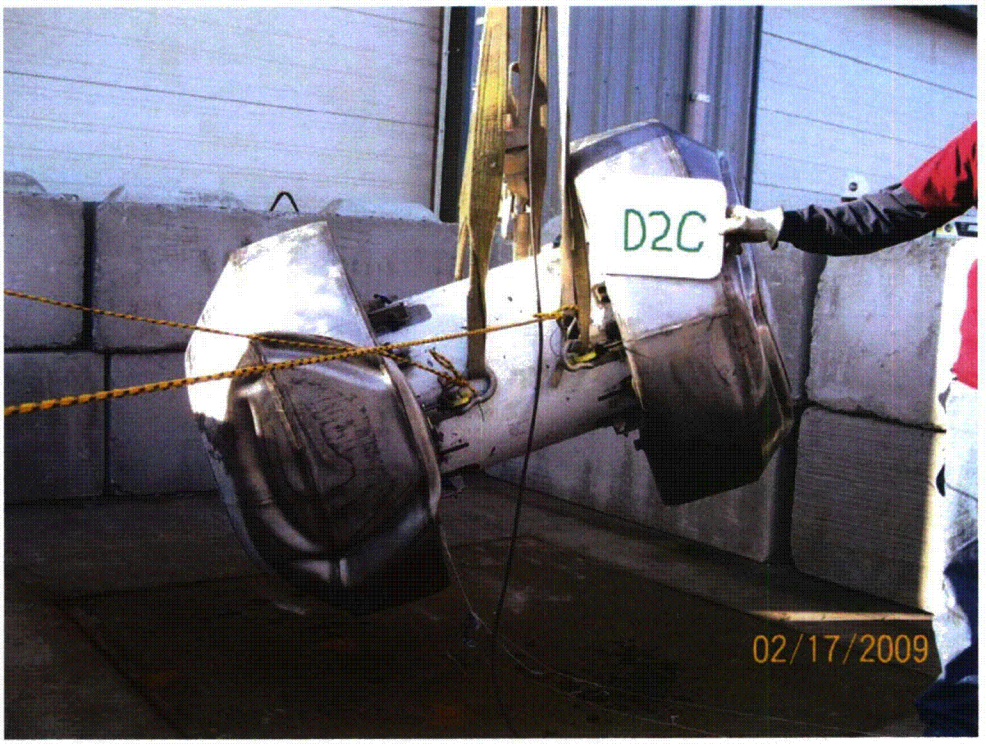

Figure 2.12.3-36 - Free Drop Test D2C Orientation

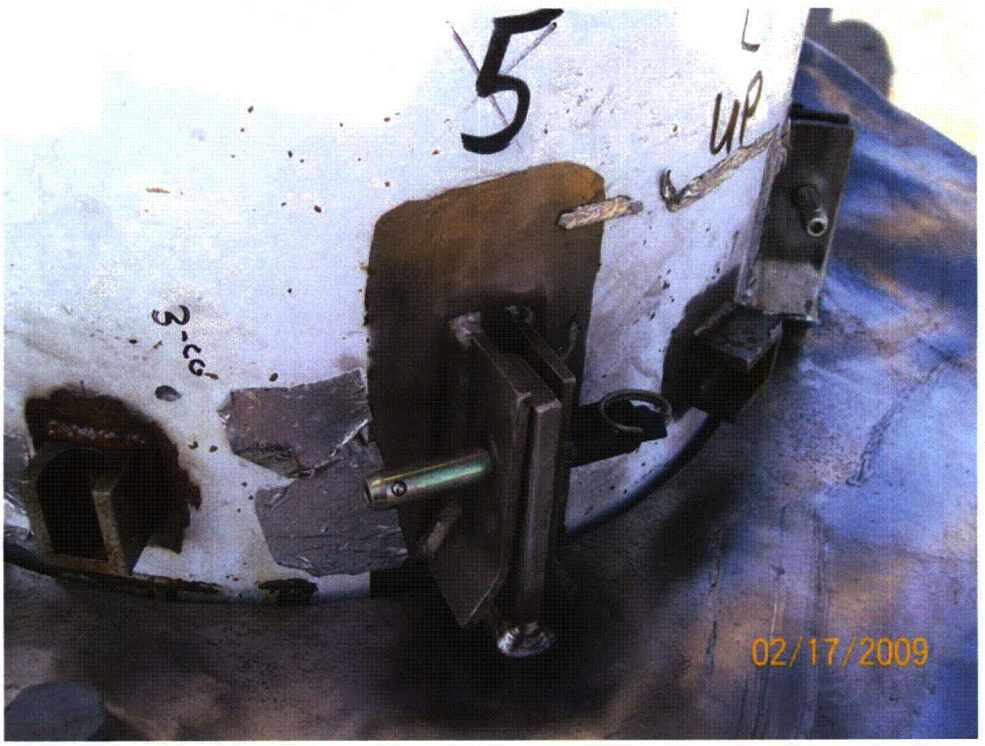

Figure 2.12.3-37 - Attachment Location #5 After Free Drop D2C

Figure 2.12.3-38 - Attachment Location #6 After Free Drop D2C

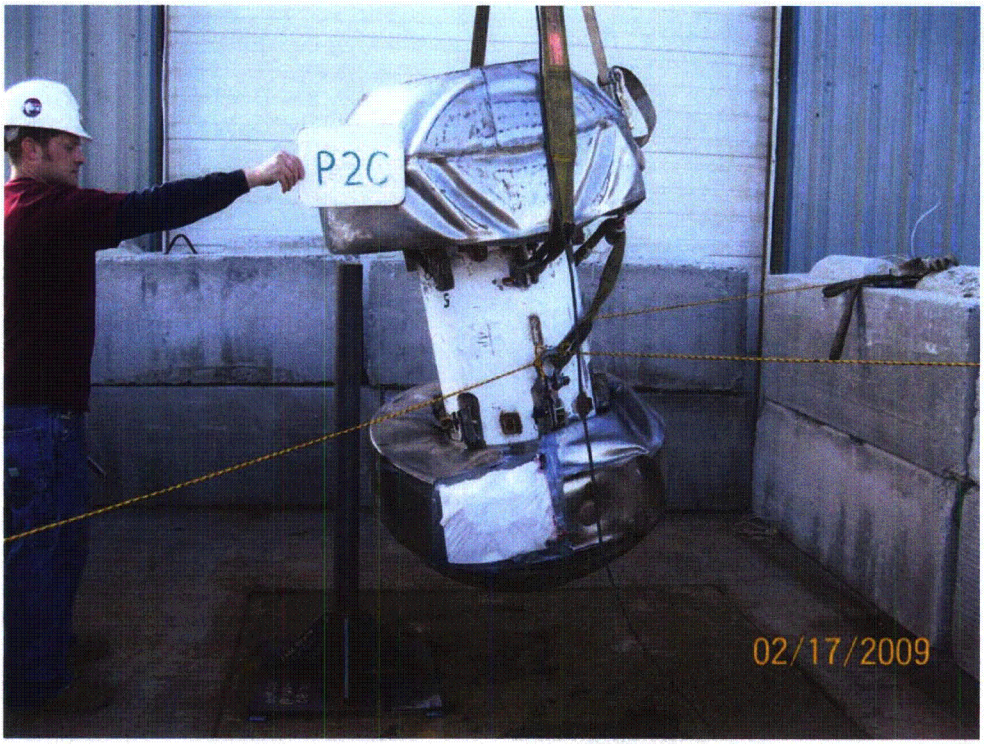

Figure 2.12.3-39 - Puncture Test P2C Orientation

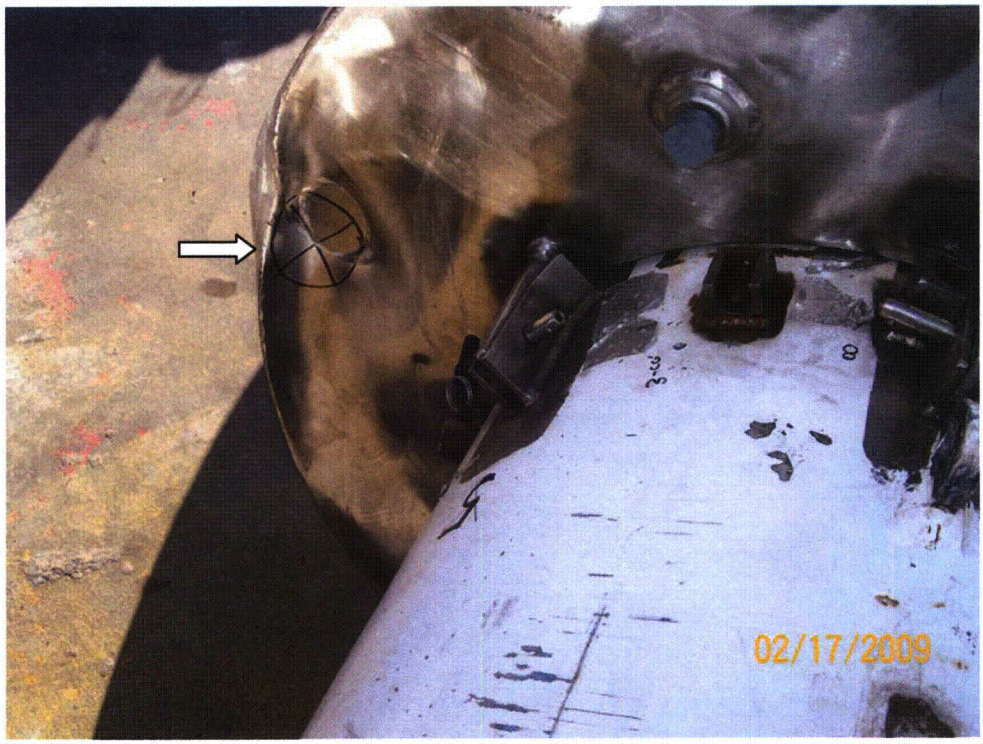

Figure 2.12.3-40 - Puncture Test P2C Result

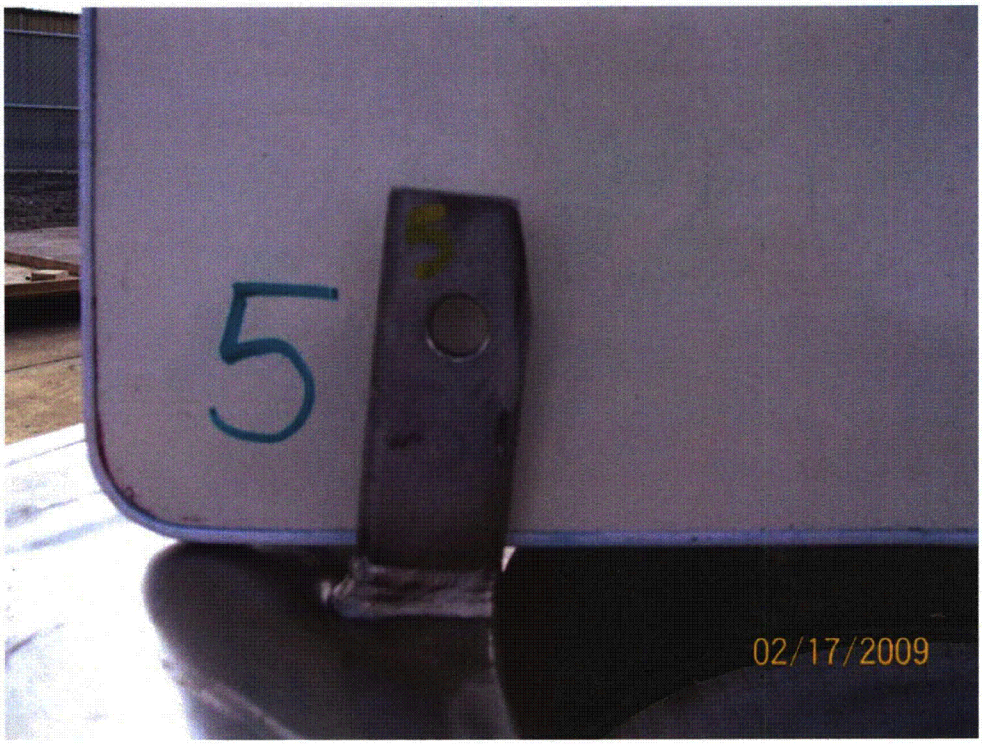

Figure 2.12.3-41 - Blade Location #5 Post-test Configuration

Figure 2.12.3-42 - Blade Location #6 Post-test Configuration

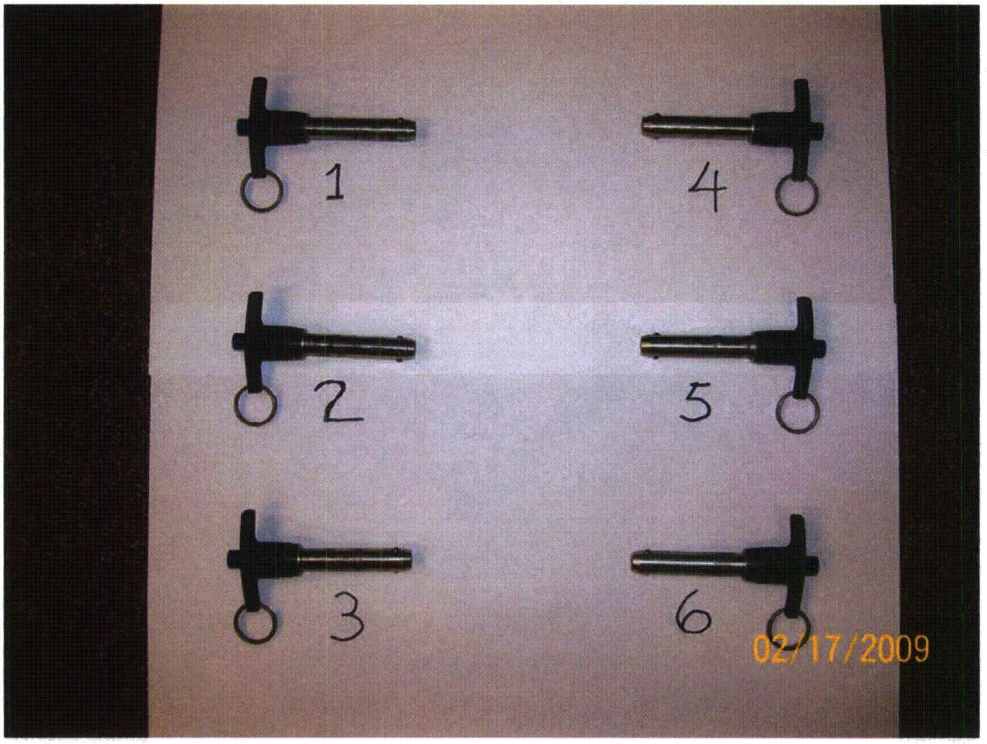

Figure 2.12.3-43 - Primary Impact Limiter Attachment Ball Lock Pins, Post-test

2.12.3.7 Accelerometer Plots

The following figures show the filtered time history accelerometer responses by channel number. Results for all instrumented tests (D1, D2, D2R, and D3) are given. Test D1 used two accelerometers at each end; all other tests used four at each end. For the slapdown cases (D2 and D2R), channels 12 – 15 were located at the secondary end, and channels 16 – 19 were located at the primary end. The time histories in these plots are the result of filtering the accelerometer outputs at 1019Hz. They are not adjusted for the accelerometer calibration constants.

Table 2.12.3-6 (on the following page) lists the estimated rigid body peak accelerations obtained from the plots. Notes for Table 2.12.3-6:

1. The 'Peak From Plots' (column A) is the peak value taken directly off of the following acceleration time histories. For example, for test D1, channel 12, the peak value is 103g.
2. The 'From Plots, Calibration Adjusted' (column B) is found by dividing the 'Peak From Plots' data by the accelerometer calibration constant found in Table 2.12.3-5. For channel 12, the constant is 0.935. Therefore the adjusted peak value of the example is 103/0.935 = 110g.
3. The 'Estimated Rigid Body Peak' (column C) is made by inspection of the corresponding accelerometer output plot. For the example case, the estimated rigid body peak is 95g.
4. The 'Rigid Body, Calibration Adjusted' (column D) is found by dividing the 'Estimated Rigid Body Peak' by the accelerometer calibration adjustment constant as described above. Following the example, 95/0.935 = 102g.
5. The 'Reduction, ½ Scale' (column E) is the reduction in peak impact which could be credited if the estimated rigid body peak is used instead of the peak from the plot. For the example case, the reduction is 110 (column B) minus 102 (column D) = 8g in half-scale. The average reduction for each set of four acceleromters corresponding to each impact is also given in column E.

Table 2.12.3-6 – Rigid Body Results Estimates (see notes on previous page)

Test No.	Channel	Peak from Plots, g	From Plots, Calibration Adjusted, g	Estimated Rigid Body Peak, g	Rigid Body, Calibration Adjusted, g	Reduction, ½ Scale, g
		A	B	C	D	E
D1	12	103	110	95	102	8
(Primary)	13	112	121	104	112	9
	14	105	113	101	109	4
	15	111	118	105	112	6
					Avg.	**7**
D2	12	95	102	91	97	5
(Secondary)	13	100	108	97	105	3
	14	102	110	100	108	2
	15	102	108	97	103	5
					Avg.	**4**
D2	16	Severed wire	---	---	---	---
(Primary)	17	118	133	106	119	14
	18	124	137	110	122	15
	19	131	135	116	119	16
					Avg.	**15**
D2R	12	105	113	96	103	10
(Secondary)	13	103	111	97	105	6
	14	99	106	93	100	6
	15	117	124	95	101	23
					Avg.	**11**
D2R	16	102	111	92	100	11
(Primary)	17	103	116	97	109	7
	18	96	106	85	94	12
	19	103	106	90	92	14
					Avg.	**11**
D3	12	99	106	85	91	15
(Primary)	13	103	111	87	94	17
	14	102	110	84	90	20
	15	97	103	85	90	13
					Avg.	**16**

BEA Research Reactor Package Half-Scale Free Drop Test
Test D1 (End), Channel 12

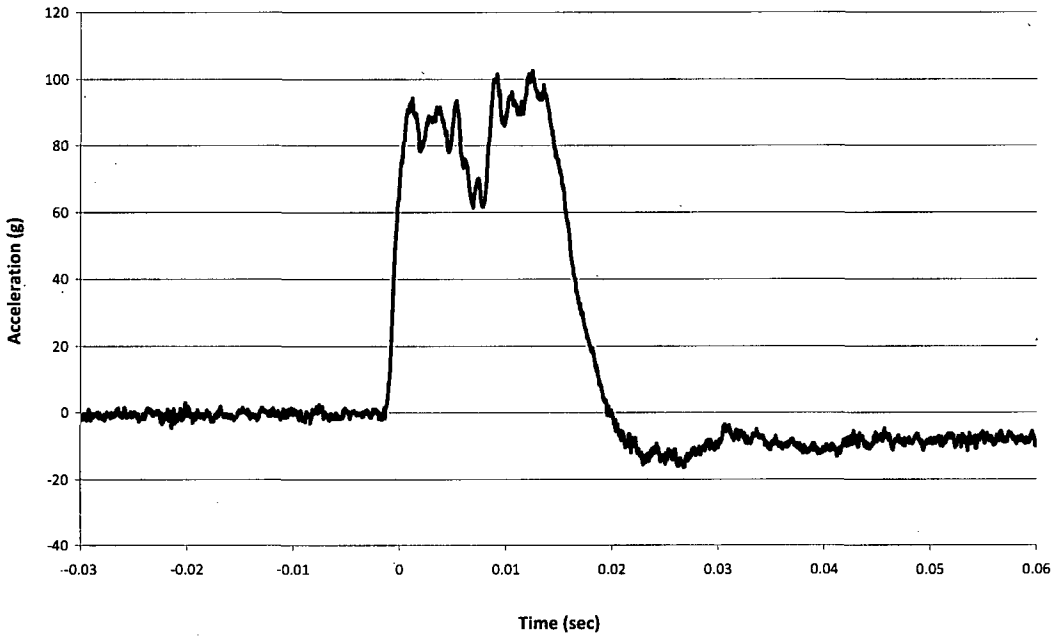

BEA Research Reactor Package Half-Scale Free Drop Test
Test D1 (End), Channel 13

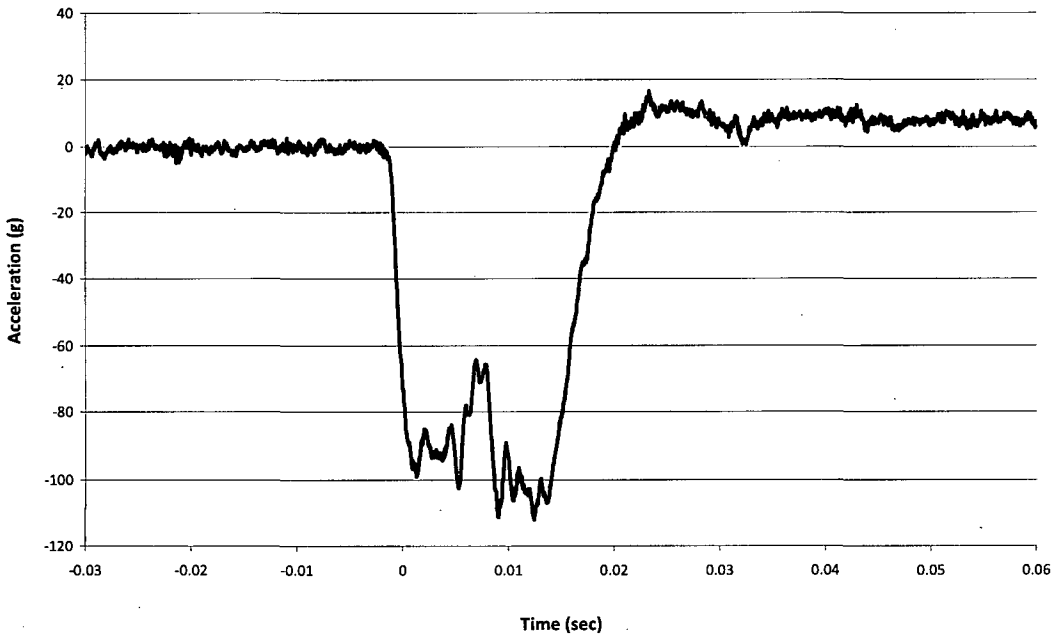

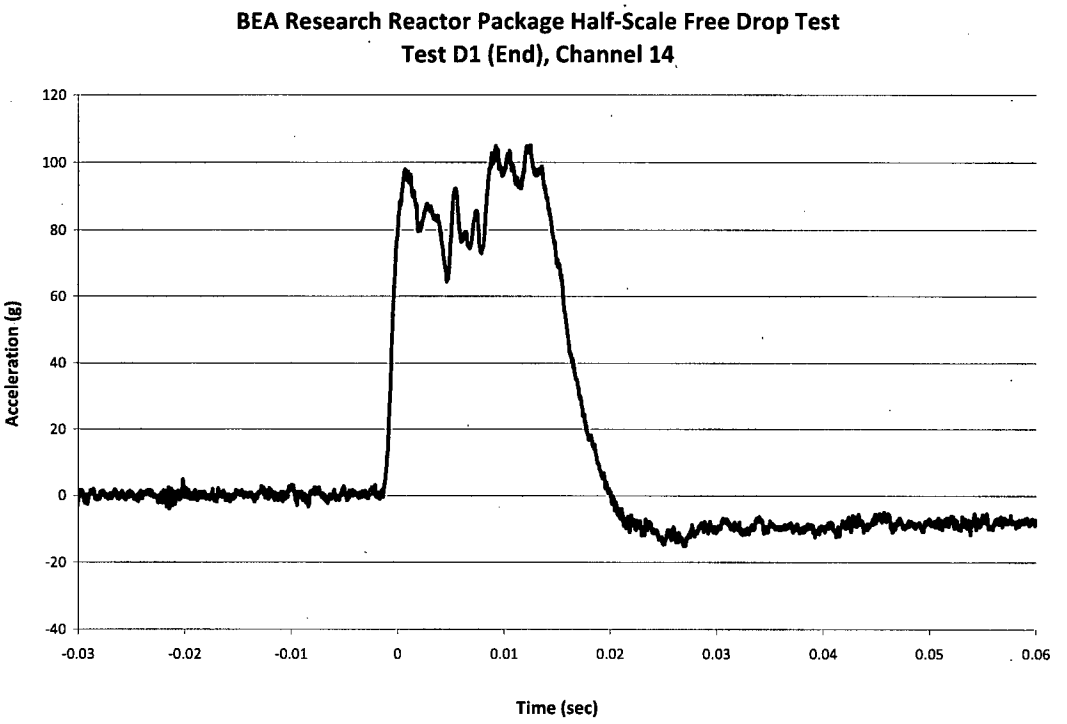
BEA Research Reactor Package Half-Scale Free Drop Test
Test D1 (End), Channel 14
Acceleration (g)
120
100
80
60
40
20
0
-20
-40
-0.03
-0.02
-0.01
0
0.01
0.02
0.03
0.04
0.05
0.06
Time (sec)

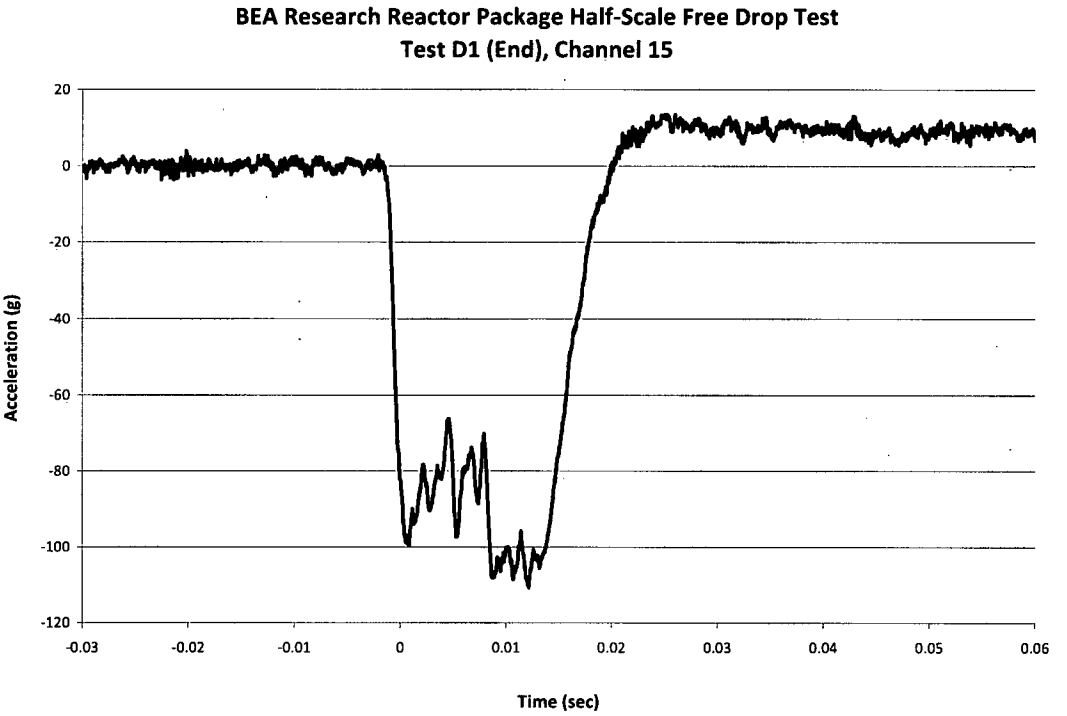
BEA Research Reactor Package Half-Scale Free Drop Test
Test D1 (End), Channel 15
Acceleration (g)
20
0
-20
-40
-60
-80
-100
-120
-0.03
-0.02
-0.01
0
0.01
0.02
0.03
0.04
0.05
0.06
Time (sec)

BEA Research Reactor Package Half-Scale Free Drop Test
Test D2 (15° Oblique), Channel 12 (Secondary Impact)

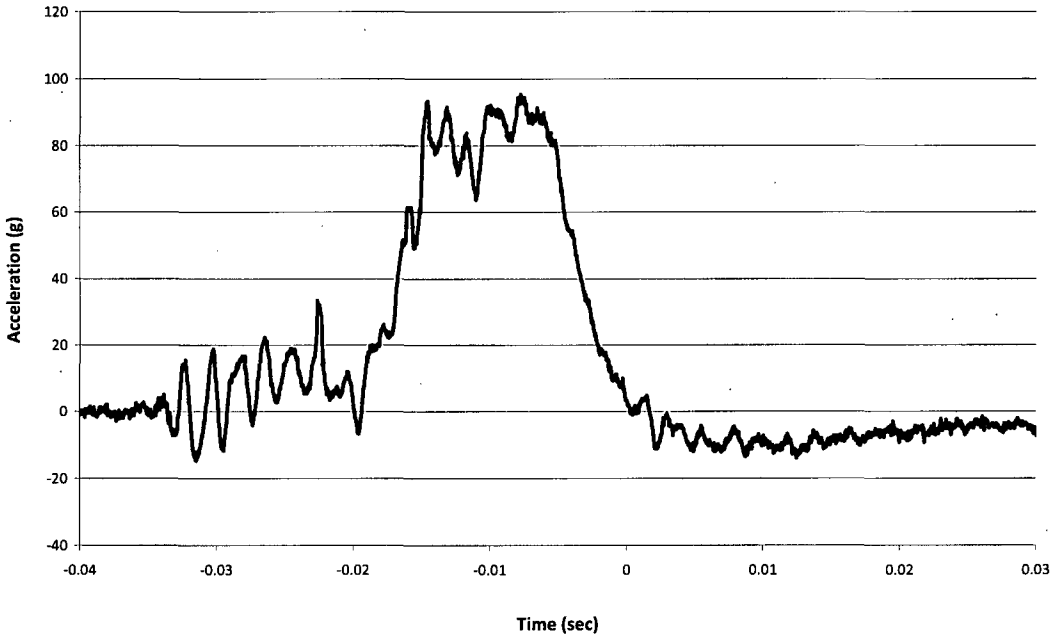

BEA Research Reactor Package Half-Scale Free Drop Test
Test D2 (15° Oblique), Channel 13 (Secondary Impact)

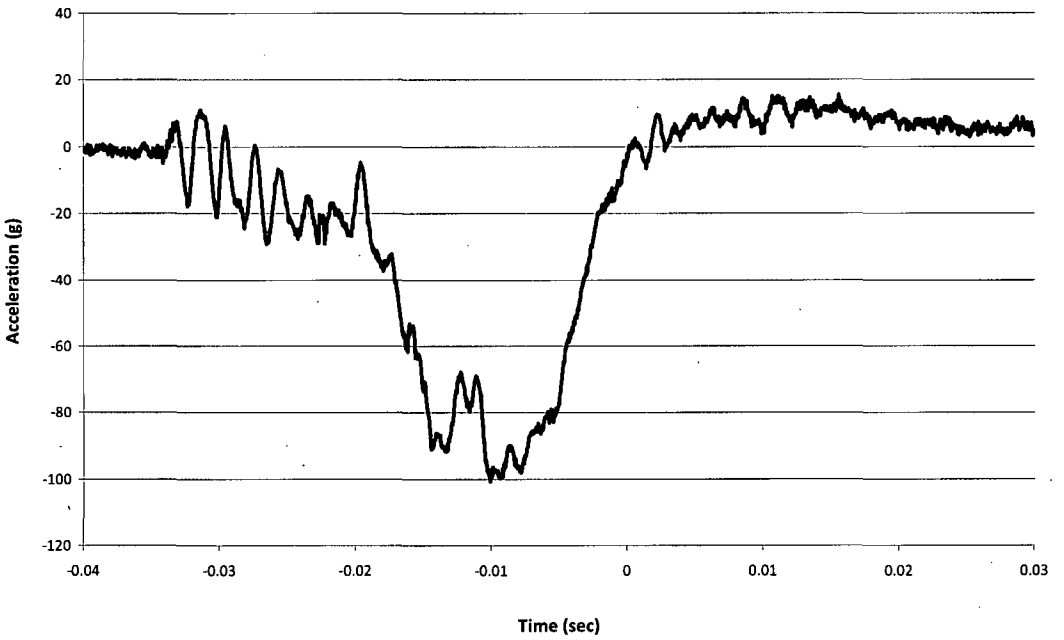

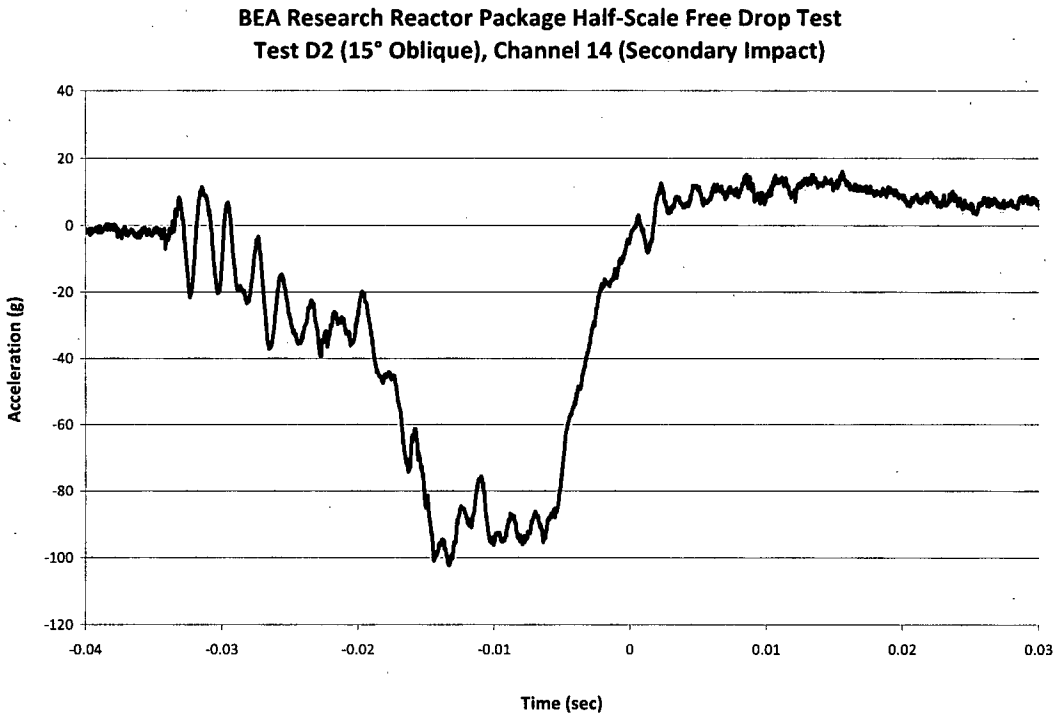
BEA Research Reactor Package Half-Scale Free Drop Test
Test D2 (15° Oblique), Channel 14 (Secondary Impact)
Acceleration (g)
40
20
0
-20
-40
-60
-80
-100
-120
-0.04
-0.03
-0.02
-0.01
0
0.01
0.02
0.03
Time (sec)

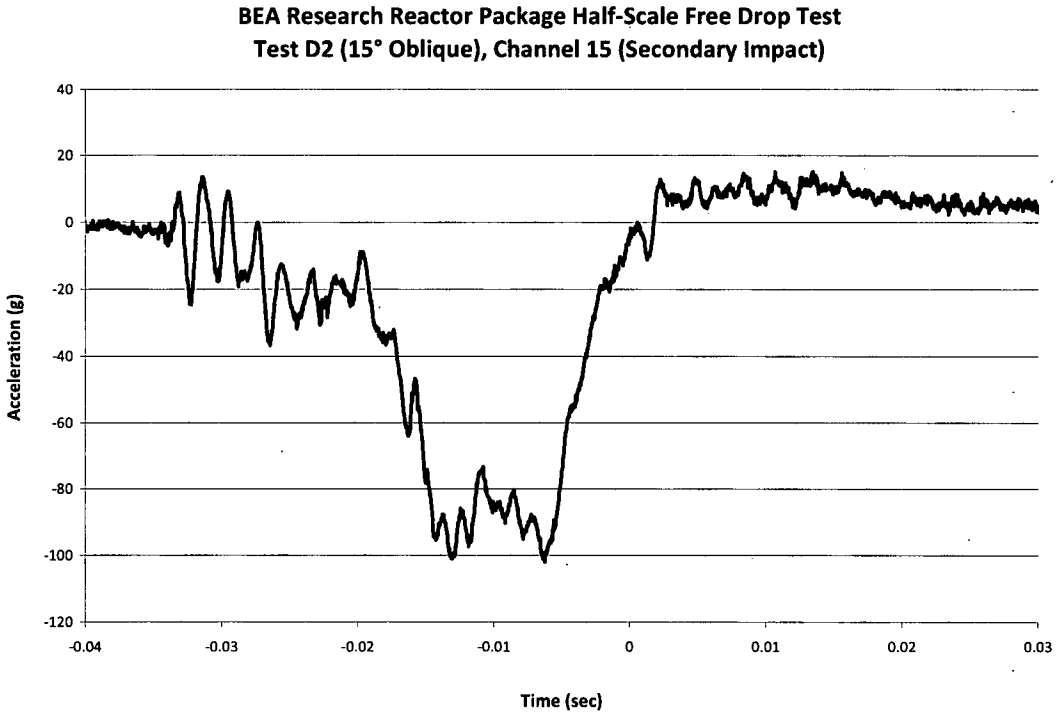
BEA Research Reactor Package Half-Scale Free Drop Test
Test D2 (15° Oblique), Channel 15 (Secondary Impact)
Acceleration (g)
40
20
0
-20
-40
-60
-80
-100
-120
-0.04
-0.03
-0.02
-0.01
0
0.01
0.02
0.03
Time (sec)

BEA Research Reactor Package Half-Scale Free Drop Test
Test D2 (15° Oblique), Channel 16 (Primary Impact)

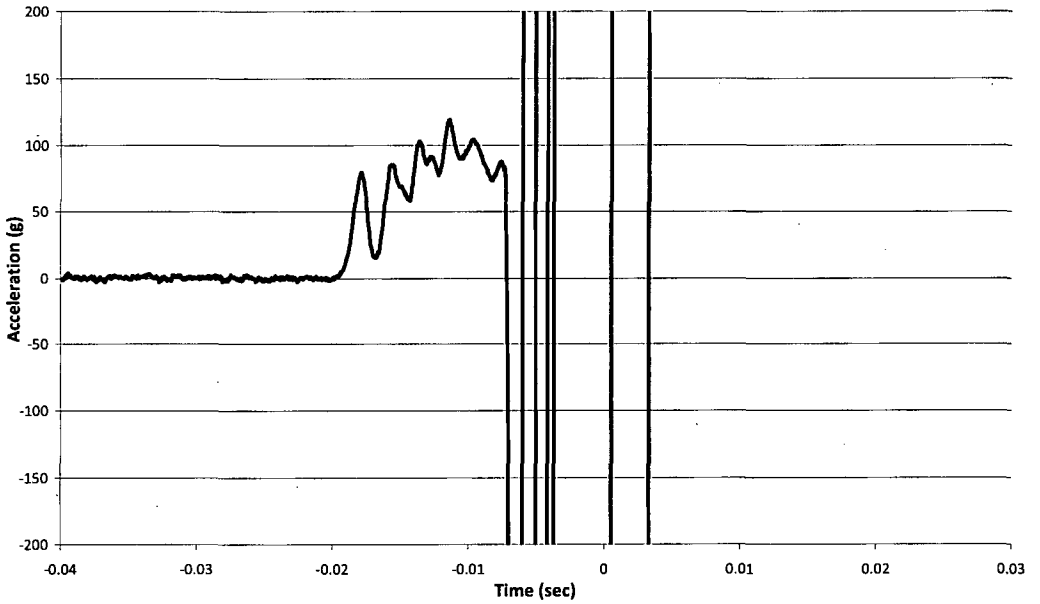

BEA Research Reactor Package Half-Scale Free Drop Test
Test D2 (15° Oblique), Channel 17 (Primary Impact)

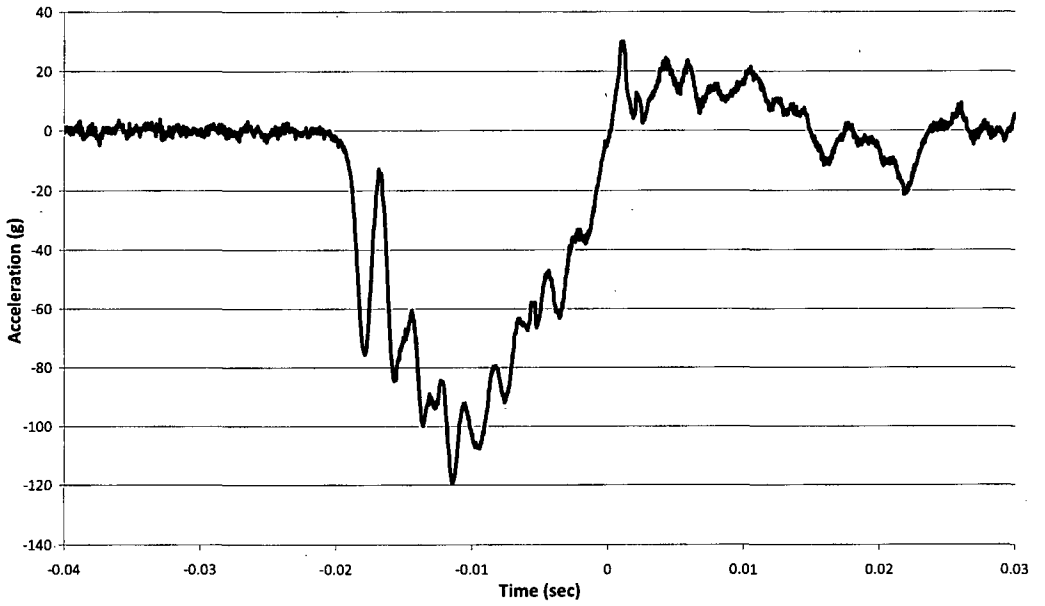

BEA Research Reactor Package Half-Scale Free Drop Test
Test D2 (15° Oblique), Channel 18 (Primary Impact)

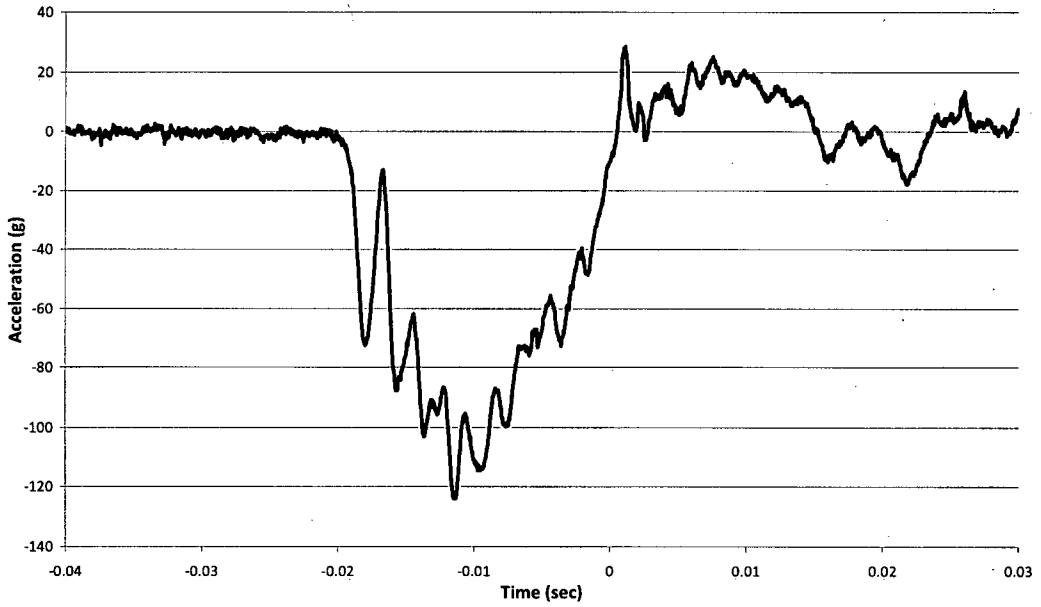

BEA Research Reactor Package Half-Scale Free Drop Test
Test D2 (15° Oblique), Channel 19 (Primary Impact)

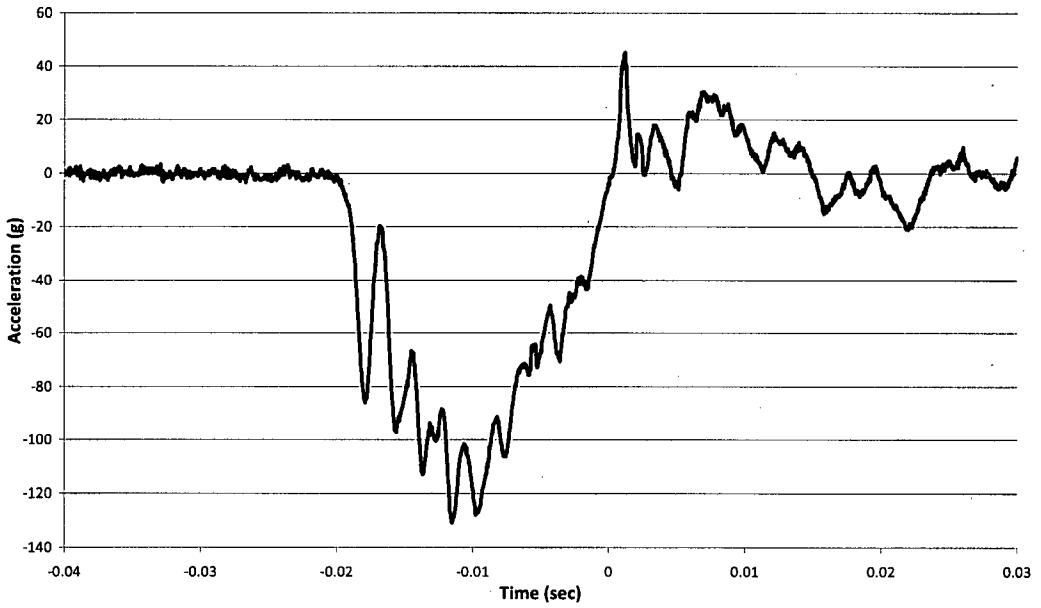

BEA Research Reactor Package Half-Scale Free Drop Test
Test D2R (15° Oblique), Channel 12 (Secondary Impact)

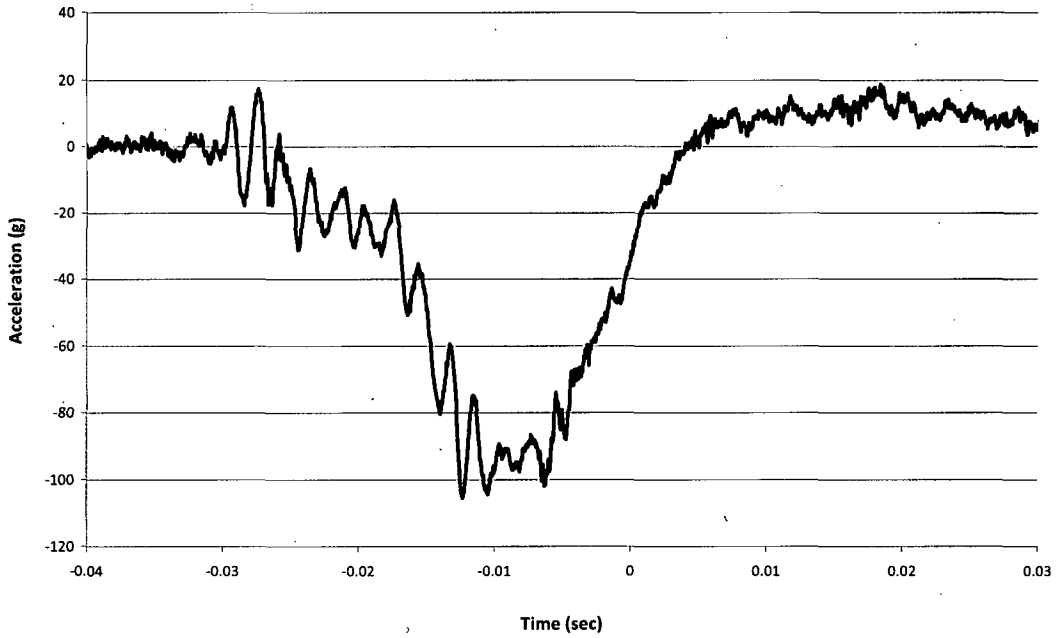

BEA Research Reactor Package Half-Scale Free Drop Test
Test D2R (15° Oblique), Channel 13 (Secondary Impact)

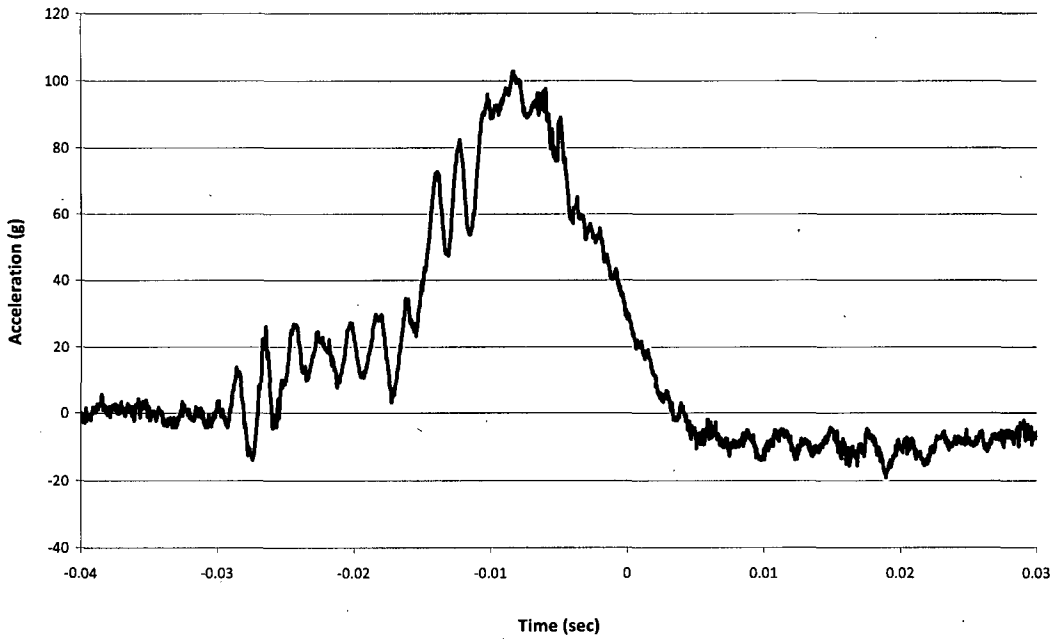

BEA Research Reactor Package Half-Scale Free Drop Test
Test D2R (15° Oblique), Channel 14 (Secondary Impact)

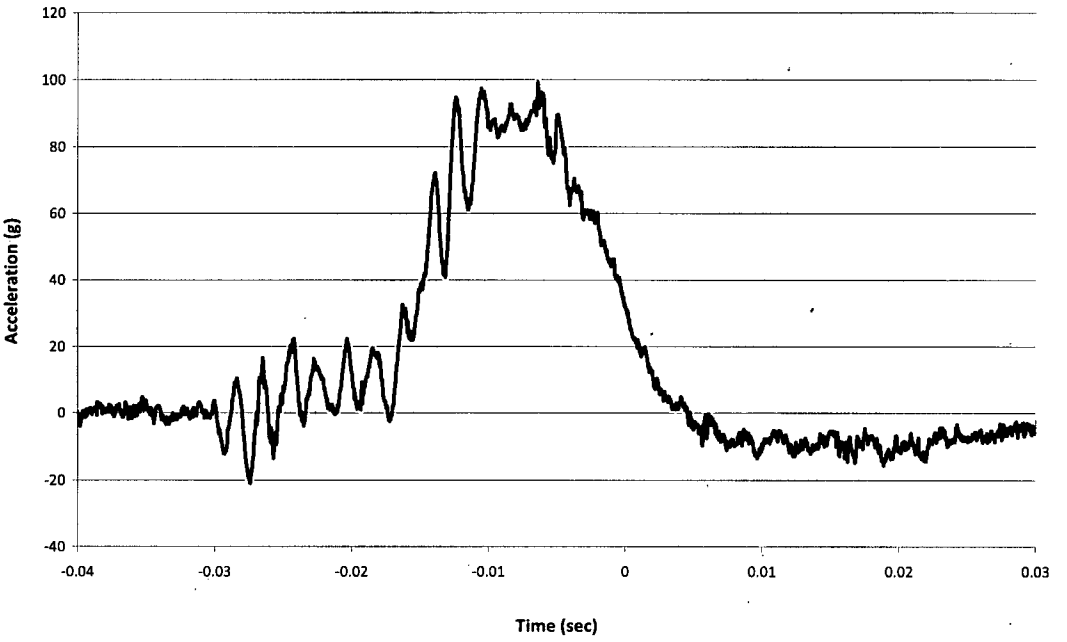

BEA Research Reactor Package Half-Scale Free Drop Test
Test D2R (15° Oblique), Channel 15 (Secondary Impact)

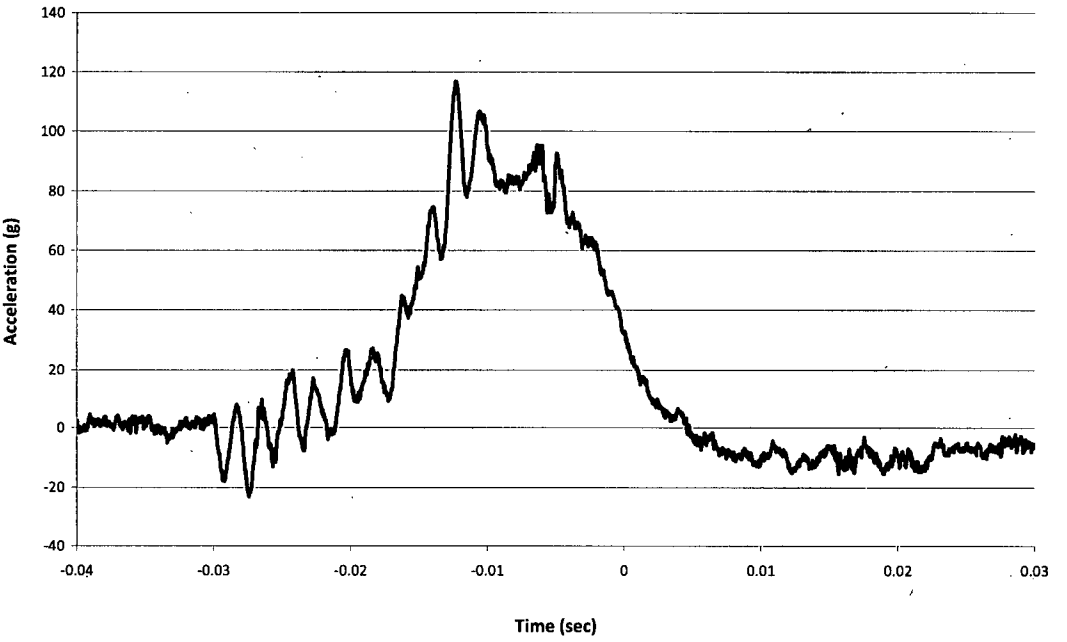

BEA Research Reactor Package Half-Scale Free Drop Test
Test D2R (15° Oblique), Channel 16 (Primary Impact)

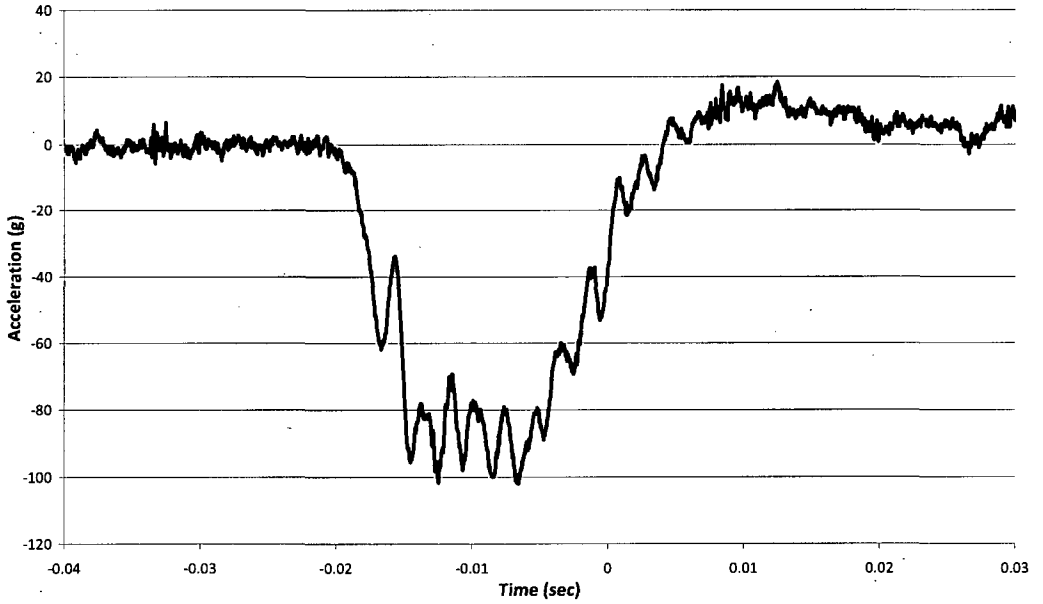

BEA Research Reactor Package Half-Scale Free Drop Test
Test D2R (15° Oblique), Channel 17 (Primary Impact)

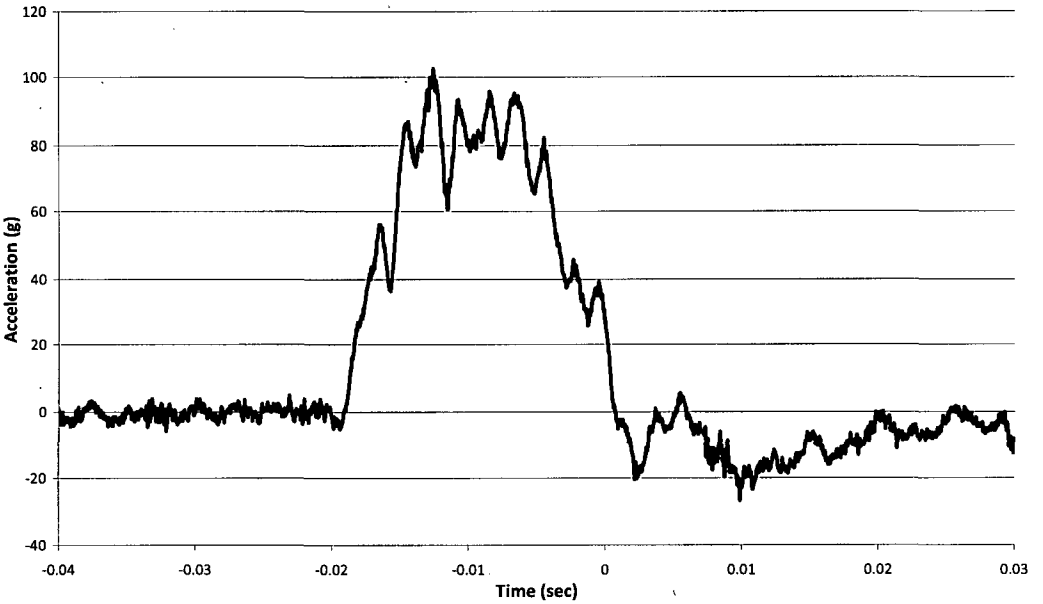

BEA Research Reactor Package Half-Scale Free Drop Test
Test D2R (15° Oblique), Channel 18 (Primary Impact)

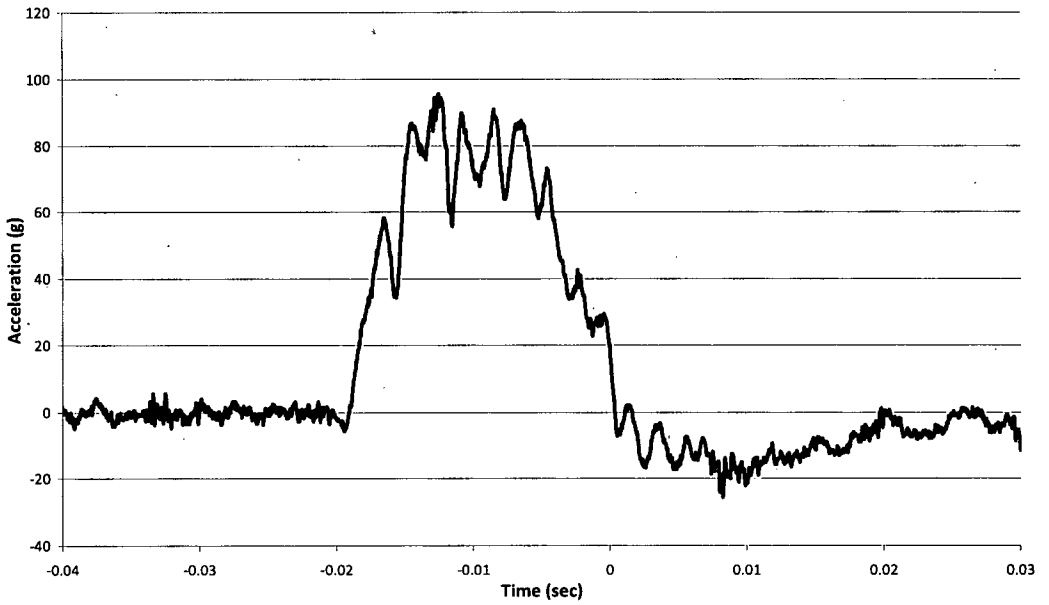

BEA Research Reactor Package Half-Scale Free Drop Test
Test D2R (15° Oblique), Channel 19 (Primary Impact)

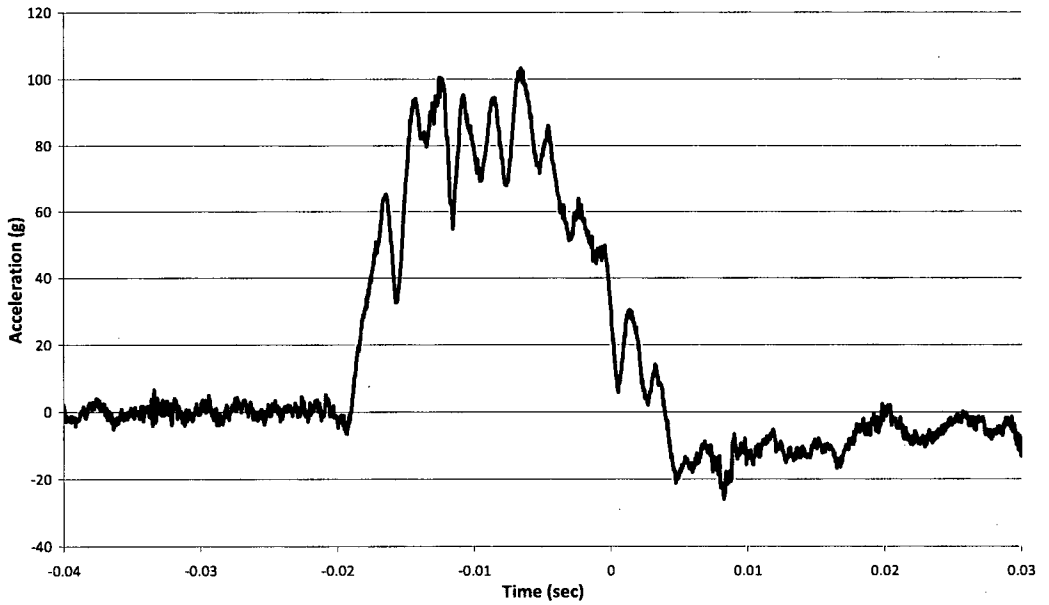

BEA Research Reactor Package Half-Scale Free Drop Test
Test D3 (CG Over Corner), Channel 12

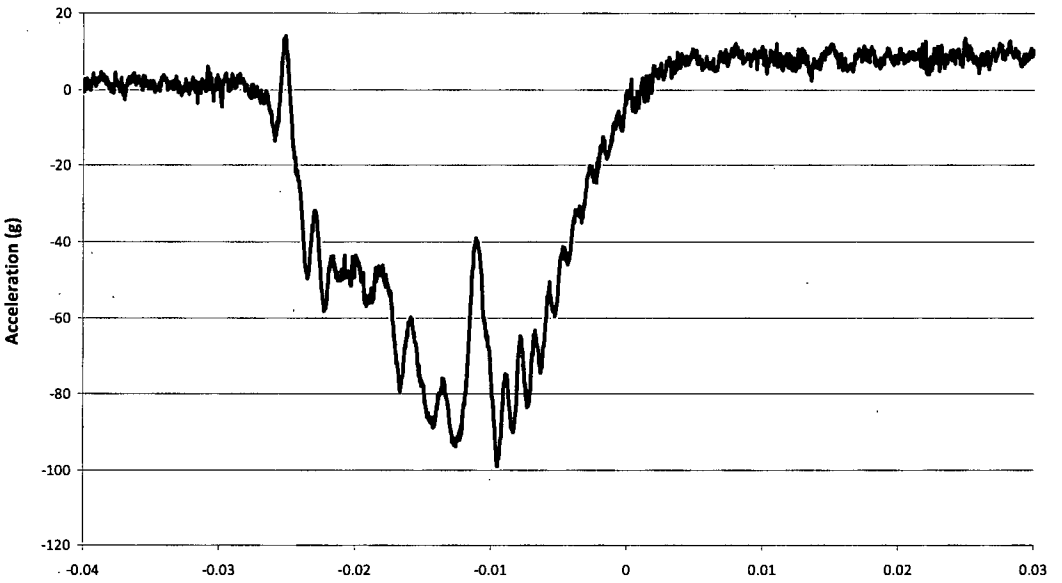

BEA Research Reactor Package Half-Scale Free Drop Test
Test D3 (CG Over Corner), Channel 13

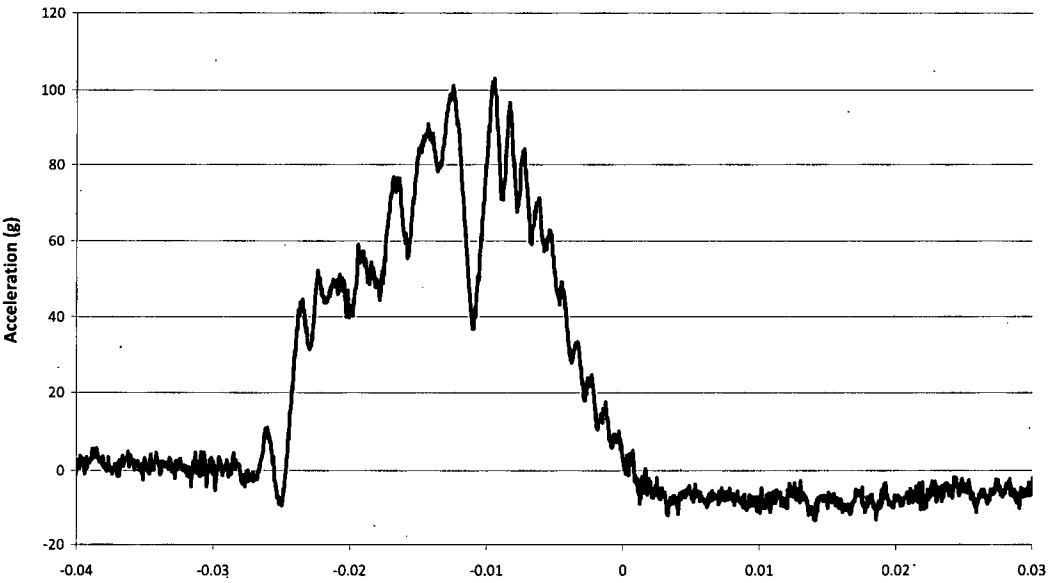

BEA Research Reactor Package Half-Scale Free Drop Test
Test D3 (CG Over Corner), Channel 14

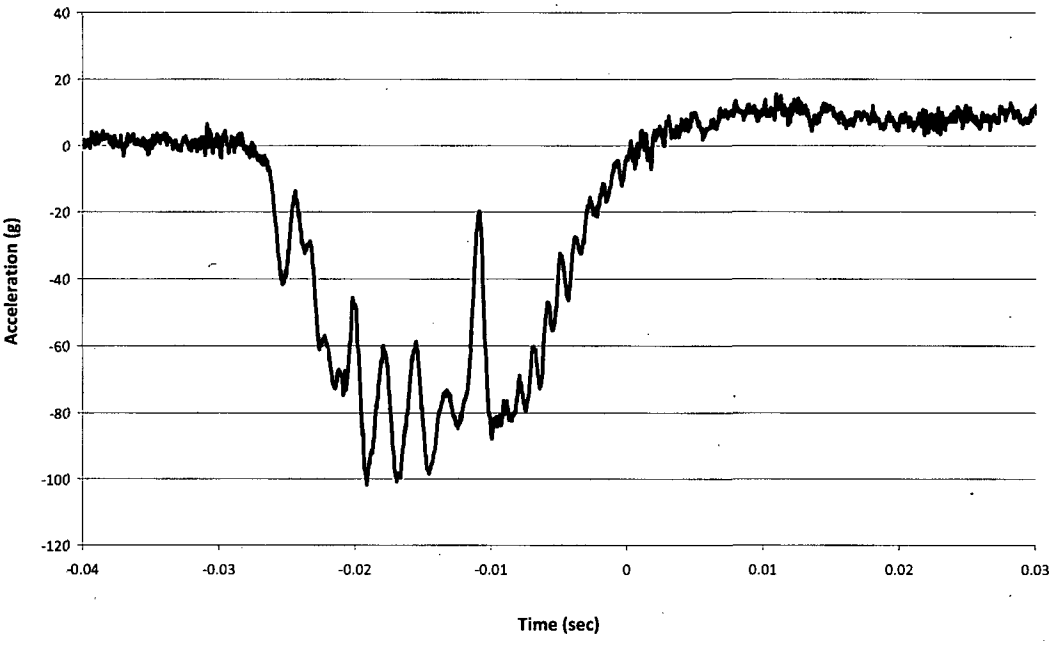

BEA Research Reactor Package Half-Scale Free Drop Test
Test D3 (CG Over Corner), Channel 15

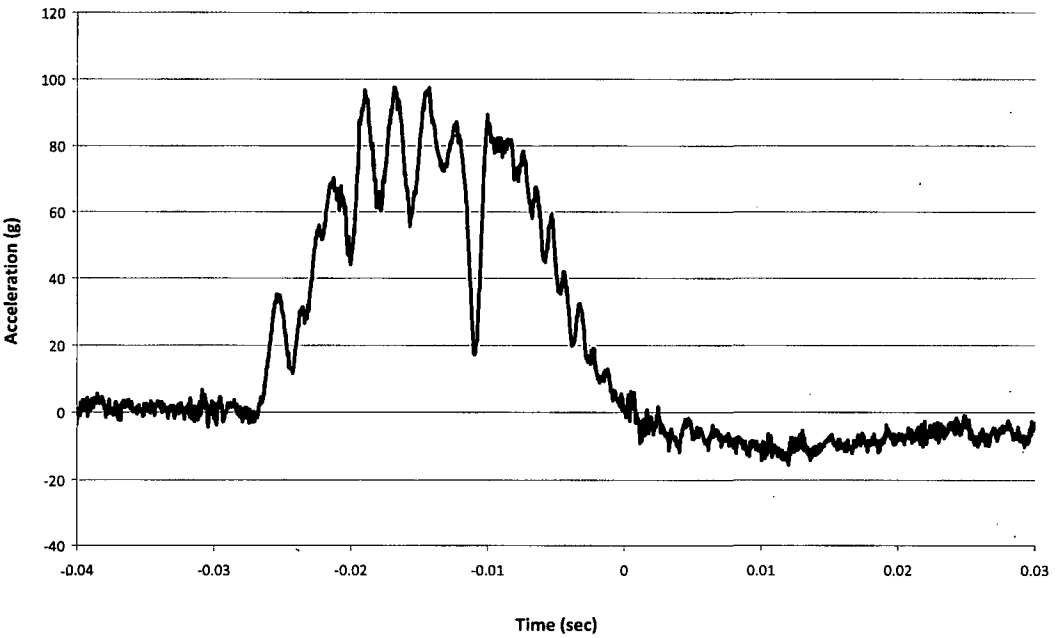

BEA Research Reactor Package Half-Scale Free Drop Test
Test D3 (CG Over Corner), Channel 16

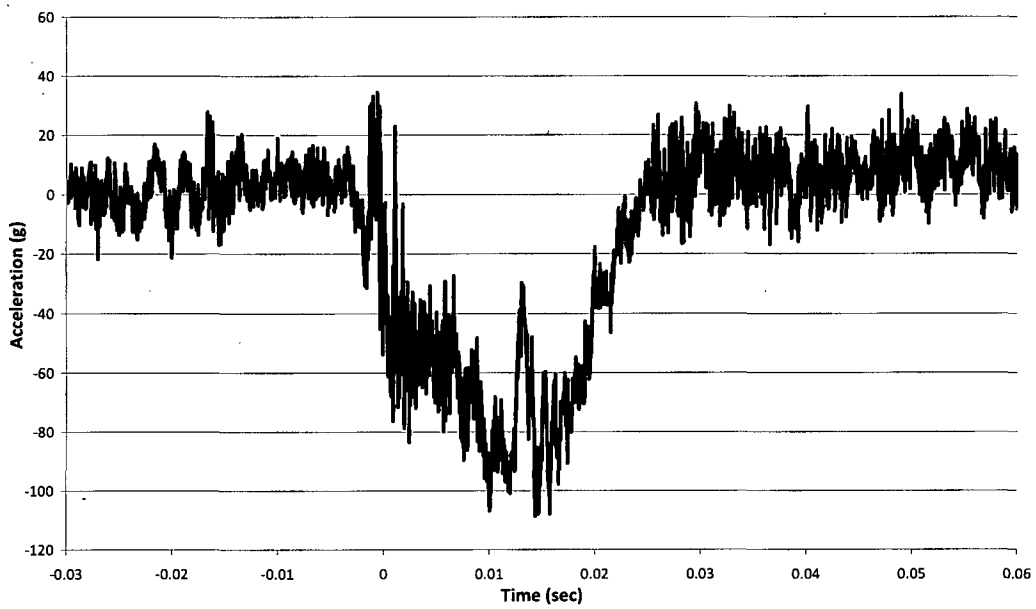

BEA Research Reactor Package Half-Scale Free Drop Test
Test D3 (CG Over Corner), Channel 17

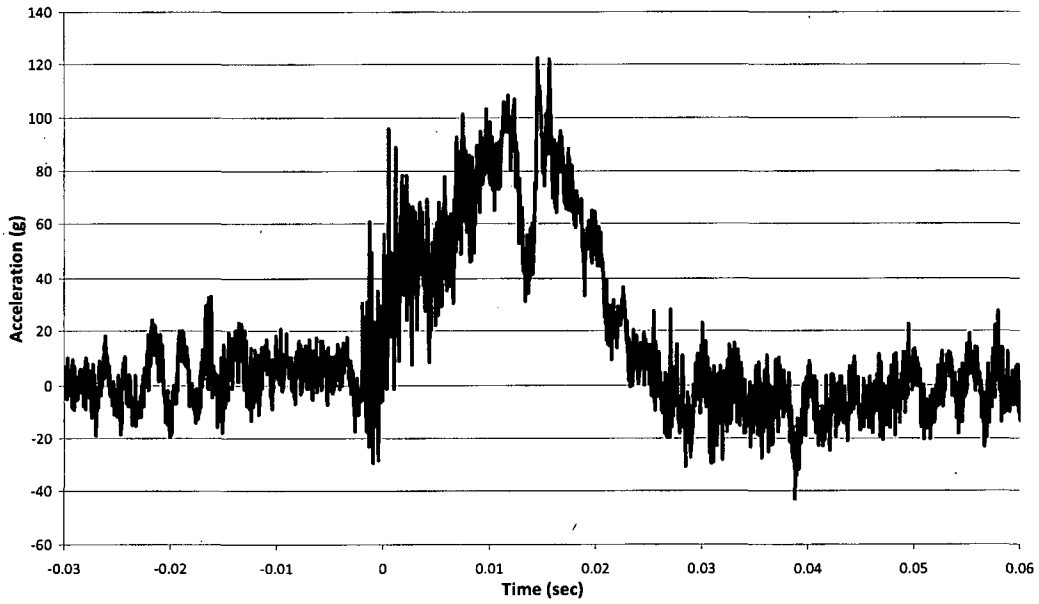

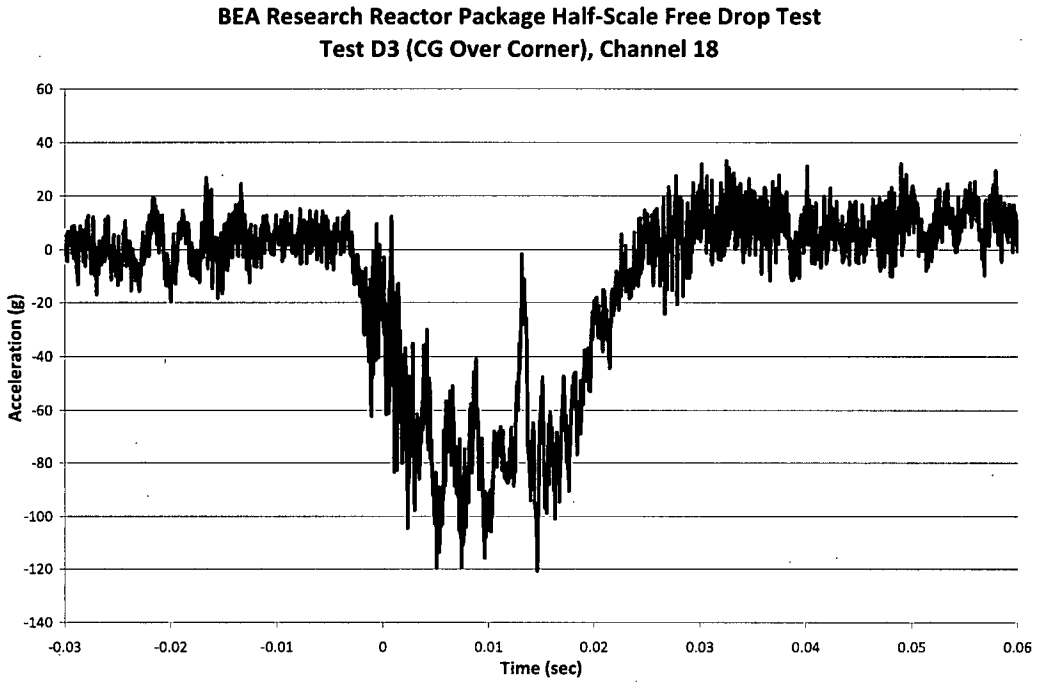
BEA Research Reactor Package Half-Scale Free Drop Test
Test D3 (CG Over Corner), Channel 18
Acceleration (g)
60
40
20
0
-20
-40
-60
-80
-100
-120
-140
-0.03
-0.02
-0.01
0
0.01
0.02
0.03
0.04
0.05
0.06
Time (sec)

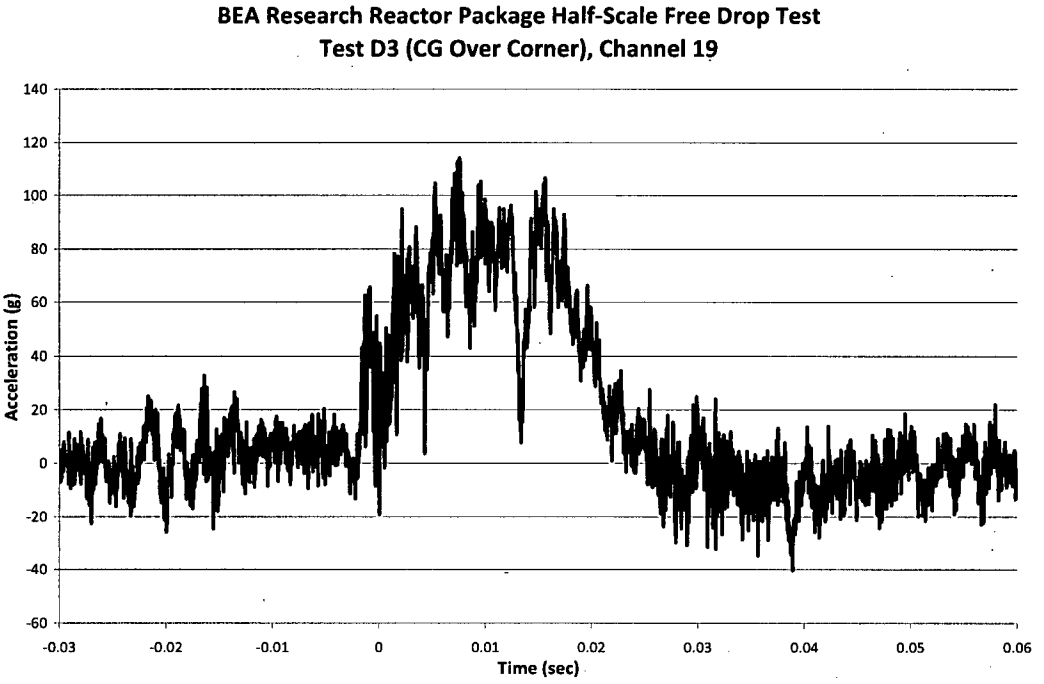
BEA Research Reactor Package Half-Scale Free Drop Test
Test D3 (CG Over Corner), Channel 19
Acceleration (g)
140
120
100
80
60
40
20
0
-20
-40
-60
-0.03
-0.02
-0.01
0
0.01
0.02
0.03
0.04
0.05
0.06
Time (sec)

2.12.4 Stress Analysis Finite Element Models

This appendix describes the finite element analysis of the BRR package body. The structural components considered are the upper and lower end structures, the inner shell, and the outer shell. The shield plug, closure lid, and fuel baskets are analyzed separately. Both Normal Conditions of Transport (NCT) and Hypothetical Accident Conditions (HAC) are considered. Loading types include design pressure, thermal, and free drop impact.

2.12.4.1 Analysis Model Description

The finite element model of the BRR package body is used to calculate stress under NCT and HAC in the structural members of the cask, which consist of the upper and lower massive end structures, the inner shell, and the outer shell. The impact limiters, the fuel baskets, the shield plug, the thermal shield, the impact limiter attachments, and the closure lid are not modeled structurally, but their mass is accounted for as discussed below. The lead shielding material in the sides and bottom of the cask body is also not explicitly modeled, and is further discussed below. The model is built in ANSYS Revision 11.0 using half symmetry along a vertical plane through the cask center. The structural elements are SOLID95, 20-node bricks, and the thermal elements are SOLID90, 20-noded bricks. A pressure of 25 psi, corresponding to the design pressure identified in Section 2.6.1.1, *Summary of Pressures and Temperatures*, is applied to the interior surface of the model in each case. The pressure is applied to all element interior surfaces which fall within the location of the inner (containment) O-ring. The pressure creates a small net force which is reacted by forces in the opposite direction applied at the bolt circle of the closure lid. For load cases which do not include inertia forces, the model is constrained by the symmetry plane and by fixed nodes at the edge of the cask outer bottom surface. When inertia loads are applied, the model constraint is individually discussed in the following sections. The finite element mesh is shown in Figure 2.12.4-1.

2.12.4.2 Loading of the Model

Besides the design pressure discussed above, the model is loaded by thermal loads and by free drop impact loads.

2.12.4.2.1 Thermal Loads

A detailed thermal analysis is performed in Chapter 3, *Thermal Evaluation.* The thermal analysis performed using the model described in this section is done only to transform the thermal results obtained in Chapter 3 into the form required by the stress analysis model. This is done by assigning selected key nodal temperatures taken from the Chapter 3 analysis, and running the thermal/stress model described in this section using thermal elements (SOLID90) to obtain temperatures at each node of the model. The location of the key nodes at which the Chapter 3 NCT temperatures were transferred directly to the thermal/stress model are shown in Figure 2.12.4-2. Convection and radiation are set to zero. Thermal conductivity is a required SOLID90 input but does not affect the result and is therefore set to an arbitrary value of 1. The resulting temperature distribution is essentially the same as that obtained in Chapter 3, and is shown in Figure 2.12.4-3. The nodal temperatures are used in the stress analysis along with

temperature-dependent coefficients of thermal expansion taken from Table 2.2-1 and Table 2.2-2 to obtain thermal stress.

Another source of thermal loading is the lead gamma shield used in the annulus between the inner and outer shells. Due to different thermal expansion coefficients, the lead gamma shielding applies a radial pressure to the outer surface of the inner shell under NCT hot conditions. As shown in Section 2.6.1.2.3, *Lead*, this pressure can be assigned an upper bound value of 350 psi. For the NCT hot case, this pressure is applied to the inner shell outer surface over the entire length of the side lead cavity. The treatment of lead in load cases which include free drop impact loads is discussed below.

2.12.4.2.2 Free Drop Impact Loads

Stress is generated in the BRR cask body in a free drop impact through self weight of the components and the applied loads of components not modeled. The resulting forces are reacted over the interface areas of the impact limiter(s). A bounding impact deceleration field of 40g is applied for the NCT cases as discussed in Section 2.6.7, *Free Drop*, and 120g is applied for the HAC cases as discussed in Section 2.7.1, *Free Drop*. As shown in Section 2.7.1, the governing orientations for stress analysis are the end drop (top end down and bottom end down), and the side drop.

The weight of the shield plug, fuel basket, closure lid, and the impact limiter not in contact with the ground (e.g., the one on top in an end drop) are accounted for by applying pressure to the region of contact. The applied load is equal to the weight of the component multiplied by the appropriate impact g-load, divided by the contact area. Component weights are taken from Table 2.1-2, (half of these values are used for half symmetry) and the contact areas are calculated using the drawings in Appendix 1.3.3, *Packaging General Arrangement Drawings*. The density of stainless steel is 0.29 lb/in^3. The weight of the thermal shield and impact limiter attachments is included in the cask body model by a slight adjustment of the material density.

The lead gamma shielding is not explicitly modeled. Instead, for simplicity and conservatism, it is treated as a liquid material, thus applying a hydrostatic pressure within the side and lower lead cavities. The magnitude of the pressure is:

$$p = \gamma g h$$

where the pressure at any point, p, is applied on the side and lower surfaces of the lead cavity, g is the acceleration of gravity, h is the depth of the lead, and γ is the density of lead, equal to 0.41 lb/in^3. Due to the conservatism of this assumption, it is not necessary to additionally apply the lead thermal load of 350 psi (see Section 2.12.4.2.1, *Thermal Loads*) to any free drop load cases.

Once all of the impact loads have been applied, the model is constrained at a minimum number of nodes for stability. The impact limiter support loads are then adjusted until near-perfect balance is achieved between the applied loads (inertia loads of the cask structure, lead, and separate components) and the impact reaction (the impact limiter). In each case, the total reaction force is essentially equal to the total decelerated weight (i.e., total weight of the BRR package, less the weight of the limiter(s) contacting the ground) times 40 (NCT) or 120 (HAC). Greater detail on the application of the inertia loads, the lead hydrostatic pressure loads, and the displacement constraints is provided in the sections discussing each load case.

These analyses do not include a dynamic load factor (DLF), since the impact acceleration used is nearly 50 % higher than the maximum test result (see Section 2.12.5.3, *Reconciliation with Certification Test Results*), and because the cask structures are relatively stiff, which would result in a DLF not significantly different from unity.

2.12.4.3 Material Properties

For load cases that do not evaluate thermal stress, the modulus of elasticity is evaluated at the bounding NCT hot temperature of 250 °F, or $E = 27.3 \times 10^6$ psi from Table 2.6-1. Poisson's ratio is equal to 0.3. For load cases in which thermal stress is included, both the modulus of elasticity and the thermal expansion coefficient are evaluated at the nodal temperatures determined in the thermal run, using data from Table 2.2-1 and Table 2.2-2. All allowable stresses are evaluated at the NCT hot temperature of 250 °F.

2.12.4.4 Load Cases and Allowable Stress

Load cases are identified which allow the evaluation of the model stresses using the allowable stresses defined in Table 2.1-1. For NCT, numerical values of allowable stress are taken from Table 2.6-1 for a temperature of 250 °F. The primary membrane (P_m) allowable stress is S_m, which is equal to 20,000 psi. The primary membrane plus bending ($P_m + P_b$) stress allowable is $1.5S_m$, or 30,000 psi, and the primary plus bending plus secondary ($P_m + P_b + Q$) stress allowable is $3.0S_m$, or 60,000 psi.

For HAC, the numerical values depend on the value of S_u, which is smaller for the forged or cast materials used for the upper and lower end structures and the inner shell (see Table 2.2-2). At a temperature of 250 °F, the minimum value of S_u = 64,050 psi. The primary membrane (P_m) allowable stress is the lesser of $2.4S_m$ or $0.7S_u$, or a minimum of 44,835 psi. The primary membrane plus bending ($P_m + P_b$) stress allowable is the lesser of $3.6S_m$ or S_u, or a minimum of 64,050 psi.

Because, in the NCT cases, the resulting stresses are relatively low and it is not necessary to separately identify the membrane stress. Therefore the margin of safety may be conservatively determined by applying the maximum stress intensity to the primary membrane stress allowable.

For the HAC cases, the maximum stress resulting from the model is evaluated by decoupling the primary stress from bending and secondary stress. Thus, in each HAC case, the stresses are linearized to distinguish between the decoupled stresses and separate allowables are applied.

The load cases and allowable stresses are listed in the following table. Note: the design pressure of 25 psig is present in all load cases.

Case No.	Section No.	Description	Stress Evaluated
1	2.12.4.4.1	Design pressure only	Primary
2	2.12.4.4.2	Lead shrinkage pressure with thermal	Secondary
3	2.12.4.4.3	NCT bottom-down end drop	Primary
4	2.12.4.4.4	NCT bottom-down end drop with thermal	Secondary
5	2.12.4.4.5	HAC bottom-down end drop	Primary
6	2.12.4.4.6	NCT top-down end drop	Primary
7	2.12.4.4.7	NCT top-down end drop with thermal	Secondary
8	2.12.4.4.8	HAC top-down end drop	Primary
9	2.12.4.4.9	NCT side drop	Primary
10	2.12.4.4.10	NCT side drop with thermal	Secondary
11	2.12.4.4.11	HAC side drop	Primary

2.12.4.4.1 Case No. 1, Design Pressure Only

In this case, the only applied load is the design pressure of 25 psig, applied to the interior of the cask body at a radius less than or equal to that of the inner (containment) O-ring. The design pressure loading is shown in Figure 2.12.4-4. The model is constrained by the symmetry plane and by nodes at the outer edge of the cask bottom surface.

Results are shown in Figure 2.12.4-5. The maximum stress intensity is 281 psi at the midpoint of the payload cavity bottom. Conservatively using the NCT membrane stress allowable of 20,000 psi, the margin of safety is:

$$MS = \frac{20{,}000}{281} - 1 = +70.2$$

2.12.4.4.2 Case No. 2, Lead Shrinkage Pressure With Thermal

Case No. 2 starts with the 25 psig pressure of Case No. 1 and adds the lead shrinkage pressure to the outside surface of the inner shell, all along the side lead cavity. In addition, thermal stress is calculated using the NCT hot case temperatures and temperature dependent coefficients of thermal expansion. Both of these loads are described in Section 2.12.4.2.1, *Thermal Loads*. The model is constrained by the symmetry plane and by nodes at the outer edge of the cask bottom surface.

Results are shown in Figure 2.12.4-6. The maximum stress intensity is 6,933 psi at the top of the inner shell cross section. Since this result includes secondary stress, the allowable is 60,000 psi. The margin of safety is:

$$MS = \frac{60{,}000}{6{,}933} - 1 = +7.65$$

2.12.4.4.3 Case No. 3, NCT Bottom-Down End Drop

In this case, the applied loads are the design pressure from Case No. 1 and the free drop weight of the shield plug, fuel basket, closure lid, and impact limiter. The free drop loads are described in Section 2.12.4.2.2, *Free Drop Impact Loads*. The cask body orientation is vertical, with the bottom end down. The weight of the side lead applies a hydrostatic pressure based on depth as described in Section 2.12.4.2.2. The weight of the lower lead is modeled as two separate hydrostatic loads based the inner and outer lead columns above the upper surface of the lower closure plate. The bottom-down end drop loading is shown in Figure 2.12.4-7. The model is constrained by the symmetry plane and by nodes at the outer edge of the cask bottom surface.

Results are shown in Figure 2.12.4-8. The maximum stress intensity is 15,202 psi at the outside surface of the bottom end structure. Conservatively using the NCT membrane stress allowable of 20,000 psi, the margin of safety is:

$$MS = \frac{20{,}000}{15{,}202} - 1 = +0.32$$

2.12.4.4.4 Case No. 4, NCT Bottom-Down End Drop With Thermal

Case No. 4 adds the thermal loading described in Section 2.12.4.2.1, *Thermal Loads*, to Case No. 3.

Results are shown in Figure 2.12.4-9. The maximum stress intensity is 14,586 psi at the top of the inner shell cross section. Since this result includes secondary stress, the allowable is 60,000 psi. The margin of safety is:

$$MS = \frac{60{,}000}{14{,}586} - 1 = +3.11$$

2.12.4.4.5 Case No. 5, HAC Bottom-Down End Drop

Case No. 5 is the same as Case No. 3, except with an HAC inertia field of 120g.

Results are shown in Figure 2.12.4-10. The maximum stress intensity is 45,681 psi at the outside surface of the bottom end structure. In the prior NCT load cases, the membrane allowable has been conservatively applied to the maximum stress intensity, which makes it unnecessary to differentiate the actual membrane stress from the membrane plus bending stress. Since this is an HAC case, the less conservative approach is applied; the stress is linearized through the lower massive end structure cross section. Results are shown in Figure 2.12.4-11. The maximum primary membrane stress is 22,680 psi. The HAC membrane stress allowable is 44,835 psi. The margin of safety is:

$$MS = \frac{44{,}835}{22{,}680} - 1 = +0.98$$

The maximum membrane plus bending stress is 43,080 psi. The HAC membrane plus bending stress allowable is 64,050. The margin of safety is:

$$MS = \frac{64{,}050}{43{,}080} - 1 = +0.49$$

2.12.4.4.6 Case No. 6, NCT Top-Down End Drop

In this case, the weight of the shield plug, fuel basket and closure lid are modeled as forces located at the lid bolt circle. The shield plug is modeled as a pressure distributed on the impact limiter contact area. Design pressure is applied as in Case No. 1. The cask body orientation is vertical, with the top end down. The weight of the side lead applies a hydrostatic pressure based on depth as described in Section 2.12.4.2.2, *Free Drop Impact Loads.* The weight of the lower lead is modeled as two separate hydrostatic loads based the inner and outer lead columns above the upper and lower shelves of the lower lead cavity. The top-down end drop loading is shown in Figure 2.12.4-12. The model is constrained by the symmetry plane and by nodes at the outer edge of the cask top surface.

Results are shown in Figure 2.12.4-13. The maximum stress intensity is 13,248 psi at the top of the inner shell. Conservatively using the NCT membrane stress allowable of 20,000 psi, the margin of safety is:

$$MS = \frac{20,000}{13,248} - 1 = +0.51$$

2.12.4.4.7 Case No. 7, NCT Top-Down End Drop With Thermal

Case No. 7 adds the thermal loading described in Section 2.12.4.2.1, *Thermal Loads*, to Case No. 6.

Results are shown in Figure 2.12.4-14. The maximum stress intensity is 13,258 psi at the top of the inner shell. Since this result includes secondary stress, the allowable is 60,000 psi. The margin of safety is:

$$MS = \frac{60,000}{13,258} - 1 = +3.53$$

2.12.4.4.8 Case No. 8, HAC Top-Down End Drop

Case No. 8 is the same as Case No. 6, except with an HAC inertia field of 120g.

Results are shown in Figure 2.12.4-15. The maximum stress intensity is 40,140 psi at the top of the inner shell. In this HAC case, the stress is linearized, through the line of highest stress intensity in the top inner shell cross section. The linearized results are shown in Figure 2.12.4-16. The maximum primary membrane stress is 22,720 psi. The HAC membrane stress allowable is 44,835 psi. The margin of safety is:

$$MS = \frac{44,835}{22,720} - 1 = +0.97$$

The maximum membrane plus bending stress is 33,400 psi. The HAC membrane plus bending stress allowable is 64,050. The margin of safety is:

$$MS = \frac{64,050}{33,400} - 1 = +0.92$$

2.12.4.4.9 Case No. 9, NCT Side Drop

In this case, the applied loads are the design pressure from Case No. 1 and the free drop weight of the shield plug, fuel basket, and closure lid. The applied loads and supporting pressures are applied as pressures over an included angle of 30°, which represents the circumferential extent of contact. The cask body orientation is horizontal. The weight of the side and bottom lead shields are modeled as a hydrostatic pressures as described in Section 2.12.4.2.2, *Free Drop Impact Loads*. The side drop loading is shown in Figure 2.12.4-17 and Figure 2.12.4-18. The model is constrained by the symmetry plane and by two nodes at the top and bottom of the cask and one node at the top to constrain radial and axial motion respectively.

Results are shown in Figure 2.12.4-19. The maximum stress intensity is 18,935 psi at the bottom outside edge of the lower lead cavity. Conservatively using the NCT membrane stress allowable of 20,000 psi, the margin of safety is:

$$MS = \frac{20{,}000}{18{,}935} - 1 = +0.06$$

2.12.4.4.10 Case No. 10, NCT Side Drop With Thermal

Case No. 10 adds the thermal loading described in Section 2.12.4.2.1, *Thermal Loads*, to Case No. 9.

Results are shown in Figure 2.12.4-20. The maximum stress intensity is 22,704 psi at the shield plug shelf. Since this result includes secondary stress, the allowable is 60,000 psi. The margin of safety is:

$$MS = \frac{60{,}000}{22{,}704} - 1 = +1.64$$

2.12.4.4.11 Case No. 11, HAC Side Drop

Case No. 11 is the same as Case No. 9, except with an HAC inertia field of 120g.

Results are shown in Figure 2.12.4-21. The maximum stress intensity is 56,810 psi at the bottom outside edge of the lower lead cavity. The stress, as in prior HAC cases, is linearized through the lower closure plate cross section. Results are shown in Figure 2.12.4-22. The maximum primary membrane stress is 16,330 psi. The HAC membrane stress allowable is 44,835 psi. The margin of safety is:

$$MS = \frac{44{,}835}{16{,}330} - 1 = +1.75$$

The maximum membrane plus bending stress is 51,990 psi. The HAC membrane plus bending stress allowable is 64,050. The margin of safety is:

$$MS = \frac{64{,}050}{51{,}990} - 1 = +0.23$$

2.12.4.5 Summary

Table 2.12.4-1 summarizes the margins of safety of the BRR package finite element analysis, as established in the sections above. Since all margins of safety are positive, the structural components considered (the upper and lower end structures, the inner shell, and the outer shell) are not of concern.

Table 2.12.2-1 – Finite Element Analysis Results

Analysis Description	Reference Section	Margin of Safety
Case No. 1, Design Pressure Only	2.12.4.4.1	+ 70.2
Case No. 2, Lead Shrinkage Pressure With Thermal	2.12.4.4.2	+ 7.65
Case No. 3, NCT Bottom-Down End Drop	2.12.4.4.3	+ 0.32
Case No. 4, NCT Bottom-Down End Drop With Thermal	2.12.4.4.4	+ 3.11
Case No. 5, HAC Bottom-Down End Drop	2.12.4.4.5	+ 0.49①
Case No. 6, NCT Top-Down End Drop	2.12.4.4.6	+ 0.51
Case No. 7, NCT Top-Down End Drop With Thermal	2.12.4.4.7	+ 3.53
Case No. 8, HAC Top-Down End Drop	2.12.4.4.8	+ 0.92①
Case No. 9, NCT Side Drop	2.12.4.4.9	+ 0.06
Case No. 10, NCT Side Drop With Thermal	2.12.4.4.10	+ 1.64
Case No. 11, HAC Side Drop	2.12.4.4.11	+ 0.23①

Notes:

1. Minimum value shown.

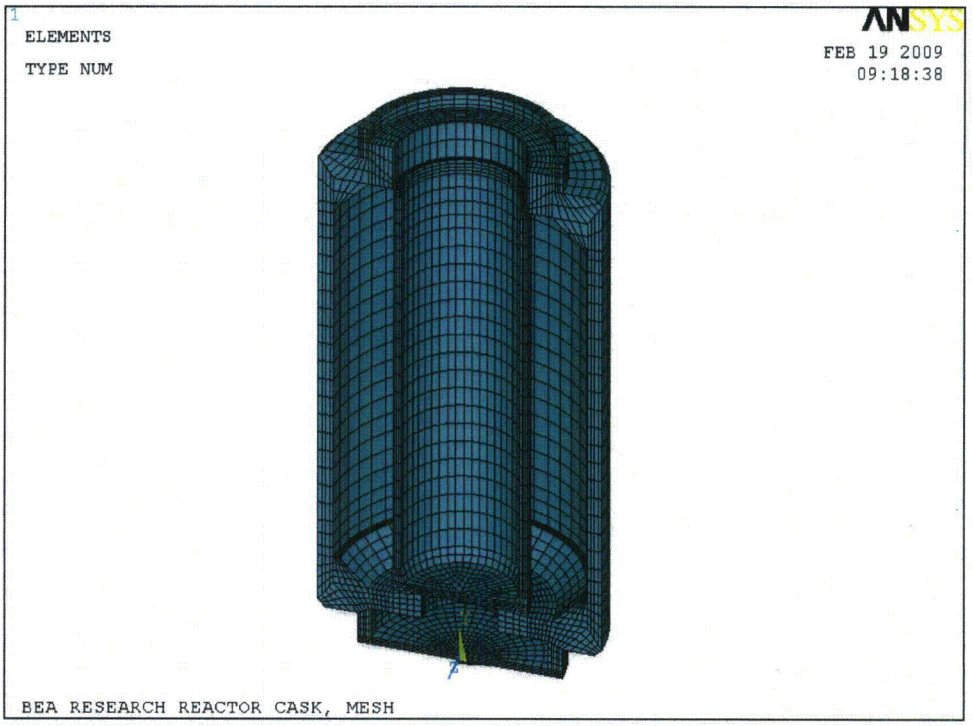

Figure 2.12.4-1 – Finite Element Mesh

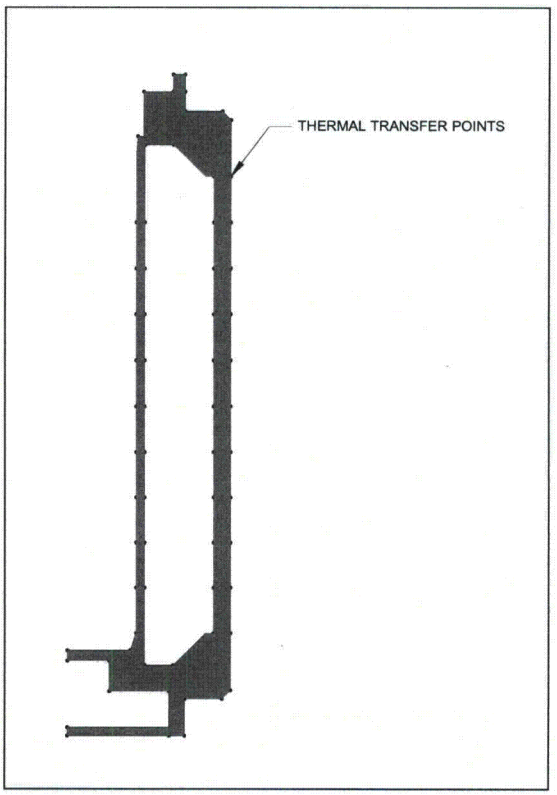

Figure 2.12.4-2 – Thermal Transfer Points

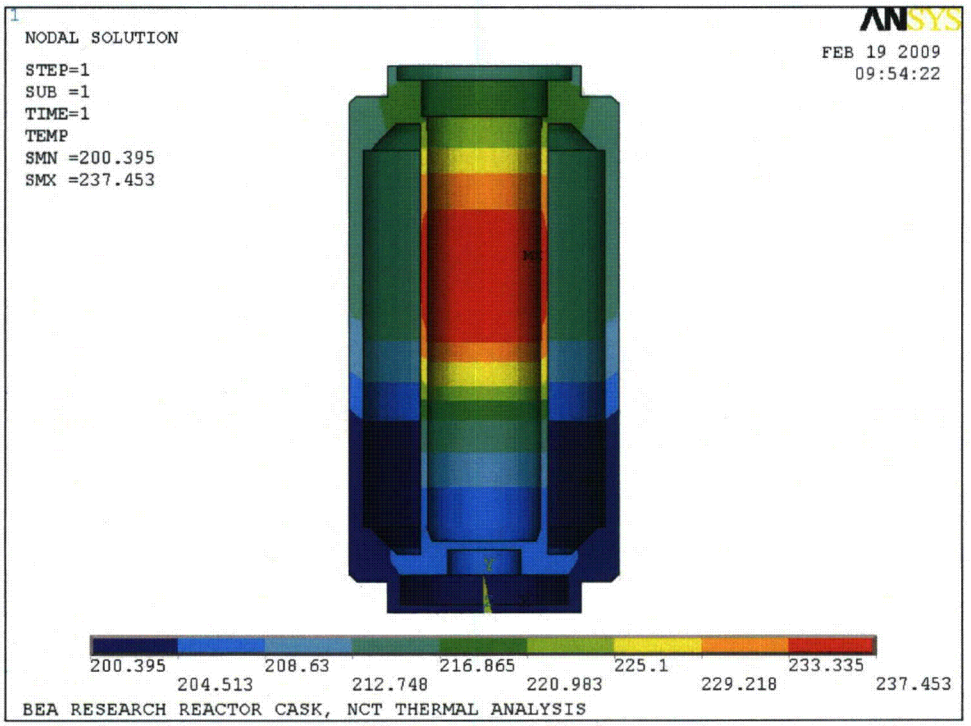

Figure 2.12.4-3 – Temperature Distribution

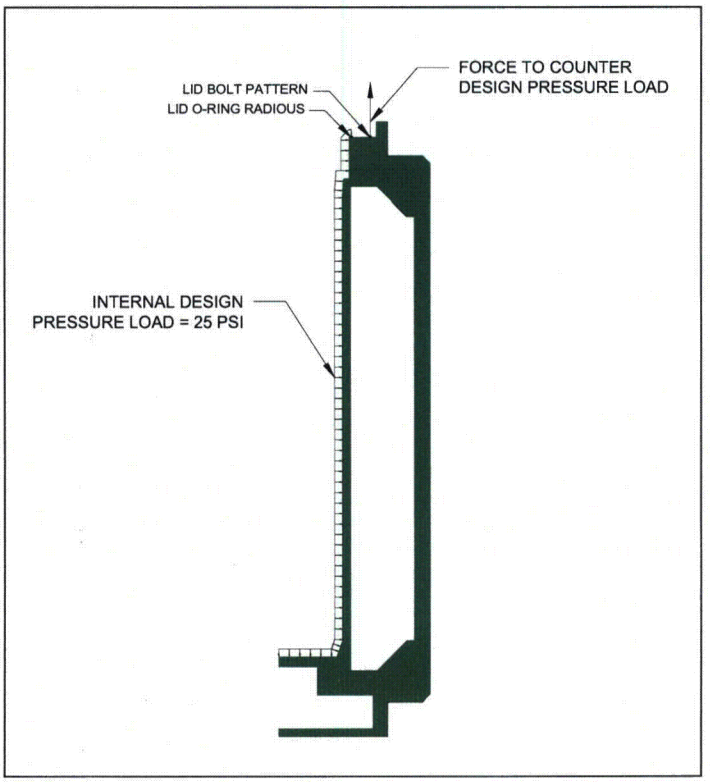

Figure 2.12.4-4 – Design Pressure Loading

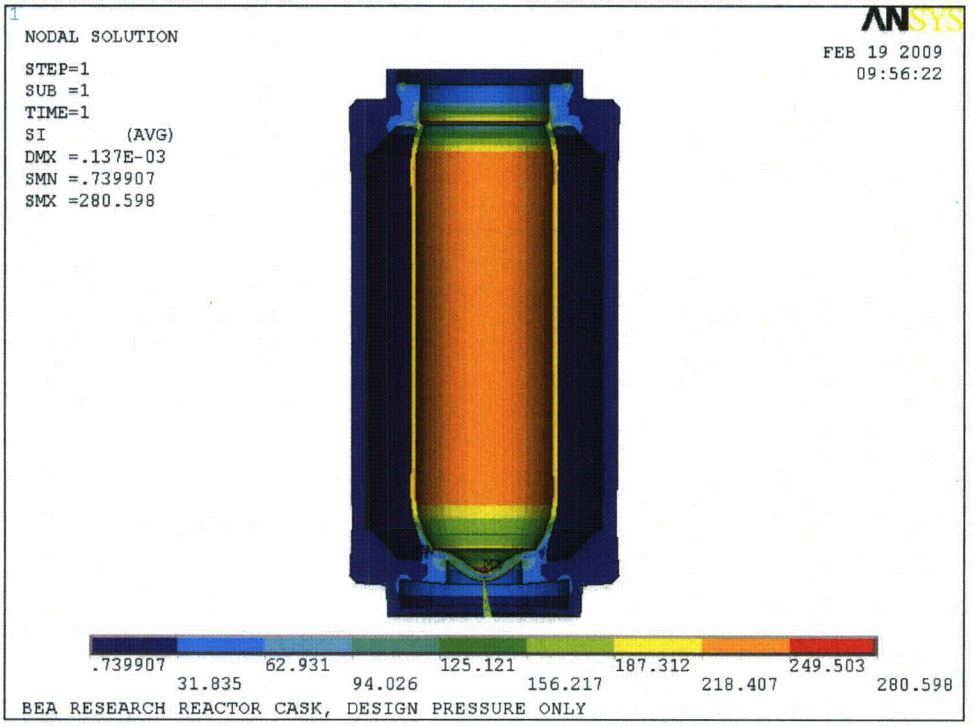

Figure 2.12.4-5 – Internal Pressure Only

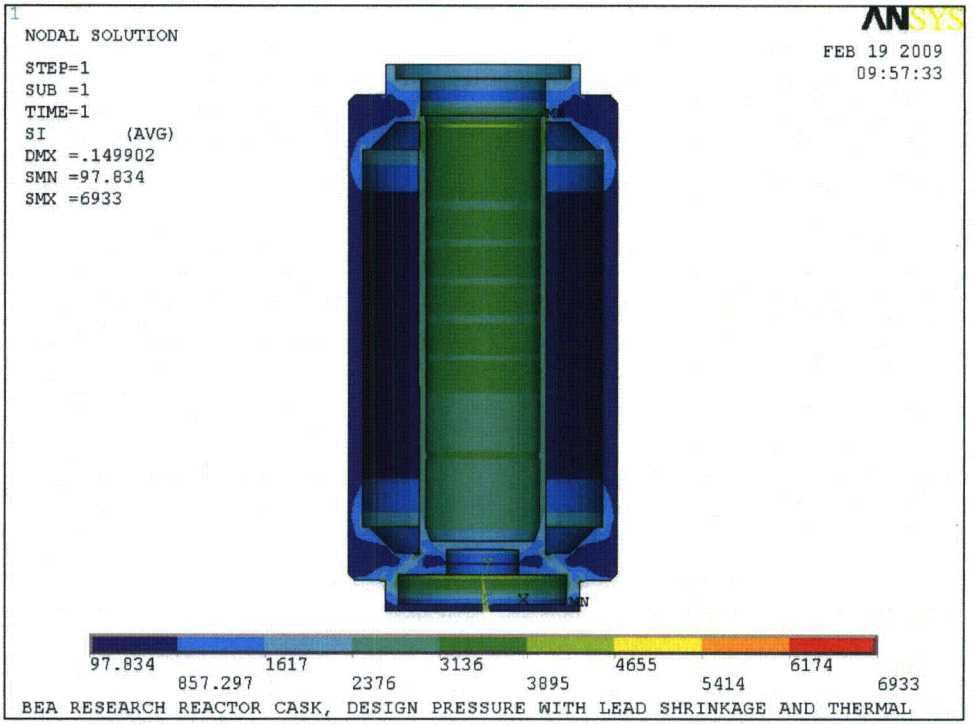

Figure 2.12.4-6 – Lead Shrinkage Pressure With Thermal

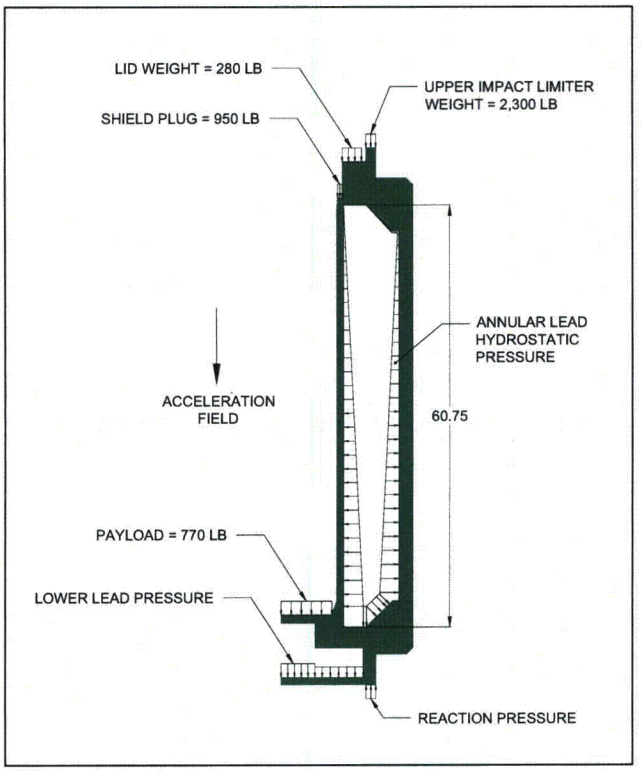

Figure 2.12.4-7 –Bottom-Down End Drop Loading

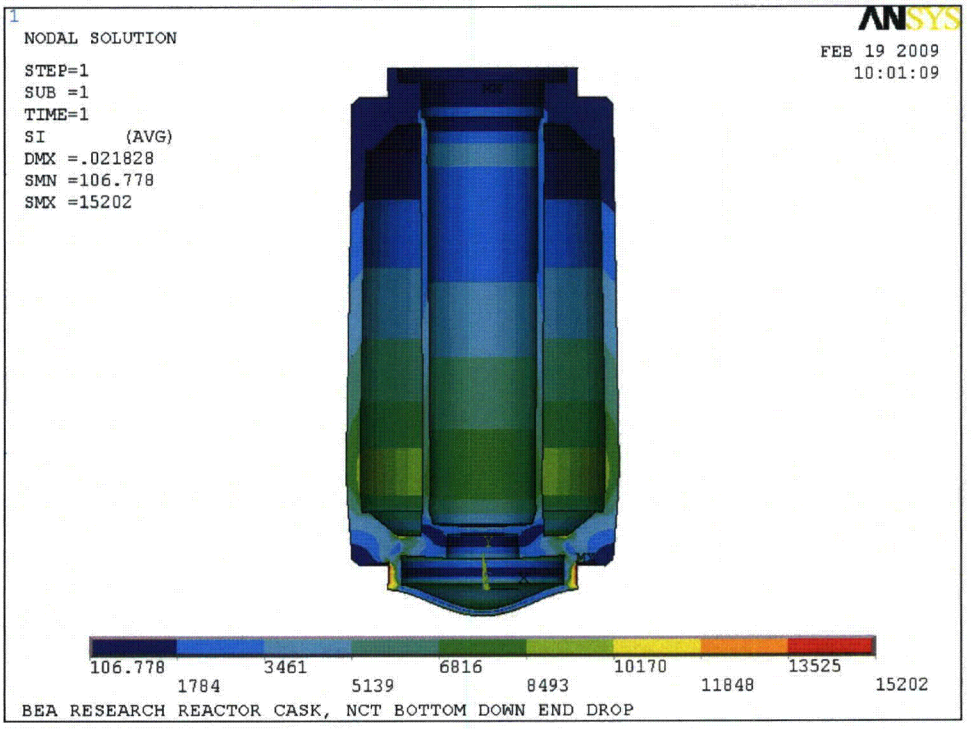

Figure 2.12.4-8 – NCT Bottom-Down End Drop

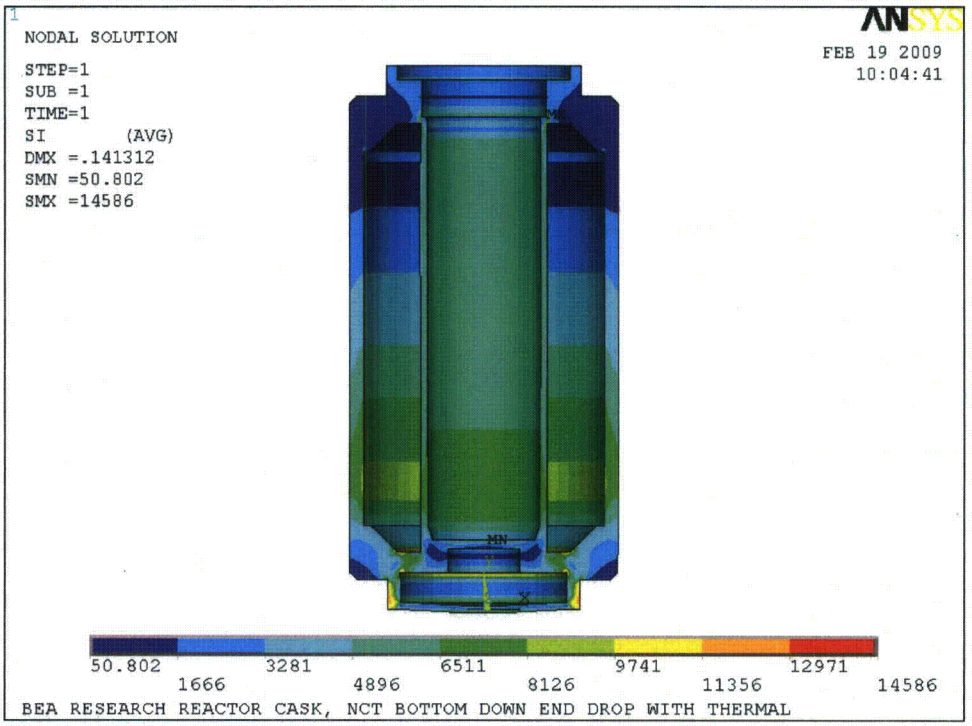

Figure 2.12.4-9 – NCT Bottom-Down End Drop With Thermal

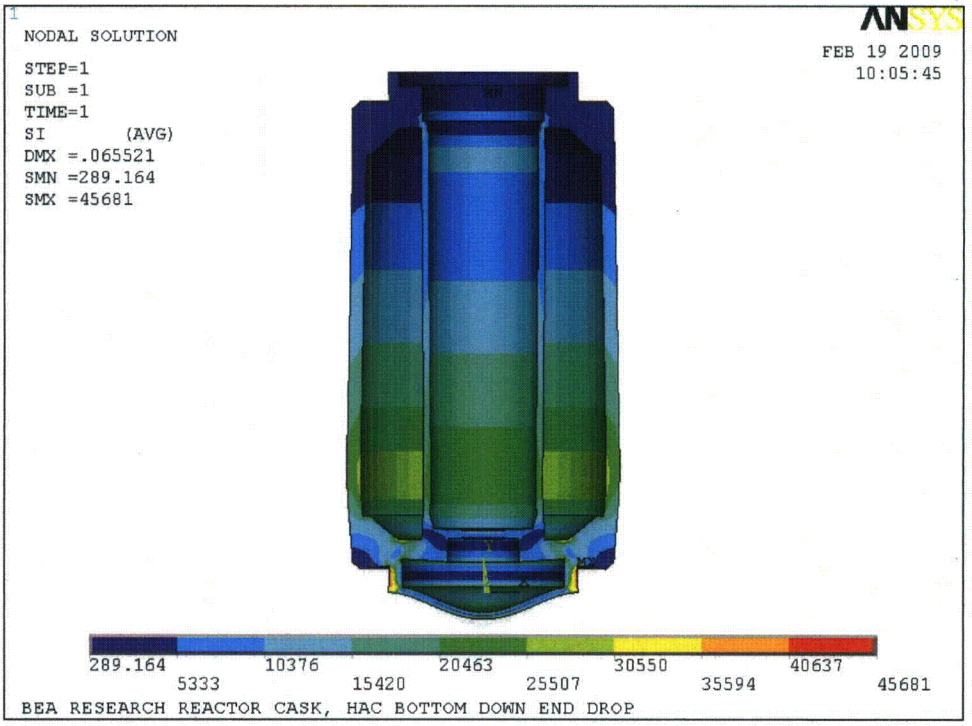

Figure 2.12.4-10 – HAC Bottom-Down End Drop

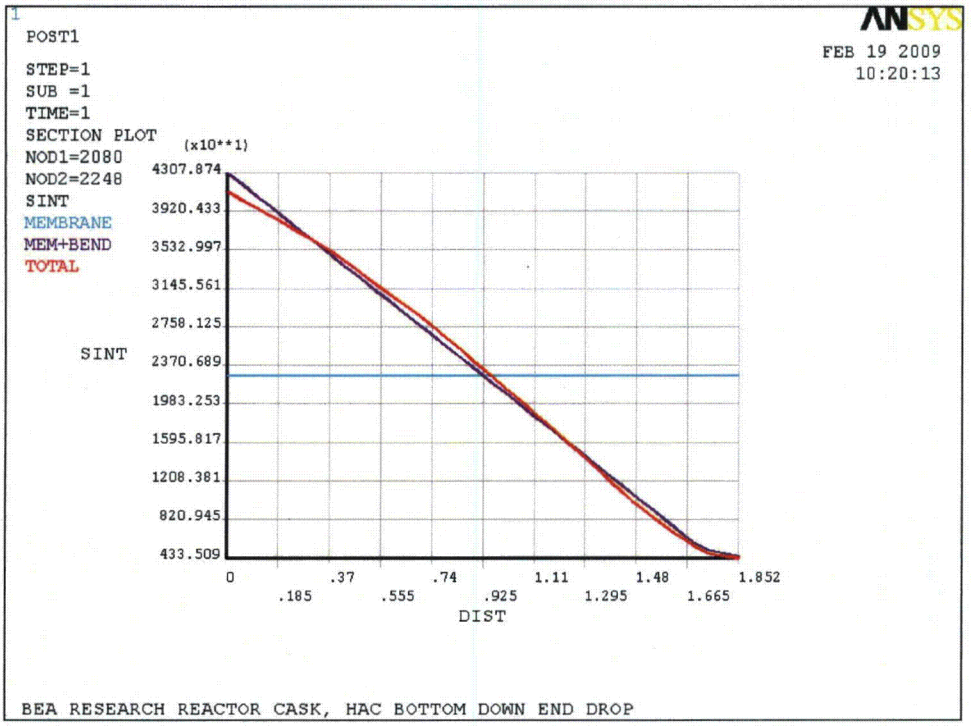

Figure 2.12.4-11 – HAC Bottom-Down End Drop Linearized Stress

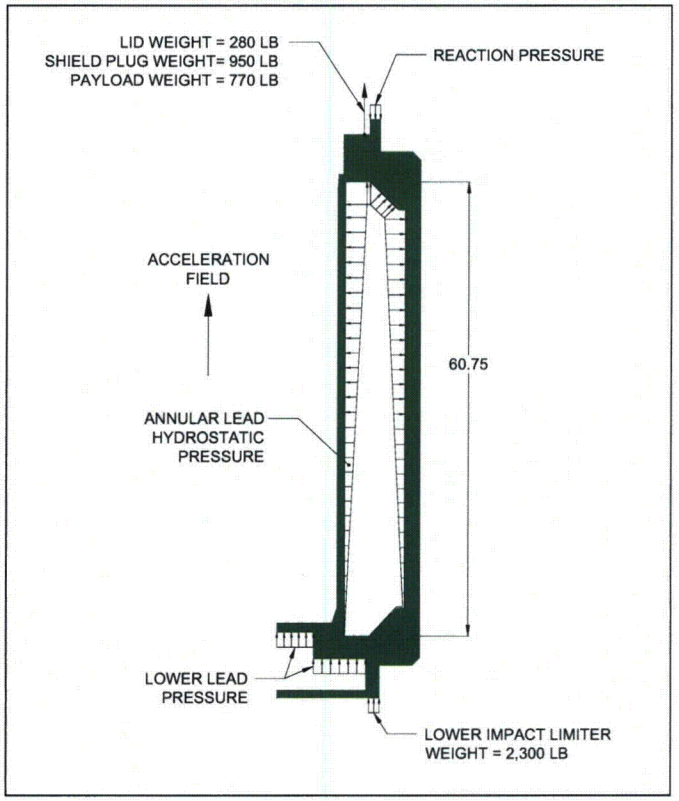

Figure 2.12.4-12 –Top-Down End Drop Loading

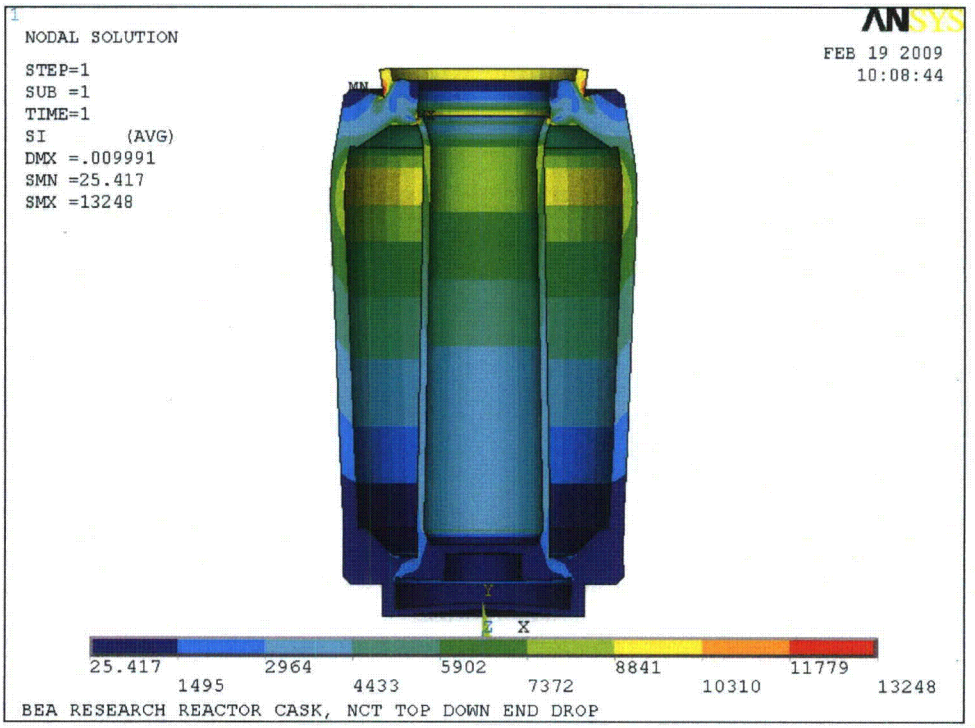

Figure 2.12.4-13 – NCT Top-Down End Drop

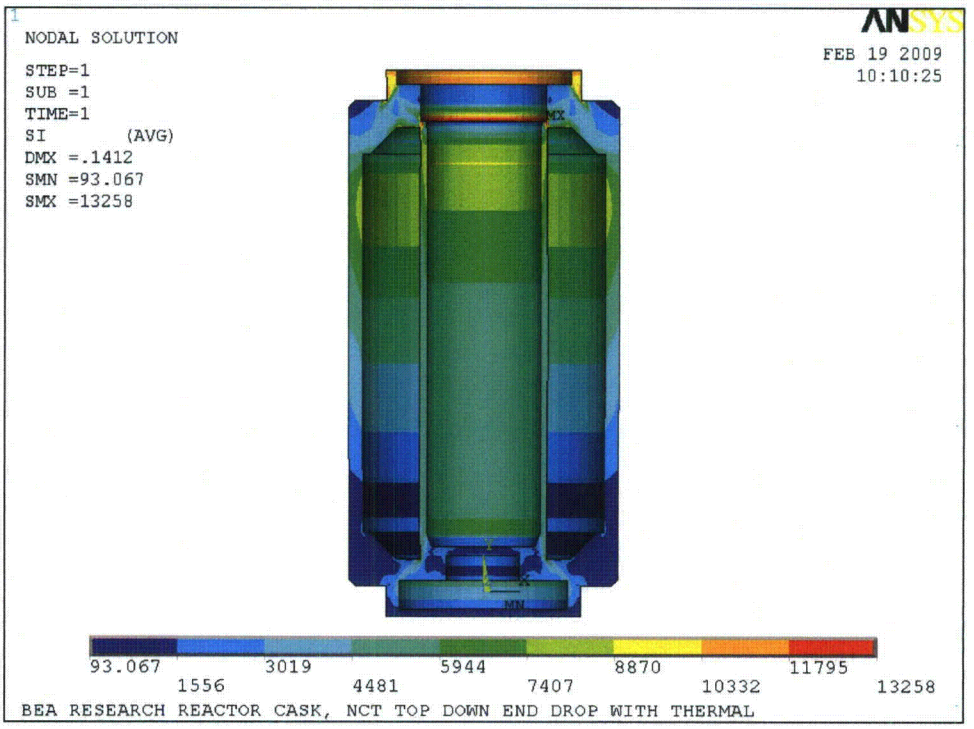

Figure 2.12.4-14 – NCT Top-Down End Drop With Thermal

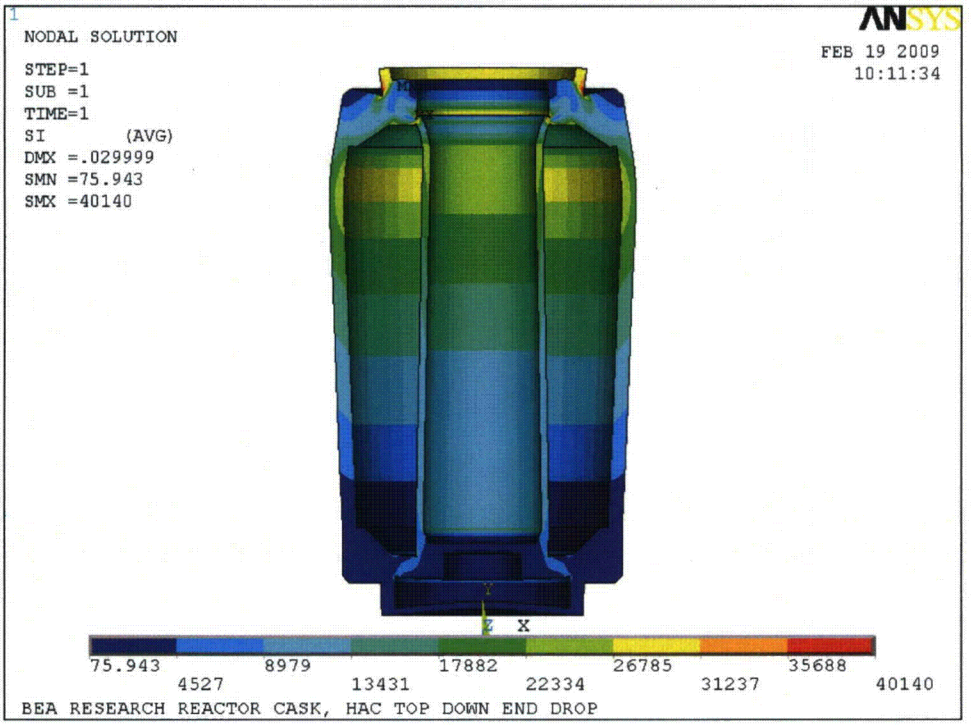

Figure 2.12.4-15 – HAC Top-Down End Drop

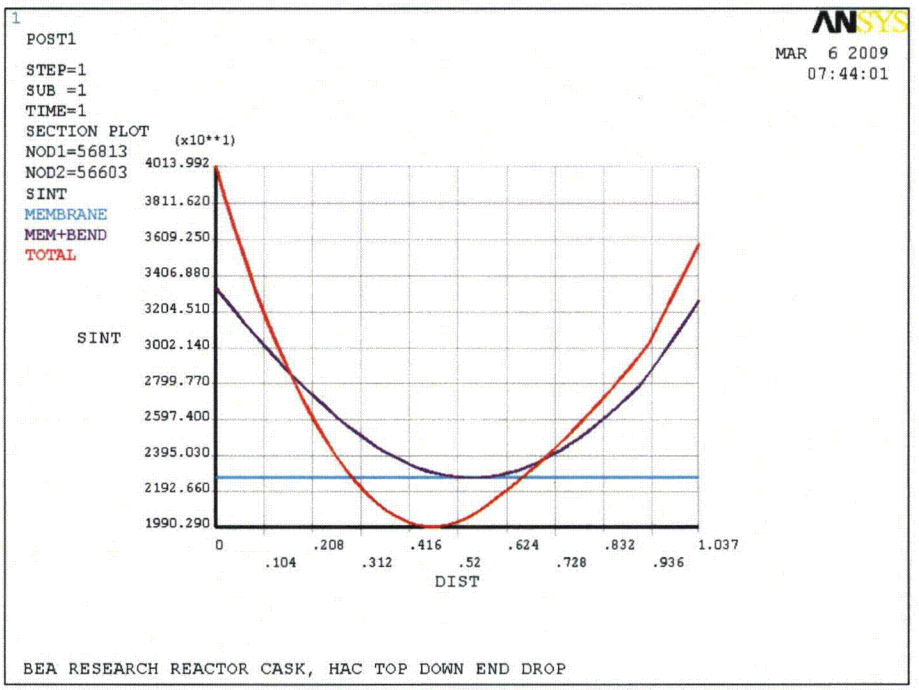

Figure 2.12.4-16 – HAC Top-Down End Drop Linearized Stress

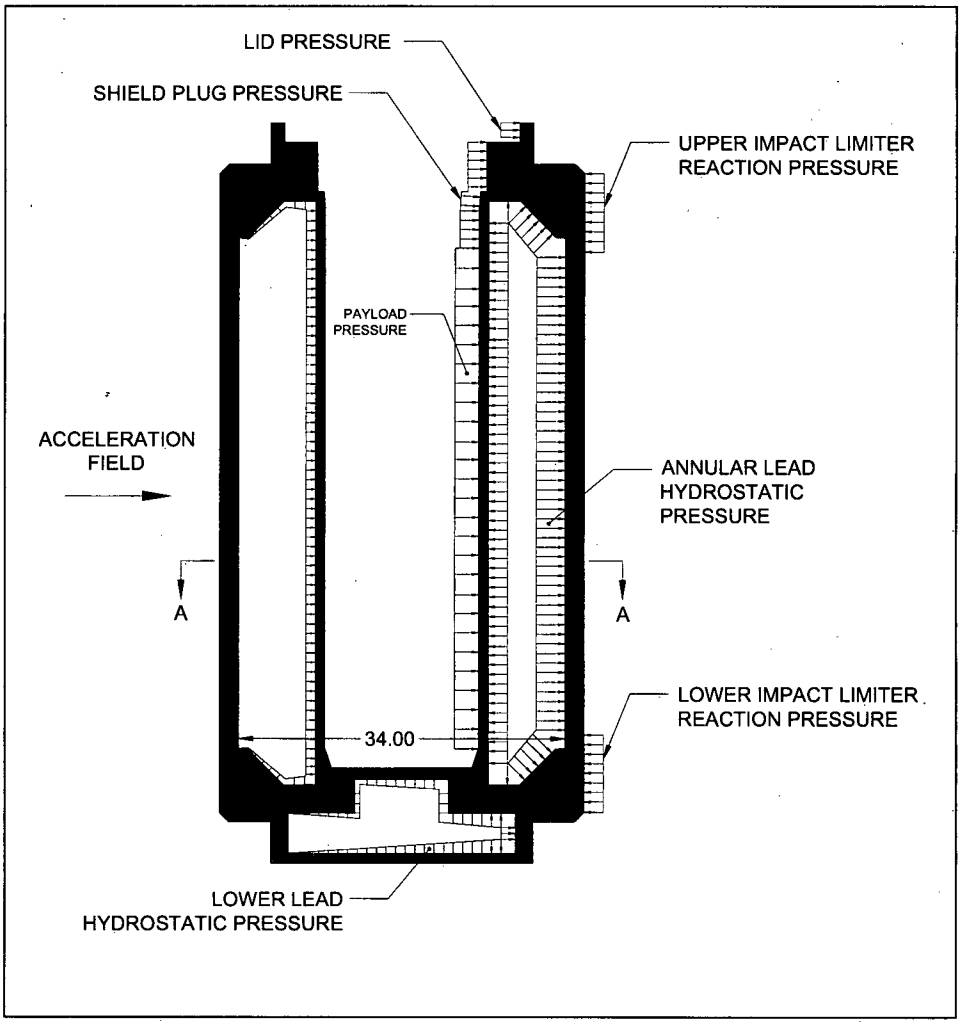

Figure 2.12.4-17 – NCT Side Drop Loading

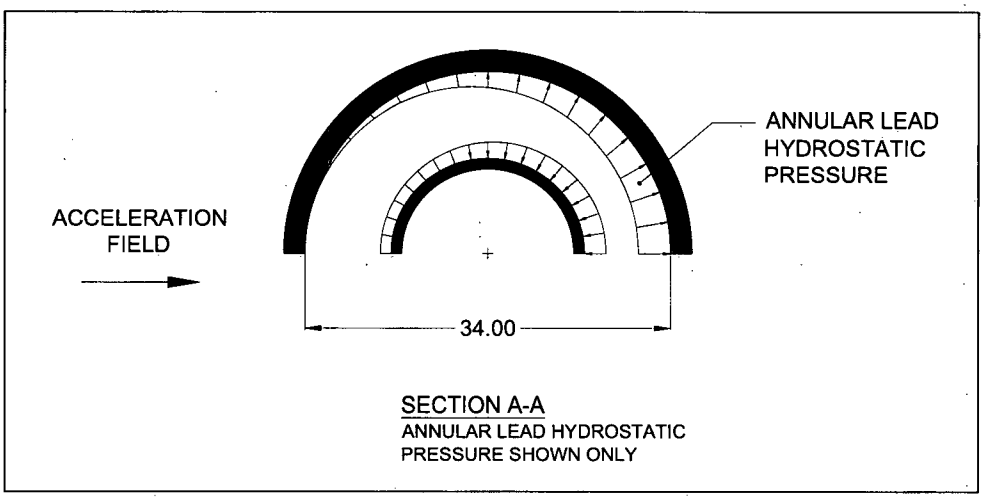

Figure 2.12.4-18 – NCT Side Drop Loading

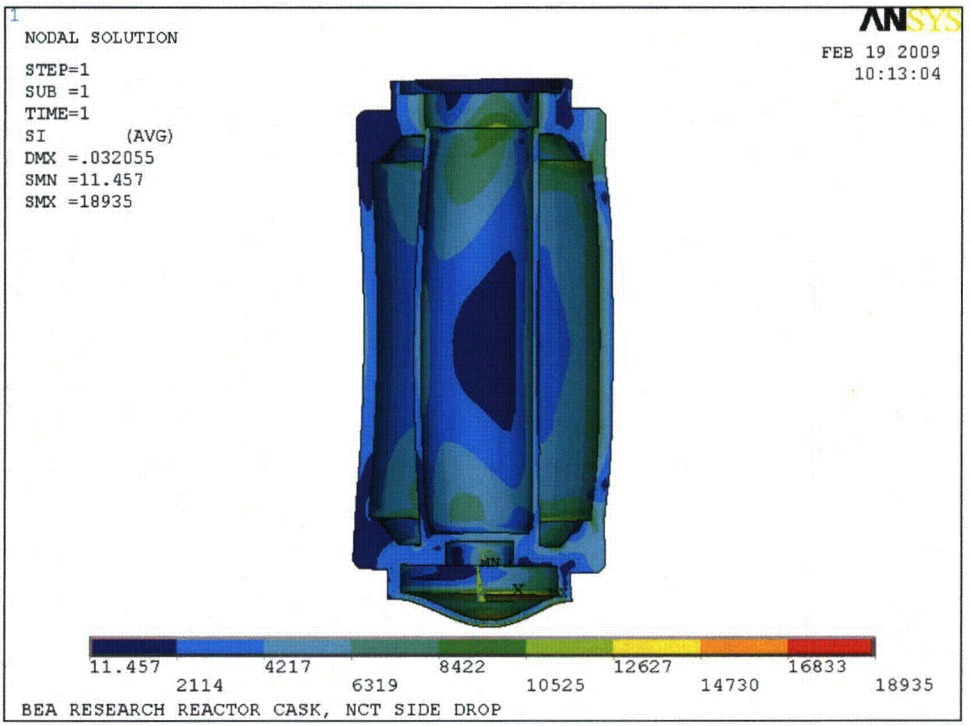

Figure 2.12.4-19 – NCT Side Drop

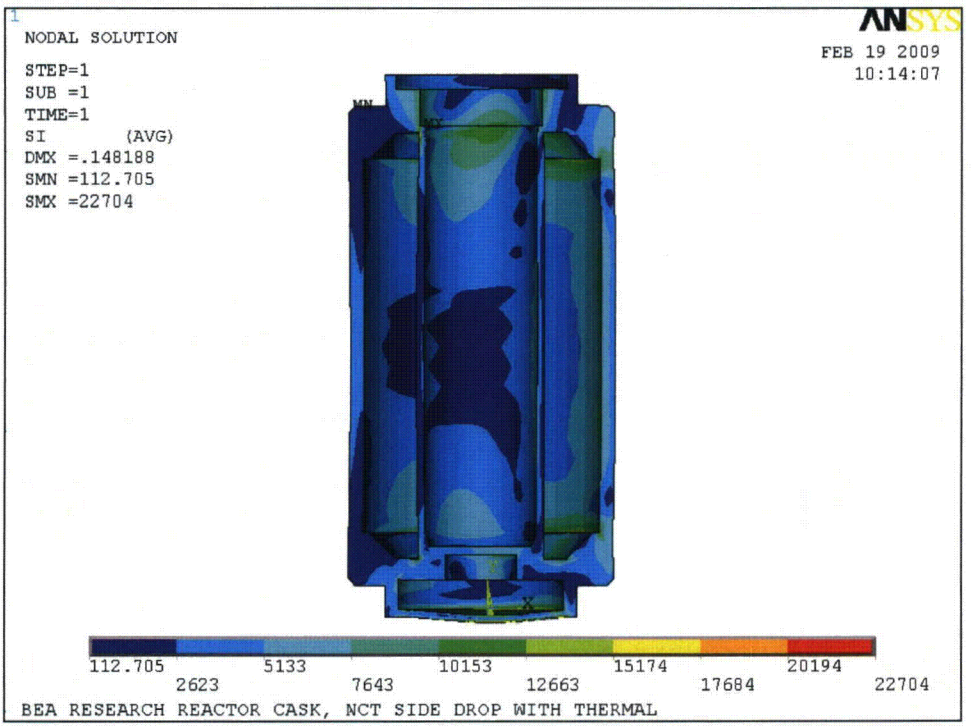

Figure 2.12.4-20 – NCT Side Drop With Thermal

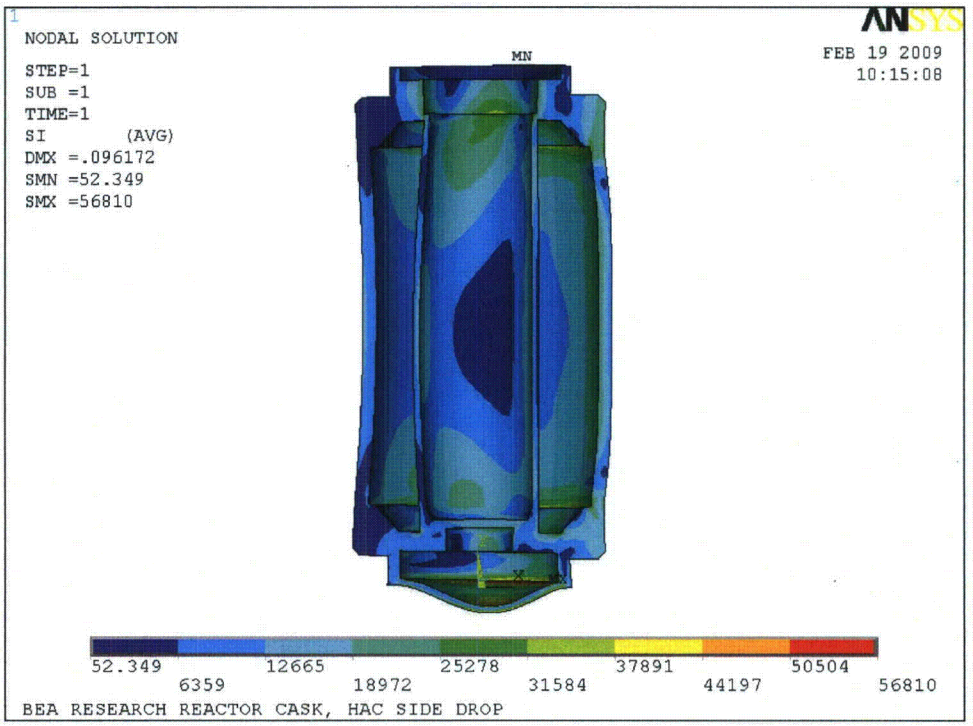

Figure 2.12.4-21 – HAC Side Drop

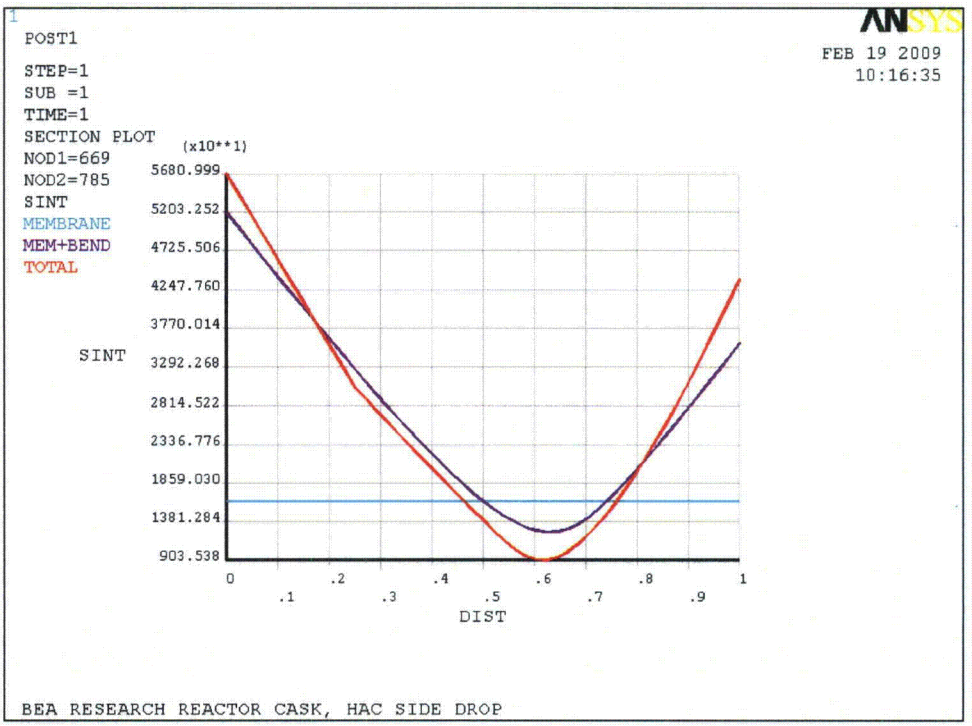

Figure 2.12.4-22 – HAC Side Drop Linearized Stress

2.12.5 Impact Limiter Performance Evaluation

This appendix presents the analytical evaluation of the impact and crush performance of the BRR package impact limiters. The impact magnitude and crush deformation of the limiters in several impact orientations, and at hot and cold bounding temperatures, is presented. Each step of the analysis is presented in detail, including the establishment of the crush properties of the polyurethane energy-absorbing foam, the calculation of the impact limiter force-deflection curves using the CASKDROP computer program, and the calculation of the impact response of the package using the SLAPDOWN computer program. A description of CASKDROP and SLAPDOWN are given in Appendix 2.12.6, *Analysis Software Descriptions*.

This appendix concludes with a reconciliation between the analysis results and test results, which shows that the analysis results are generally bounding. Of note, the impact magnitude used for stress analysis of 120g is nearly 50% greater than the highest test or analysis result.

2.12.5.1 Introduction

The analysis procedure of the impact limiter performance proceeds in three steps:

1. Calculate the effective stress-strain properties of the 9 lb/ft^3 polyurethane foam used within the limiter to absorb energy. The analysis begins with the room temperature, quasi-static stress-strain curves obtained from the foam manufacturer, and then adjusts the curves for minimum (-20 °F) and maximum (150 °F) temperature, for manufacturing tolerance (± 10% on the bulk average strength property), for a dynamic (strain rate) effect, for the difference between the crush axis and the axes of material orthotropy, and for the effect of the outer steel shell.
2. Calculate the overall force-deflection relation for the limiter in each orientation, using the fully adjusted stress-strain curve established above and the geometry of the limiter. The result is a force-deflection curve for each orientation at each extreme temperature.
3. Calculate the overall response of the cask and impact limiters, modeling the cask as a rigid rod and the impact limiters as non-linear springs. The result is the impact magnitude and crush deformation of each impact limiter. If the impact orientation is not stable (i.e., a "slapdown"), calculate the acceleration at the end of the payload cavity farthest from the c.g. of the package.

These steps will now be presented in detail. The impact limiter geometry is found on drawing 1910-01-02-SAR in Appendix 1.3.3, *Packaging General Arrangement Drawings*. The basic, room temperature, quasi-static polyurethane foam stress-strain properties are taken from the database provided by the foam manufacturer, General Plastics Manufacturing Co. of Tacoma, WA. Pertinent pages from their web site are shown in Figure 2.12.5-1. Both limiters are taken to be identical, since the only actual difference is the presence of lifting bosses in the upper limiter. The maximum foam temperature of 150 °F is established in Section 2.6.1.1, *Summary of Pressures and Temperatures*. The minimum temperature is -20 °F as defined in [1].

The polyurethane foam is introduced into the impact limiter steel shells as a liquid, which then solidifies. During solidification, orthotropy of properties is established along an axis perpendicular to the ground ("parallel-to-rise") and on the orthogonal axis ("perpendicular-to-rise"). The parallel-to-rise direction is the same as the axis of the package.

2.12.5.1.1 Foam Stress-Strain Determination

The foam stress-strain curves are a function of the given strain, temperature, manufacturing tolerance, dynamic crush factor, drop orientation, and a steel shell adjustment. This procedure is illustrated by means of example calculations for 10% strain and a drop orientation of 15° from the horizontal. The static crush strength at ambient temperature (75 °F) for both perpendicular and parallel-to-foam rise are calculated using the method and formulas given in Tables 7 and 8 of the manufacturer's data sheet shown in Figure 2.12.5-1. The resulting static, room temperature crush strengths are shown in the left-hand columns of Table 2.12.5-1 (parallel-to-rise) and Table 2.12.5-2 (perpendicular-to-rise). The basic equation for static crush strength is:

$$\sigma = Y\rho^S$$

where σ is the crush strength in psi, ρ is the foam density in lb/ft^3, and Y and S are constants which depend on the strain level. As an example, for 10% strain,

$$\sigma_{Para}(\varepsilon = 10\%) = Y\rho^S = (7.3058)(9)^{1.6590} = 280 \text{ psi}$$

$$\sigma_{Perp}(\varepsilon = 10\%) = Y\rho^S = (6.3841)(9)^{1.7182} = 278 \text{ psi}$$

The static crush strength is modified by a temperature coefficient and a manufacturing tolerance for both the hot (150 °F) and cold (-20 °F) conditions. The manufacturing tolerance is included by entering a ± 10% variation in the crush strength. These two effects are conservatively combined such that the -10% manufacturing tolerance is applied to the hot temperature case (both tend to reduce crush strength) and the +10% manufacturing tolerance is applied to the cold temperature case (both tend to increase crush strength).

Static crush strength using the C_T values found in Tables 7 and 8 of Figure 2.12.5-1 combining the cold (-20 °F) temperature with the plus manufacturing tolerance is illustrated by the following example for 10% strain:

$$\sigma_{Para}(\varepsilon = 10\%) = C_T(\sigma_{Para})(1 + \text{Bias}) = 1.29(280)(1 + 0.1) = 397 \text{ psi}$$

$$\sigma_{Perp}(\varepsilon = 10\%) = C_T(\sigma_{Perp})(1 + \text{Bias}) = 1.32(278)(1 + 0.1) = 404 \text{ psi}$$

Similarly, static crush strength at the hot (150 °F) temperature with the minus manufacturing tolerance gives:

$$\sigma_{Para}(\varepsilon = 10\%) = C_T(\sigma_{Para})(1 - \text{Bias}) = 0.71(280)(1 - 0.1) = 179 \text{ psi}$$

$$\sigma_{Perp}(\varepsilon = 10\%) = C_T(\sigma_{Perp})(1 - \text{Bias}) = 0.72(278)(1 - 0.1) = 180 \text{ psi}$$

The manufacturer's data extends as far as a strain of 70%. In some drop orientations at the hot temperature, local strains are expected to exceed this value. In order to account for this, the manufacturer's data was extrapolated between 70% and 80% strain. To demonstrate the validity of this approach, the extrapolated curve is compared to data up to 80% strain that has been previously published [34] by the same manufacturer, in Figure 2.12.5-18[1]. The curves shown in Figure 2.12.5-18 are for a temperature of 150 °F and parallel to rise. Note that between zero and

[1] Note from Figure 2.12.5-18 that polyurethane foam does not have a discrete "lock up" point. While the foam becomes much stiffer at high strains, this occurs relatively gradually compared to other materials such as aluminum honeycomb.

70% strain, the two curves are quite similar, which demonstrates that foam behavior has not changed significantly since the previous data was published. As shown in the figure, the lower curve (current data, extrapolated above 70%) has a slower rise in stress with increasing strain than the upper (previously published) data curve. Use of the extrapolated curve (according to the procedure used in this appendix) will result in a conservatively greater crush deformation prediction than the upper curve. Since the actual foam behavior may tend to be more in line with the upper stress-strain curve, a calculation of package impact acceleration was made using the upper curve, according to the procedure described in Section 2.12.5.1, *Introduction.* This calculation results in the largest impact acceleration that would be expected from the hot case utilizing foam stress-strain behavior like that previously published in the region beyond 70% strain. Since the largest impact was desired, the stress-strain curve was conservatively increased by 10% for manufacturing variability. The results are given in Table 2.12.5-25, which compare the results of the two curves utilizing the governing 15° slapdown orientation. The results, as expected, show less strain and higher impact for the previously published stress-strain data. Although the maximum impact of 89.6g is slightly higher than the cold case maximum value of 86.8g, it is still far below the bounding value used in stress calculations of 120g. Therefore, the method of extrapolating the hot case foam stress-strain values is acceptable. Note that in the one case where a strain of up to 83.2% is needed (see Table 2.12.5-14), the stress for 80% is used, adding further conservatism to the maximum impact limiter deformation strain result.

The resulting static crush strengths at the temperature extremes are shown in the right-hand columns of Table 2.12.5-1 (parallel-to-rise) and Table 2.12.5-2 (perpendicular-to-rise).

The static crush strength is further modified to account for the dynamic loading of the impact limiter. Table 9 in the manufacture's datasheet (reproduced in Figure 2.12.5-1) provides the method used to calculate the dynamic crush strength. The formula used is:

$$\sigma_{Dynamic} = Y_{int}(\sigma_{Static})^{S}$$

where Y_{int} and S are different values than those defined above, and σ_{Static} is the static crush strength given on the right-hand side of Table 2.12.5-1 and Table 2.12.5-2. Examples for 10% strain at room temperature and the two temperature extremes are given as follows:

Dynamic crush strength at room temperature:

$$\sigma_{Para}(\varepsilon = 10\%) = Y\sigma_{Para}^{S} = (1.2971)(280)^{1.0330} = 437 \text{ psi}$$

$$\sigma_{Perp}(\varepsilon = 10\%) = Y\sigma_{Perp}^{S} = (1.2971)(278)^{1.0330} = 434 \text{ psi}$$

Dynamic crush strength at the cold temperature:

$$\sigma_{Para}(\varepsilon = 10\%) = Y\sigma_{Para}^{S} = (1.2971)(397)^{1.0330} = 627 \text{ psi}$$

$$\sigma_{Perp}(\varepsilon = 10\%) = Y\sigma_{Perp}^{S} = (1.2971)(404)^{1.0330} = 639 \text{ psi}$$

Dynamic crush strength at the hot temperature:

$$\sigma_{Para}(\varepsilon = 10\%) = Y\sigma_{Para}^{S} = (1.2971)(179)^{1.0330} = 276 \text{ psi}$$

$$\sigma_{Perp}(\varepsilon = 10\%) = Y\sigma_{Perp}^{S} = (1.2971)(180)^{1.0330} = 277 \text{ psi}$$

Table 9 does not provide values for the dynamic crush strength for strains above 70%. The values for S and Y for 70% strain are used to extend the curve up to 80% for the hot case (the room temperature case must also be extended in order to perform the adjustment for the steel shell as shown below). This keeps the dynamic crush strength dependence on the static crush strength similar to that of the highest strain in Table 9. If the value of either variable (S or Y) is modeled too high, the dynamic crush strength will be greatly increased resulting in much lower deformation. Since much of the energy from the crush will be dissipated in the initial 70% strain, small variations of the dynamic crush strength at the highest strains are negligible. The effect of this assumption will be compared against the test data. Table 2.12.5-3 and Table 2.12.5-4 show the result of the dynamic crush adjustment.

The variation in crush strength due to drop orientation is calculated based on the angle of the drop test with respect to the horizontal plane and the axis of the cask. The rise direction of the polyurethane foam is assumed to be parallel to the axis of the cask. An ellipse function is used to combine the parallel and perpendicular crush strength curves to obtain the crush curve for a particular drop orientation. The example for 10% strain and an impact orientation of 15° is carried out below.

Room temperature crush strength adjusted for orientation:

$$\sigma_{Ambient} = \frac{1}{\sqrt{\left(\frac{\sin\theta}{\sigma_{Para}}\right)^2 + \left(\frac{\cos\theta}{\sigma_{Perp}}\right)^2}} = \frac{1}{\sqrt{\left(\frac{\sin(15°)}{437}\right)^2 + \left(\frac{\cos(15°)}{434}\right)^2}} = 434 \text{ psi}$$

Cold crush strength adjusted for orientation:

$$\sigma_{Cold} = \frac{1}{\sqrt{\left(\frac{\sin\theta}{\sigma_{Para}}\right)^2 + \left(\frac{\cos\theta}{\sigma_{Perp}}\right)^2}} = \frac{1}{\sqrt{\left(\frac{\sin(15°)}{627}\right)^2 + \left(\frac{\cos(15°)}{639}\right)^2}} = 638 \text{ psi}$$

Hot crush strength adjusted for orientation:

$$\sigma_{Hot} = \frac{1}{\sqrt{\left(\frac{\sin\theta}{\sigma_{Para}}\right)^2 + \left(\frac{\cos\theta}{\sigma_{Perp}}\right)^2}} = \frac{1}{\sqrt{\left(\frac{\sin(15°)}{276}\right)^2 + \left(\frac{\cos(15°)}{277}\right)^2}} = 277 \text{ psi}$$

Table 2.12.5-5, Table 2.12.5-6, and Table 2.12.5-7 show the stress-strain values adjusted for dynamic loading.

Finally, the stress-strain curves generated by this method were biased upward to account for the steel shell of the impact limiter. A bias equivalent to a 47 percent strength increase was applied to the foam crush strength at ambient (75 °F) temperature. This bias is based on results obtained in engineering tests of the MOX Fresh Fuel Package (MFFP, NRC Docket 71-9295, Appendix 2.12.1). The bias was applied by adding 47% of the room temperature adjusted crush strength (see Table 2.12.5-5) to either the cold or hot adjusted crush strengths (Table 2.12.5-6 and Table 2.12.5-7, respectively). Following the example,

Crush strength biased for steel shell, cold (10% strain, 15° orientation):

$\sigma(\varepsilon) = 0.47(\sigma_{Ambient}) + \sigma_{Cold} = .47(434) + 638 = 842$ psi

Crush strength biased for steel shell, hot (10% strain, 15° orientation):

$\sigma(\varepsilon) = 0.47(\sigma_{Ambient}) + \sigma_{Hot} = .47(434) + 277 = 481$ psi

Table 2.12.5-8 presents the complete set of stress-strain data that supports the calculation of impact limiter force-deflection curves. These values represent a summary of the adjustments to the static, room temperature data for temperature extremes, manufacturing tolerance, dynamic effect, impact orientation, and steel shell bias.

2.12.5.1.2 Force-Deflection Curves

The force-deflection curves are calculated using the computer program CASKDROP. Given an impact limiter external geometry, orientation to the impacting surface, and crush strength corresponding to that orientation, CASKDROP calculates the total crush force for each increment of deflection. The calculational technique is described in detail in Appendix 2.12.6, *Analysis Software Descriptions*. In summary, CASKDROP divides the crush area into small regions, and for each differential element, calculates the strain and, by means of the stress-strain table, the corresponding stress. Multiplying the stress times the differential area and summing all of the individual forces results in the total force at a given level of crush deformation. Repeating this process at a range of crush deformations results in the complete force-deflection curve.

The geometry shown in Figure 2.12.5-2 is utilized with CASKDROP. There are very small differences between the geometry shown and the drawings given in Appendix 1.3.3, *Packaging General Arrangement Drawings*, but the effect on the force-deflection curves is negligible.

The drop angle formed when the package center of gravity is directly over the conical diameter corner of the impact limiter is of particular interest. This angle is known as the center of gravity over corner, or cg-over-corner. At this angle, the impact limiter will absorb all of the drop kinetic energy on the primary impact. This angle is calculated as:

$$\theta_{cg} = \mathrm{Tan}^{-1}\frac{L}{d_c} = \mathrm{Tan}^{-1}\left[\frac{119.5}{48.1}\right] = 68°$$

where L is the total height of the cask, and d_c is the conical diameter.

CASKDROP was used to generate force-deflection curves for drop orientations of 0°, 15°, 30°, 45°, 60°, 68° and 90° from a horizontal cask orientation. Since the cg-over-corner drop orientation is considered critical for the calculation, that angle was selected instead of 75° in the sequence. Table 2.12.5-9 summarizes the input data used with the CASKDROP program for this solution. Note: because CASKDROP actually solves for the total crush in stable orientations using an energy approach, the program requires inputs of package weight and drop height. However, since only the force-deflection output is relevant here, the weight and drop height are not listed in the table.

Force-deflection curves are taken directly from the CASKDROP output files, except for the case of the horizontal side drop. Since CASKDROP outputs a single force-deflection curve, the result must be divided by 2 in this case, since two limiters are in contact with the ground. The force-deflection curves for the stated orientations, for hot and cold conditions, are shown in Figure 2.12.5-3 through Figure 2.12.5-9.

2.12.5.1.3 Impact Acceleration and Crush Deformation

The SLAPDOWN program, as described in Appendix 2.12.6, *Analysis Software Descriptions*, was used to analyze the impact response of the BRR package with the unyielding surface. It is particularly useful when the center of gravity is not directly over the impact point. Under these circumstances, the package will generally hit, begin to rotate, and strike the ground a second time as a "slapdown" impact. SLAPDOWN conducts a time-integration analysis using a model of the package as a rigid rod, and of the impact limiters as non-linear springs. Given a drop height, the package has an initial velocity at impact. The energy is absorbed first by the primary spring/impact limiter ('nose'), which imparts a rotational force to the model, until the secondary spring/impact limiter ('tail') comes in contact. Most of the energy absorbed by the springs is lost, except the portion that is restored by springback. The position, angle, velocity, and acceleration in both linear and rotational modes are calculated for each time step.

The force-deflection curves calculated by CASKDROP were input into SLAPDOWN to produce the results listed in this analysis. The primary impact limiter non-linear spring data was equal to the force-deflection curve created for the corresponding impact orientation. The secondary impact limiter non-linear spring was equal to the force-deflection curve for the zero degree orientation (i.e., horizontal) in each case. Additional input variables used in SLAPDOWN are summarized in Table 2.12.5-10, and briefly described below.

Length, Nose-to-CG – the distance along the cask axis from the location of impact to the CG of the cask. The impact location is dependent on the drop angle and ranges from one-half the total span between impact limiter springs of 77.13/2 = 38.565 inches for the side drop, to zero for the cg-over-corner drop (68°) and end drop (90°). Note that the discrete location of the impact limiter springs has been taken as coincident with the flat ends of the cask body.

Length, Tail-to-CG – the distance from the location of the secondary impact to the CG. This value remains the same as the secondary impact is considered to be a horizontal impact in all cases.

Radius, Nose Limiter – the radius of the primary impact limiter.

Radius, Tail Limiter – the radius of the secondary impact limiter.

Body Mass – the total mass of the cask and impact limiters expressed in lb_m-s^2/in, equivalent to the bounding package weight of 32,000 lb from Table 2.1-2.

Rotational Moment of Inertia – the rotational moment of inertia of the cask and assembly, calculated using the weight and geometry of the package.

Drop Height – the initial height of the cask prior to free drop measured in feet.

Impact Angle – the orientation of the primary impact, measured to the horizontal.

2.12.5.2 Results

The results of the analysis include the maximum crush and acceleration values for the given orientations. For unstable, i.e., slapdown orientations, the acceleration output is taken at a distance of 29.565 inches from the c.g. of the cask, which is conservatively further from the c.g. than either end of the payload cavity, and it is the maximum acceleration that the payload will experience.

The calculated impact limiter strain is determined as a percentage of the maximum allowable crush. The allowable crush is the distance between the point of impact on the limiter and the closest point of the internal shell of the limiter, and is calculated from the drawings for each orientation of primary impact. The allowable crush for secondary impact is the same for all cases, since the orientation is assumed to be horizontal in each case. The actual crush distance is the value provided as part of the SLAPDOWN output. The impact limiter strain is:

$$\varepsilon_{IL} = \frac{\text{Actual Crush}}{\text{Allowable Crush}}(100\%)$$

2.12.5.2.1 HAC Free Drop Results

Table 2.12.5-11 through Table 2.12.5-14 summarize the HAC free drop results. Note that maximum accelerations are governed by the cold case, and maximum impact limiter strain by the hot case. Figure 2.12.5-10 and Figure 2.12.5-11 show the maximum impact limiter strain developed for the primary and secondary impacts for the specified impact orientations. From a comparison of the two plots, the overall maximum impact limiter strain occurs in the secondary impact, hot case, for a primary impact orientation of 15°. Figure 2.12.5-12 and Figure 2.12.5-13 show the maximum acceleration of the cask for the specified drop orientations. The overall maximum impact acceleration occurs in the secondary impact, cold case, for a primary impact orientation of 15°.

2.12.5.2.2 NCT Free Drop Results

The NCT test requires the cask to be dropped from a height of two feet, per 10 CFR §71.71(c)(7). Table 2.12.5-15 through Table 2.12.5-18 summarize the NCT free drop results, using the same orientations and force-deflection curves as for the HAC cases.

Figure 2.12.5-14 and Figure 2.12.5-15 show the maximum impact limiter strain developed for the NCT primary and secondary impacts for the specified impact orientations. The maximum strain for the primary impact occurs at 68°, while the maximum strain for the secondary impact is seen to occur at a primary impact orientation of 15°. In both cases, the maximum strain is bounded by all the HAC strains for both primary and secondary impacts.

Figure 2.12.5-16 and Figure 2.12.5-17 show the maximum acceleration of the cask for the specified drop orientations. The maximum impact acceleration occurs in the 90° orientation. As expected, all NCT impact cases are bounded by the HAC cases. The NCT governing cases are different than the HAC governing cases, but this is to be expected due to the difference in impact velocity and energy absorbed.

2.12.5.2.3 Combined HAC and NCT Free Drop Results

Since 10 CFR 71 requires that the NCT free drop precede the HAC free drop, the effect of the combination of both drops is next considered. Since the impact acceleration is a function of the crush of the limiter, and the crush of the limiter is a function of the energy absorbed, a 2-foot free drop followed by a 30-foot free drop (taken in the same orientation on the same spot) may be modeled as a single 32-foot free drop. This is a conservative assumption, which neglects the effect of material springback which will occur after the initial NCT impact.

A sample of selected cold impact cases, where the acceleration was shown to be the highest, as shown in Table 2.12.5-19 and Table 2.12.5-20 demonstrates that the maximum increase in acceleration is less than 5 percent. A sample of selected hot impact cases, where the strain was shown to be greater than the cold impact cases, is shown in Table 2.12.5-21 and Table 2.12.5-22. From the results of the combined NCT and HAC drop, it is clear that the effect of the NCT free drop on the HAC free drop is negligible.

2.12.5.3 Reconciliation with Certification Test Results

To verify the BRR Package functions as intended, a half-scale CTU was tested in three drop orientations as described in Appendix 2.12.3, *Certification Test Results*. The results of the test indicate that the results predicted in this calculation are conservative. The test results for the HAC end, slapdown, and c.g.-over-corner orientations are shown in Table 2.12.5-23. To convert the half-scale results to full-scale, the acceleration is divided by 2, and the crush distance is multiplied by 2.

The transverse accelerometers were located 8.68 inches from the end of the cask, or 17.36 inches in the equivalent full-scale, whereas the SLAPDOWN calculations correspond to the end of the cask cavity at the bottom, bounded by a distance of 29.565 inches from the cask c.g. This difference does not affect the stable impact orientations such as the end (D1) and c.g. over corner (D3), but for the slapdown impact (D2R), an adjustment of the test results must be made before comparison to the SLAPDOWN calculations.

The acceleration at any point along the axis in an oblique impact can be found from:

$$a_i = a_{c.g.} + \alpha L$$

where $a_{c.g.}$ is the acceleration of the center of gravity (in/s^2), α is the rotational acceleration in rad/s^2, and L is the distance of the point i from the c.g. in inches. Since $a_{c.g.}$ was not measured in the test, it must be calculated using the known location of the transverse accelerometers and the rotational acceleration calculated using SLAPDOWN. At the moment of maximum primary impact, the rotational acceleration is calculated by SLAPDOWN to be $\alpha_P = 534$ rad/s^2. The full scale equivalent location of the accelerometers from the cask c.g. was:

$$L_{accel} = \frac{L_{cask}}{2} - 17.36 = 21.21 \text{ in}$$

where $L_{cask} = 77.13$ inches, and the full scale equivalent location of the accelerometers from the cask end was 17.36 inches. The full-scale acceleration of the cask c.g. for the primary event in the test therefore can be computed as:

$$a_{test\ c.g.-P} = a_{accel-P} - \alpha_P L_{accel} = 10{,}892 \text{ in/s}^2$$

where the full-scale measured acceleration from Table 2.12.5-23 for the primary impact of test D2R, $a_{accel\text{-}P} = 57.5$g (i.e., 22,218 in/s^2), and the location of the accelerometers , $L_{accel} = 21.21$ inches from the cask c.g. The acceleration of the test cask at the location of used for the SLAPDOWN runs (i.e., the bottom end of the payload cavity) is therefore:

$$a_{adj-P} = a_{test\ c.g.-P} + \alpha_P L_{adj} = 26{,}680 \text{ in/s}^2 = 69.0\text{g}$$

where the distance from the cask c.g. to the location of the SLAPDOWN output is L_{adj} = 29.565 inches. The corresponding SLAPDOWN calculated output acceleration for the primary impact is equal to 71.0g from Table 2.12.5-11.

Similarly, at the moment of maximum secondary impact, the rotational acceleration is calculated by SLAPDOWN to be α_S = 687 rad/s^2. The full-scale acceleration of the cask c.g. for the secondary event in the test can be computed as:

$$a_{\text{test c.g.}-S} = a_{\text{accel}-S} - \alpha_S L_{\text{accel}} = 7{,}454 \text{ in}/\text{s}^2$$

where the full-scale measured acceleration from Table 2.12.5-23 for the secondary impact of test D2R, $a_{\text{accel-S}}$ = 57.0g (i.e., 20,025 in/s^2), and L_{accel} is the same as above. The acceleration of the test cask at the location used for the SLAPDOWN runs (i.e., the bottom end of the payload cavity) is therefore:

$$a_{\text{adj}-S} = a_{\text{test c.g.}-S} + \alpha_S L_{\text{adj}} = 27{,}765 \text{ in}/\text{s}^2 = 71.8\text{g}$$

The corresponding SLAPDOWN calculated output acceleration for the secondary impact is equal to 86.8g from Table 2.12.5-12.

The results show that the corrected test accelerations are still below the maximum acceleration used in stress analysis of 120g. The maximum secondary acceleration of 71.8g is lower than the calculated value of 86.8g. The corrected primary acceleration of 69.0g is also below the calculated value of 71.0g. This indicates that the calculation is essentially bounding for all cases. The principal conclusion, however, is that the actual accelerations of the BRR package are well below the bounding value of 120g used in the stress calculations.

As stated in Section 2.12.3.3, *Test Unit Configuration*, the weight of the test cask was 3,181 lb, or when properly adjusted for scale, approximately 7% below the maximum equivalent full-scale weight of 32,000 lb. This had the effect of conservatively increasing the recorded accelerations of the CTU. Correspondingly, the crush deformations were slightly underestimated in the test, since there was less kinetic energy in the drop.

The force-deflection curves discussed in Section 2.12.5.1.2, *Force-Deflection Curves*, show that the strain increases nonlinearly with an increase in applied load. Therefore, although an increase in weight will result in an increased deformation, each succeeding crush strain increment becomes smaller as a greater force is applied, particularly as the end of crush is neared. Thus the percent change in the crush distance will be smaller in magnitude than the percent change in weight. Since the increase in the crush distance will be less than the weight increase, and since the weight increase is small in magnitude, the crush distance is bounded by the values in the calculation. This holds true for both the cold and hot temperature conditions developed in this calculation. The bounding crush strain corresponds to the 15° secondary impact in the hot case. As shown in Table 2.12.5-14, the predicted crush is 15.9 inches. Since, as shown in Table 2.12.5-24, the cold secondary crush was measured to be 36% lower than the prediction, then the small increase in weight of 7% will not invalidate the hot case maximum predicted crush. Thus the predictions are conservative.

A comparison of the calculated ('Calc') and full-scale equivalent test ('Actual') impact limiter performance is given in Table 2.12.5-24. A negative sign in the '% Less' columns indicates that the test result was lower than the calculated value.

2.12.5.4 Analysis of Optional Drain Tube

An optional drain tube may be included in the lower impact limiter. The drain tube is made from Type 304 stainless steel tube with an outer diameter of 5/8" and a wall thickness of 0.05 ± 0.02 inches.

The lower end of the drain tube is welded to the penetration in the impact limiter shell with a weld nominally equal to the thickness of the tube wall thickness.

The upper end of the tube is inserted over a transitional fitting which is welded to the inner shell of the impact limiter. This fitting is sized to allow for free axial movement between the tube and fitting. This arrangement prevents any axial load from being applied to the tube from the weight of the cask during normal use.

Under free end drop conditions, the tube is intended to crush along with the impact limiter foam. With an ultimate tensile stress of σ_U = 75 ksi, the maximum force applied by the tube may be calculated with the maximum cross-sectional area.

$$A = \frac{\pi}{4}\left[d_o^2 - d_i^2\right] = 0.123\ in^2$$

where the outer diameter of the tube is d_o = 0.63 inches, and the minimum inner diameter is d_i = 0.49 inches for a maximum wall thickness of 0.07 inches. A conservative upper bound compressive load will therefore be:

$$F = \sigma_U A = 9{,}225\ lb$$

For a package weight of 32,000 lbs, this applies an insignificant acceleration of 0.3g. This result is rather conservative as it ignores buckling of the tube and assumes uniform flow of the material at a value equal to the ultimate stress.

A bounding value for the HAC end drop impact of 120g (See Section 2.7.1.1, *Impact Forces and Deformation*) was used to bound the full-scale equivalent end drop test result of 58g (from Table 2.12.5-23.) Therefore the loading due to the drain tube on the package is of negligible concern.

2.12.5.5 Conclusion

The impact limiter evaluation is used to establish a bounding impact magnitude for stress analysis in other sections of this SAR. The maximum impact occurs in the cold temperature case. For NCT, the maximum overall impact is equal to 32.9g in the 90° orientation, from which a bounding impact for all orientations of 40g is taken. For HAC, the maximum overall impact is 86.8g in the 15° secondary slapdown impact, and a very conservative value of 120g is used as a bounding impact for all orientations.

The maximum strain occurs under HAC in the hot temperature case, and equals 83.2% in the 15° secondary slapdown case.

Table 2.12.5-1 - Parallel-to-Rise Static Compressive Strength (psi)

Strain	Room Temperature (75 °F)				-20 °F		150 °F	
	Y, int	density	S	Crush Str	C_T	Crush Str	C_T	Crush Str
10%	7.3058	9	1.6590	280	1.29	397	0.71	179
20%	6.7276	9	1.7021	283	1.36	423	0.73	186
30%	6.4961	9	1.7350	294	1.32	427	0.74	196
40%	6.9137	9	1.7255	306	1.29	434	0.75	207
50%	5.6711	9	1.8877	359	1.26	498	0.76	246
60%	5.3279	9	2.0431	474	1.28	667	0.76	324
65%	5.9871	9	2.0870	587	1.29	833	0.76	402
70%	6.2085	9	2.1868	758	1.37	1142	0.81	553
75%				952				710
80%				1,204				928

Table 2.12.5-2 - Perpendicular-to-Rise Static Compressive Strength (psi)

Strain	Room Temperature (75 °F)				-20 °F		150 °F	
	Y, int	density	S	Crush Str	C_T	Crush Str	C_T	Crush Str
10%	6.3841	9	1.7182	278	1.32	404	0.72	180
20%	6.5943	9	1.6946	273	1.35	405	0.74	182
30%	6.1154	9	1.7403	280	1.34	413	0.79	199
40%	5.7722	9	1.8023	303	1.32	440	0.77	210
50%	5.3041	9	1.9054	349	1.32	507	0.77	242
60%	5.3181	9	2.0392	470	1.33	688	0.77	326
65%	5.7864	9	2.1002	584	1.34	861	0.77	405
70%	5.7701	9	2.2255	767	1.36	1,147	0.78	538
75%				971				683
80%				1,240				878

Table 2.12.5-3 - Parallel-to-Rise Dynamic Crush Strength

Strain	Dynamic Crush Strength Coefficients		Dynamic Crush Strength (psi)		
	Y, int	S	75 °F	-20 °F	150 °F
10%	1.2971	1.0330	437	627	276
20%	1.4397	1.0069	424	635	278
30%	1.5181	0.9941	432	625	288
40%	1.3887	1.0028	432	613	292
50%	1.4419	0.9912	492	680	338
60%	1.4275	0.9831	610	853	419
65%	1.3871	0.9910	769	1088	528
70%	1.4660	0.9586	844	1251	624
75%	1.4660	0.9586	1,051		793
80%	1.4660	0.9586	1,316		1,025

Table 2.12.5-4 - Perpendicular-to-Rise Dynamic Crush Strength

Strain	Dynamic Crush Strength Coefficients		Dynamic Crush Strength (psi)		
	Y, int	S	75 °F	-20 °F	150 °F
10%	1.2971	1.0330	434	639	277
20%	1.4397	1.0069	409	608	272
30%	1.5181	0.9941	411	605	293
40%	1.3887	1.0028	428	622	296
50%	1.4419	0.9912	478	692	332
60%	1.4275	0.9831	605	879	422
65%	1.3871	0.9910	765	1124	532
70%	1.4660	0.9586	854	1256	608
75%	1.4660	0.9586	1,071		764
80%	1.4660	0.9586	1,354		972

Table 2.12.5-5 - Dynamic Strength Adjusted for Impact Angle (75 °F)

Strain	Angle of Impact (degrees)						
	0	15	30	45	60	68	90
	Compressive Stress (psi)						
10%	434	434	435	435	436	437	437
20%	409	410	413	416	420	422	424
30%	411	412	416	421	426	429	432
40%	428	428	429	430	431	431	432
50%	478	479	481	485	488	490	492
60%	605	605	606	607	609	609	610
65%	765	765	766	767	768	768	769
70%	854	853	851	849	846	845	844
75%	1,071	1,070	1,066	1,061	1,056	1,054	1,051
80%	1,354	1,351	1,344	1,335	1,325	1,321	1,316

Table 2.12.5-6 - Dynamic Strength Adjusted for Impact Angle (-20 °F)

Strain	Angle of Impact (degrees)						
	0	15	30	45	60	68	90
	Compressive Stress (psi)						
10%	639	638	636	633	630	629	627
20%	608	610	614	621	628	631	635
30%	605	606	610	615	620	622	625
40%	622	621	620	617	615	614	613
50%	692	691	689	686	683	682	680
60%	879	877	872	866	859	857	853
65%	1,124	1,121	1,115	1,106	1,097	1,093	1,088
70%	1,256	1,256	1,255	1,253	1,252	1,252	1,251

Table 2.12.5-7 - Dynamic Strength Adjusted for Impact Angle (150 °F)

Strain	Angle of Impact (degrees)						
	0	15	30	45	60	68	90
	Compressive Stress (psi)						
10%	277	277	277	276	276	276	276
20%	272	272	273	275	276	277	278
30%	293	293	292	290	289	289	288
40%	296	296	295	294	293	293	292
50%	332	332	333	335	336	337	338
60%	422	422	421	420	420	419	419
65%	532	532	531	530	529	529	528
70%	608	609	612	616	620	622	624
75%	764	766	771	778	785	789	793
80%	972	975	984	997	1,011	1,017	1,025

Table 2.12.5-8 - Fully Adjusted Polyurethane Foam Stress-Strain Data

Strain	Angle of Impact (degrees)						
	0	15	30	45	60	68	90
-20 °F Stress (psi)							
10%	843	842	840	837	835	834	832
20%	800	803	808	817	825	829	834
30%	798	800	806	813	820	824	828
40%	823	822	822	819	818	817	816
50%	917	916	915	914	912	912	911
60%	1,163	1,161	1,157	1,151	1,145	1,143	1,140
65%	1,484	1,481	1,475	1,466	1,458	1,454	1,449
70%	1,657	1,657	1,655	1,652	1,650	1,649	1,648
150 °F Stress (psi)							
10%	481	481	481	480	481	481	481
20%	464	465	467	471	473	475	477
30%	486	487	488	488	489	491	491
40%	497	497	497	496	496	496	495
50%	557	557	559	563	565	567	569
60%	706	706	706	705	706	705	706
65%	892	892	891	890	890	890	889
70%	1,009	1,010	1,012	1,015	1,018	1,019	1,021
75%	1,267	1,269	1,272	1,277	1,281	1,284	1,287
80%	1,608	1,610	1,616	1,624	1,634	1,638	1,644

Table 2.12.5-9 - CASKDROP Input Data

Input Data	Value
Impact Limiter Outside Diameter, in.	78.0
Impact Limiter Overall Length, in.	34.6
Impact Limiter Conical Diameter, in.	48.1
Impact Limiter Conical length, in.	15.0
Impact Limiter End Thickness, in.	21.2
Impact Limiter Hole Diameter, in.	0
Impact Limiter Hole Length, in.	0
Body Outside Diameter, in.	38.0
Body Overall Length, in.	77.13
Frictional Coefficient	0

Table 2.12.5-10 - SLAPDOWN Input Data

Input data	Value
Length, Nose-to-C.G., in.	Variable
Length, Tail-to-C.G., in.	38.565
Radius, Nose Limiter, in.	39.0
Radius, Tail Limiter, in.	39.0
Body Mass, lb_m-s^2/in.	82.816
Rotational Moment of inertia, in-lb_m-s^2	63,246
HAC Drop Height, ft.	30
NCT Drop Height, ft	2
HAC + NCT Drop Height, ft	32
Impact Angle (with Horizontal)	Variable
Force Deflection Curves	Variable
Friction Coefficient	0

Table 2.12.5-11 - Cold Primary Impact Results, HAC

Primary Impact Angle	Acceleration	Crush	Allowable Crush	Crush Margin	Limiter Strain
(deg)	(g)	(in)	(in)	(in)	%
0	63.3	11.0	19.1	8.1	57.6
15	71.0	10.7	21.4	10.7	50.0
30	79.7	12.3	22.1	9.8	55.7
45	80.4	11.0	21.4	10.4	51.4
60	82.6	13.1	22.6	9.5	58.0
68	69.6	13.3	22.5	9.2	59.1
90	72.4	7.3	20.2	12.9	36.1

Table 2.12.5-12 - Cold Secondary Impact Results, HAC

Primary Impact Angle	Acceleration	Crush	Allowable Crush	Crush Margin	Limiter Strain
(deg)	(g)	(in)	(in)	(in)	%
0	63.3	11.0	19.1	8.1	57.6
15	**86.8**	12.1	19.1	7.0	63.4
30	66.2	9.3	19.1	9.8	48.7
45	56.0	7.7	19.1	11.4	40.3
60	40.1	5.1	19.1	14.0	26.7

Table 2.12.5-13 - Hot Primary Impact Results, HAC

Primary Impact Angle	Acceleration	Crush	Allowable Crush	Crush Margin	Limiter Strain
(deg)	(g)	(in)	(in)	(in)	%
0	55.1	14.5	19.1	4.6	75.9
15	53.4	13.6	21.4	7.8	63.6
30	60.8	15.8	22.1	6.3	71.5
45	66.6	14.4	21.4	7.0	67.3
60	67.9	16.5	22.6	6.1	73.0
68	55.4	16.6	22.5	5.9	73.8
90	54.8	10.5	20.2	9.7	52.0

Table 2.12.5-14 - Hot Secondary Impact Results, HAC

Primary Impact Angle	Acceleration	Crush	Allowable Crush	Crush Margin	Limiter Strain
(deg)	(g)	(in)	(in)	(in)	%
0	55.1	14.5	19.1	4.6	75.9
15	83.2	15.9	19.1	3.2	**83.2**
30	54.2	12.5	19.1	6.6	65.4
45	43.4	10.5	19.1	8.6	55.0
60	29.9	7.1	19.1	12.0	37.2

Table 2.12.5-15 - Cold Primary Impact Results, NCT

Primary Impact Angle	Acceleration	Crush	Allowable Crush	Crush Margin	Limiter Strain
(deg)	(g)	(in)	(in)	(in)	%
0	19.7	2.8	19.1	16.3	14.7
15	19.1	4.1	21.4	17.3	19.2
30	21.2	4.7	22.1	17.4	21.3
45	25.9	3.0	21.4	18.4	14.0
60	24.2	5.0	22.6	17.6	22.1
68	15.2	5.2	22.5	17.3	23.1
90	**32.9**	1.5	20.2	18.7	7.4

Table 2.12.5-16 - Cold Secondary Impact Results, NCT

Primary Impact Angle	Acceleration	Crush	Allowable Crush	Crush Margin	Limiter Strain
(deg)	(g)	(in)	(in)	(in)	%
0	19.7	2.8	19.1	16.3	14.7
15	29.6	3.7	19.1	15.4	19.4
30	29.5	3.4	19.1	15.7	17.8
45	30.1	3.5	19.1	15.6	18.3
60	28.2	3.2	19.1	15.9	16.8

Table 2.12.5-17 - Hot Primary Impact Results, NCT

Primary Impact Angle	Acceleration	Crush	Allowable Crush	Crush Margin	Limiter Strain
(deg)	(g)	(in)	(in)	(in)	%
0	13.9	3.7	19.1	15.4	19.4
15	15.7	4.9	21.4	16.5	22.9
30	16.8	5.8	22.1	16.3	26.2
45	20.0	3.9	21.4	17.5	18.2
60	19.0	6.1	22.6	16.5	27.0
68	12.4	6.4	22.5	16.1	**28.4**
90	23.9	2.0	20.2	18.2	9.9

Table 2.12.5-18 - Hot Secondary Impact Results, NCT

Primary Impact Angle	Acceleration	Crush	Allowable Crush	Crush Margin	Limiter Strain
(deg)	(g)	(in)	(in)	(in)	%
0	13.9	3.7	19.1	15.4	19.4
15	22.5	5.1	19.1	14.0	26.7
30	21.8	4.5	19.1	14.6	23.6
45	20.8	4.6	19.1	14.5	24.1
60	21.1	4.3	19.1	14.8	22.5

Table 2.12.5-19 - Cold Primary Impact Results, HAC + NCT

Primary Impact Angle	HAC Acceleration	HAC+NCT Acceleration	Acceleration Increase	Percent Increase
(deg)	(g)	(g)	(g)	%
15	71.0	73.2	2.2	3.1
68	69.6	71.9	2.3	3.3
90	72.4	73.9	1.5	2.1

Table 2.12.5-20 - Cold Secondary Impact Results, HAC + NCT

Primary Impact Angle	HAC Acceleration	HAC+NCT Acceleration	Acceleration Increase	Percent Increase
(deg)	(g)	(g)	(g)	%
15	86.8	90.1	3.3	3.8

Table 2.12.5-21 - Hot Primary Impact Results, HAC + NCT

Primary Impact Angle	HAC Crush	HAC+NCT Crush	Crush Increase	Percent Increase
(deg)	(in)	(in)	(in)	%
15	13.6	14.0	0.4	2.9
68	16.6	17.0	0.4	2.4
90	10.5	10.9	0.4	3.8

Table 2.12.5-22 - Hot Secondary Impact Results, HAC + NCT

Primary Impact Angle	HAC Crush	HAC+NCT Crush	Crush increase	Percent Increase
(deg)	(in)	(in)	(in)	%
15	15.9	16.3	0.4	2.5

Table 2.12.5-23 - CTU Test Results

Test #	Type	Location	Half-Scale*			Full-Scale**			
			Measured Accel. (g)		Crush Distance (in)	Measured Accel. (g)			Crush Distance (in)
			1019 Hz Cutoff	Rigid Body Estimate		1019 Hz Cutoff	Rigid Body Estimate	Δ	
D1	End Drop	Primary	116	109	3.4	58.0	54.5	3.5	6.8
D2R	Oblique Slapdown	Primary	115	104	4.0	57.5	52.0	5.5	8.0
		Secondary	114	103	3.9	57.0	51.5	5.5	7.8
D3	CG Over Corner	Primary	117	101	5.5	58.5	50.5	8.0	11.0

*Values in the '1019Hz Cutoff' and 'Crush Distance' columns are obtained from Section 2.12.3.5. The 'Rigid Body Estimate' in half-scale is formed by subtracting the average reduction value for the impact event (found in column 'E' of Table 2.12.3-6) from the 1019Hz cutoff accelerometer response. For example, for test D1, the average reduction value is 7g, and therefore the rigid body estimate is 116 – 7 = 109g.

**Full-scale accelerations are one-half of the half-scale results. The column labeled 'Δ' is equal to the difference between the 1019Hz cutoff result and the rigid body estimate in full scale. For example, for test D1, the rigid body estimate is 58.0 – 54.5 = 3.5g lower than the 1019Hz cutoff result. From this it can be seen that the 1019Hz cutoff results are reasonable, and moderately conservative.

Table 2.12.5-24 - CTU Percentage of Predicted Results (Full-Scale)

Test #	Location	Acceleration (g)*			Crush Distance (in)		
		Calc	Actual	% Less	Calc	Actual	% Less
D1	Primary	72.4	58.0/54.5	-19.9/-24.7	7.3	6.8	-6.8
D2R	Primary	71.0	69.0/63.5	-2.8/-10.6	10.7	8.0	-25
	Secondary	86.8	71.8/66.3	-17.3/-23.6	12.1	7.8	-36
D3	Primary	69.6	58.5/50.5	-15.9/-27.4	13.3	11.0	-17

* Calculated accelerations are taken from Table 2.12.5-11 and Table 2.12.5-12. Actual acceleration values are given as A/B, where A is the value derived from the 1019 Hz cutoff data, and B is the value for the rigid body estimate. The actual acceleration values for tests D1 and D3 are taken directly from Table 2.12.5-23. The actual acceleration values for test D2R are taken from the results of the adjustment procedure described in Section 2.12.5.3. The rigid body estimates for D2R are formed by subtracting the 'Δ' value (see Table 2.12.5-23) from the adjusted values. For example, for the D2R primary case, the adjusted value derived from the 1019Hz cutoff data in Section 2.12.5.3 is 69.0g, and the 'Δ' value from Table 2.12.5-23 is 5.5g, thus the rigid body estimate for D2R primary is 69.0 – 5.5 = 63.5g. The two values in the '% Less' column correspond to the two values in the 'Actual' column, and show the amount that the actual values are less than the calculated values.

Table 2.12.5-25 - Comparison of Results Using Previously Published Stress-Strain Data*

	Primary Impact		Secondary Impact	
Dataset	Deflection, in	Acceleration, g	Deflection, in	Acceleration, g
Current Data	13.6	53.4	15.9	83.2
Previous Data	13.0	57.3	15.2	89.6

* HAC, 15° slapdown, 150 °F. "Current Data" results correspond to Table 2.12.5-13 and Table 2.12.5-14.

Design Guide for use of LAST-A-FOAM FR-3700 for Crash and Fire Protection of Radioactive Material Shipping Containers

Table 7: Static Nominal Crush Strength, *Parallel* to Direction of Rise (see **Table 8** for *Perpendicular* to Rise)

For 4 to 10 lb_m/ft^3									
Temp	Correlation Factors	Crush Strength, psi, Parallel to Direction of Rise							
		10%	20%	30%	40%	50%	60%	65%	70%
-20°F	C_T	1.29	1.36	1.32	1.29	1.26	1.28	1.29	1.37
75°F	Y_{int}	**7.3058**	**6.7276**	**6.4961**	**6.9137**	**5.6711**	**5.3279**	**5.9871**	**6.2085**
	S	**1.6590**	**1.7021**	**1.7350**	**1.7255**	**1.8877**	**2.0431**	**2.0870**	**2.1868**
100°F	C_T	0.87	0.88	0.89	0.89	0.90	0.91	0.91	0.96
140°F	C_T	0.73	0.75	0.76	0.77	0.78	0.78	0.79	0.84
180°F	C_T	0.65	0.66	0.67	0.68	0.69	0.68	0.68	0.71
220°F	C_T	0.61	0.60	0.60	0.61	0.61	0.59	0.59	0.61
260°F	C_T	0.45	0.44	0.46	0.47	0.48	0.49	0.49	0.52
For 11 to 40 lb_m/ft^3									
Temp	Correlation Factor	Crush Strength, psi, Parallel to Direction of Rise							
		10%	20%	30%	40%	50%	60%	65%	70%
-20°F	C_T	1.35	1.33	1.32	1.31	1.31	1.30	1.28	1.26
75°F	Y_{int}	**4.3422**	**3.8755**	**3.5241**	**3.0307**	**3.0402**	**3.4889**	**5.8935**	**5.6055**
	S	**1.8809**	**1.9321**	**1.9872**	**2.0755**	**2.1451**	**2.2143**	**2.1041**	**2.2368**
100°F	C_T	0.86	0.87	0.88	0.88	0.89	0.90	0.90	0.97
140°F	C_T	0.72	0.74	0.75	0.75	0.75	0.76	0.76	0.81
180°F	C_T	0.62	0.63	0.65	0.65	0.65	0.65	0.64	0.68
220°F	C_T	0.56	0.56	0.57	0.57	0.56	0.54	0.54	0.57
260°F	C_T	0.40	0.40	0.41	0.42	0.41	0.43	0.43	0.47

The room temperature (75°F) foam crush strength is calculated at each %-Crush and is a function of density; $\sigma = Y_{int}(\rho)^S$, where Y_{int} and S are defined above, ρ is the nominal foam density in lb/ft^3, and σ in the resulting crush stress in psi at the indicated strain. The foam crush strength at temperatures other than 75°F is calculated at each %-Crush and is a function of the strength at 75°F; $\sigma = \sigma_{75°F} C_T$. General Plastics Mfg. Co. is re-investigating the correlations factors at temperatures above and below 75°F. Please contact us for more specific and detailed data, as needed.

Figure 2.12.5-1 - General Plastics Data (Page 1 of 3)

Design Guide for use of LAST-A-FOAM FR-3700 for Crash and Fire Protection of Radioactive Material Shipping Containers

Table 8: Static Nominal Crush Strength, *Perpendicular* to Direction of Rise (see **Table 7** for *Parallel* to Rise)

Temp	Correlation Factors (see below)	For 4 to 10 lb_m/ft^3 Crush Strength, psi, Perpendicular to Direction of Rise							
		10%	20%	30%	40%	50%	60%	65%	70%
-20°F	C_T	1.32	1.35	1.34	1.32	1.32	1.33	1.34	1.36
75°F	Y_{int}	**6.3841**	**6.5943**	**6.1154**	**5.7722**	**5.3041**	**5.3181**	**5.7864**	**5.7701**
	S	**1.7182**	**1.6946**	**1.7403**	**1.8023**	**1.9054**	**2.0392**	**2.1002**	**2.2255**
100°F	C_T	0.85	0.87	0.88	0.89	0.90	0.91	0.91	0.92
140°F	C_T	0.75	0.77	0.78	0.79	0.79	0.79	0.79	0.80
180°F	C_T	0.63	0.66	0.68	0.69	0.69	0.70	0.69	0.70
220°F	C_T	0.59	0.59	0.60	0.61	0.60	0.60	0.59	0.60
260°F	C_T	0.45	0.45	0.47	0.48	0.48	0.48	0.48	0.48
Temp	Correlation Factors (see below)	For 11 to 40 lb_m/ft^3 Crush Strength, psi, Perpendicular to Direction of Rise							
		10%	20%	30%	40%	50%	60%	65%	70%
-20°F	C_T	1.34	1.33	1.32	1.33	1.30	1.28	1.24	1.17
75°F	Y_{int}	**4.1342**	**3.5581**	**3.2664**	**2.8352**	**2.8988**	**3.3972**	**6.5439**	**5.6464**
	S	**1.8957**	**1.9593**	**2.0109**	**2.0955**	**2.1602**	**2.2242**	**2.0660**	**2.2321**
100°F	C_T	0.84	0.85	0.86	0.88	0.87	0.88	0.88	0.90
140°F	C_T	0.72	0.73	0.74	0.76	0.75	0.76	0.76	0.79
180°F	C_T	0.62	0.63	0.64	0.65	0.65	0.65	0.65	0.67
220°F	C_T	0.53	0.53	0.54	0.55	0.54	0.54	0.54	0.56
260°F	C_T	0.39	0.39	0.40	0.41	0.41	0.40	0.40	0.42

The room temperature (75°F) foam crush strength is calculated at each %-Crush and is a function of density; $\sigma = Y_{int}(\rho)^S$, where Y_{int} and S are defined above, ρ is the nominal foam density in lb/ft^3, and σ in the resulting crush stress in psi at the indicated strain. The foam crush strength at temperatures other than 75°F is calculated at each %-Crush and is a function of the strength at 75°F; $\sigma = \sigma_{75°F} C_T$. General Plastics Mfg. Co. is re-investigating the correlations factors at temperatures above and below 75°F. Please contact us for more specific and detailed data, as needed.

Figure 2.12.5-1 - General Plastics Data, continued (Page 2 of 3)

Design Guide for use of LAST-A-FOAM FR-3700 for Crash and Fire Protection of Radioactive Material Shipping Containers

Dynamic Crush Strength

The crush strength of LAST-A-FOAM®, like many materials, is modestly sensitive to strain rate. The static to dynamic adjustment shown in Table 9 is based on a significant testing program and included strain rates in the range of 30 sec^{-1} to 100 sec^{-1}. It is expected that the adjustment will provide good predictions of dynamic impact strength of FR-3700 for most Packaging design conditions. This information is intended to be a guide for designers of impact mitigating devices. The constitutive material models may be useful in targeting a foam density or rage for a particular application. However, each design should be thoroughly analyzed or tested to understand the implications of the complete design.

Table 9: Static to Dynamic Crush Strength Adjustment

Strain	10%	20%	30%	40%	50%	60%	65%	70%
Y_{Int}	1.2971	1.4397	1.5181	1.3887	1.4419	1.4275	1.3871	1.4660
S	1.0330	1.0069	0.9941	1.0028	0.9912	0.9831	0.9910	0.9586

The dynamic crush strength is calculated at each %-strain and a function of the static crush strength at the same %-strain;

$\sigma_{Dynamic} = y_{Int}(\sigma_{Static})^{S}$.

CAUTION: Use only units of PSI for input σ_{Static} value.

General Plastics Manufacturing Company
4910 Burlington Way • P.O. box 9097
Tacoma, WA 98409

Telephone: (800) 806-6051 or (253) 473-5000
Facsimile: (253) 473-5104

See our World Wide Wed Site at:
www.generalplastics.com
E-mail address: sales@generalplastics.com

Figure 2.12.5-1 - General Plastics Data, continued (Page 3 of 3)

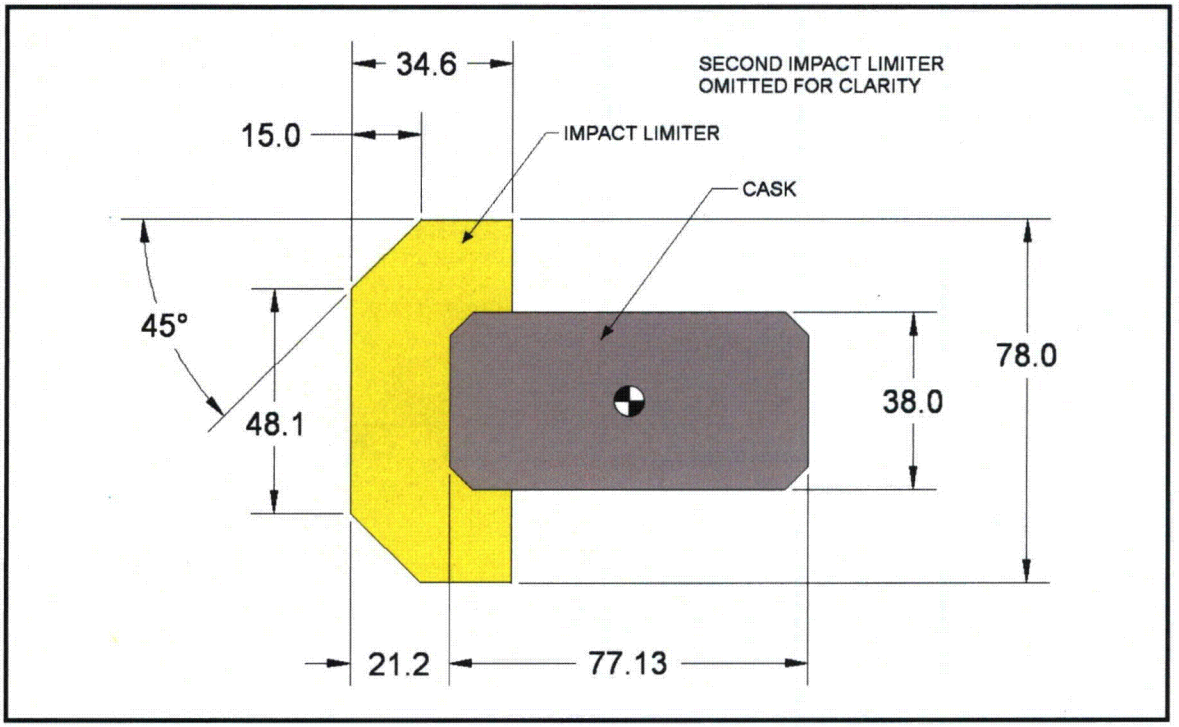

Figure 2.12.5-2 - Dimensions Used in CASKDROP

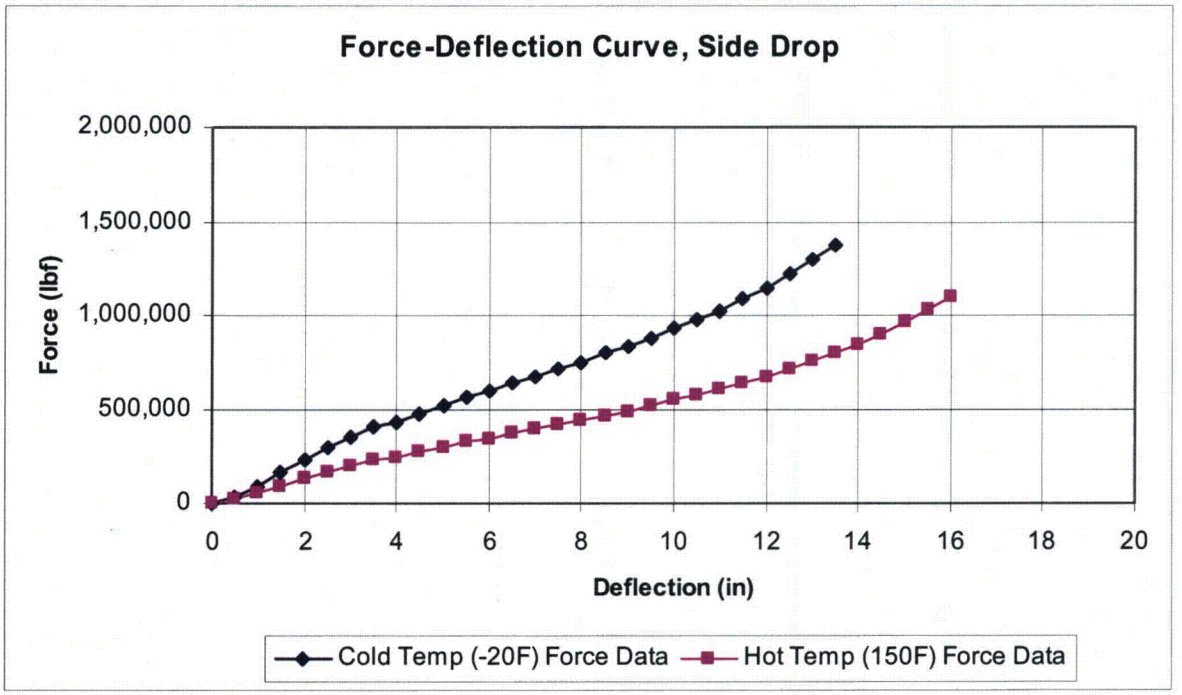

Figure 2.12.5-3 - Force-Deflection Curve, Side Orientation

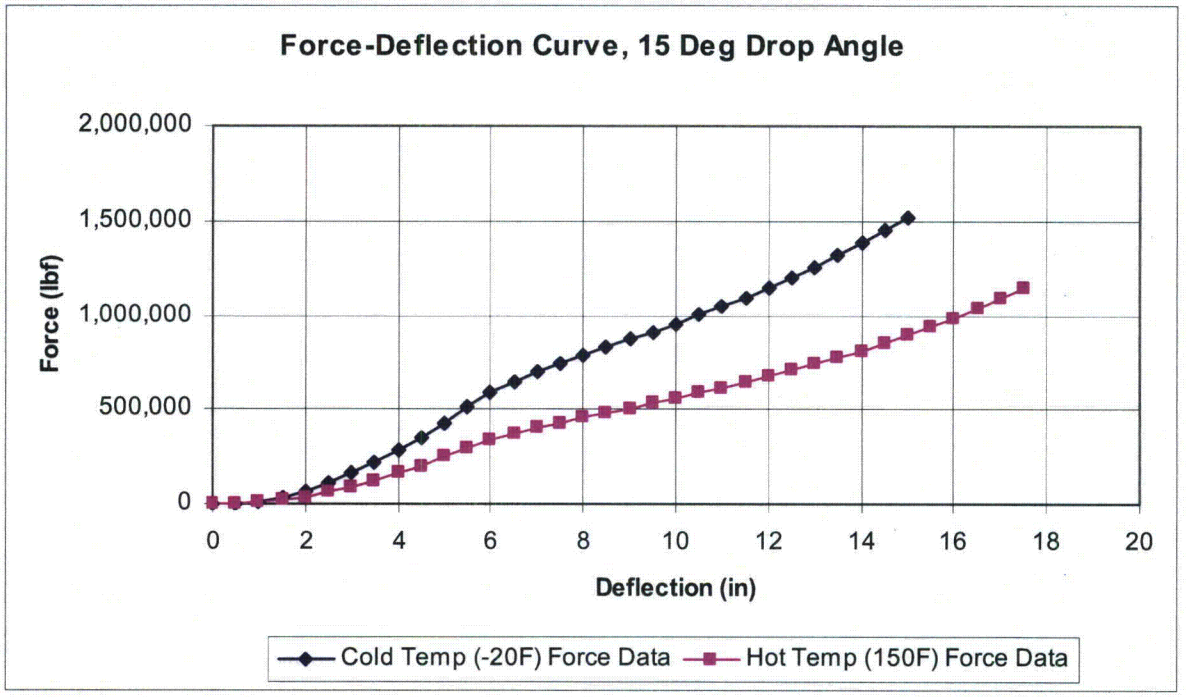

Figure 2.12.5-4 - Force-Deflection Curve, 15° Orientation

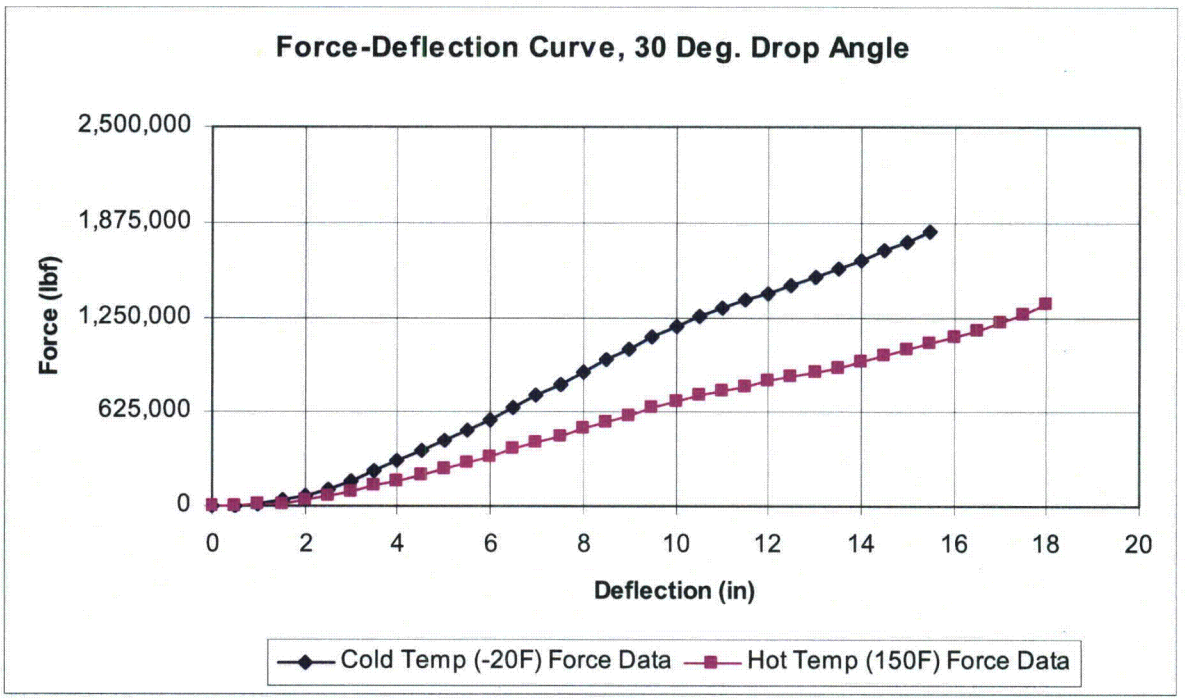

Figure 2.12.5-5 - Force-Deflection Curve, 30° Orientation

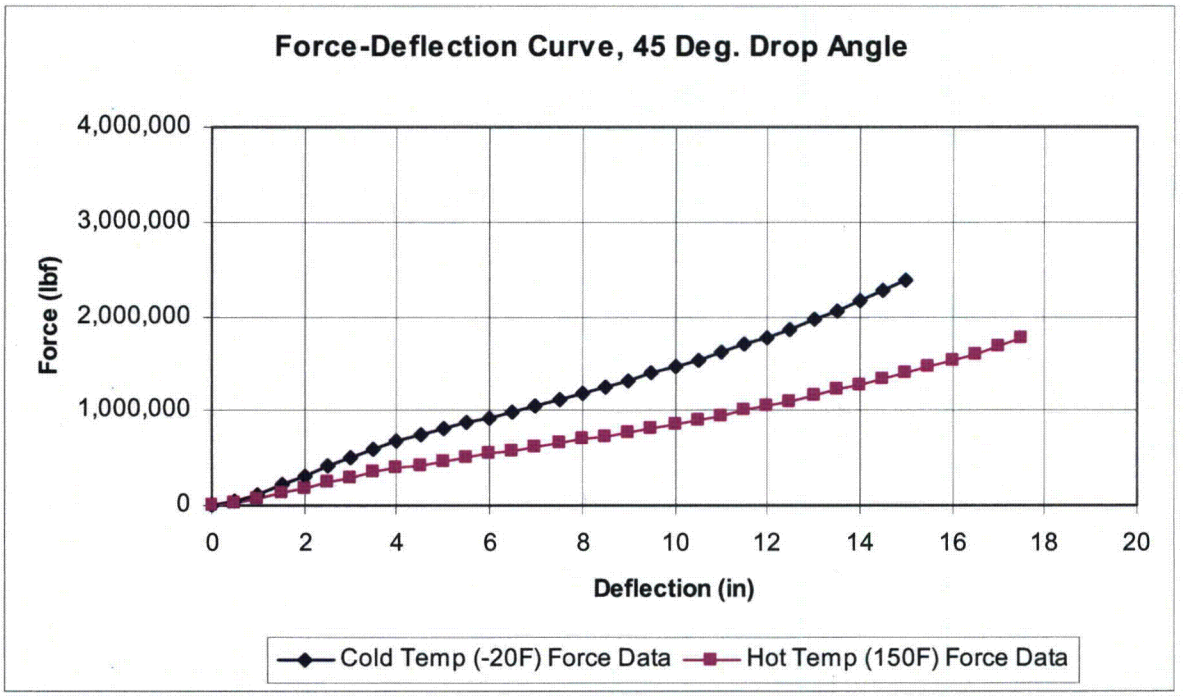

Figure 2.12.5-6 - Force-Deflection Curve, 45° Orientation

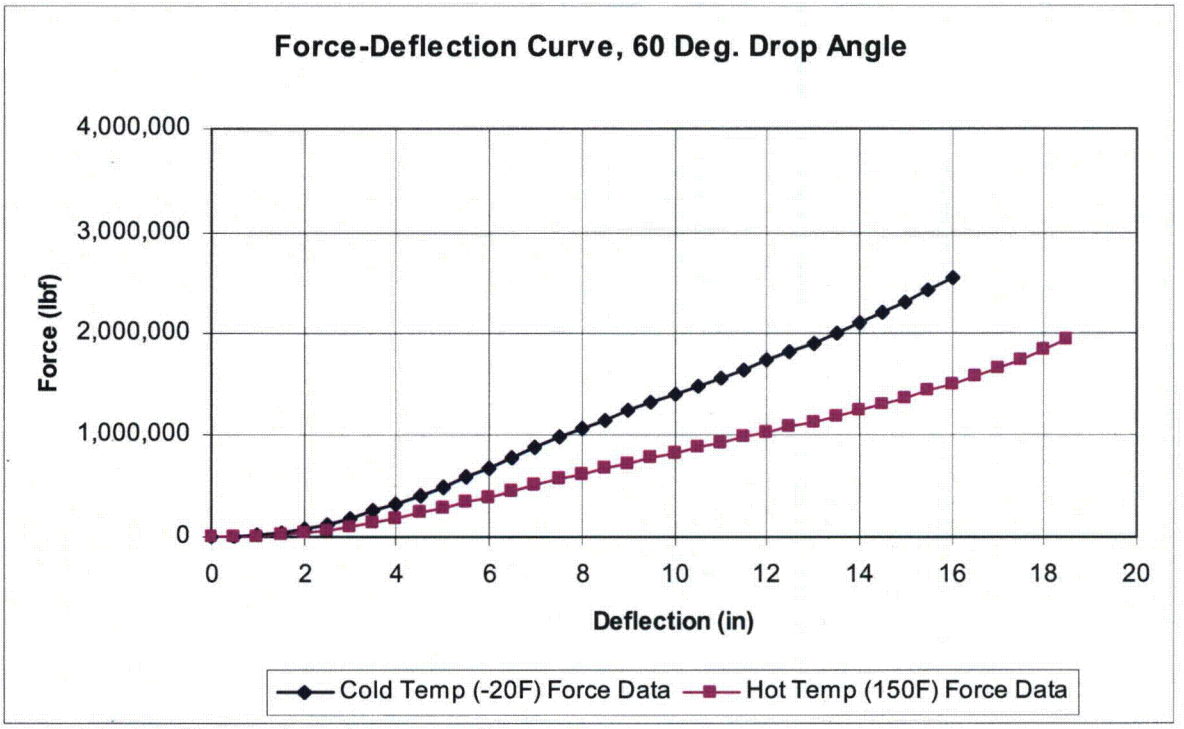

Figure 2.12.5-7 - Force-Deflection Curve, 60° Orientation

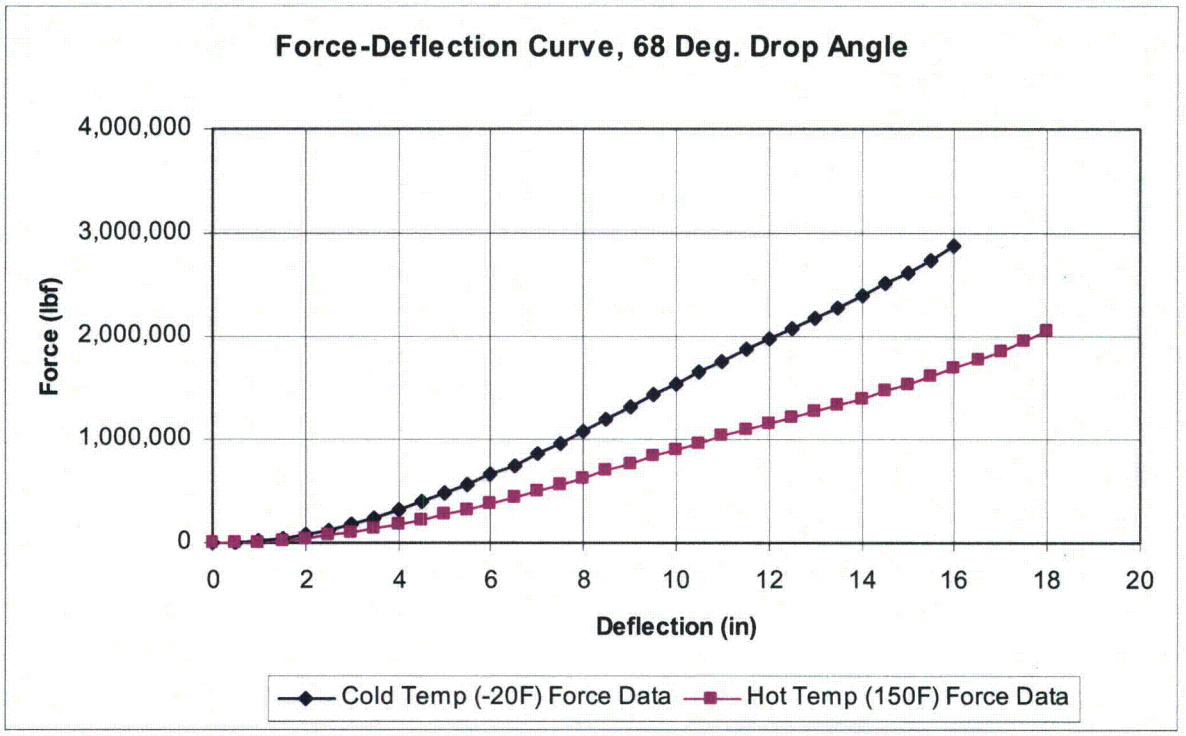

Figure 2.12.5-8 - Force-Deflection Curve, 68° Orientation

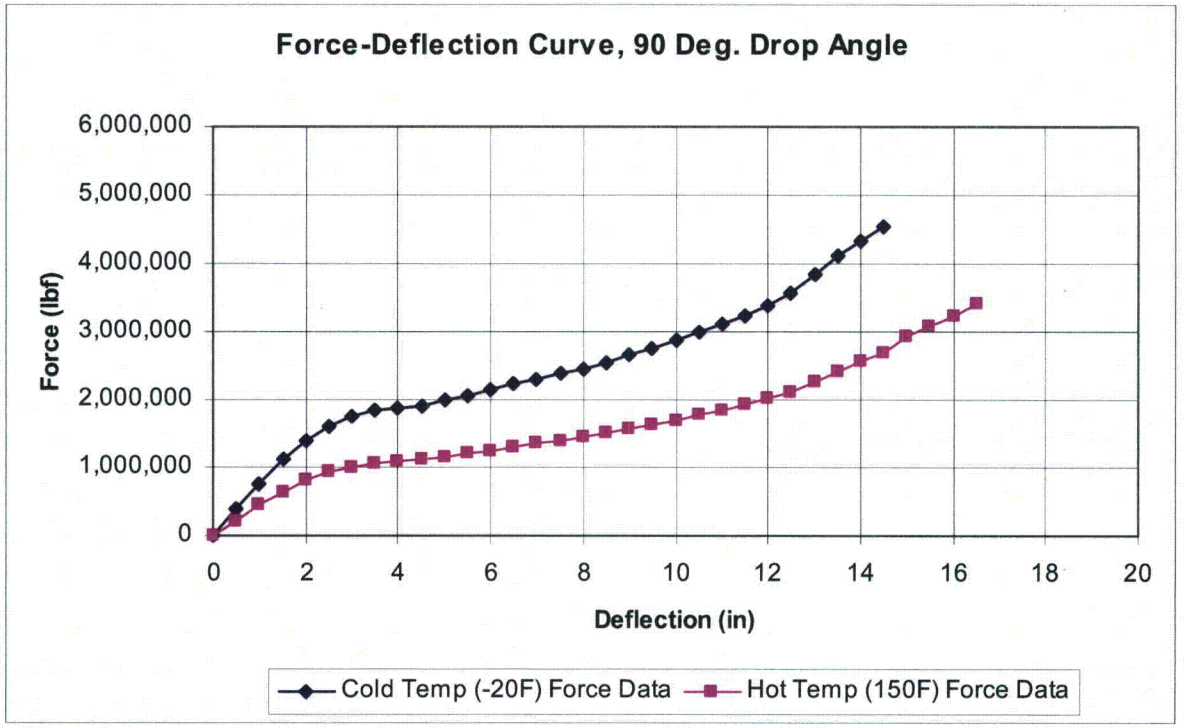

Figure 2.12.5-9 - Force-Deflection Curve, 90° Orientation

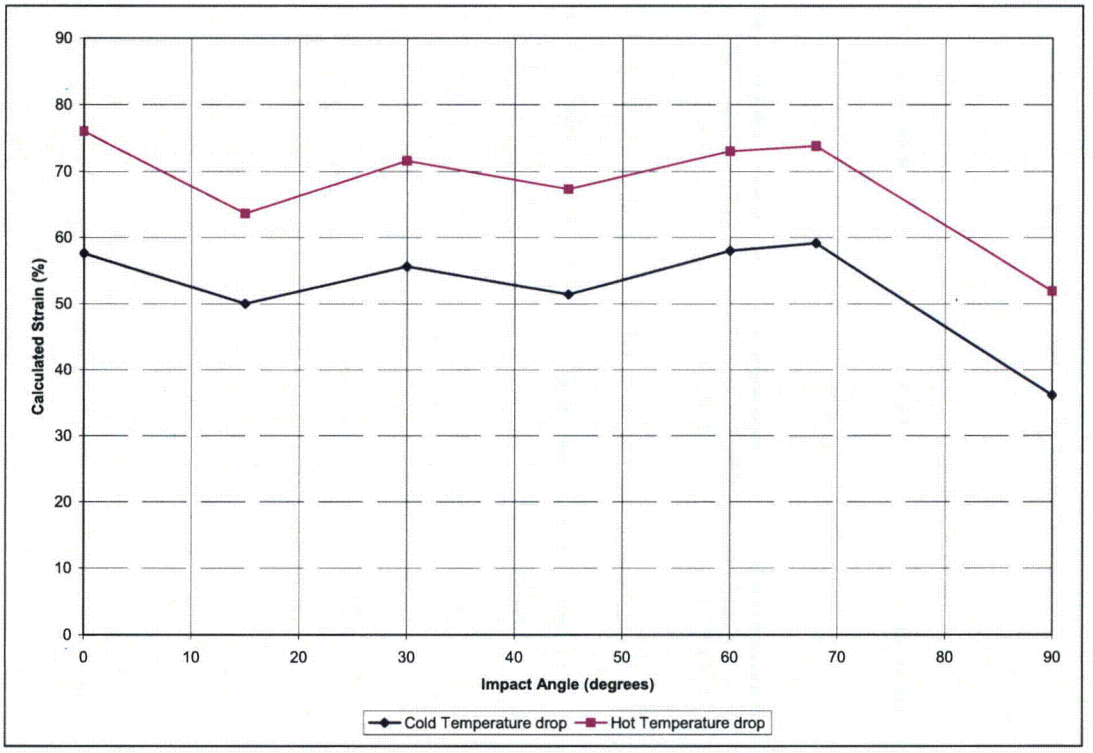

Figure 2.12.5-10 - Primary Impact Limiter Strain, HAC

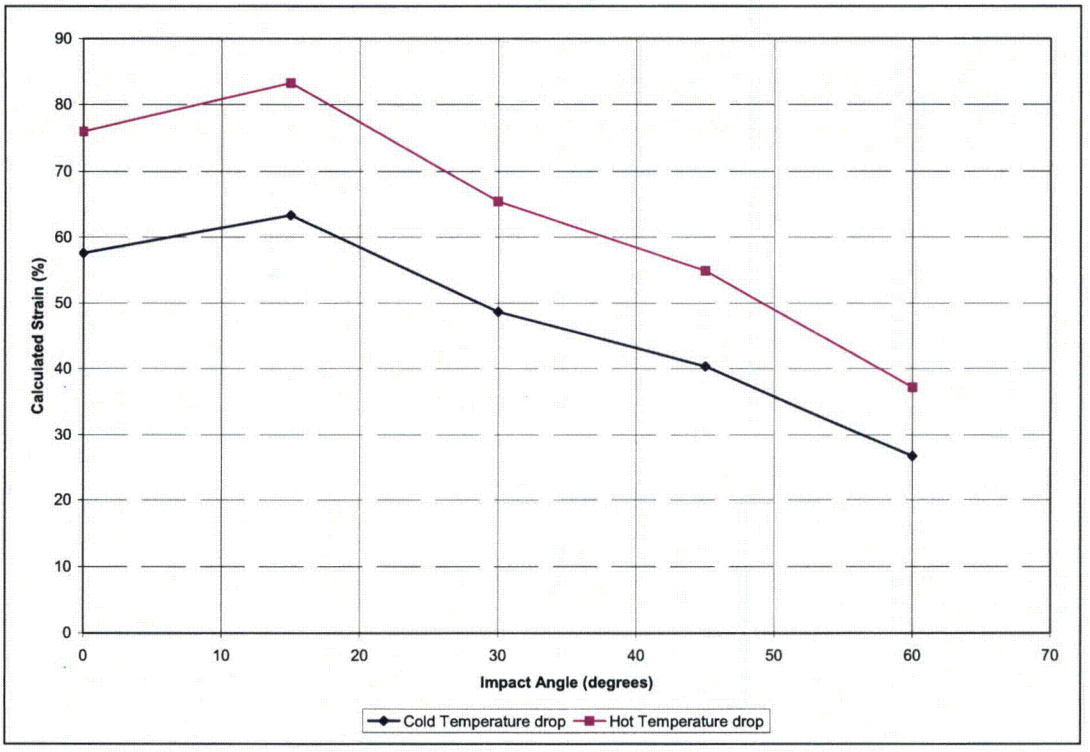

Figure 2.12.5-11 - Secondary Impact Limiter Strain, HAC

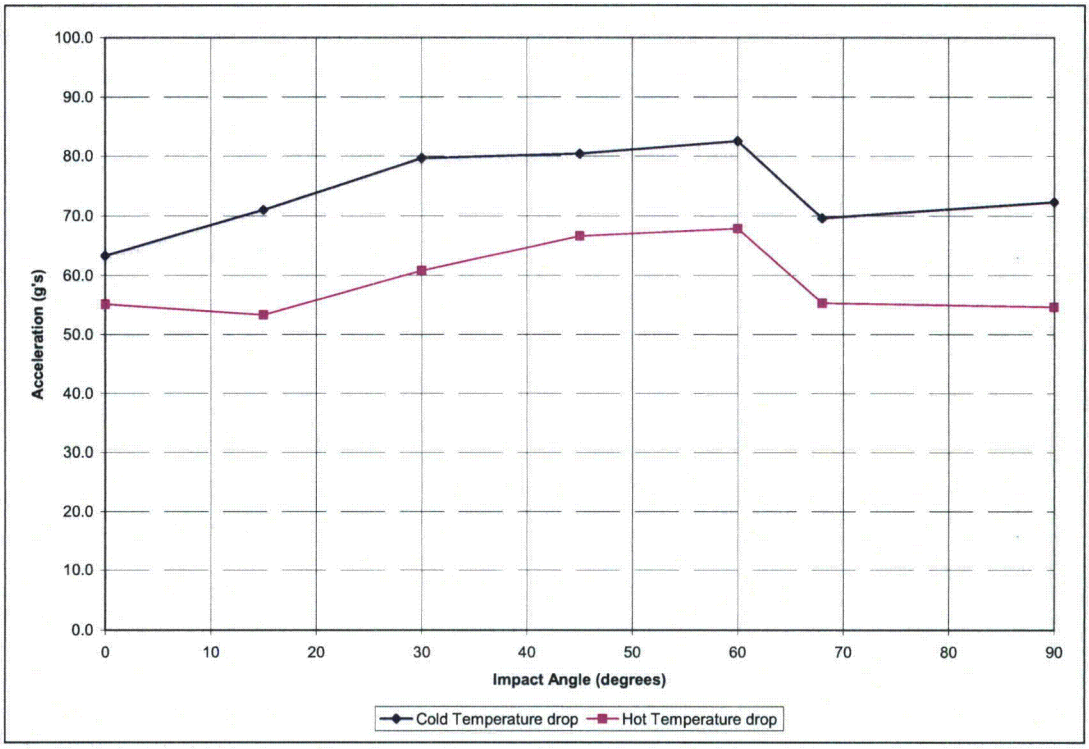

Figure 2.12.5-12 - Primary Impact Acceleration, HAC

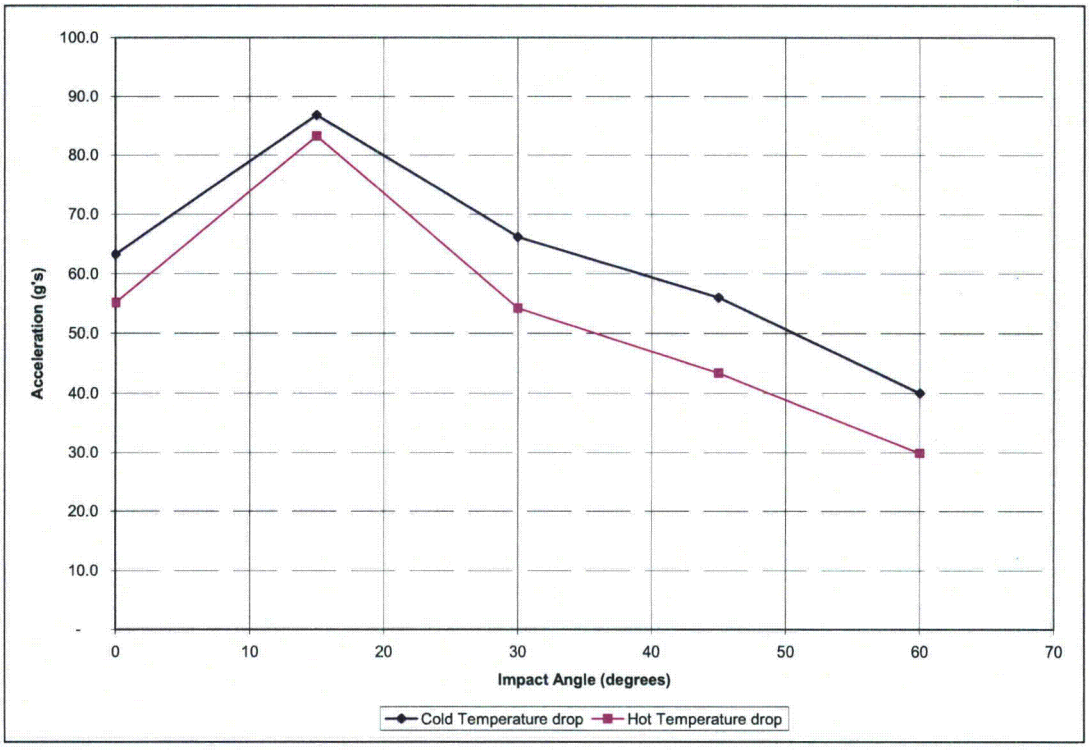

Figure 2.12.5-13 - Secondary Impact Acceleration, HAC

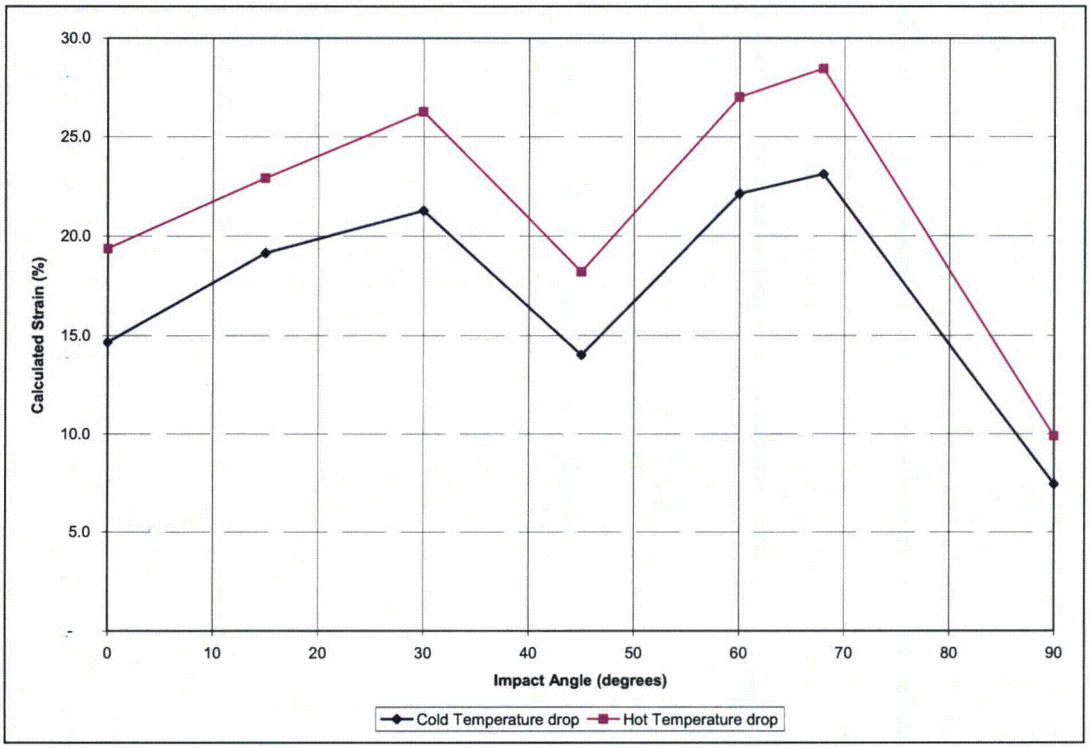

Figure 2.12.5-14 - Primary Impact Limiter Strain, NCT

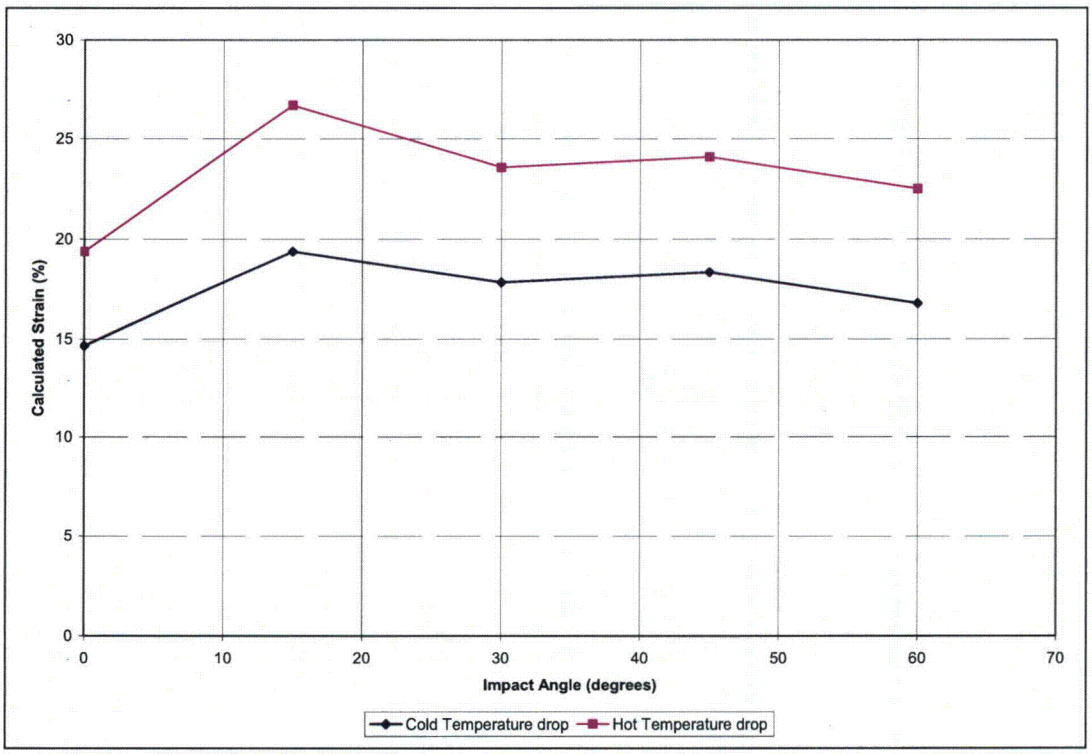

Figure 2.12.5-15 - Secondary Impact Limiter Strain, NCT

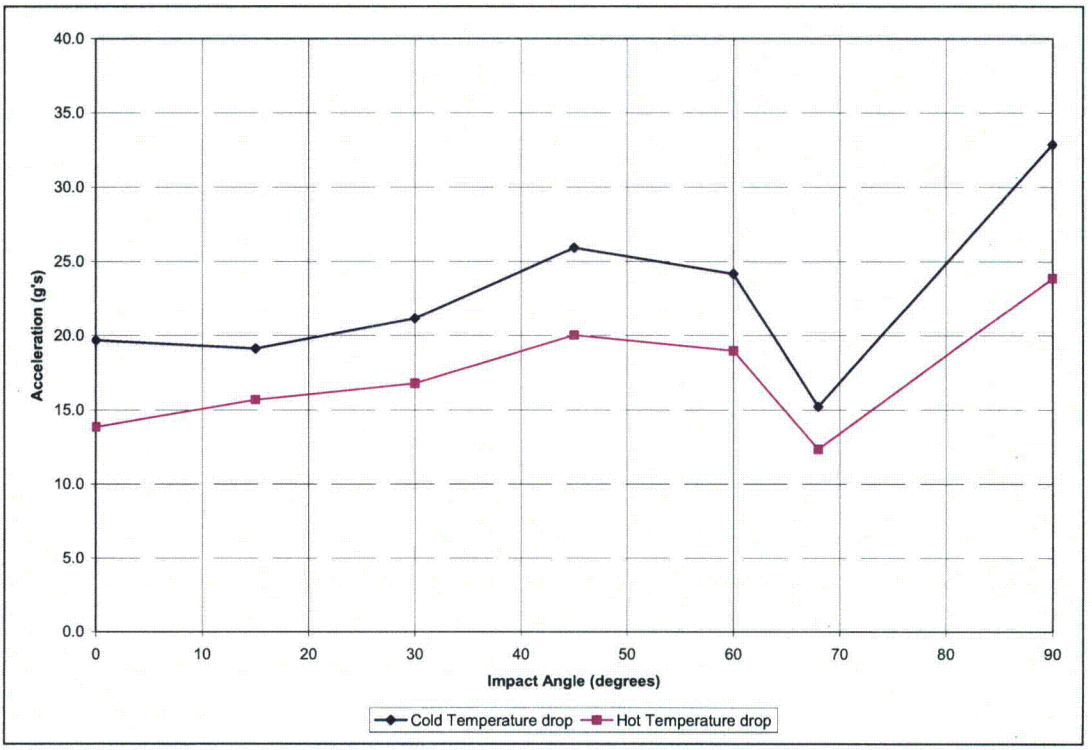

Figure 2.12.5-16 - Primary Impact Acceleration, NCT

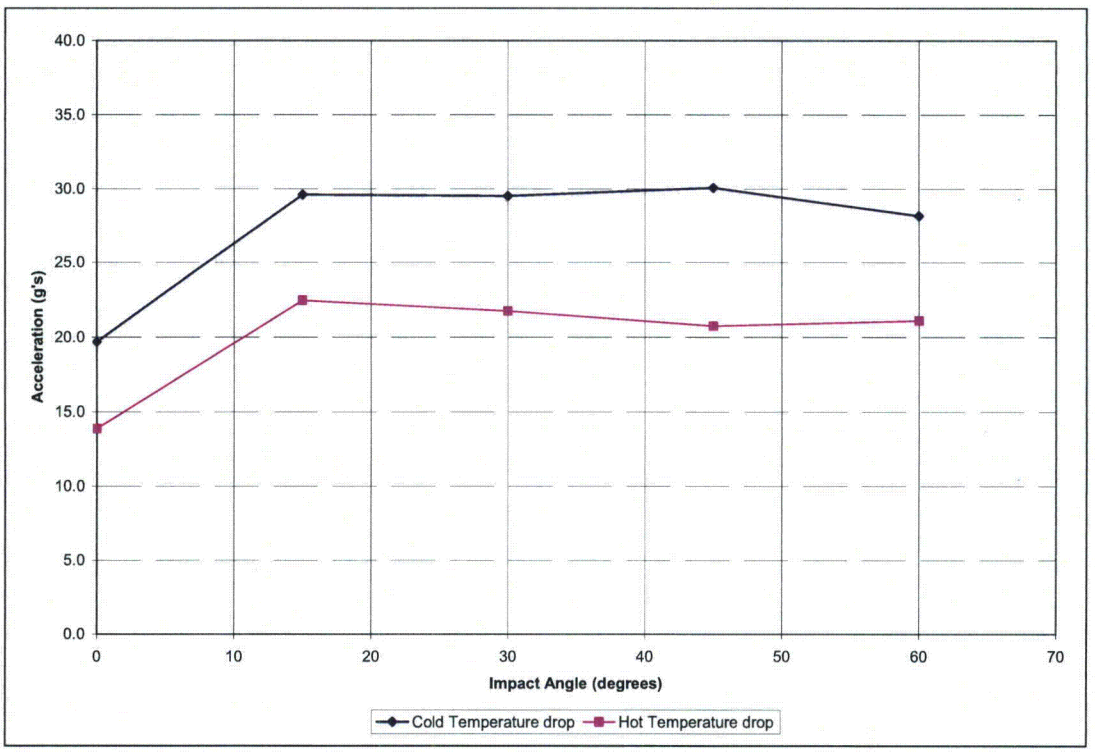

Figure 2.12.5-17 - Secondary Impact Acceleration, NCT

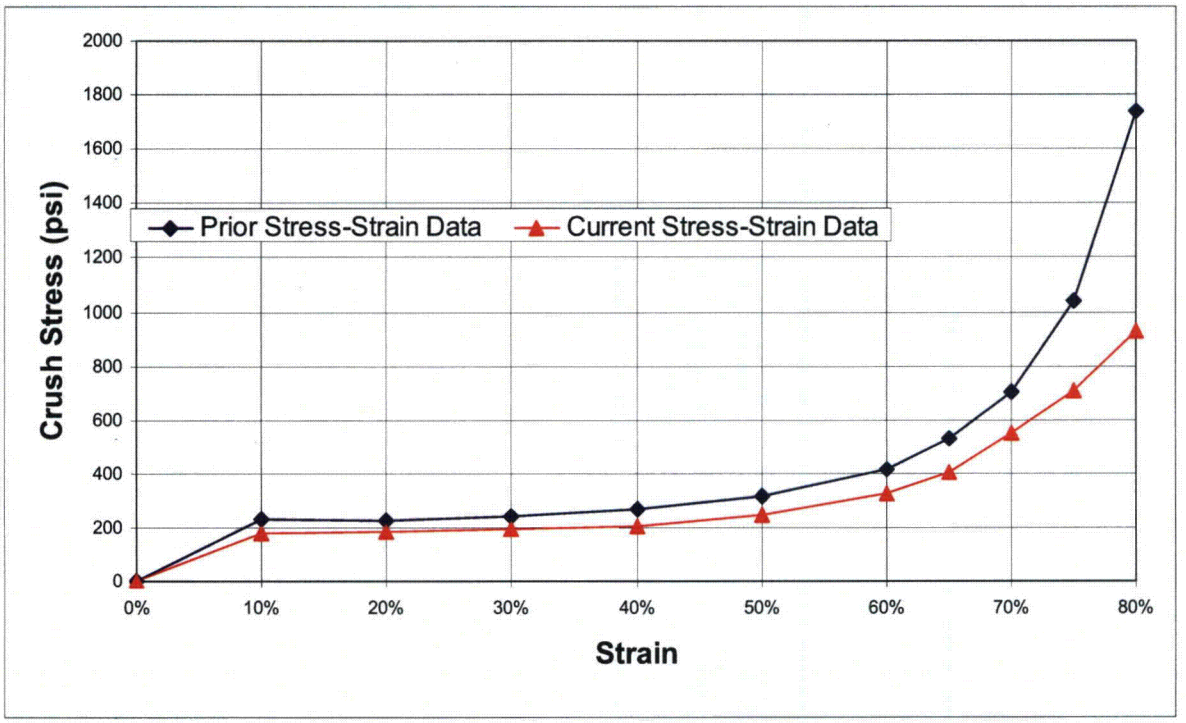

Figure 2.12.5-18 - Previously Published vs. Current Stress-Strain Data (150 °F)

2.12.6 Analysis Software Descriptions

This appendix contains descriptions of the computer codes CASKDROP and SLAPDOWN. Both of these programs are used in Appendix 2.12.5, *Impact Limiter Performance Evaluation.*

2.12.6.1 CASKDROP

This appendix briefly documents the methodology employed by the AREVA Federal Services proprietary computer program CASKDROP. Used in conjunction with an appropriate packaging dynamic analysis computer code (see Section 2.12.6.2, *SLAPDOWN*), the computer program CASKDROP is used to demonstrate compliance of the package with 10 CFR §71.71(c)(7) and 10 CFR §71.73(c)(1) for normal conditions of transport (NCT) and hypothetical accident conditions (HAC) of transport free drop analyses, respectively.

2.12.6.1.1 Using CASKDROP to Determine Impact Limiter Deformation Behavior

CASKDROP evaluates all angles of drop from 0° (horizontal) to 90° (vertical) by performing a quasi-static analysis that ignores rotational effects. At orientations where rotational effects are important, use of a dynamic analysis computer program such as SLAPDOWN is required utilizing the force-deflection data developed by CASKDROP. Note that although CASKDROP is capable of completely solving the impact analysis for orientations where rotation effects are not important (e.g., end, side, and c.g.-over-corner), the only program output which is utilized in the evaluation of the BRR Package free drop events is the formulation of the force-deflection relation for the impact limiters. The program SLAPDOWN, using the force-deflection input from CASKDROP, is utilized for the final evaluation of all orientations. The following material is a general documentation of CASKDROP, and is not limited to the features utilized for the BRR package.

CASKDROP assumes the package is protected by polyurethane foam-filled, energy absorbing impact limiters. Since the impact surface is unyielding, the impact limiters are assumed to absorb all of the potential energy of the drop event.

For all orientations of impact, the prediction of impact limiter deformation behavior can be approached from straightforward energy balance principles:

$$E = W(h + \delta) = \int_0^{\delta} F_x dx$$

where W is the package gross weight, h is the drop height, δ is the maximum impact limiter deformation, and F_x is the force imposed on the target at an impact limiter deformation of x. The left-hand term represents the potential energy of the free drop. The right-hand term represents the strain energy of the deformed impact limiter(s).

Given a specific drop angle, θ, and impact limiter deformation, δ, as illustrated in Figure 2.12.6-1, the result is an impact limiter crush plane "footprint." Integration of the impact limiter crush plane yields a total crush force and centroidal distance of:

$$F = \iint \sigma\{\varepsilon\}\, dA \qquad \text{and} \qquad \overline{X} = \left(\frac{1}{F}\right) \iint \overline{x}\sigma\{\varepsilon\}\, dA$$

respectively, where F is the total integrated force, $\sigma\{\varepsilon\}$ is the differential stress as a function of strain, dA is the differential area (i.e., dA is a function of the "x" and "y" directions, or dx and dy), $\overline{X}$ is the total integrated centroidal distance from the package center of gravity, and $\overline{x}$ is the differential centroidal distance from the package center of gravity.

With reference to Figure 2.12.6-1, the geometric calculations for the impact surface (crush plane) and the associated strains are carried out using a translating X'-Y'-Z' coordinate system, with the X'-Y' plane corresponding to the crush plane. Due to the cylindrical nature of the problem, the overall crush plane is comprised of a segment of an ellipse corresponding to the outside surface of the impact limiter. The optional end hole requires removal of its associated elliptical segment. Similarly, the optional conical surface is an elliptical, parabolic, or hyperbolic segment depending on both the drop angle, θ, and angle of the cone.

Calculation of the differential strain is somewhat more complex. As illustrated in Figure 2.12.6-2, the differential strain, $\varepsilon\{x,y\}$, is calculated at the center of the differential area, dA. The differential strain is determined by calculating the amount of vertical deformation at the (x, y) location on the crush plane. The vertical distance from point (x, y) on the impact surface to the package or upper impact limiter surface is found and denoted z_{TOP}. Similarly, the vertical distance from point (x, y) on the impact surface to the undeformed lower impact limiter surface is found and denoted z_{BOT}. In equation format the differential strain at location (x, y) is simply:

$$\varepsilon = \frac{z_{BOT}}{z_{BOT} + z_{TOP}}$$

This strain is used to determine the corresponding crush stress from an implicit tabular definition of the crushable media stress-strain characteristics. For each differential area, dA, the differential force, dF, is found. The total force, F, is therefore the summation of the differential forces. Similarly, the centroidal distance, $\overline{X}$, is the summation of the moments, $\overline{x} \times dF$, divided by the total force.

Unbacked regions are defined as having an (x, y) location where z_{TOP} is calculated to occur outside the package's "shadow" (i.e., or backing, occurring on the impact limiter surface). Unbacked regions usually utilize the nominal crush strength of the crushable media (typically 10% for polyurethane foam material) for integrated force purposes. The crush strength for unbacked regions is user-definable in the program CASKDROP.

For most drop angles, θ, and impact limiter deformations, δ, the impact limiter crush force, F, is transmitted to the package body in direct compression. Hence, the forces transmitted to the circumferential impact limiter attachments are essentially zero. However, for nearly vertical or horizontal orientations at small deformations where the crush force occurs beyond the edge of the package, the forces transmitted to the impact limiter attachments can be substantially large. It is important to note that only the nearly vertical or nearly horizontal orientations are required to produce the prying motion; all other orientations will always compress the impact limiter onto the package body. Figure 2.12.6-3 illustrates the near vertical and near horizontal orientations producing impact limiter separation forces.

For the near vertical orientation, the moment about point "a" determines whether a separation force exists at the impact limiter attachments. Assuming for this case that a counterclockwise moment is positive (i.e., will tend to "pry" the impact limiter off the package), the equation for the moment about point "a," M_a, is:

$$M_a = Fx_F + F_{IL}x_{IL}$$

Similarly, for the near horizontal orientation, the moment about point "b" determines whether a separation force exists at the impact limiter attachments. Assuming for this case that a clockwise moment is positive (i.e., will tend to "pry" the impact limiter off the package), the equation for the moment about point "b," M_b, is:

$$M_b = Fx_F - F_{IL}x_{IL}$$

If M_a or M_b are positive, a separation force will occur at the impact limiter attachments whereas if M_a or M_b are zero or negative, a separation force will not occur. Note that use of a conically shaped impact limiter typically eliminates the impact limiter separation force by causing the crush force, F, to almost always occur between points "a" and "b."

2.12.6.1.2 An Example Problem for the CASKDROP Program

An example problem is illustrated in Figure 2.12.6-4. The CASKDROP program utilizes a variety of physical input data to determine package and impact limiter geometry. In all cases, the package and impact limiter are assumed axisymmetric. The package is cylindrical, as is the impact limiter. Two fundamental variations in the basic cylindrical shape of the impact limiter are an optional end hole and optional conical end. The end hole may extend part or all of the way from the outside surface of the impact limiter to the package end. The conical end may be a truncated or fully developed cone, defined by a cone diameter and a cone length at the outside surface of the impact limiter. By varying the impact limiter dimensions the result is a wide variety of possible impact limiter shapes, from a totally enclosing "overpack" to pointed end-only buffers.

The CASKDROP program was primarily developed as an impact limiter design tool. Geometry and analysis control input to the CASKDROP program is fully interactive allowing changes "on the fly." Figure 2.12.6-5 illustrates the CASKDROP screen for data entry into the *Input Window*.

The CASKDROP program allows for three types of crushable media definition:

1. CONSTANT: a constant crush stress independent of calculated strain.
2. VARIABLE: a variable, user-defined stress-strain definition. The BRR package analysis uses this option by inputting the adjusted stress-strain curves as discussed in Appendix 2.12.5.
3. POLYFOAM: a built-in polyurethane foam database providing accurate stress-strain definition for 5 to 25 pound per cubic foot (pcf) density and temperatures of -20 °F to +300 °F based on extensive sample testing.

The example problem assumes 20 pcf polyurethane foam at a temperature of -20 °F. A +60% bias is applied to the temperature-corrected stress-strain data to account for dynamic strain rate effects for the example problem. Figure 2.12.6-6 illustrates the CASKDROP input screen for the polyurethane foam crush media for the example problem.

For the example problem, the CASKDROP program utilizes polyurethane foam where "parallel to rise" foam curing occurs in the axial direction and "perpendicular to rise" foam curing occurs in the radial direction, although the difference between these two directions is small. The user may optionally select the "parallel-to-rise" or "perpendicular-to-rise" properties to be reversed or global for all drop orientations. For orientations other than axial (end drop) and radial (side drop), the CASKDROP program interpolates foam properties using an ellipse function. For the case where

crush stress "parallel-to-rise" is in the axial direction, σ_{PAR}, and crush stress "perpendicular-to-rise" is in the radial direction, σ_{PER}, the interpolation equation at drop angle, θ, is:

$$\sigma_\theta = \sqrt{\frac{1}{\left(\frac{\sin\theta}{\sigma_{PAR}}\right)^2 + \left(\frac{\cos\theta}{\sigma_{PER}}\right)^2}}$$

Similarly, for the case where crush stress "perpendicular-to-rise" is in the axial direction, σ_{PER}, and crush stress "parallel-to-rise" is in the radial direction, σ_{PAR}, the interpolation equation is:

$$\sigma_\theta = \sqrt{\frac{1}{\left(\frac{\sin\theta}{\sigma_{PER}}\right)^2 + \left(\frac{\cos\theta}{\sigma_{PAR}}\right)^2}}$$

The *Control Window* allows the user to specify various analysis and output controls. The *Control Window* is separated into *Analysis, Crush, Angle, Static, Dynamic, Print, and File.*

Three *Analysis* options are available: dXY defines the number of integration elements in the crush plane, 25 for the example problem; Sln defines the analysis methodology (Global versus Local Strain Theory), *Global* for the example problem; ε/σ defines the strain (or crush stress) value to be utilized in unbacked regions (e.g., if a value is specified between 0 and 1, it is assumed a strain value and the corresponding crush stress at that strain is used; if a value is specified greater than 1, it is assumed to be a crush stress), 0.1 for the example problem corresponding to a crush stress at 10% strain from the polyurethane foam database.

The *Crush* options define the incremental deformations to be analyzed. The example problem specifies analyzing for crush deformations from 0.25 inch to 20 inch in 0.25 inch increments. Specifying a *Max* value greater than the actual maximum available crush depth (as determined geometrically) flags the CASKDROP program to not exceed the maximum available crush depth.

Similarly, the *Angle* options define the incremental angular orientations to be analyzed. The example problem specifies analyzing for drop angles from 0° to 90° in 15° increments.

The *Static* options allow the user to specify quasi-static analyses providing *Full* display output, *Smry* (summary) output, or *Both*. The example problem specifies *Full* output to the display only. Similarly, the *Dynamic* options allow the user to specify dynamic analyses providing *Full* display output, *Smry* (summary) output, or *Both*. The example problem does not specify a dynamic analysis as that module is not completed in the CASKDROP program.

The *Print* and *File* options allow the user to specify *Full* display output, *Smry* (summary) output, or *Both* to the printer or a file. The example problem specifies *Full* output to an output file only.

The *Output Window* provides the location for *Static* and *Dynamic* display output. A quasi-static solution is achieved when the strain energy of the crushable media (*SE*) is equal to the free-falling kinetic energy of the package (*KE*), or *SE/KE = 1*. The following tables provide a sample file output at 0° (side drop), at 45°, and at 90° (end drop).

Side Drop
05-16-1995, 15:38:39

*** PACKAGING TECHNOLOGY ***

CASKDROP, v2.21
Jul 01, 1994

SAMPLE PROBLEM FOR QUALITY ASSURANCE CHECK (AREAS AND VOLUMES)			
Impact Limiter Weight (each) -	1,000 lbs	Cask and Payload Weight -	10,000 lbs
Impact Limiter Outside Diameter -	60.0000 in	Cask Outside Diameter -	40.0000 in
Impact Limiter Overall Length -	24.0000 in	Cask Overall Length -	48.0000 in
Impact Limiter Conical Diameter -	48.0000 in	Dynamic Unloading Modulus -	1.000E+07 lbs/in
Impact Limiter Conical Length -	10.0000 in	Rad Mass Moment of Inertia -	12,235 lb-in-s²
Impact Limiter End Thickness -	12.0000 in	Frictional Coefficient -	0.0000
Impact Limiter Hole Diameter -	20.0000 in	Drop Height -	30.0000 ft
Impact Limiter Hole Length -	8.0000 in	Drop Angle from Horizontal -	0.0000°
Unbacked Area Threshhold Strain -	0.1000 in/in	Crush Analysis Theory -	Global
Unbacked Area Crush Stress -	2,675 psi	Number of Integration Incs -	25

POLYFOAM CRUSH STRESS
(Axial: "∥" to rise)

Density = 20.000 pcf
Temp = -20.000 °F
σ-yield = 2,552.3 psi
Bias = 60.000%

ε (in/in)	σ (psi)
0.000	0.0
0.100	2,552.3
0.200	2,687.0
0.300	2,868.8
0.400	3,302.9
0.500	4,115.1
0.600	6,074.3
0.650	7,942.0
0.700	10,925.0
0.750	15,001.8
0.800	26,829.5

POLYFOAM CRUSH STRESS
(Radial: "⊥" to rise)

Density = 20.000 pcf
Temp = -20.000 °F
σ-yield = 2,675.0 psi
Bias = 60.000%

ε (in/in)	σ (psi)
0.000	0.0
0.100	2,675.0
0.200	2,785.4
0.300	2,959.9
0.400	3,345.9
0.500	4,147.7
0.600	6,062.8
0.650	7,868.8
0.700	10,180.0
0.750	15,554.4
0.800	29,704.8

POLYFOAM CRUSH STRESS
(Actual Data @ 0.0°)

Density = 20.000 pcf
Temp = -20.000 °F
σ-yield = 2,675.0 psi
Bias = 60.000%

ε (in/in)	σ (psi)
0.000	0.0
0.100	2,675.0
0.200	2,785.4
0.300	2,959.9
0.400	3,345.9
0.500	4,147.7
0.600	6,062.8
0.650	7,868.8
0.700	10,180.0
0.750	15,554.4
0.800	29,704.8

DEFL (in)	MAX ε (%)	AREA (in2)	VOLUME (in3)	XBAR (in)	IMPACT FORCE (lbs)	ACCEL (g's)	I/L MOMENT (in-lbs)	STRAIN ENERGY (in-lbs)	KINETIC ENERGY (in-lbs)	SE/KE RATIO
0.250	2.50	221	37	0.00	106,881	8.9	0	13,360	4,323,000	0.00
0.500	5.00	318	105	0.00	289,508	24.1	0	62,909	4,326,000	0.01
0.750	7.50	396	194	0.00	518,875	43.2	0	163,957	4,329,000	0.04
1.000	10.00	465	302	0.00	733,200	61.1	0	320,466	4,332,000	0.07

Side Drop
05-16-1995, 15:38:39

*** PACKAGING TECHNOLOGY ***
(continued...)

CASKDROP, v2.21
Jul 01, 1994

DEFL (in)	MAX ε (%)	AREA (in2)	VOLUME (in3)	XBAR (in)	IMPACT FORCE (lbs)	ACCEL (g's)	I/L MOMENT (in-lbs)	STRAIN ENERGY (in-lbs)	KINETIC ENERGY (in-lbs)	SE/KE RATIO
1.250	12.49	528	425	0.00	955,009	79.6	0	531,492	4,335,000	0.12
1.500	14.99	587	565	0.00	1,107,366	92.3	0	789,289	4,338,000	0.18
1.750	17.49	644	719	0.00	1,270,225	105.9	0	1,086,488	4,341,000	0.25
2.000	19.99	699	886	0.00	1,371,441	114.3	0	1,416,697	4,344,000	0.33
2.250	22.49	752	1,068	0.00	1,509,207	125.8	0	1,776,778	4,347,000	0.41
2.500	24.99	804	1,262	0.00	1,668,937	139.1	0	2,174,046	4,350,000	0.50
2.750	27.49	855	1,469	0.00	1,761,221	146.8	0	2,602,815	4,353,000	0.60
3.000	29.99	906	1,690	0.00	1,946,101	162.2	0	3,066,230	4,356,000	0.70
3.250	32.49	955	1,921	0.00	2,044,813	170.4	0	3,565,095	4,359,000	0.82
3.500	34.98	1,005	2,167	0.00	2,249,052	187.4	0	4,101,828	4,362,000	0.94
3.614	36.13	1,027	2,285	0.00	2,326,676	193.9	0	4,363,372	4,363,372	1.00
3.750	37.48	1,053	2,424	0.00	2,419,003	201.6	0	4,956,582	4,365,000	1.14
4.000	39.98	1,101	2,692	0.00	2,640,297	220.0	0	5,588,994	4,368,000	1.28
4.250	42.48	1,149	2,975	0.00	2,759,520	230.0	0	6,263,971	4,371,000	1.43
4.500	44.98	1,197	3,267	0.00	2,956,003	246.3	0	6,978,412	4,374,000	1.60
4.750	47.48	1,244	3,571	0.00	3,208,534	267.4	0	7,748,979	4,377,000	1.77
5.000	49.98	1,292	3,889	0.00	3,357,376	279.8	0	8,569,718	4,380,000	1.96
5.250	52.48	1,339	4,219	0.00	3,603,141	300.3	0	9,439,782	4,383,000	2.15
5.500	54.97	1,385	4,556	0.00	3,906,997	325.6	0	10,378,550	4,386,000	2.37
5.750	57.47	1,432	4,909	0.00	4,215,273	351.3	0	11,393,833	4,389,000	2.60
6.000	59.97	1,479	5,275	0.00	4,573,066	381.1	0	12,492,376	4,392,000	2.84
6.250	62.47	1,520	5,650	0.00	4,961,100	413.4	0	13,684,147	4,395,000	3.11
6.500	64.97	1,559	6,035	0.00	5,404,072	450.3	0	14,979,793	4,398,000	3.41
6.750	67.47	1,597	6,430	0.00	5,893,283	491.1	0	16,391,963	4,401,000	3.72
7.000	69.97	1,632	6,834	0.00	6,440,254	536.7	0	17,933,655	4,404,000	4.07
7.250	72.47	1,666	7,246	0.00	7,087,717	590.6	0	19,624,651	4,407,000	4.45
7.500	74.96	1,698	7,667	0.00	8,001,352	666.8	0	21,510,785	4,410,000	4.88
7.750	77.46	1,730	8,095	0.00	9,446,226	787.2	0	23,691,732	4,413,000	5.37
8.000	79.96	1,760	8,532	0.00	11,484,412	957.0	0	26,308,062	4,416,000	5.96
8.250	82.46	1,790	8,976	0.00	13,964,555	1,163.7	0	29,489,183	4,419,000	6.67
8.500	84.96	1,818	9,427	0.00	16,801,077	1,400.1	0	33,334,887	4,422,000	7.54
8.750	87.46	1,846	9,885	0.00	19,931,256	1,660.9	0	37,926,428	4,425,000	8.57
9.000	89.96	1,873	10,350	0.00	23,276,639	1,939.7	0	43,327,415	4,428,000	9.78
9.250	92.45	1,899	10,822	0.00	26,896,391	2,241.4	0	49,599,044	4,431,000	11.19
9.500	94.95	1,925	11,300	0.00	30,724,250	2,560.4	0	56,801,624	4,434,000	12.81
9.750	97.45	1,950	11,784	0.00	34,740,688	2,895.1	0	64,984,741	4,437,000	14.65
10.000	99.95	1,974	12,275	0.00	38,887,797	3,240.6	0	74,188,302	4,440,000	16.71

Corner Drop
05-16-1995, 15:38:39

*** PACKAGING TECHNOLOGY ***

CASKDROP, v2.21
Jul 01, 1994

SAMPLE PROBLEM FOR QUALITY ASSURANCE CHECK (AREAS AND VOLUMES)			
Impact Limiter Weight (each) -	1,000 lbs	Cask and Payload Weight -	10,000 lbs
Impact Limiter Outside Diameter -	60.0000 in	Cask Outside Diameter -	40.0000 in
Impact Limiter Overall Length -	24.0000 in	Cask Overall Length -	48.0000 in
Impact Limiter Conical Diameter -	48.0000 in	Dynamic Unloading Modulus -	1.000E+07 lbs/in
Impact Limiter Conical Length -	10.0000 in	Rad Mass Moment of Inertia -	12,235 lb-in-s²
Impact Limiter End Thickness -	12.0000 in	Frictional Coefficient -	0.0000
Impact Limiter Hole Diameter -	20.0000 in	Drop Height -	30.0000 ft
Impact Limiter Hole Length -	8.0000 in	Drop Angle from Horizontal -	45.0000°
Unbacked Area Threshhold Strain -	0.1000 in/in	Crush Analysis Theory -	Global
Unbacked Area Crush Stress -	2,611 psi	Number of Integration Incs -	25

POLYFOAM CRUSH STRESS (Axial: "∥" to rise)	
Density = 20.000 pcf	
Temp = -20.000 °F	
σ-yield = 2,552.3 psi	
Bias = 60.000%	
ε (in/in)	σ (psi)
0.000	0.0
0.100	2,552.3
0.200	2,687.0
0.300	2,868.8
0.400	3,302.9
0.500	4,115.1
0.600	6,074.3
0.650	7,942.0
0.700	10,925.0
0.750	15,001.8
0.800	26,829.5

POLYFOAM CRUSH STRESS (Radial: "⊥" to rise)	
Density = 20.000 pcf	
Temp = -20.000 °F	
σ-yield = 2,675.0 psi	
Bias = 60.000%	
ε (in/in)	σ (psi)
0.000	0.0
0.100	2,675.0
0.200	2,785.4
0.300	2,959.9
0.400	3,345.9
0.500	4,147.7
0.600	6,062.8
0.650	7,868.8
0.700	10,180.0
0.750	15,554.4
0.800	29,704.8

POLYFOAM CRUSH STRESS (Actual Data @ 45.0°)	
Density = 20.000 pcf	
Temp = -20.000 °F	
σ-yield = 2,611.5 psi	
Bias = 60.000%	
ε (in/in)	σ (psi)
0.000	0.0
0.100	2,611.5
0.200	2,734.9
0.300	2,913.3
0.400	3,324.2
0.500	4,131.3
0.600	6,068.5
0.650	7,905.2
0.700	10,532.8
0.750	15,270.6
0.800	28,157.6

DEFL (in)	MAX ε (%)	AREA (in2)	VOLUME (in3)	XBAR (in)	IMPACT FORCE (lbs)	ACCEL (g's)	I/L MOMENT (in-lbs)	STRAIN ENERGY (in-lbs)	KINETIC ENERGY (in-lbs)	SE/KE RATIO
0.250	1.44	7	1	-8.30	1,351	0.1	0	169	4,323,000	0.00
0.500	2.88	20	4	-8.11	7,756	0.6	0	1,307	4,326,000	0.00
0.750	4.33	36	11	-7.90	21,631	1.8	0	4,981	4,329,000	0.00
1.000	5.79	55	22	-7.68	44,807	3.7	0	13,286	4,332,000	0.00
1.250	7.25	78	39	-7.44	78,737	6.6	0	28,729	4,335,000	0.01
1.500	8.71	102	61	-7.19	124,483	10.4	0	54,131	4,338,000	0.01
1.750	10.18	129	90	-6.92	182,320	15.2	0	92,481	4,341,000	0.02

Corner Drop
05-16-1995, 15:38:39

*** PACKAGING TECHNOLOGY ***
(continued...)

CASKDROP, v2.21
Jul 01, 1994

DEFL (in)	MAX ε (%)	AREA (in2)	VOLUME (in3)	XBAR (in)	IMPACT FORCE (lbs)	ACCEL (g's)	I/L MOMENT (in-lbs)	STRAIN ENERGY (in-lbs)	KINETIC ENERGY (in-lbs)	SE/KE RATIO
2.000	11.66	158	126	-6.65	250,919	20.9	0	146,636	4,344,000	0.03
2.250	13.14	189	169	-6.39	327,791	27.3	0	218,975	4,347,000	0.05
2.500	14.63	222	221	-6.15	409,985	34.2	0	311,197	4,350,000	0.07
2.750	16.12	256	280	-5.92	495,229	41.3	0	424,349	4,353,000	0.10
3.000	17.64	290	349	-5.70	581,988	48.5	0	559,001	4,356,000	0.13
3.250	19.14	321	425	-5.53	666,955	55.6	0	715,119	4,359,000	0.16
3.500	21.04	350	509	-5.39	750,161	62.5	0	892,258	4,362,000	0.20
3.750	23.53	379	600	-5.30	832,241	69.4	0	1,090,058	4,365,000	0.25
4.000	26.04	407	698	-5.24	913,114	76.1	0	1,308,228	4,368,000	0.30
4.250	28.58	435	804	-5.21	993,967	82.8	0	1,546,613	4,371,000	0.35
4.500	31.14	462	916	-5.20	1,075,026	89.6	0	1,805,237	4,374,000	0.41
4.750	33.55	490	1,035	-5.22	1,157,389	96.4	0	2,084,289	4,377,000	0.48
5.000	35.86	517	1,161	-5.24	1,240,678	103.4	0	2,384,048	4,380,000	0.54
5.250	38.16	545	1,293	-5.27	1,325,202	110.4	0	2,704,783	4,383,000	0.62
5.500	40.44	573	1,433	-5.30	1,413,119	117.8	0	3,047,073	4,386,000	0.69
5.750	42.71	600	1,579	-5.33	1,503,231	125.3	0	3,411,616	4,389,000	0.78
6.000	44.96	628	1,733	-5.37	1,596,230	133.0	0	3,799,049	4,392,000	0.86
6.250	47.21	656	1,894	-5.40	1,692,397	141.0	0	4,210,127	4,395,000	0.96
6.359	48.17	668	1,966	-5.41	1,735,814	144.7	0	4,396,303	4,396,303	1.00
6.500	49.43	684	2,061	-5.42	1,792,981	149.4	0	4,837,403	4,398,000	1.10
6.750	51.75	711	2,236	-5.44	1,897,584	158.1	0	5,298,723	4,401,000	1.20
7.000	54.19	739	2,417	-5.46	2,009,560	167.5	0	5,787,116	4,404,000	1.31
7.250	56.65	767	2,605	-5.47	2,128,316	177.4	0	6,304,351	4,407,000	1.43
7.500	59.12	795	2,800	-5.48	2,255,709	188.0	0	6,852,354	4,410,000	1.55
7.750	61.60	824	3,002	-5.48	2,392,365	199.4	0	7,433,363	4,413,000	1.68
8.000	64.10	852	3,212	-5.47	2,538,941	211.6	0	8,049,776	4,416,000	1.82
8.250	66.60	881	3,429	-5.47	2,701,943	225.2	0	8,704,887	4,419,000	1.97
8.500	69.12	909	3,652	-5.45	2,882,629	240.2	0	9,402,959	4,422,000	2.13
8.750	71.65	938	3,883	-5.43	3,079,002	256.6	0	10,148,162	4,425,000	2.29
9.000	74.19	967	4,121	-5.38	3,300,885	275.1	0	10,945,648	4,428,000	2.47
9.250	76.75	995	4,367	-5.32	3,573,055	297.8	0	11,804,891	4,431,000	2.66
9.500	79.31	1,024	4,619	-5.26	3,901,592	325.1	0	12,739,222	4,434,000	2.87
9.750	81.89	1,053	4,879	-5.17	4,292,510	357.7	0	13,763,484	4,437,000	3.10
10.000	84.49	1,082	5,146	-5.06	4,763,070	396.9	0	14,895,432	4,440,000	3.35
10.250	87.09	1,109	5,419	-4.95	5,316,128	443.0	0	16,155,332	4,443,000	3.64
10.500	89.71	1,134	5,698	-4.83	5,947,562	495.6	0	17,563,293	4,446,000	3.95
10.750	92.34	1,161	5,985	-4.74	6,665,548	555.5	0	19,139,932	4,449,000	4.30
11.000	94.98	1,184	6,270	-4.63	7,465,195	622.1	0	20,906,275	4,452,000	4.70
11.250	97.64	1,206	6,563	-4.54	8,360,345	696.7	0	22,884,467	4,455,000	5.14

End Drop
05-16-1995, 15:38:39

*** PACKAGING TECHNOLOGY ***

CASKDROP, v2.21
Jul 01, 1994

SAMPLE PROBLEM FOR QUALITY ASSURANCE CHECK (AREAS AND VOLUMES)			
Impact Limiter Weight (each) -	1,000 lbs	Cask and Payload Weight -	10,000 lbs
Impact Limiter Outside Diameter -	60.0000 in	Cask Outside Diameter -	40.0000 in
Impact Limiter Overall Length -	24.0000 in	Cask Overall Length -	48.0000 in
Impact Limiter Conical Diameter -	48.0000 in	Dynamic Unloading Modulus -	1.000E+07 lbs/in
Impact Limiter Conical Length -	10.0000 in	Rad Mass Moment of Inertia -	12,235 lb-in-s²
Impact Limiter End Thickness -	12.0000 in	Frictional Coefficient -	0.0000
Impact Limiter Hole Diameter -	20.0000 in	Drop Height -	30.0000 ft
Impact Limiter Hole Length -	8.0000 in	Drop Angle from Horizontal -	90.0000°
Unbacked Area Threshhold Strain -	0.1000 in/in	Crush Analysis Theory -	Global
Unbacked Area Crush Stress -	2,552 psi	Number of Integration Incs -	25

POLYFOAM CRUSH STRESS (Axial: "∥" to rise)	
Density = 20.000 pcf Temp = -20.000 °F σ-yield = 2,552.3 psi Bias = 60.000%	
ε (in/in)	σ (psi)
0.000	0.0
0.100	2,552.3
0.200	2,687.0
0.300	2,868.8
0.400	3,302.9
0.500	4,115.1
0.600	6,074.3
0.650	7,942.0
0.700	10,925.0
0.750	15,001.8
0.800	26,829.5

POLYFOAM CRUSH STRESS (Radial: "⊥" to rise)	
Density = 20.000 pcf Temp = -20.000 °F σ-yield = 2,675.0 psi Bias = 60.000%	
ε (in/in)	σ (psi)
0.000	0.0
0.100	2,675.0
0.200	2,785.4
0.300	2,959.9
0.400	3,345.9
0.500	4,147.7
0.600	6,062.8
0.650	7,868.8
0.700	10,180.0
0.750	15,554.4
0.800	29,704.8

POLYFOAM CRUSH STRESS (Actual Data @ 90.0°)	
Density = 20.000 pcf Temp = -20.000 °F σ-yield = 2,552.3 psi Bias = 60.000%	
ε (in/in)	σ (psi)
0.000	0.0
0.100	2,552.3
0.200	2,687.0
0.300	2,868.8
0.400	3,302.9
0.500	4,115.1
0.600	6,074.3
0.650	7,942.0
0.700	10,925.0
0.750	15,001.8
0.800	26,829.5

DEFL (in)	MAX ε (%)	AREA (in2)	VOLUME (in3)	XBAR (in)	IMPACT FORCE (lbs)	ACCEL (g's)	I/L MOMENT (in-lbs)	STRAIN ENERGY (in-lbs)	KINETIC ENERGY (in-lbs)	SE/KE RATIO
0.250	2.08	1,518	377	0.00	810,360	67.5	0	101,295	4,323,000	0.02
0.500	4.17	1,541	759	0.00	1,592,808	132.7	0	401,691	4,326,000	0.09
0.750	6.25	1,564	1,147	0.00	2,311,804	192.7	0	889,768	4,329,000	0.21
1.000	8.33	1,587	1,541	0.00	2,931,701	244.3	0	1,545,206	4,332,000	0.36
1.250	10.42	1,610	1,941	0.00	3,416,844	284.7	0	2,338,774	4,335,000	0.54
1.500	12.50	1,634	2,346	0.00	3,752,646	312.7	0	3,234,960	4,338,000	0.75
1.750	14.58	1,657	2,758	0.00	3,971,661	331.0	0	4,200,498	4,341,000	0.97

End Drop
05-16-1995, 15:38:39

*** PACKAGING TECHNOLOGY ***
(continued...)

CASKDROP, v2.21
Jul 01, 1994

DEFL (in)	MAX ε (%)	AREA (in2)	VOLUME (in3)	XBAR (in)	IMPACT FORCE (lbs)	ACCEL (g's)	I/L MOMENT (in-lbs)	STRAIN ENERGY (in-lbs)	KINETIC ENERGY (in-lbs)	SE/KE RATIO
1.785	14.88	1,661	2,816	0.00	3,995,461	333.0	0	4,341,425	4,341,425	1.00
2.000	16.67	1,681	3,175	0.00	4,112,712	342.7	0	5,354,946	4,344,000	1.23
2.250	18.75	1,705	3,598	0.00	4,214,497	351.2	0	6,395,847	4,347,000	1.47
2.500	20.83	1,729	4,027	0.00	4,287,704	357.3	0	7,458,622	4,350,000	1.71
2.750	22.92	1,753	4,462	0.00	4,351,294	362.6	0	8,538,497	4,353,000	1.96
3.000	25.00	1,777	4,904	0.00	4,445,683	370.5	0	9,638,119	4,356,000	2.21
3.250	27.08	1,801	5,351	0.00	4,562,636	380.2	0	10,764,159	4,359,000	2.47
3.500	29.17	1,826	5,804	0.00	4,693,990	391.2	0	11,921,237	4,362,000	2.73
3.750	31.25	1,851	6,264	0.00	4,831,784	402.6	0	13,111,959	4,365,000	3.00
4.000	33.33	1,875	6,730	0.00	4,973,522	414.5	0	14,337,622	4,368,000	3.28
4.250	35.42	1,900	7,202	0.00	5,120,673	426.7	0	15,599,396	4,371,000	3.57
4.500	37.50	1,925	7,680	0.00	5,274,868	439.6	0	16,898,839	4,374,000	3.86
4.750	39.58	1,951	8,164	0.00	5,437,800	453.2	0	18,237,922	4,377,000	4.17
5.000	41.67	1,976	8,655	0.00	5,611,685	467.6	0	19,619,108	4,380,000	4.48
5.250	43.75	2,002	9,152	0.00	5,802,397	483.5	0	21,045,868	4,383,000	4.80
5.500	45.83	2,027	9,656	0.00	6,018,789	501.6	0	22,523,516	4,386,000	5.14
5.750	47.92	2,053	10,166	0.00	6,268,472	522.4	0	24,059,424	4,389,000	5.48
6.000	50.00	2,079	10,682	0.00	6,560,063	546.7	0	25,662,991	4,392,000	5.84
6.250	52.08	2,105	11,205	0.00	6,900,740	575.1	0	27,345,591	4,395,000	6.22
6.500	54.17	2,131	11,735	0.00	7,296,837	608.1	0	29,120,288	4,398,000	6.62
6.750	56.25	2,158	12,271	0.00	7,751,903	646.0	0	31,001,381	4,401,000	7.04
7.000	58.33	2,184	12,814	0.00	8,272,373	689.4	0	33,004,415	4,404,000	7.49
7.250	60.42	2,211	13,363	0.00	8,862,880	738.6	0	35,146,322	4,407,000	7.98
7.500	62.50	2,238	13,919	0.00	9,556,877	796.4	0	37,448,792	4,410,000	8.49
7.750	64.58	2,265	14,482	0.00	10,454,871	871.2	0	39,950,260	4,413,000	9.05
8.000	66.67	2,606	15,051	0.00	11,632,851	969.4	0	42,711,226	4,416,000	9.67
8.250	68.75	2,633	15,706	0.00	13,506,993	1,125.6	0	45,853,706	4,419,000	10.38
8.500	70.83	2,660	16,368	0.00	14,954,954	1,246.2	0	49,411,449	4,422,000	11.17
8.750	72.92	2,688	17,037	0.00	16,218,008	1,351.5	0	53,308,070	4,425,000	12.05
9.000	75.00	2,715	17,712	0.00	18,519,890	1,543.3	0	57,650,307	4,428,000	13.02
9.250	77.08	2,743	18,394	0.00	22,571,268	1,880.9	0	62,786,702	4,431,000	14.17
9.500	79.17	2,771	19,084	0.00	27,794,818	2,316.2	0	69,082,462	4,434,000	15.58
9.750	81.25	2,799	19,780	0.00	33,405,583	2,783.8	0	76,732,513	4,437,000	17.29
10.000	83.33	2,827	20,483	0.00	39,286,171	3,273.8	0	85,818,982	4,440,000	19.33
10.250	85.42	2,827	21,190	0.00	45,050,964	3,754.2	0	96,361,124	4,443,000	21.69
10.500	87.50	2,827	21,897	0.00	51,018,884	4,251.6	0	108,369,855	4,446,000	24.37
10.750	89.58	2,827	22,604	0.00	57,507,705	4,792.3	0	121,935,678	4,449,000	27.41
11.000	91.67	2,827	23,311	0.00	64,451,479	5,371.0	0	137,180,576	4,452,000	30.81
11.250	93.75	2,827	24,017	0.00	74,690,773	6,224.2	0	154,573,358	4,455,000	34.70
11.500	95.83	2,827	24,724	0.00	85,563,336	7,130.3	0	174,605,121	4,458,000	39.17
11.750	97.92	2,827	25,431	0.00	96,435,898	8,036.3	0	197,355,026	4,461,000	44.24
12.000	100.00	2,827	26,138	0.00	107,308,461	8,942.4	0	222,823,071	4,464,000	49.92

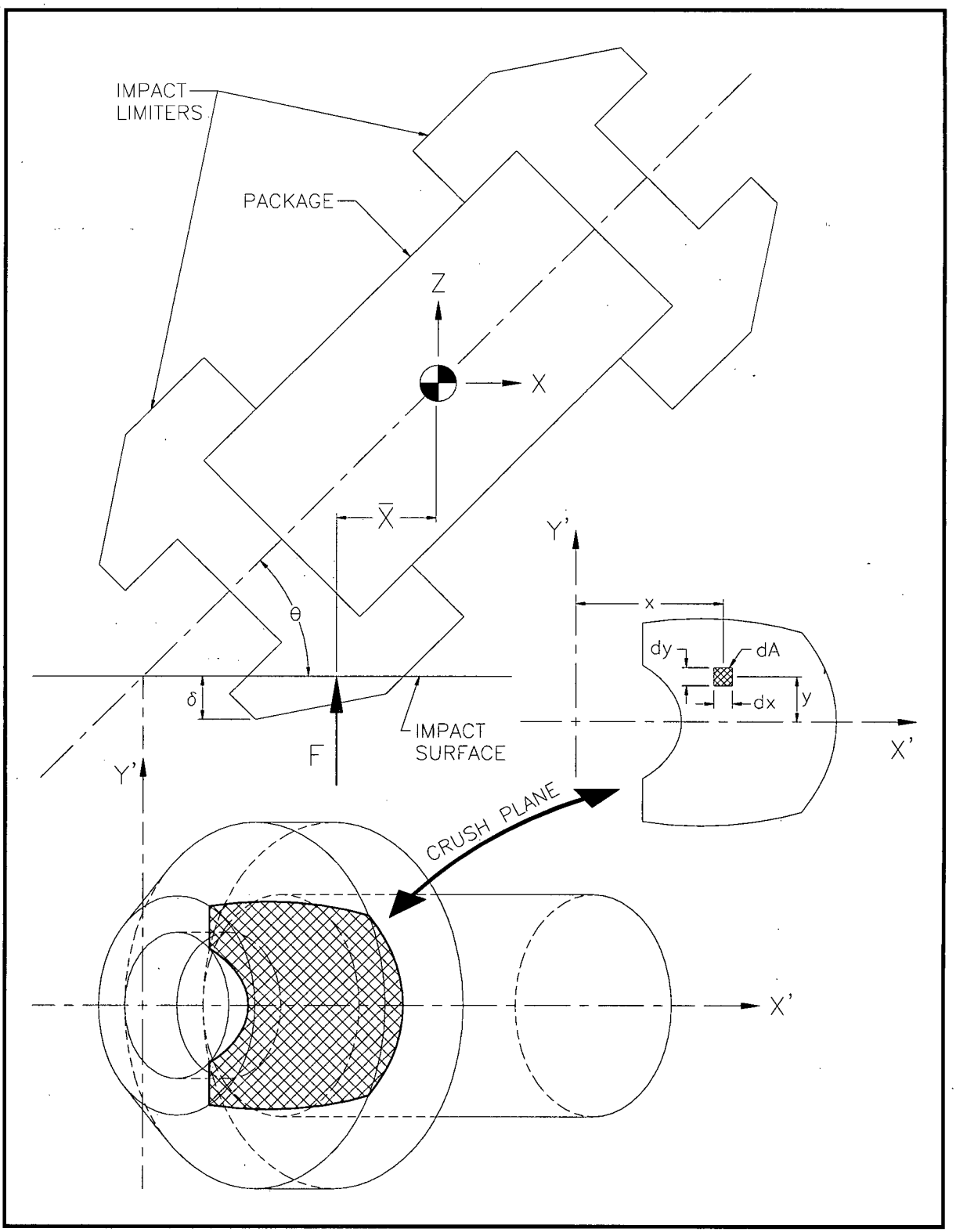

Figure 2.12.6-1 – Impact Limiter Force and Centroid Development

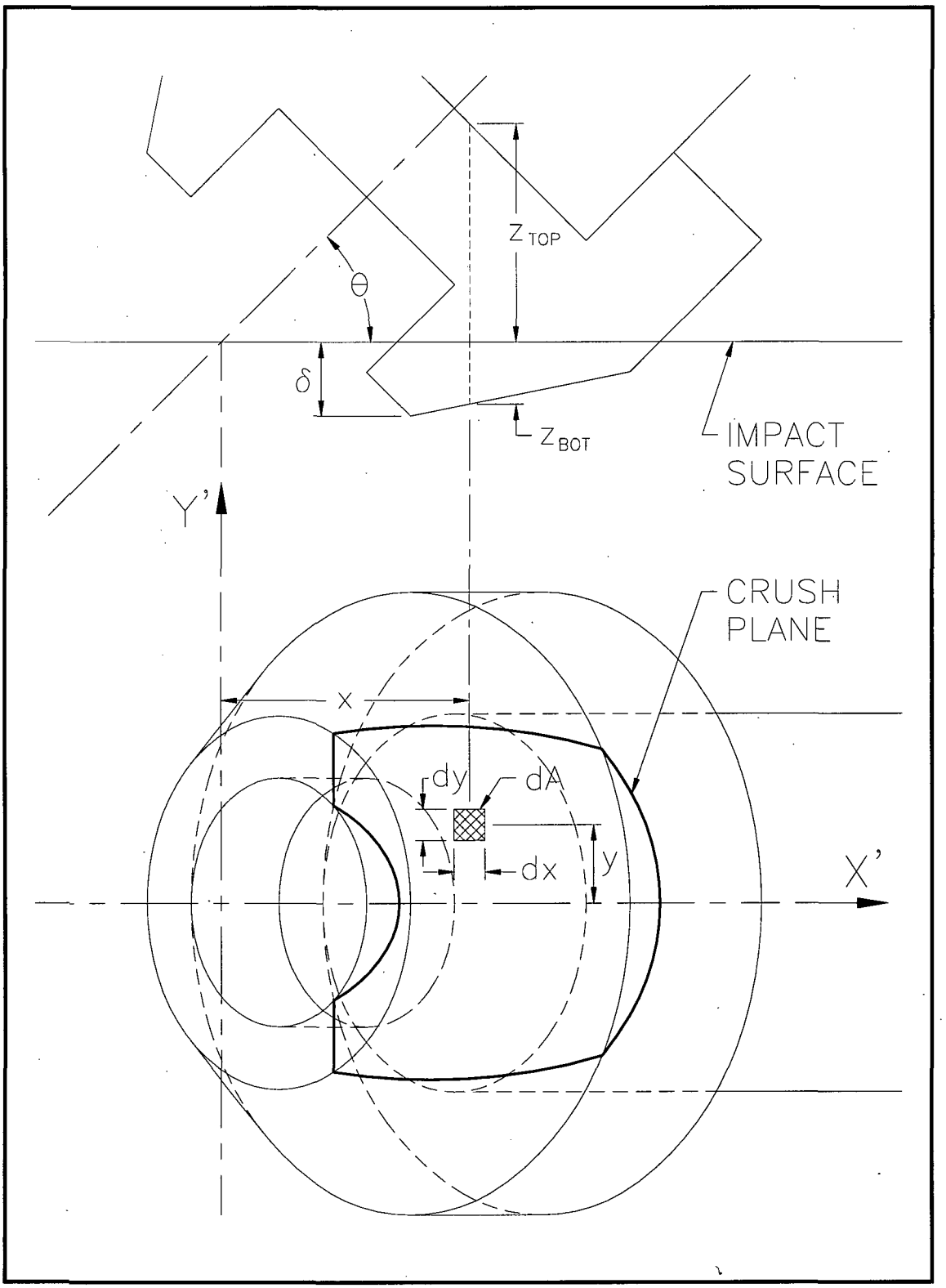

Figure 2.12.6-2 – Strain Determination

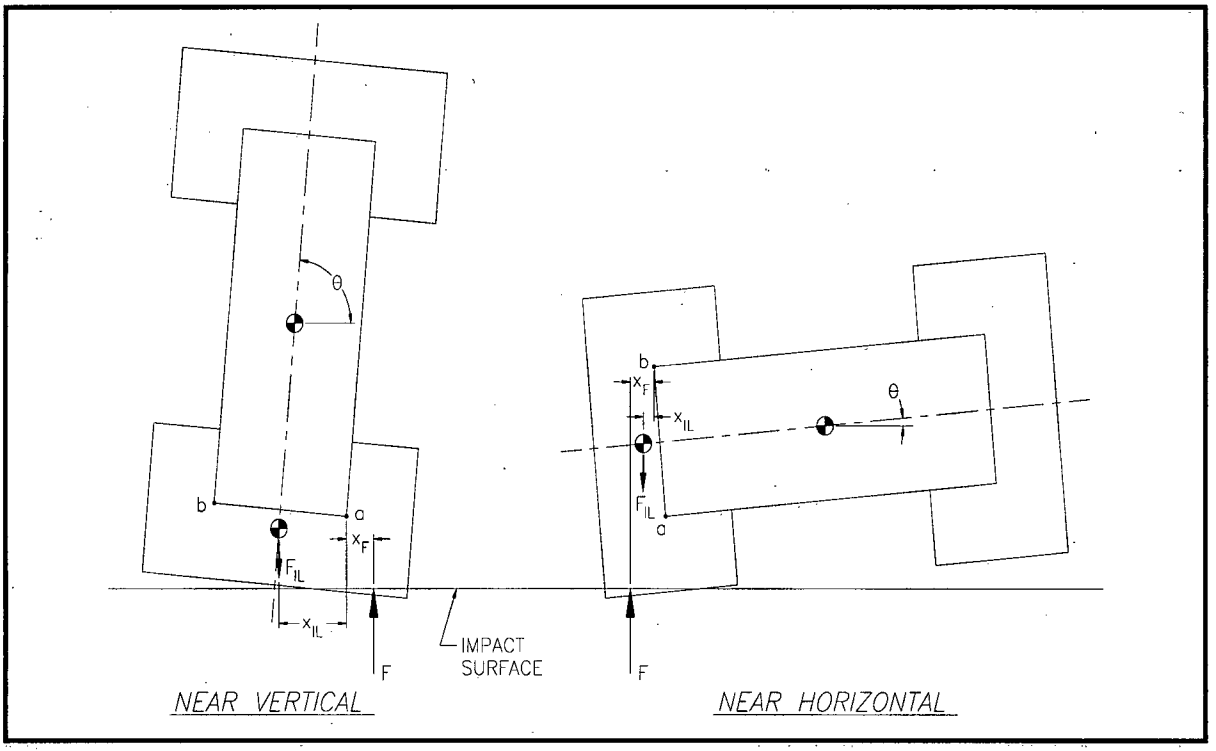

Figure 2.12.6-3 – Determination of Impact Limiter Separation Moments

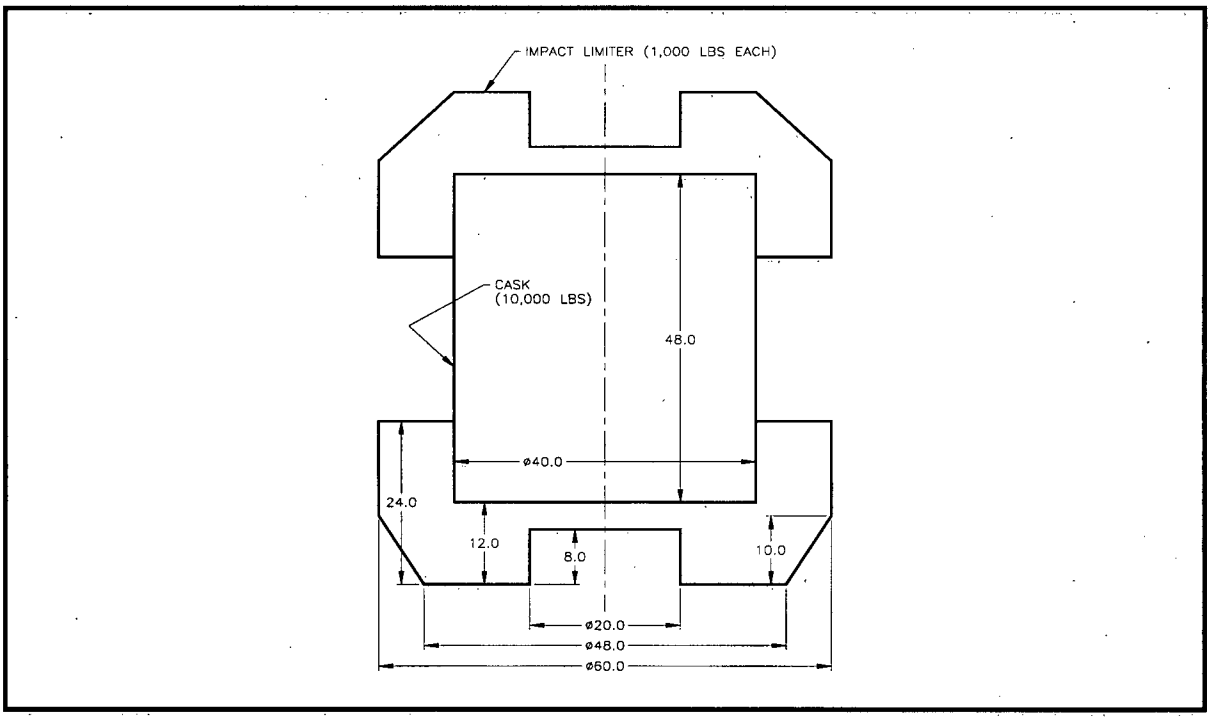

Figure 2.12.6-4 – Example Problem for CASKDROP

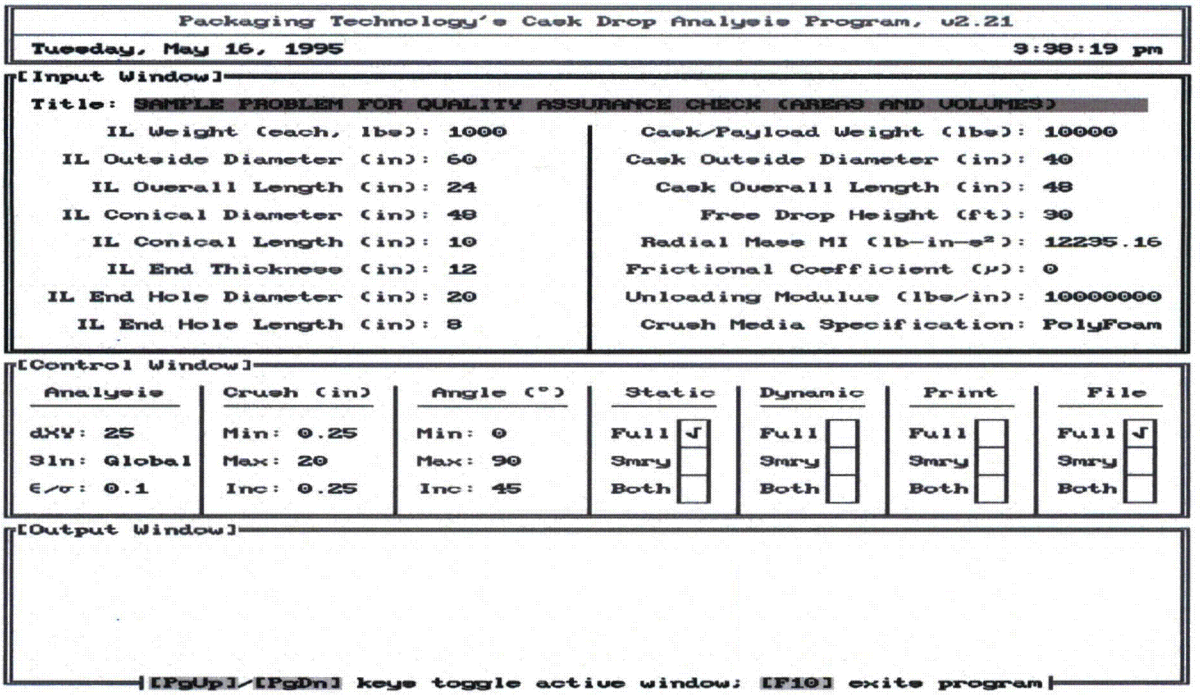

Figure 2.12.6-5 – The CASKDROP Program *Input Window*

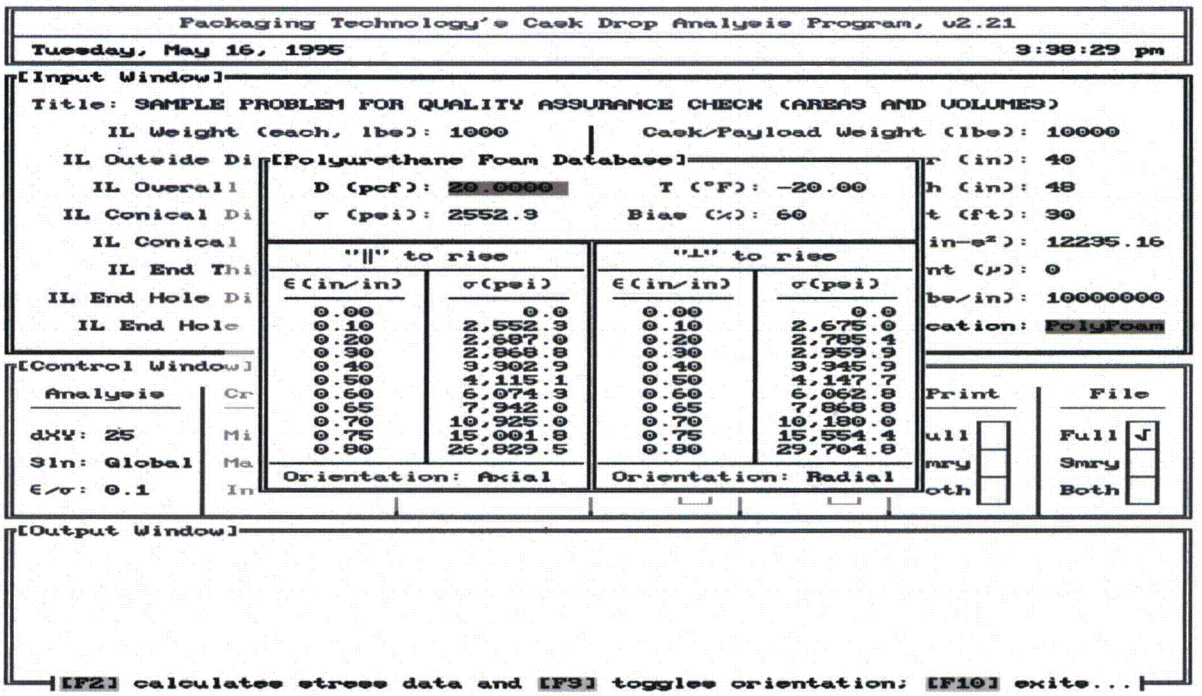

Figure 2.12.6-6 – The CASKDROP Program *Polyurethane Foam Window*

2.12.6.2 SLAPDOWN

Impact limiter deflections and package accelerations are calculated using the Sandia National Laboratories-developed computer code SLAPDOWN [30]. This program solves the rigid-body equations of motion for a transportation package, given parameters such as weight, rotational moment of inertia, geometric relationships, and impact limiter force-deflection curves. The output consists of maximum impact limiter deformations and a time history of the parameters of motion (of principal interest, the acceleration at the center of gravity and angular acceleration). From these outputs, accelerations at any point on the package are found. Figure 2.12.6-7 shows the geometric parameters used, and Table 2.12.6-1 lists the required input parameters.

With respect to Figure 2.12.6-7, the line connecting points 1, 2, and 3 is the centerline axis of the cask. Points 4 and 5 represent the points of contact of the impact limiter with the impact surface. It is shown with the cask axis at an angle θ to the horizontal, but may impact the ground at any angle, up to and including vertical. The primary end is the end of the cask which strikes the ground first, and the secondary end (the slapdown end) is the end which strikes the ground second. The distances R1 and R2 are the outer radii, respectively, of each impact limiter. The impact limiter forces (which act along the lines of R1 and R2) are assumed to be always perpendicular to the impact surface, which is consistent with the assumption for each orientation that the force-deflection curve is defined perpendicular to the surface. The impact limiters are modeled as nonlinear, inelastic springs, and consist of the force-deflection relations developed in Section 2.12.6.1, *CASKDROP*. The elastic rebound stiffness determines how much of the energy absorbed by the limiter (the area under the force-deflection curve) is elastically recovered. Elastic rebound stiffness has a small effect on SLAPDOWN response, and is normally set at a value of 10^7 lb/in. The equations of motion are solved for all five nodes. The center of gravity (C.G.) is taken as the geometric center of the cask. Friction is assigned a value of zero, since this maximizes the impact forces and deflections for the secondary (slapdown) impact limiter.

Table 2.12.6-1 shows a listing of sample input for the SLAPDOWN program. Table 2.12.6-2 shows a listing of sample force-deflection data for the SLAPDOWN program. The force-deflection data for the primary impact limiter are obtained from CASKDROP for the stated primary impact orientation. The secondary impact limiter data is for a horizontal orientation. Table 2.12.6-3 shows a sample output of the SLAPDOWN program from the general output file. This is performed for a 15° primary oblique orientation. The angle of secondary contact with the ground surface is displayed at the end of the output list ("Tail Impact Angle"), and is nearly equal to zero, thus the horizontal orientation force-deflection data for the secondary impact is justified.

Table 2.12.6-4 shows a portion of the corresponding time history output file, showing the results only through the end of the primary impact. The time variable is given in the first column. In the second, third and fourth columns are given the results at the cask center of gravity (SLAPDOWN node 2): the vertical position is in the column headed POSY(2) (inches), the velocity is in the column headed VELY(2) (in/s), and the acceleration is in the column headed ACCY(2) (in/s^2). The last three columns give the rotational parameters of angular position: the angle THETA (radians, horizontal is zero), the angular velocity OMEGA (r/s) and the angular acceleration ALPHA (r/s^2).

As verification of the SLAPDOWN code analysis methodology, the sample problem described above was compared to output from the public domain program SCANS [31]. The results compare well, as demonstrated in Table 2.12.6-5. Input data for the comparison is taken from Table 2.12.6-1.

Table 2.12.6-1 – Sample Inputs to the SLAPDOWN Program

Input Parameter	Description	Sample Value
Z1, Z2	Length from primary end to C.G., and from C.G. to secondary end, respectively (inch)*	90.38 (both sides)
R1, R2	Length from cask axis to impact limiter contact point, primary and secondary ends, respectively (inch)	63.0 (both ends)
$\mu 1$, $\mu 2$	Coefficient of friction, primary and secondary ends, respectively	0.0 (both ends)
m	Overall package mass (lb-s^2/inch)	611.0
I_{cg}	Radial mass moment of inertia about the package C.G. (in-lb-s^2)	$3.1(10)^6$
h	Drop height (ft)	30
θ	Angle with respect to horizontal of primary impact	Variable (15° used for example)
k	Elastic rebound stiffness of the impact limiter material (lb/inch)	10^7

*This dimension is measured from the cask C.G. to the center of the cylindrical portion of the impact limiter, which is the location of the line of action of side drop impact force.

Table 2.12.6-2 – Sample Force-Deflection to the SLAPDOWN Program

Primary Impact Limiter		Secondary Impact Limiter	
Deflection (in)	**Force (lb)**	**Deflection (in)**	**Force (lb)**
0	0	0	0
1	207,100	1	2,383,000
2	583,900	2	3,363,000
3	1,069,000	3	3,963,000
4	1,640,000	4	4,450,000
5	2,285,000	5	4,885,000
6	2,998,000	6	5,289,000
7	3,767,000	7	5,671,000
8	4,444,000	8	6,041,000
9	5,146,000	9	6,310,000
10	5,756,000	10	6,513,000
11	6,304,000	11	6,721,000
12	6,818,000	12	6,936,000
13	7,223,000	13	7,157,000
14	7,573,000	14	7,384,000
15	7,926,000	15	7,614,000

Table 2.12.6-3 – Sample of SLAPDOWN General Output

```
Sample Cask, 15 Degree Oblique

****** SEQUENCE OF EVENTS ******

 ** NOSE HIT      AT TIME 0.000E+0 VELOCITY = -5.275E+2  RATIO =  1.00E+0
 ** NOSE REBOUND AT TIME 3.311E-2 VELOCITY =  1.506E+1  RATIO = -2.86E-2
 ** NOSE UNLOAD  AT TIME 4.008E-2 VELOCITY =  1.346E+2  RATIO = -2.55E-1
 ** TAIL HIT      AT TIME 7.318E-2 VELOCITY = -7.061E+2  RATIO =  1.34E+0
 ** TAIL REBOUND AT TIME 1.037E-1 VELOCITY =  2.410E+1  RATIO = -4.57E-2
 ** TAIL UNLOAD  AT TIME 1.106E-1 VELOCITY =  1.422E+2  RATIO = -2.70E-1

Event over at time    0.11152      Time step size  0.00087
Time step multiplier  0.10         128 Plot times written to database


          DISPLACEMENT  VELOCITY    ACCELERATION

   NOSE    1.159E+1     1.346E+2    2.7317E+4  (MAX)
                       -5.275E+2   -7.2971E+3  (MIN)

   TAIL    1.206E+1     1.422E+2    2.9272E+4  (MAX)
                       -7.061E+2   -6.4780E+3  (MIN)

     CG                 2.781E+1    1.0987E+4  (MAX)
                       -5.277E+2   -3.8600E+2  (MIN)

ANGULAR                 1.267E+0    2.0245E+2  (MAX)
                       -4.623E+0   -1.8804E+2  (MIN)

MAXIMUM ENERGY:              3.4879E+7(NOSE)
MAXIMUM ENERGY:              5.9471E+7(TAIL)
IMPACT AT 80 IN FROM C.G. (x-n)       65.93(g)
IMPACT AT 80 IN FROM C.G. (x-t)       70.35(g)
TAIL IMPACT ANGLE =          1.91 DEG.
```

Table 2.12.6-4 – Sample of SLAPDOWN Time History Output

Title: Sample Cask, 15 Degree Oblique

9/29/2008 10:39:46 AM

Time,S	POSY(2)	VELY(2)	ACCY(2)	THETA	OMEGA	ALPHA
.0000E+0	.8639E+2	-.5275E+3	-.3860E+3	.2618E+0	.0000E+0	.0000E+0
.8712E-3	.8593E+2	-.5277E+3	-.2302E+3	.2618E+0	-.2335E-2	-.2680E+1
.1742E-2	.8547E+2	-.5277E+3	-.7449E+2	.2618E+0	-.7005E-2	-.5360E+1
.2614E-2	.8501E+2	-.5276E+3	.1862E+3	.2618E+0	-.1558E-1	-.9846E+1
.3485E-2	.8455E+2	-.5271E+3	.4689E+3	.2618E+0	-.2840E-1	-.1471E+2
.4356E-2	.8409E+2	-.5264E+3	.8029E+3	.2618E+0	-.4622E-1	-.2046E+2
.5227E-2	.8364E+2	-.5254E+3	.1164E+4	.2617E+0	-.6946E-1	-.2668E+2
.6098E-2	.8318E+2	-.5241E+3	.1552E+4	.2617E+0	-.9851E-1	-.3334E+2
.6970E-2	.8272E+2	-.5224E+3	.1972E+4	.2616E+0	-.1339E+0	-.4057E+2
.7841E-2	.8227E+2	-.5203E+3	.2399E+4	.2614E+0	-.1756E+0	-.4792E+2
.8712E-2	.8181E+2	-.5178E+3	.2863E+4	.2613E+0	-.2243E+0	-.5592E+2
.9583E-2	.8136E+2	-.5149E+3	.3321E+4	.2611E+0	-.2799E+0	-.6380E+2
.1045E-1	.8091E+2	-.5116E+3	.3817E+4	.2609E+0	-.3429E+0	-.7233E+2
.1133E-1	.8047E+2	-.5078E+3	.4306E+4	.2606E+0	-.4133E+0	-.8076E+2
.1220E-1	.8003E+2	-.5036E+3	.4807E+4	.2602E+0	-.4912E+0	-.8939E+2
.1307E-1	.7959E+2	-.4990E+3	.5312E+4	.2598E+0	-.5766E+0	-.9809E+2
.1394E-1	.7915E+2	-.4939E+3	.5801E+4	.2593E+0	-.6694E+0	-.1065E+3
.1481E-1	.7872E+2	-.4885E+3	.6221E+4	.2587E+0	-.7686E+0	-.1138E+3
.1568E-1	.7830E+2	-.4827E+3	.6628E+4	.2580E+0	-.8738E+0	-.1208E+3
.1655E-1	.7788E+2	-.4766E+3	.7025E+4	.2573E+0	-.9850E+0	-.1277E+3
.1742E-1	.7746E+2	-.4702E+3	.7416E+4	.2564E+0	-.1102E+1	-.1344E+3
.1830E-1	.7705E+2	-.4634E+3	.7790E+4	.2554E+0	-.1225E+1	-.1409E+3
.1917E-1	.7665E+2	-.4563E+3	.8132E+4	.2544E+0	-.1353E+1	-.1469E+3
.2004E-1	.7625E+2	-.4490E+3	.8426E+4	.2532E+0	-.1485E+1	-.1520E+3
.2091E-1	.7586E+2	-.4414E+3	.8704E+4	.2519E+0	-.1622E+1	-.1568E+3
.2178E-1	.7547E+2	-.4336E+3	.8964E+4	.2505E+0	-.1762E+1	-.1614E+3
.2265E-1	.7510E+2	-.4256E+3	.9189E+4	.2489E+0	-.1906E+1	-.1653E+3
.2352E-1	.7472E+2	-.4174E+3	.9391E+4	.2473E+0	-.2054E+1	-.1689E+3
.2439E-1	.7436E+2	-.4090E+3	.9577E+4	.2455E+0	-.2204E+1	-.1722E+3
.2527E-1	.7400E+2	-.4005E+3	.9746E+4	.2436E+0	-.2356E+1	-.1752E+3
.2614E-1	.7366E+2	-.3919E+3	.9897E+4	.2415E+0	-.2511E+1	-.1779E+3
.2701E-1	.7331E+2	-.3832E+3	.1002E+5	.2393E+0	-.2668E+1	-.1802E+3
.2788E-1	.7298E+2	-.3744E+3	.1013E+5	.2370E+0	-.2827E+1	-.1822E+3
.2875E-1	.7265E+2	-.3654E+3	.1023E+5	.2345E+0	-.2987E+1	-.1839E+3
.2962E-1	.7234E+2	-.3565E+3	.1030E+5	.2319E+0	-.3148E+1	-.1853E+3
.3049E-1	.7203E+2	-.3474E+3	.1036E+5	.2292E+0	-.3311E+1	-.1864E+3
.3136E-1	.7172E+2	-.3384E+3	.1040E+5	.2263E+0	-.3474E+1	-.1873E+3
.3223E-1	.7143E+2	-.3293E+3	.1042E+5	.2233E+0	-.3638E+1	-.1878E+3
.3311E-1	.7114E+2	-.3202E+3	.1043E+5	.2201E+0	-.3801E+1	-.1880E+3
.3398E-1	.7086E+2	-.3111E+3	.1042E+5	.2168E+0	-.3965E+1	-.1880E+3
.3485E-1	.7059E+2	-.3027E+3	.9658E+4	.2134E+0	-.4118E+1	-.1749E+3
.3572E-1	.7033E+2	-.2951E+3	.8787E+4	.2098E+0	-.4257E+1	-.1598E+3
.3659E-1	.7007E+2	-.2884E+3	.7627E+4	.2061E+0	-.4378E+1	-.1397E+3
.3746E-1	.6982E+2	-.2830E+3	.6214E+4	.2022E+0	-.4479E+1	-.1152E+3
.3833E-1	.6957E+2	-.2790E+3	.4593E+4	.1983E+0	-.4555E+1	-.8695E+2
.3920E-1	.6933E+2	-.2766E+3	.2814E+4	.1944E+0	-.4603E+1	-.5594E+2
.4008E-1	.6909E+2	-.2757E+3	.9348E+3	.1904E+0	-.4623E+1	-.2310E+2
.4095E-1	.6885E+2	-.2761E+3	-.3860E+3	.1863E+0	-.4623E+1	.0000E+0

Table 2.12.6-5 – Comparison of SLAPDOWN and SCANS Results

Parameter	SLAPDOWN Result	SCANS Result
Primary impact limiter deflection, inch	11.6	11.6
Secondary impact limiter deflection, inch	12.1	12.1
Primary vertical acceleration (e.g.), g	26.9	26.8
Secondary vertical acceleration (e.g.), g	28.5	28.5
Primary angular acceleration, radians/s^2	-188	-186
Secondary angular acceleration, radians/s^2	202	218

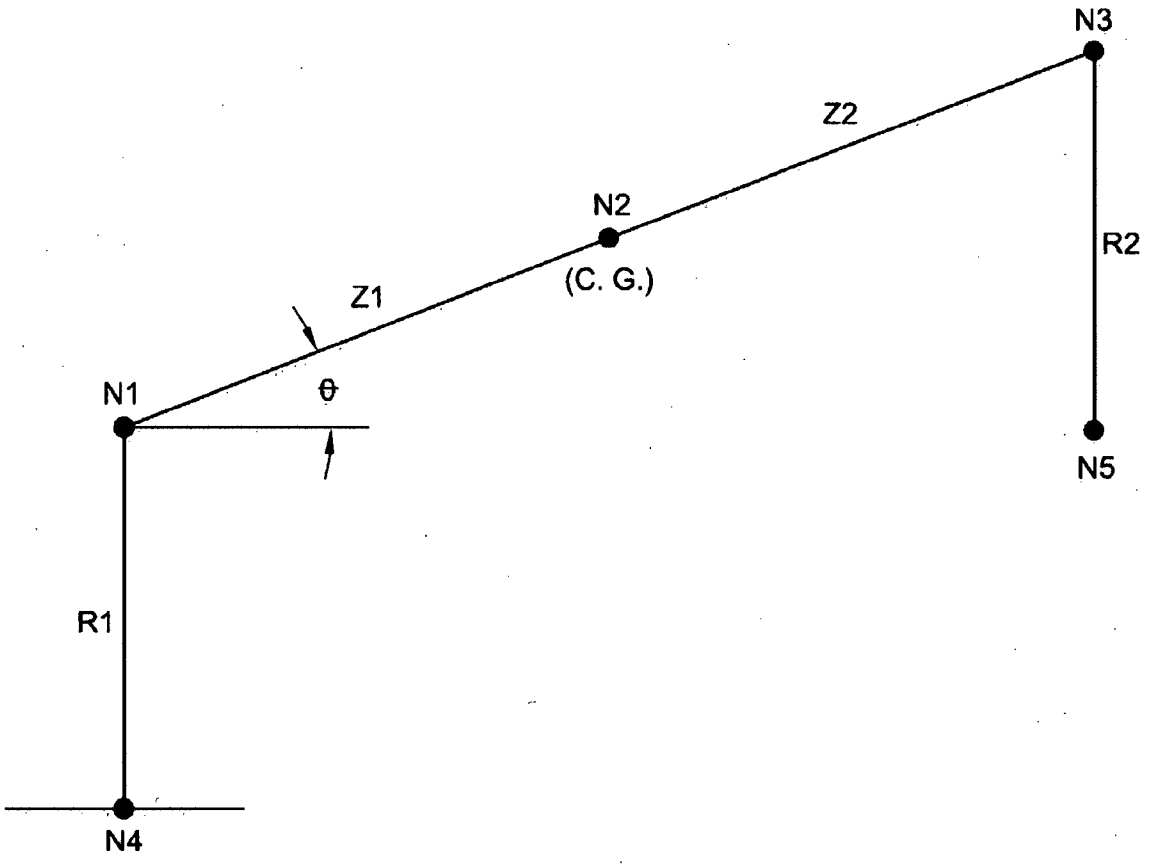

Figure 2.12.6-7 – SLAPDOWN Analytical Model

2.12.7 Seal Performance Tests

This appendix contains descriptions of the performance tests which have been run on the butyl rubber compound used for the containment O-ring seal and sealing washers used in the BRR package. The material is designated as Rainier Rubber R-0405-70. The performance tests which will be discussed have demonstrated the ability of this material to maintain a leaktight[1] containment boundary under minimum compression, minimum temperature, and maximum temperature conditions which are beyond those experienced in the BRR package.

2.12.7.1 Performance Tests Associated with the TRUPACT-II Package

Two sets of butyl rubber performance tests have been done in support of the TRUPACT-II package certification (NRC Docket 71-9218). All relevant tests have used a bore-type fixture which is consistent with the configuration of the O-ring seals in the TRUPACT-II.

The test configuration and procedure was similar between the two tests and will now be briefly described. More details are available in Section 2.10.7.4 and Section 2.10.7.4A of [2]. Only the small test fixture is considered, since it was used in both sets of tests. The test fixture consists of an inner ring containing two O-ring grooves on its outer diameter and an outer ring which fits over the inner ring and provides compression of the two test O-rings. The cross-sectional diameter of the test O-rings was nominally 0.400 inches, which is essentially equivalent to the 0.375 nominal dimension of the BRR package containment O-ring seal. To vary the O-ring compression in the test fixture, the radial position of the inner ring was controlled by jacking screws. When the inner ring was shifted to one side within the outer ring, a maximum compression was obtained on the side toward which the inner ring was shifted, and a minimum compression was obtained on the opposite side. The entire fixture could be placed in an environmental chamber and either cooled or heated for a set time. A helium leakage rate test was performed at various stages by testing the leakage rate between the outside of the fixture and the space between the two test O-rings.

The first set of tests was performed in 1989 and is documented in Section 2.10.7.4 of [2]. A typical test sequence consisted of the following steps:

1. Assemble the test fixture at ambient conditions.
2. Perform a leakage rate test with the inner ring centered in the outer ring.
3. Chill the fixture to -40 °F and perform a helium leakage rate test.
4. Allow the fixture to warm to -20 °F.
5. Shift the inner ring laterally within the outer ring to achieve maximum compression on one side and minimum compression on the other side.
6. Perform a helium leakage rate test with the fixture still at -20 °F.
7. Heat to an elevated temperature, maintaining the inner ring in the shifted position.

[1] Leaktight is defined as a maximum leakage rate of 1×10^{-7} ref-cc/sec, air, per [1].

8. Hold at temperature for 8 hours. Create a hard vacuum between the two test O-rings to confirm their integrity. A helium leakage rate test was not performed due to the tendency toward rapid saturation of the O-rings with helium at elevated temperature.
9. Chill the fixture to -20 °F, maintaining the inner ring in the shifted position.
10. Perform a final helium leakage rate test with the fixture still at -20 °F.

For each test, the maximum and minimum compressions were calculated using the dimensions of the fixture and of the test O-rings. The principal result of these tests was a demonstration that the subject rubber compound is capable of maintaining a leaktight condition at -20 °F with a minimum compression of 14.9% subsequent to an 8 hour soak at 400 °F. Details of the five small fixture tests are given in Table 2.12.7-1, adapted from Table 2.10.7-1 of [2]. Note that the term 'disk' in the table corresponds to the term 'inner ring' used in this description.

The second set of tests was performed in 1999, and are documented in Section 2.10.7.4A of [2]. These tests served to lower the minimum compression value at which a leaktight condition was demonstrated to be maintained. The tests used the same small test fixture, modified to allow it to achieve a lower minimum compression. The same test procedure was followed, except that all tests were run at a temperature of 400 °F. The principal result of these tests was a demonstration that the subject rubber compound is capable of maintaining a leaktight condition at -20 °F with a minimum compression of 12.9% subsequent to an 8 hour soak at 400 °F. Details of the three tests are given in Table 2.12.7-2, adapted from Table 2.10.7.4A-2 of [2].

2.12.7.2 Performance Tests Associated with the RTG Package

2.12.7.2.1 Face Seal Tests

O-ring tests were also performed in support of the Radioisotope Thermoelectric Generator (RTG) package certification (DOE Docket 94-6-9904). The results are reported in Section 2.10.6 of [3]. In these tests, a face-type fixture was used which permitted four different compressions to be tested at once. Unlike the TRUPACT-II testing, and consistent with the conditions in a face-type configuration, the O-rings were not mechanically moved or disturbed throughout the test. The fixture consisted of an inner plate having three concentric grooves on each side. Each groove had a different depth and contained an O-ring made from butyl compound R-0405-70 as described above. The inner and outer O-rings on each side were the test specimens; the center O-rings were used only to support leakage rate testing of the test specimens. The O-rings were compressed by outer plates which were set off from the inner plate by shims which, along with the groove depths, controlled the amount of compression of each test O-ring. The nominal test O-ring cross-sectional diameter was 0.275 inches. The minimum compression created by the fixture was 10%, which was uniform around the entire circumference of the fixture. Compressions of 12%, 14%, and 15.5% were tested at the same time. The dimensions of the fixture and of the test specimens, and the resulting compression values, are shown in Table 2.12.7-3.

The time/temperature sequence was as follows:

1. Assemble the test fixture at ambient conditions and perform a helium leakage rate test.
2. Chill the fixture to -40 °F and perform a helium leakage rate test.

3. Heat the fixture to 380 °F, and hold for 24 hours. Confirm integrity of the test O-rings by placing a hard vacuum on the test cavity (less than 0.2 mbar).
4. Allow the fixture to cool to 350 °F, and hold for 144 hours. The total time at elevated temperature is 168 hours, or one full week. Confirm integrity of the test O-rings by placing a hard vacuum on the test cavity (less than 0.2 mbar).
5. Cool the fixture to -20 °F and perform a final helium leakage rate test.

Each of the helium leakage rate tests demonstrated a leakage rate below the leaktight criterion of 1×10^{-7} ref-cc/sec, air, as defined by [1]. Of note, only the results from the outer O-ring tests (10% and 14% compression) were available at the time of publication of [3]. The successful completion of the inner O-ring tests (12% and 15.5% compression) was confirmed in [4].

2.12.7.2.2 Bore Seal Tests

Further O-ring tests were performed by Westinghouse Hanford Company in association with the RTG package, and documented in [5] and [6][2]. In these tests, the same bore-type fixture was used as that used for the TRUPACT-II tests described in Section 2.12.7.1, *Performance Tests Associated with the TRUPACT-II Package*. The procedure differed slightly in that a cold shift (step no. 5 from Section 2.12.7.1) was not performed. The test sequence was as follows:

1. Assemble the fixture at ambient conditions, and shift the inner ring fully to one side, generating minimum compression on one side and maximum on the other. Perform a helium leakage rate test.
2. Chill the fixture to -40 °F and perform a helium leakage rate test.
3. Heat to the specified elevated temperature and hold for the specified time. At the end of the hold time, perform a helium leakage rate test (saturation with helium at the high temperature was not reported to have had an effect on the helium leakage rate test).
4. Chill the fixture to -20 °F and perform the final helium leakage rate test.

For each test, the maximum and minimum compressions were calculated using the dimensions of the fixture and of the test O-rings. A number of different time/temperature tests were run, showing leaktight performance of the butyl material for 430 °F for one hour [6], 375 °F for 25 hours [6], and 350 °F for 168 hours [5]. Data is summarized in Table 2.12.7-4.

2.12.7.3 Long Term Performance of Butyl Rubber Seals

The tests of the Rainier Rubber R-0405-70 compound described in this appendix were performed at relatively high temperatures for relatively short times, consistent with the HAC fire event. Demonstration of the performance of the material at the lower temperature and longer duration associated with the NCT hot environment is made by extrapolation of this data.

Reference 7 uses thermogravimetric analysis to predict the relative lifetimes of some elastomers. One of the results of this study is to show that elastomer lifetime is linear when plotted on a log-

[2] Note that some of the test reports refer to the material as 'RR-0405-70' while in some instances, 'R-0405-70' is used. Both refer to the same compound, where 'RR' is used for uncured material, and 'R' for a cured product form. All testing was performed on cured material.

lifetime (ordinate) vs. 1000/Temp (K) (abscissa) scales. This is shown in figure 3 of [7], which is reproduced as Figure 2.12.7-1. The curve for butyl will not necessarily have the same slope or be placed in the same position relative to the scales as is shown in the figure. The position and slope for butyl will need to be established using the test data. Then, using linear extrapolation, its performance at longer lifetimes can be found. Note, since the abscissa is based on the inverse of temperature, temperature is actually decreasing along the abscissa towards the right, even though the values of 1000/Temp (K) are increasing. Consequently, the longest lifetimes correlate to the lowest temperature, as expected.

Figure 2.12.7-2 shows several time/temperature data points from the tests discussed above, along with the best-fit line through the data. For consistency, only data from the bore-type test fixture are considered. Note that this is not a locus of exact failure points (points defining the border between pass/fail), but of tests that passed (i.e., met the leaktight requirements of [1]). The possibility exists that some or all of these tests were "undertests", i.e., were not tested to the extreme limit of the material. Because the margin to failure may be different for each test, the actual locus of borderline results (zero-margin pass) may have a shallower slope than the best-fit curve to the data. If that curve were used to extrapolate upward to longer lifetimes, it might over predict the acceptable temperature (recall that temperature is decreasing to the right).

For the BRR package, it is desired to determine the acceptable temperature for leaktight performance for a duration of one year (8,760 hours). The most conservative extrapolation (the lowest acceptable temperature) will be generated from the data curve fit having the shallowest (conservative) slope. To find the shallowest slope, a data point for a test failure (450 °F for 8 hours) is introduced, as shown in Figure 2.12.7-3. This is taken from the TRUPACT-II test results shown in Table 2.12.7-1. The straight line between this failure point and the longest-term successful data point (350 °F for 168 hours) has the shallowest slope which is consistent with the known data points. This can be concluded from the following observations:

1. The 450 °F/8 hour data point cannot be an undertest, since it is a known failure. Therefore, the actual zero-margin pass temperature must lie to the right of, but not to the left of, the test data point.
2. The 350 °F/168 hour data point is likely somewhat undertested. Therefore, the actual zero-margin pass temperature must lie to the left of, but not to the right of, the test data point.
3. Consequently, the actual locus of zero-margin performance could be steeper than, but could not be shallower than, the line formed by joining the 450 °F/8 hour and 350 °F/168 hour data points.

The equation of the line connecting these two data points is:

$$\mathrm{Log}_{10}(\mathrm{hrs}) = 5.396(1000/\mathrm{T(K)}) - 9.775$$

Using this expression, the maximum leak tight temperature for 8,760 hours (one year) is 249 °F. Therefore, the R-0405-70 butyl material can be held at at least 249 °F for one full year (constant temperature night/day) and is expected to be leak tight per ANSI N14.5. This is the most conservative extrapolation that can be made from the known data and is essentially equal to the long term limit for the butyl material of 250 °F which is stated in Section 3.2.2, *Technical Specification of Components*.

2.12.7.4 Summary

The butyl rubber compound used for the BRR package containment seals was tested in both a bore-type and a face-type test fixture at low compression and elevated temperature. In the bore-type testing, the O-rings were demonstrated to be helium leaktight at a temperature of -20 °F after a soak at 400 °F for 8 hours at a minimum compression of 11.9%. In the face-type testing, the O-rings were demonstrated to be helium leaktight at a temperature of -20 °F after a soak at 380 °F for 24 hours followed by a soak at 350 °F for 144 hours at a minimum compression of 10%. These compression and temperature/time conditions exceed the severity of those experienced in the BRR package. In addition, the seals are expected to be leaktight after one full year at a constant temperature of at least 249 °F. Because this value was conservatively obtained, the value of 250 °F used in Section 3.2.2, *Technical Specification of Components* is acceptable. The minimum compression of the BRR package containment seal O-ring is calculated in Section 4.1.3, *Seals*, and the maximum temperature under NCT and HAC is discussed in Chapter 3, *Thermal Evaluation.*

Table 2.12.7-1 – TRUPACT–II O-ring Seal Performance Test Results (1989)⑦

Test Number	O-ring Seal Cross-Sectional Diameter (inches)				Stretch (%)		Maximum Gap (inches)		Minimum Compression (%)				Soak Temperature and Helium Leakage Rate Test Results ④				
	O-ring Seal No. 1		O-ring Seal No. 2				Disk Center	Disk Offset	Disk Centered		Disk Offset		Disk Centered		Disk Offset		
	Min	Max	Min	Max	Min	Max			Min	Max	Min	Max	Ambient	-40 °F	-20 °F	8 hrs⑤	-20 °F
1	0.387	0.397	0.387	0.396	2.0	4.1	0.026	③	22.1	25.6	14.9	20.0	Yes	Yes	Yes	350 °F	Yes
2	0.388	0.398	0.387	0.398	2.0	4.1	0.029	0.050	21.3	25.1	15.7	19.7	Yes	Yes	⑥	450 °F	No
3	0.387	0.397	0.387	0.399	2.0	4.1	0.027	0.052	21.9	25.8	15.2	19.4	Yes	Yes	Yes	400 °F	Yes
4	②	②	②	②	2.0	4.1	0.027	0.053	21.9	25.8	**14.9**	19.1	Yes	Yes	Yes	**400 °F**	**Yes**
5	②	②	②	②	2.0	4.1	0.026	0.050	22.1	26.0	15.7	19.9	Yes	Yes	Yes	400 °F	Yes

Notes:

① Material for all O-ring seal test specimens was butyl rubber compound R-0405-70, Rainier Rubber Co., Seattle, WA.

② Not measured; calculations assume the worst case range as taken from Tests Numbers 1 - 3 (i.e., Ø0.387 minimum to Ø0.399 maximum).

③ Range of values is 0.048 in. minimum to 0.053 in. maximum due to an indirect method of gap measurement (used for this test only).

④ A "Yes" response indicates that helium leakage rate testing demonstrated a leaktight condition as defined in [1], i.e., the leakage rate was less than or equal to 1×10^{-7} ref-cc/sec, air. In all cases, measured leak rates were less than or equal to 2.0×10^{-8} ref cc/s, helium, for tests with a "Yes" response.

⑤ No helium leakage rate tests were performed at elevated temperatures due to O-ring seal permeation and saturation by helium gas. The ability of the test fixture to establish a rapid, hard vacuum between the O-ring seals was used as the basis for leakage rate test acceptance at elevated temperatures. All tests rapidly developed a hard vacuum, with the exception of Test Number 2 at an elevated temperature of 450 °F, which slowly developed a vacuum.

⑥ Initial leakage rate of 1.0×10^{-5} ref cc/s, helium; became leaktight approximately one minute later.

⑦ Adapted from Table 2.10.7-1 of [2].

Table 2.12.7-2 – Supplementary TRUPACT–II O-ring Seal Performance Test Results (1999)④

Test No.	Disk Centered % Comp.		Disk Offset % Comp.		Helium Leak Tight②				
	O-ring #1	O-ring #2	O-ring #1	O-ring #2	Ambient Temp.	-40 °F	-20 °F (Disk Offset)	Hot Soak (Disk Offset)③	-20 °F (Disk Offset)
1	18.5	17.9	12.7	12.0	Yes	Yes	Yes	Held Vacuum	Yes
2	20.8	20.0	12.9	**11.9**	Yes	Yes	Yes	Held Vacuum	**Yes**
3	19.2	19.2	12.1	12.1	Yes	Yes	Yes	Held Vacuum	Yes

Notes:

① Material for all O-ring seal test specimens was butyl rubber compound R-0405-70, Rainier Rubber Co., Seattle, WA.

② Seal is considered to be leaktight if the actual leakage rate is less than or equal to 8×10^{-8} atm-cc/sec.

③ Hot soak was 8 hours at a uniform temperature of 400 °F.

④ Adapted from Table 2.10.7.4A-2 of [2].

Table 2.12.7-3 – RTG O-ring Face Seal Performance Test Parameters③

Fixture Side	Outer groove depth, in.	Inner groove depth, in.	Shim Thickness, in.	Outer O-ring X- section, in.	Inner O-ring X- section, in.	Outer O-ring compression, %	Inner O-ring compression, %
Side A	0.2053	0.2000	0.044	0.2770	0.2773	10	12
Side B	0.2075	0.2033	0.031	0.2776	0.2774	14	15.5

Notes:

① Material for all O-ring seal test specimens was butyl rubber compound R-0405-70, Rainier Rubber Co., Seattle, WA.

② Each of the four test O-ring seals were leaktight per [1] when tested at a temperature of -20 °F following the time/temperature sequence of 380 °F for 24 hours followed by 350 °F for 144 hours.

③ Adapted from Table 4.1-1 and Table 4.1-2 of [3].

Table 2.12.7-4 – RTG O-ring Bore Seal Performance Test Parameters

Test No.	Min Compression, %	Max Compression, %	Max Temperature, °F	Hold Time, hours	Data Source
4	17.5	30.5	350	168	Table 3 of [5]
4B	17.8	31.3	375	25	Table 3 of [6]
3	19.2	32.3	430	1	Table 3 of [6]

Notes:

① Material for all O-ring seal test specimens was butyl rubber compound R-0405-70, Rainier Rubber Co., Seattle, WA.

② O-ring seals were leaktight per [1] when tested initially at room temperature, at a temperature of -40 °F, again at the stated maximum temperature at the end of the hold time, and finally when chilled to -20 °F.

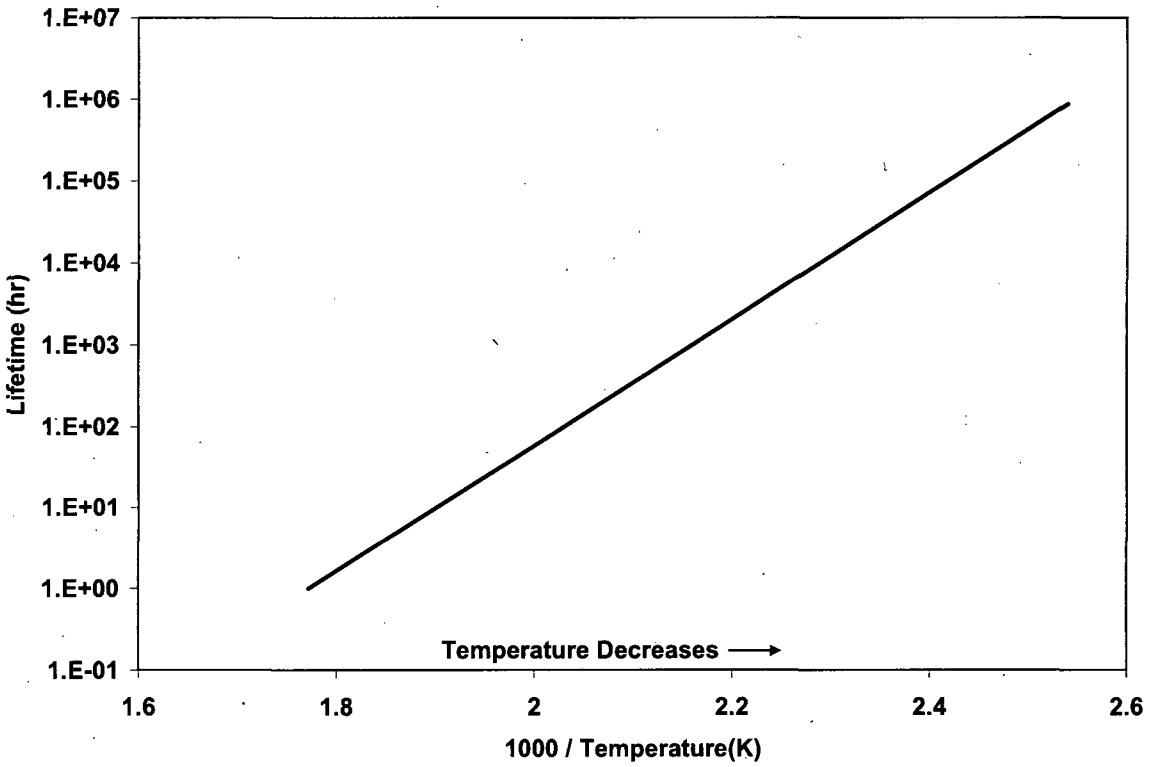

Figure 2.12.7-1 – Elastomer Time-Temperature Behavior (adapted from Figure 3 of [7])